Microfluidic production of liposomal adjuvants for subunit vaccines

A thesis presented for the degree of

Doctor of Philosophy

from the Institute of Pharmacy and Biomedical Science

at the University of Strathclyde

by

Cameron Marcus Webb

Declaration of Authenticity

'This thesis is the result of the author's original research. It has been composed by the author and has not been previously submitted for examination which has led to the award of a degree.'

'The copyright of this thesis belongs to the author under the terms of the United Kingdom Copyright Acts as qualified by University of Strathclyde Regulation 3.50. Due acknowledgement must always be made of the use of any material contained in, or derived from, this thesis.'

Signed: Cameron Marcus Webb

Date: 7th February 2022

Acknowledgements

First and foremost, I would like to thank my supervisor Professor Yvonne Perrie for her continued support during this PhD. I am incredibly grateful to have been allowed to work within her laboratory, which has not only broadened my horizons but has allowed me to publish, attended international conferences and challenged myself in a truly exciting field but most importantly, saved me years of counting tablets. I am also hugely appreciative of her drive to keep the lab open during the pandemic, which allowed me to work on exciting collaborations and keep the PhD on track! I would also like to thank Professor Craig Roberts and Professor Ed Lavelle from Trinity College Dublin for their immunological insights and to those at Precision NanoSystems Inc, Canada, and the Staten Serum Institut, Denmark, for your time and for welcoming me into your institutions.

To everyone I have met in RW315/17 thank you for all your help (and ears), particularly when experiments weren't working. There are now too many names to list in the lab but I would like to pay special thanks to Carla, Neil, Swapnil, Rachel, Rob and Despo, who were hugely helpful during my first year in training me up and getting my research going. I would also like to thank Stuart for all your help with the *in vivo* experiments; I hope the blueberry muffins and costa coffees were suitable payments for your time! In addition to Natalie, Edward and Muattaz thank you for all your assistance with the *in vivo* surgerys and cell work… in particular to the very early starts and not forgetting the 11.30 pm finish on one occasion...

To all my friends, thank you for providing much-needed distractions and breaks from work and to Si for the Thursday trips to The Arlington - I think we both benefitted from this!

To my parents, Maria and Marcus, thank you for everything you have done for my brothers and me. I am confident that if it were not for your advice and emphasis/investments in education, I would not be in the position I am now in. I cannot thank you enough.

Finally, I would like to thank my girlfriend, Ilaria. I cannot truly express my appreciation for your support and motivating me to keep going when times were getting tough, but ultimately, thank you for your patience to sit, listen, and understand my grumblings. Thank you again.

University of Strathclyde

Microfluidic production of liposomal adjuvants for subunit vaccines

Cameron Marcus Webb

Abstract

Nanomedicines are highly effective drug delivery formulations and improve therapeutic outcomes. Since 1990 and the first approved lipid nanomedicine product, a range of lipid nanomedicines have followed and led to the rapid development and regulatory approval of two novel lipid nanomedicines following the COVID-19 outbreak. While mRNA has shown to be an innovative development for vaccines and other treatments, subunit vaccines remain an attractive vaccination route due to their high levels of safety, allowing their use within immunocompromised patients. However, as subunit proteins are not sufficiently immunogenic, an adjuvant is required to boost an innate immune response. Liposomes fulfil this requirement by incorporating immunogenic antigens and their ability to enhance immunostimulatory potency by the addition of surface charges and modifications of their physical characteristics. However, as liposome geometry is primarily determined from the method of manufacture, the method of manufacture must be scalable with tightly controlled process parameters to reduce physical vesicle changes during the scale-up process.

The aim of the work outlined was to develop and explore microfluidic manufacturing techniques to produce liposomal subunit vaccine candidates. The formulations were then physically characterised in terms of size, uniformity, charge, morphology, antigen loading, stability and antigen release kinetics. These systems were then assessed as vaccine adjuvants using *in vivo* mouse models to investigate biodistribution of liposomes and antigen as well as vaccine immunogenicity which was conducted either by ELISAs or bead-based immunoassays.

Microfluidic manufacturing of nanomedicines is a promising method that already has established process parameters. Building on this work, an additional novel microfluidic process parameter was described which utilises organic solvent polarity to control vesicle size. Using a selected formulation, DSPC:Chol, a protein subunit model antigen was entrapped and successfully scaled from a volume of < 1 mL to volumes of 200 mL/min without modifying any additional process parameters, other than the throughput speed. Using developed controlled microfluidic methods for antigen adsorption, *in vivo* biodistribution studies indicated the formation of a depot using DSPC:Chol:DDA liposomes which remained at the injection site for 9 days. This lead to high IgG antigen-specific antibody titres, at a high L:P ratio, when using the protein subunit major outer membrane protein (MOMP) from *C. trachomatis*. Finally, liposomes containing the adjuvants trehalose or a synthetic analogue of monophosphoryl Lipid A (PHAD) were coated with a trimeric spike protein from SARS-CoV-2 with immune responses assessed *in vivo*. The immune responses highlighted PHAD as a potent adjuvant when compared against TDB, leading to a robust Th1 humoral response and Th2 cell-mediated response. The use of DDA:PHAD strongly stimulated Th1 and Th17 pathways and activated caspase-I receptors at the injection site, demonstrating the adjuvant's effectiveness in the production of T cell responses and neutralising antibodies against antibodies SARS-CoV-2. The work outlined in the thesis confirms microfluidics as a scalable production method to control liposome adjuvant physical properties and effectively encapsulate or surface adsorb protein subunits allowing for robust immune responses to produce safe and efficacious protein subunit vaccines for different modalities.

List of Publications

C. Webb and Y Perrie, Pharmaceutical Formulation: Technologies and Processing Techniques (in preparation).

C. Webb, S. Ip, N.V. Bathula, P. Popova, S.K.V. Soriano, H.H. Ly, B. Eryilmaz, V.A.N. Huu, R. Broadhead, M. Rabel, I. Villamagna, S. Abraham, V. Raeesi, A. Thomas, S. Clarke, E.C. Ramsay, Y. Perrie, A.K. Blakney, Current Status and Future Perspectives on mRNA Drug Manufacturing. Molecular Pharmaceutics, 19 (2022).

N. Munoz-Wolf, R.W. Ward, C.H. Hearnden, F.A. Sharp, J. Geoghegan, K. O'Grady, C.P. McEntee, K.A. Shanahan, C. Guy, A.G. Bowie, M. Campbell, C.B. Roces, G. Anderluzzi, **C. Webb**, Y. Perrie, E. Creagh, E.C. Lavelle, Non-canonical inflammasome activation mediates the adjuvanticity of nanoparticles. Immunity (pre-press, 2022).

C. Webb, N. Forbes, C.B. Roces, G. Anderluzzi, G. Lou, S. Abraham, L. Ingalls, K. Marshall, T.J. Leaver, J.A. Watts, J.W. Aylott, Y. Perrie, Using microfluidics for scalable manufacturing of nanomedicines from bench to GMP: A case study using protein-loaded liposomes, International Journal of Pharmaceutics, 582 (2020).

C. Webb, S. Khadke, S.T. Schmidt, C.B. Roces, N. Forbes, G. Berrie, Y. Perrie, The Impact of Solvent Selection: Strategies to Guide the Manufacturing of Liposomes Using Microfluidics, Pharmaceutics, 11 (2019).

List of Poster Presentations

Webb C., Perrie Y (2021). Microfluidic preparation of adjuvanted SARS-CoV-2 subunit protein: DDAB:TDB vs DDAB:PHAD. *American Association of Pharmaceutical Scientists*. 17-20th October 2021 (virtual)

Webb C., Perrie Y (2021). Continuous production of liposomal vaccines: solvent reduction strategies. *CRS Annual Meeting & Exposition.* July 25-29th 2021 (virtual)

Webb C., Perrie Y (2020). Production of cationic PLGA nanoparticles for the delivery of RNA therapies. *Genetic Medicine Summit: Evolution Revolution. Precision NanoSystems inc.* November 17-18th 2020 (virtual).

Webb C., Forbes N., Perrie Y (2020). From lab bench to GMP: A direct path to high throughput formulation production with protein-loaded liposomes. *Genetic Medicine Summit: Evolution Revolution. Precision NanoSystems inc.* November 17-18th 2020 (virtual).

Webb C., Forbes N., Perrie Y (2020). Implementation of a novel microfluidic structure to transition protein-loaded liposome production from bench to GMP. UKICRS annual meeting, 14th October 2020 (virtual).

Webb C., Forbes N., Perrie Y (2019). High-throughput production of liposomes entrapping proteins using a novel microfluidic architecture. *American Association of Pharmaceutical Scientists, San Antonio Texas*, 3-6th November 2019

Webb C., Perrie Y (2019). Comparing purification techniques for scalable liposomal formulations*. Liposome Research Days, Sapporo Japan,* 15-18th September

Webb C., Berrie G., Perrie Y (2019). Microfluidic controlled manufacturing for liposomal vaccine formulations. *UK PharmSci, Greenwich UK,* 11-13th September 2019

Webb C., Berrie G., Perrie Y (2019). Developing microfluidic processes for the manufacture of liposomal vaccines. *CRS Annual Meeting & Exposition, Valencia Spain,* 21-24th July 2019

Webb C., Berrie G., Perrie Y (2019). Exploring microfluidic-controlled manufacturing for liposomal vaccines. *UKICRS Symposium, Liverpool UK,* 3-4th June 2019

Webb C., Berrie G., Perrie Y (2019). Optimising microfluidic parameters for the manufacture of lipid nanoparticles. *Bioinspired Nanomaterials, Glasgow UK,* 18-19th March 2019

List of Oral Presentations

Manufacturing of Nanomedicines by microfluidics. *The Academy of Pharmaceutical Sciences*. October 21st 2021 (Virtual)

Facilitating RNA genetic medicine development using scalable production methods. Genetic Medicine Summit: Evolution Revolution. Precision NanoSystems Inc. November 17th 2020 (Virtual).

From bench to GMP: A scale-independent approach to protein-loaded liposomes production using a novel microfluidic architecture. CRS Annual Meeting, June 29th to July 2nd 2020 (Virtual)

Use of a novel microfluidic technology to accelerate lipid nanomedicine development: From the lab bench to GMP. *Doctoral School Multidisciplinary Symposium, Glasgow UK, 27th April 2020 (Virtual)*

Investigating microfluidic cartridge design to support rapid scale-up*. PrecisionNanosystems: Create Transformative Medicine Europe User Group Meeting, Glasgow UK*, 9th October 2019 Comparing purification techniques for scalable liposomal formulations. *Liposome Research Days, Sapporo Japan*, 11-13th September 2019

Developing microfluidic processes for the manufacture of liposomal vaccines. *CRS Annual Meeting, Valencia Spain,* 21-24th July 2019

Table of Contents

Chapter 3 Implementation of a novel microfluidic manufacturing parameter: Exploiting organic solvent polarities to fine-tune vesicle physical properties

Chapter 4 Bench to GMP: Systematic mapping analysis of microfluidic geometries to permit scale-up production of liposomal drug delivery systems

List of Tables

List of Figures

adsorption a cationic liposomal formulation of DSPC:Chol:DDA (10:5:4 w/w) was manufactured by microfluidics at a FRR of 1:1 and 15 mL/min in MeOH (solvent phase) and Tris 10 mM (aqueous phase) which was purified by dialysis method (14 kD membrane) immediately after leaving a final liposome concentration of 2 mg/mL. Sizes were then measured by suspending OVA Tris 10 mM and either pipetted directly onto the liposomes (1:1 v/v) (A); vortexed while pipetting (1:1 v/v) (B) or mixed with liposomes via microfluidics (C) at a FRR of 1:1 and zeta potentials recorded for the respective methods (D, E and F). The final liposome concentration after OVA adsorption was 1 mg/mL with OVA concentrations between 0.016 – 10 mg/mL depending on the investigated L:P ratio. Results represent mean ± SD from 3 independent batches. 168

Figure 5.2 Assessing the influence of L:P ratios by microfluidic adsorption on liposomal stability and loading efficiencies. The effect of liposomal stability was measured over 14 days with size (A), PDI (B), zeta potential (C) and loading efficiencies (D) recorded at specific time points to plot the degree of change as a result of L:P ratios. DSPC:Chol:DDA (10:5:4 w/w) liposomes were manufactured at a 1:1 FRR and 15 mL/min at a final liposome concentration of 2 mg/mL using MeOH (solvent phase) and Tris 10 mM (aqueous phase) with solvent removed by dialysis (14 kD membrane). OVA, suspended in Tris 10 mM (pH 7.4) was then adsorbed to liposomes at a FRR of 1:1 and TFR of 15mL/min leaving a final liposome concentration of 1 mg/mL and OVA concentrations between 0.005 - 0.125 mg/mL. Samples were stored at 4 °C between time points. Results represent mean ± SD from 3 independent batches. 170

Figure 5.3 Tracking liposome stability over 14 h. Liposome size and PDI was measured for 10:1 L:P (A); 30:1 L:P (B) and 60:1 L:P (C) over 14 h recorded at each hour. A method was set up to cool samples to 4 °C between measurements to simulate the storage conditions in figure 5.2 with samples heated at to the required 25 °C during the measurement. The same method of liposome production, purification and protein adsorption used in figure 5.2 was used to obtain figure 5.3. 172

Figure 5.4 Effect of flow rate ratios on liposome physical characteristics and influence of solvent selection. The impact of solvent on liposomes size and PDI for MeOH (A) and EtOH (C) in addition to zeta potential for MeOH (B) and EtOH (D) were investigated along with FRR to refine optimal liposomal manufacturing parameters for DSPC:Chol:DDA (10:5:4 w/w) liposomes. A TFR of 15 mL/min was used with Tris 10 mM used for both the aqueous phase

Abstract

Abbreviations

AF647	Alexa fluor 647
Ag	Antigen
ANOVA	Analysis of variance
APC	Antigen presenting cell
API	Active pharmaceutical ingredient
ATX	proprietary ionizable amino lipids
BCA	Bicinchoninic acid assay
BM	Batch manufacturing
CAF	Cationic adjuvant formulation
CAN	Acetonitrile
CH_3COOH	Acetic acid
Chol	Cholesterol
CM	Continuous manufacturing
ConA	Concanavalin A
Cryo-TEM	Cryogenic transmission electron microscope
$d.H_2O$	Deionised water
DDA	Dimethyldioctadecylammonium
DF	Dilution factor
DiR	DiIC18(7); (1,1'-Dioctadecyl-3,3,3',3'-Tetramethylindotricarbocyanine Iodide)
DLS	Dynamic light scattering
DMG-PEG	DMG-PEG (1,2-Dimyristoyl-sn-glycerol, methoxypolyethylene glycol
DMPC	1,2-dimyristoyl-sn-glycero-3-phosphocholine
DMSO	Dimethyl sulfoxide
DOTAP	1,2-dioleoyl-3-trimethylammonium-propane
DSPC	1,2-distearoyl-sn-glycero-3-phosphocholine
EDTA	Ethylenediaminetetraacetic acid
EE%	Encapsulation efficiency
EMA	European Medicines Agency
EPR	Enhanced permeability and retention

ESP	Empirical solvent polarity
EtOH	Ethanol
Ex/em	Excitation/emission
FBS	Foetal bovine serum
FDA	Food and Drug Administration
FRR	Flow rate ratio
GMP	Good manufacturing practice
GUV	Giant unilamellar vesicles
H56	Hybrid 56
HBSS	Hanks balanced salt solution
HRP	Horseradish peroxidase
ICH	International Conference of Harmonisation
IFN-γ	Interferon gamma
IgG	Immunoglobulin
IL	Interleukin
IPA	Isopropanol alcohol or 2-propanol
IVIS	In vivo imaging system
LFH	Lipid film hydration
LNP	Lipid nanoparticle
LOD	Limit of detection
LOQ	Limit of quantification
LUV	Large unilamellar vesicles
MeOH	Methanol
MHC	Major histocompatibility comples
MHC	Major histocompatibility complex
MHRA	Medicines & Healthcare Products Regulatory Agency
MLV	Multilamellar vesicles
MMG	Mycobacterial monomyolated glycerol
MOMP	Major outer membrane protein
mPES	Modified polyethersulfone
MPL/MPLA	Monophosphoryl Lipid A

MVV	Multi-vesicular vesicles
MW	Molecular weight
NTA	Nanoparticle tracking analysis
OVA	Ovalbumin
PAGE	Polyacrylamide gelelectrophoresis
PAMP	Pathogen-associated molecular patterns
PAT	Process analytical technology
PC	Phosphatidyl choline
PDI	Polydispersity index
Pe	Péclets number
PEG	Polyethylene glycol
PEG$_{2000}$	1,2-distearoyl-sn-glycero-3-phosphoethanolamine-N-[amino(polyethylene glycol)-2000
PHAD®	Synthetic structural analogue of monophosphoryl Lipid A
PLGA	poly(lactic-co-glycolic acid)
POPC	1-palmitoyl-2-oleoyl-sn-glycero-3-phosphocholine
PRR	Pattern recognition receptor
Re	Reynolds number
RP-HPLC	Reverse phase high performance liquid chromatography
RPMI	Roswell Park Memorial Institute medium
SD	Standard deviation
SDS	Sodium dodecyl sulfate
SHM	Staggered herringbone micromixer
Spike	Recombinant SARS-CoV-2 Spike His-tag
SUV	Small unilamellar vesicles
TAP	Transported associated with antigen processing
TCR	T cell receptor
TDB	Trehalose 6,6'-dibehenate
TFA	Trifluoroacetic acid
TFF	Tangential flow filtration
TFR	Total flow rate

Th	T helper cell
TLR	Toll like receptor
T_m	High phase transition temperature
TMB	3,3',5,5'-Tetramethylbenzidine
TMP	Transmembrane pressure
TNF	Tumour necrosis factor
Tris	2-amino-2-(hydroxymethyl)-1,3-propanediol
TrM	Toroidal micromixer
UV	Ultraviolet
WHO	World Health Organisation
ZP	Zeta potenial

Chapter 1

General Introduction

1.1 Lipid vesicles for drug delivery

Liposomes were first described in 1965 by a British haematologist, Alec Bangham, where artificial lipid vesicles were shown to resemble a cell membrane with close similarity, providing cellular biologists with a unique tool for studying cell membrane functions [1]. However, it was not until the pioneering work conducted in the 1970s by Gregory Gregoriadis and colleagues which led to their innovative use as a drug delivery platform for therapeutic use [2, 3]. Within nanomedicines, liposomes comprise of lipids such as phosphatidylcholines. When in an aqueous phase, lipids arrange into lipid bilayers due to their structural attributes and, subsequently, these bilayers close and form vesicles composed of an aqueous core and non-polar region within the bilayer (figure 1.1A). Phospholipids are amphiphilic and incorporate a backbone region (e.g. glycerol), a hydrophilic head (polar; e.g. phosphatidylcholine) and two hydrophobic hydrocarbon tails (non-polar). The degree of polarity of the hydrophilic head governs the liposome's surface charge [4], with the alkyl chain providing an essential role in the liposome stability [5] which can exist in either a saturated or unsaturated state. When lipids are placed into an aqueous medium, they orientate themselves to reduce unfavourable interactions between the non-polar alkyl chain and the polar aqueous medium, leading to liposomes closing off the aqueous core (figure 1.1C; [6, 7]).
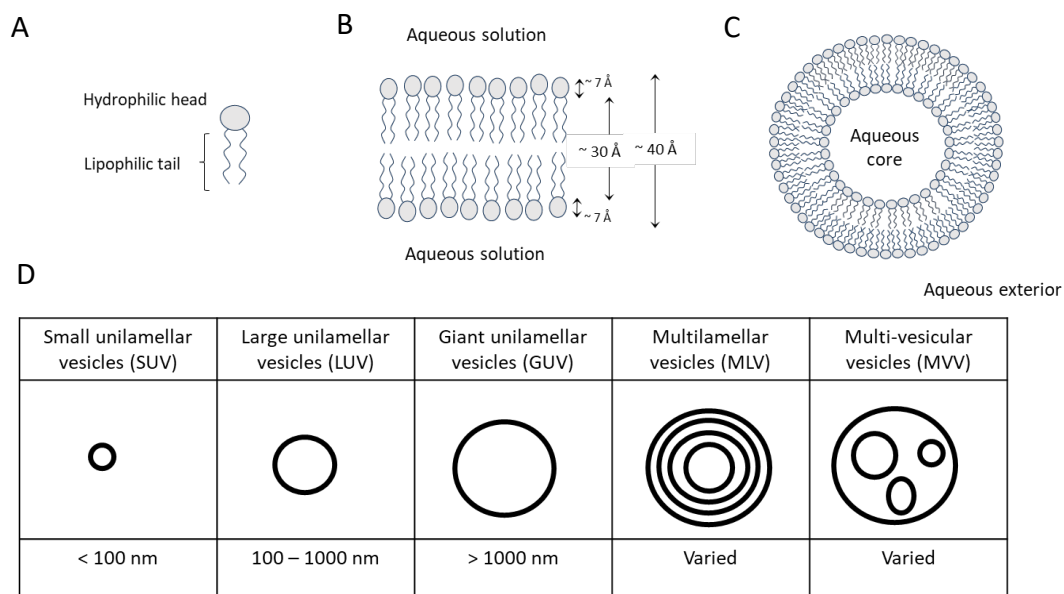
Figure 1.1 *Schematic representation of the components and structures of liposomes. (A) represents the amphilic phospholipid which forms the (B) liposomes bilayer (sizes from [8]) and closure into (C) liposomes with (D) the representation of sizes and structures that can formed.*

Liposomes can then be classified according to their size and structural features, as shown in figure 1.1D. Their biocompatible and amphiphilic nature makes them a promising candidate for drug delivery due to their ability to incorporate hydrophilic and hydrophobic compounds within their structure, offering physical protection [9], or compounds can be attached to the liposomal surface through covalent or electrostatic bonding [10] which further increases their flexibility as a drug delivery method.

1.2 Liposomes used in the clinic

Liposomes can alter the biodistribution of drugs [11] and improve the controlled release of entrapped material, enhancing bioavailability [12], and this has resulted in the translation of 19 marketed liposomes products in the FDA and EMA regions for therapeutic use (table 1.1; [13]). The use of liposomal formulations enabling the controlled-release of entrapped medicines can be demonstrated clinically using a well-described liposomal formulation in the form of Doxil® (table 1.1) to passively deliver doxorubicin to tumour cells that have 'leaky' vessels as a result of the enhanced permeability and retention effect (EPR). The EPR effect describes dilated capillary junctions within solid tumours allowing greater extravasation of the vesicles where they release doxorubicin in and around the tumour cells [14]. Using hydrogenated soy phosphatidylcholine (HSPC) as a high phase transition temperature (Tm) phospholipid, cholesterol for improved stability and a lipopolymer 1,2-distearoyl-sn-glycero-3-phosphoethanolamine-N-[biotinyl(polyethylene glycol)-2000] (PEG$_{2000}$-DSPC; table 1.1) that creates a hydrophilic layer around the liposome, has led to sterically stabilised liposomes which prolonged circulation times [15]. Using PEG within formulations causes a hydrophilic hydration layer around vesicles, with one molecule of polyethylene glycol-2000 (PEG$_{2000}$), when covalently bound to a lipid molecule, binding approximately 200 water molecules [16]. This hydration layer reduces non-specific interactions with proteins thus prolonging blood-circulation time [17] and reducing phagocytic uptake through the reduction of opsonisation by circulating proteins binding to the lipid bilayer [14]. Furthermore, as a result of the small vesicle size (< 120 nm), liposomes can effectively pass through gaps in tumour vasculature, as a result of the EPR effect [18, 19], and selectively release their payload upon internalisation within the tumour cells thus improving drug targeting and reducing systemic cytotoxicity [15].

Alternatively, formulations such as those within DepoDur™ achieve sustained release of the active pharmaceutical ingredient (API) by creating a "depot effect" [20] and as such allows the formulation to remain localised and permit the sustained release of the payload at therapeutic levels [21, 22]. Using DepoDur as an example, slow release of 10 mg/mL morphine sulphate is achieved by encapsulation within liposomal bilayers (composed of cholesterol 3.3 mg; dioleoylphosphatidylcholine (DOPC) 4.2 mg/mL; dipalmitoylphosphatidylglycerol (DPPG) 0.9 mg/mL; tricaprylin 0.3 mg/mL and triolein 0.1 mg/mL [23]). With this formulation, one dose before surgery or after a cesarean section reduces postoperative opioid more effectively than the use of IV morphine [24].

Table 1.1 *Commercially available liposome products adapted from [13].*

Clinical Product (approved year)	Administration	API	Lipid/Lipid (molar ratio)	Indication	Vesicle size
Ambisome (1997)	i.v.	Amphotericin B	HSPC:DSPG:Chol: Amphotericin B (2:0.8:1:0.4)	Fungal infection	< 100 nm
Arikayce (2018)	Inhalation	Amikacin	DPPC:chol	*Mycobacterium avium* complex lung disease	300 nm
DaunoXome (1996)	i.v.	Daunorubicin	DSPC:Chol (2:1)	AIDs-related Kaposi's sarcoma	40 – 80 nm
Depocyt (1999*)	Spinal	Cyarabine/ AraC	DOPC:DPPG:Chol: Triolein	Neoplastic meningitis	20 μm
DepoDur (2004*)	Epidural	Morphine sulfate	DOPC:DPPG:Chol: Triolein	Analgesia	17– 23 μm
Doxil/Caelyx(1995)	i.v.	Doxorubicin	HSPC:Chol:PEG2K-DSPE (56:39:5)	Ovarian. Breast cancer, Kaposi's sarcoma	100 nm
Doxorubicin (2017)	i.v	Doxorubicin	HSPC:chol:DSPE-PEG	Breast neoplasms	100 nm
Epaxal (1993)	i.m.	Inactivated hepatitis A virus	DOPC:DOPE (75:25)	Hepatitis A	150 nm
Exparel (2011)	i.v.	Bupivaciane	DEPC:DPPG:Chol: Tricaprylin	Analgesia	24– 31 μm
Lipodox (2013)	i.v	Doxorubici-n	HSPC:chol:DSPE-PEG (56:39:5)	Breast Neoplasts	100 nm

Marqibo (2012)	i.v.	Vincristine	SM:Chol (60:40)	Acute lymphoblastic leukaemia	100 nm
Mepact (2009)	i.v.	Mifamurtide	DOPS:POPC (3:7)	Non-metastatic osteosarcoma	1–5 μm
Mosquirix (2015)	i.m	Antigen based vaccine	DOPC:Chol	Vaccination to help against malaria caused by the parasite *Plasmodium falciparum*	50 – 100 nm
Myocet (2000)	i.v.	Doxorubicin	EPC:Chol (55:45)	Metastatic breast cancer	80–90 nm
Nocita (2017)	Local infiltration	Bupivacaine	DEPC:DPPG:chol:tricaprylin	Anaesthetic	25–31 μm
Onivyde (2015)	i.v.	Irinotecan	DSPC:MPEG2K:DSPE (3:2:0.015)	Pancreatic metastatic adenocarcinoma	110 nm
Shingrix (2017)	i.m	vaccine for prevention of herpes zoster	DOPC:chol	Glycoprotein E based vaccine	50–100 nm
Visudyne (2000)	i.v.	Verteporfin	Verteporphin:DMPC and EPG (1:8)	Choroidal neovascularisation	18–104 nm
Vyxeos (2017)	i.v	Daunorubicin Cytarabine	DSPC:DSPG:chol (7:2:1)	Acute myeloid leukaemia	107 nm

i.v. (intravenous); i.m. (intramuscular); Chol (cholesterol); HSPC (hydrogenated soy phosphatidylcholine); PEG (polyethylene glycol); DSPE (distearoyl-sn-glycero-phosphoethanolamine); DSPC (distearoylphosphatidylcholine); DOPC (dioleoylphosphatidylcholine); DPPG (dipalmitoylphosphatidylglycerol); EPC (egg phosphatidylcholine); DOPS (dioleoylphosphatidylserine); POPC (palmitoyloleoylphosphatidylcholine); SM (sphingomyelin); MPEG (methoxy polyethylene glycol); DMPC (dimyristoyl phosphatidylcholine); DMPG (dimyristoyl phosphatidylglycerol); DSPG (distearoylphosphatidylglycerol); DEPC (dierucoylphosphatidylcholine); DOPE (dioleoly-sn-glycero-phophoethanolamine). Discontinued products are noted with the symbol (*)

1.3 Liposomes and their role in vaccination

1.3.1 *Vaccines*

Arguably, vaccination is one of the most outstanding humanitarian achievements that has significantly reduced the mortality rate. Prolonging human longevity by artificially inducing immune responses is not a new concept and can be dated back as early as 15th century China when they recognised that those infected with smallpox, and survived the infection, were not reinfected. The novel idea to crush dried preserved scabs from smallpox sufferers into a

powder and blow them up the nostrils of boys (right nostril) and girls (left nostril) was practised as a way to inoculate those against the virus [25]. However, it was not until the 18th century when the British physician Edward Jenner was credited with developing the first and clear demonstration of immunity to smallpox using material extracted from cowpox scabs. The ground-breaking discovery laid the foundation for a range of treatments to be developed for various diseases [26]. Childhood diseases, including polio and measles, were significantly reduced due to the global vaccination adoption [27].

Vaccine development is a complex effort as a biological product must be safely produced to be used within a wide range of healthy individuals, resulting in careful monitoring of vaccine candidates. This can make vaccine research and production costly as many healthy participants need to be recruited and monitored for a long duration to establish vaccine efficacy. Excluding the COVID-19 vaccine effort, Gouglas et al., extensively screen 224 vaccine candidates from preclinical to phase 2 for 11 infectious diseases and highlighted that the costs from development to licensure can exceed a billion dollars with a 94% chance of failure during phase 1-4 clinical trials [28, 29]. This process often takes upwards of 10 years [29]. However, due to the global pressures and need for a COVID-19 vaccine, within 5 months 73 vaccine candidates were under pre-clinical experimentation with six in phase 1/2 trials [30]. The significant progress within nanomedicines, particularly lipid nanomedicines, successfully unlocked the potential of mRNA as vaccine candidate encoding for the spike protein region of the virus. This led to the use of lipid nanoparticles (LNPs) by both Pfizer/BioNTech and Moderna to deliver their mRNA product encoding for the spike region. The vaccines produced by the two companies were subsequently granted emergency approval on the 2nd of December 2020 and 8th of January 2021 respectively.

Regardless of the vaccine innovation and development, the key and fundamental attribute that all vaccines commonly share is immunity against a pathogen without prior exposure to the specific disease in question. To achieve this, the vaccine aims to closely copy foreign pathogens' mechanism of action that induces the immune response without the pathogenicity and strong immune responses associated with the pathogen's exposure. To achieve this, both innate and acquired immune responses need to be activated [31].

1.3.1.1 Pathogen recognition and its role in innate immune responses

At the start of infection, the innate immune response is the dominant non-specific immune response. The pathogen is met by phagocytes such as dendritic cells or monocytes, leading to the rapid activation of the innate immune response, with more specific responses activating after several days. Despite the innate immune response being non-specific, its activation relies heavily on cellular receptors with pathogen markers known as pathogen-associated molecular patterns (PAMPs) [32] on their membrane, including lipopolysaccharides, lipids, proteins and viral or bacterial nucleic acids. Pathogen recognition receptors (PRRs), such as toll-like receptors (TLRs), on phagocytes, interact with one of the ligands on the plasma membrane, leading to the secretion of inflammatory mediators such as IL-1, IL-12 and TNF-α [33], which are proliferated by the release of nuclear factor - κB (NF-κB) [34]. This cascade also allows the immune system to distinguish itself from non-self [35]. Such inflammatory mediators encourage the migration of monocytes, neutrophils and dendritic cells to the site of infection, leading to a localised immune response. A notable characteristic of this response is the increased vascular permeability permitting extraversion and secretion of chemokines from the recruited immune cells leads to further chemotaxis of additional leukocytes [36]. Upon pathogen recognition, depending on the size and nature of the pathogen, it is internalised either by endocytosis, micropinocytosis, pinocytosis or phagocytosis [37]. Consequently, the digested pathogen is destroyed with portions of digested proteins from the pathogen that are then expressed as peptide fragments on major histocompatibility complexes (MHC; [38]). This process additionally acts as a fail-safe mechanism to prevent the immune system from becoming hypersensitive, known as MHC restriction [39].

1.3.1.2 Acquired immunity

MHC peptide expression plays a pivotal role in the adaptive immune response and its capacity to distinguish the host "self" cells from pathogens. After PRR is activated, dendritic cells migrate to draining lymph nodes to interact with naïve T cells specific to that antigen [40]. The acquired immunity comprises a multitude of antigen-specific B and T lymphocytes with unique receptors that allow them to bind to many different antigens and, as such, take time to become established. By a process known as "lymphocyte repertoire" during lymphocyte development, random gene reshuffling within the variable regions of the immunoglobulin

receptors provides B and T lymphocytes with the capability to recognise a vast spectrum of pathogens [41]. An essential aspect of T-cells is their ability to recognise self MHC from foreign antigens by a mechanism known as T cell tolerance. Briefly, in the thymus, T cells are challenged by positive selection to ensure they have MHC affinity to bind to peptides by either MHC I or MHC II. Those that have sufficient affinity are selected for survival. Secondly, during negative selection, T cells are examined to ensure they do not bind to "self-peptide", which, if they do, are subsequently destroyed via apoptosis. Depending on the T cells, MHC binding affinity and those that survive both positive and negative selection migrate to secondary lymph nodes for maturation.

Different MHCs are upregulated depending on the location of the pathogen. For pathogens located within circulating fluid (such as bacteria, parasites and fungi) which are engulfed by phagocytes interaction with Golgi apparatus containing pre-formed MHC II molecules which leads to complexation and subsequent expression on the cell surface [42], which lead to activated T-helper cells (CD4) [43]. Such a mechanism is known as the humoral response (figure 1.2A), also called antibody-mediated immunity, and has a central role in the activation of B cells assisted by Th cells. MHC II molecules are only associated with dendritic cells, macrophages and B cells (professional antigen-presenting cells) and activated CD4 cells. Antibody production by B cell occurs within a secondary lymphoid organ when it binds to its epitope and subsequently binds with migratory specific CD4 cells expressing the peptide [33]. Upon activation, the B-cell matures into plasma cells that produce specific antibodies or memory B-cells, allowing rapid production of antibodies in a secondary infection.

Intracellular antigens such as viruses, which uses host cells to replicate, are processed in the cytosol to allow entry into the endoplasmic reticulum by the transporter associated with antigen processing (TAP). TAP activation results in the interaction with MHC I and expression on the cell surface by a transport vesicle [44] and activation of cytotoxic T cells (CD8). As all nucleated cells are susceptible to being targets by viruses for viral replication, almost all nucleated cells can express MHC I molecules causing clonal selection of CD8 when the T-cell receptor (TCR) is stimulated. This process leads to the rapid division of effector CD8 cells that travel throughout the systemic circulation to target infected host cells bearing the same MHC I peptide. Those cells expressing the MHC I peptide are subjected to the release granzymes

from CD8 cells to induce apoptosis of the host cell. After the infection, many CD8 cells remain as memory cells allowing rapid cell proliferation if the same infection is re-encountered (figure 1.2B).

A. Humoral immunity

B. Cell mediated immunity
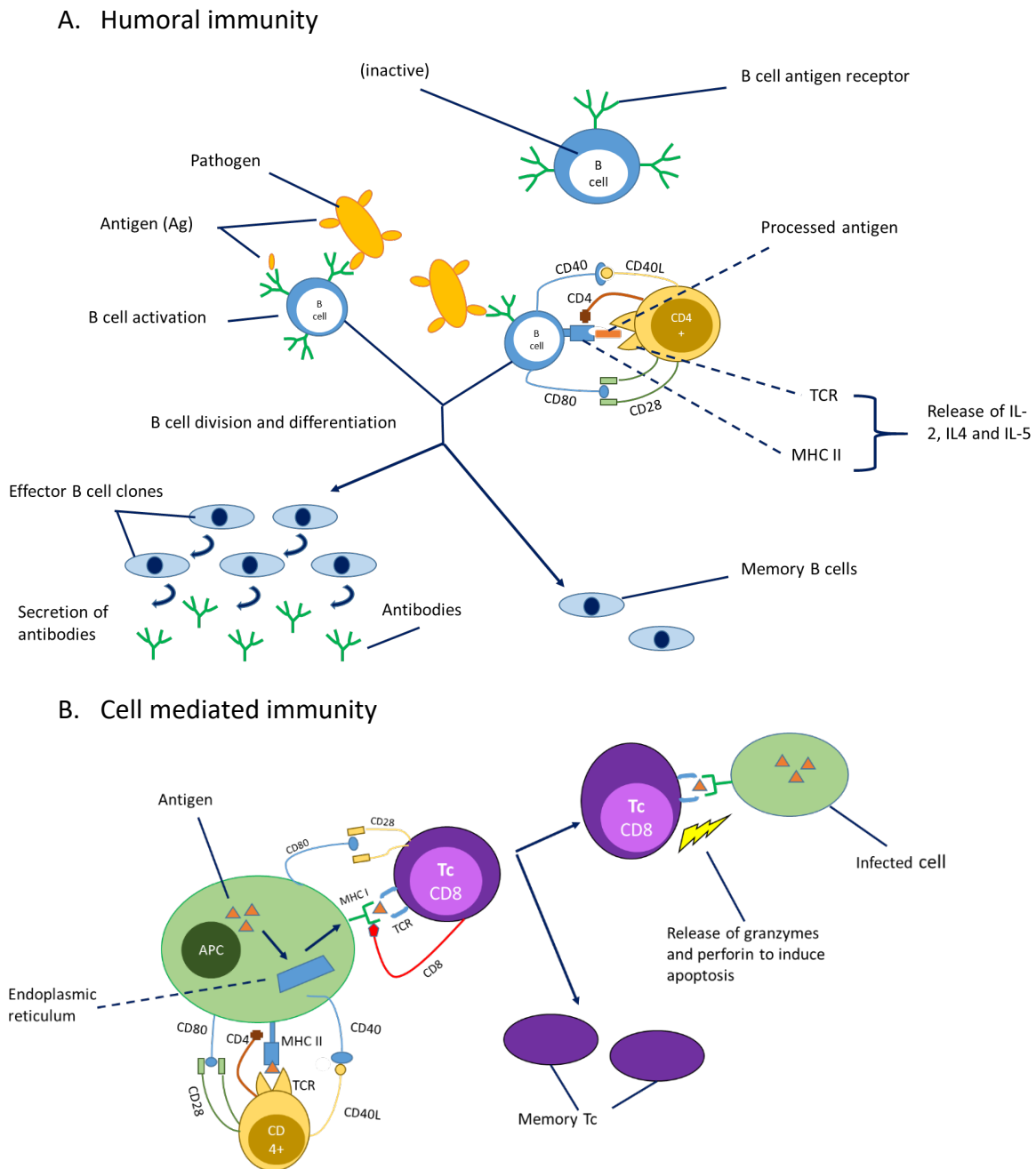
Figure 1.2 *Schematic illustrating the adaptive immune response. A) Activation of the humoral response occurs after the antigen expression on the B cell receptor surface and presentation on the MHC II receptor. An activated CD4 cell recognises the antigen via the T cell receptor (TCR) and co-stimulation of CD40-CD40L and CD80-CD28 triggering the humoral response and subsequent antibody production. B) Much like (A), an activated CD4 binds to an antigen-presenting cell and endogenous antigens expressed on MHC I; CD8+ are activated by CD80-CD28 interactions proliferating the cell-mediated cascade.*

1.3.2 Alive, dead or neither?

Traditionally, vaccines can be grouped into four main categories: live-attenuated, inactivated, toxoid and subunit vaccines. Much of the early discoveries involved live pathogens that were attenuated to reduce their virility but still be able to infect human cells. The first of these vaccines developed for humans was a live-attenuated viral vaccine for rabies in the 1880s, with attenuation of the virus achieved by inactivation with formaldehyde [45]. Live-attenuated vaccines are are still used today within the clinic in the form of bacillus Calmette-Guérin (BCG), MMR (measles, mumps, rubella) and yellow fever. Current viral attenuation for vaccines can be achieved through *in vitro* cell cultures (such as chicken embryo cells). Over a series of passages through different cell cultures, virus strains are selected where increased infectivity towards the cell culture is demonstrated through a series of mutations and will loose its ability to infect human cells with each passage [46]. While an established manufacturing process, it has remained unchanged since the 1920s and has led to manufacturing issues for BCG vaccines and countries unable to obtain supplies [47]. As they are weakened forms of the wild-type vaccine, they can induce a robust immune response by activating both humoral and cell-mediated immune responses leading to a long-lasting immunity [48]. However, there are drawbacks to their use making them not suitable for immunocomprimised or pregnant individuals without sufficient benefit-risk analysis due to the is a risk that the attenuated strain could revert to a virulent form. An example of this was the oral polio vaccine (OPV) which was effective by closely eradicating the wild poliovirus, however, in regions with low vaccine coverage the use of the vaccine has led to circulating vaccine-derived polioviruses [49, 50].

In contrast, inactivated vaccines are pathogens killed through heat or chemical inactivation and therefore can no longer replicate. When compared against live-attenuated vaccines, this is advantageous, as because the virus or bacteria has been inactivated there is no risk of reversion and so cannot cause the disease they were designed to protect againt which allow them to be used within an immunocomprimised population. However, chemical modification with reagents such as formalin could damage the antigenic protein, further reducing the vaccine immunogenicity. Typically, multiple booster vaccinations are required to maintain immunity within rabies, trivalent influenza vaccine (TIV; annual dose) and Hepatitis A vaccines currently used in the clinic.

In the case of subunit vaccines, they are based on highly purified antigens such as peptides and recombinant proteins to create an immune response making them safe and suitable for those that are immunocompromised with less adverse effect; however, the fragments used within the vaccine have insufficient immunogenicity [51]. Therefore, to maintain the safety profile of the subunit vaccines, immunostimulators, also known as vaccine adjuvants, have been heavily investigated as a strategy to improve immunogenicity. COVID-19 catapulted the clinical use mRNA vaccines using LNP as delivery carriers, which has shown to be a safe and promising new technology for other therapeutic indications such the treatment of hereditary transthyretin amyloidosis using the first small interfering RNA (siRNA) therapeutic Onpattro (patisiran) [52]. Furthermore, self-amplifying RNA is an exciting new technology that has shown to be highly efficacious when delivered using LNPs, affording high SARS-CoV-2 neutralising antibody titres in murine models [53] and could reduce the vaccine manufacturing burden, as studies by Vogel et al., and Brito et al., have found that saRNA is at least 64-fold more potent than mRNA [54, 55]

1.3.3 Use of liposomes as adjuvants

The underlying mechanism of adjuvanted formulations is to create an immune response and activate antigen-presenting cells, initiating an acquired immune response to the antigen expressed on the pathogen. The immune response can be artificially enhanced by adding adjuvants, allowing purified antigens with poor immunostimulatory abilities to be used in vaccines thus improving the vaccine's overall safety profile. The discovery of vaccine adjuvants can be referenced back to 1925, where Gaston Ramon combined his diphtheria toxoid with reagents such as starch oil, lecithin and others which lead to an improved antitoxin response when challenged against diphtheria [56]. Many agents used to encourage immune responses, such as alum (aluminium hydroxide), saponins and Freunds adjuvant (emulsified antigen in oil with an immune booster), were investigated in early preliminary research [57]. However, many of these elicited toxic adverse effects hampering their further use within vaccine formulations [58].

Herein, the need for an inexpensive, non-immunogenic and non-toxic adjuvant that provides humoral and cellular mediated immunity like their predecessors was needed [57]. Gregoriadis gave an early insight into liposomes as adjuvants [59]; since then, the field has expanded with liposomes providing a platform to deliver a range of antigens for various conditions [60, 61].

Adjuvants assist in the initial acquired immune response though locally activating APC (such as at the injection site), leading to their translocation to draining lymph nodes, allowing the desired acquired immune response with the degree of the immune response controlled depending on the balance of adjuvant and antigen used within the formulation [62]. Much of the current focus concerning vaccines involves using pathogen subunits [63], which allow for specific immune responses; however, their overall immunogenicity is poor, meaning that an adjuvant needs to be used to induce this vaccination method and initiate an acquired immune response [64]. The use of subunits allows for specific immune responses to be activated, unlike inactivated or attenuated vaccines that have far greater immunostimulatory actions but reduce the vaccine's overall safety [60]. Such immunostimulators act on PRRs expressed on APCs of which toll-like receptors (TLR), a class of PRR, are a particularly attractive target for adjuvants [40, 65]. Improvements in immunstimulatory properies can be further improved by modification of liposome physical qualities such as the choice of lipid [66], vesicle size [67, 68], surface charge [69, 70] and surface modification (such as PEGylation [71]).

1.3.3.1 Effect of liposome size

The size of the manufactured liposomes is an important physiochemical consideration in the development of a formulation and plays a critical overall role in therapeutic efficiency. As such, it is vitally important that the vesicle size is maintained [72]. For example, the importance on vesicle size can be shown liposomes where first used to deliver chemotherapy drugs to tumours as the vesicle size can be tuned to exploit the EPR effect in solid tumours. The EPR effect occurs in malignant tissue due to highly expressed vasculature facilitating rapid tumour growth, causing increased permeability factors such as bradykinin and nitric oxide [73]. This allows liposomes within the correct size requirements to pass through the tumour vasculature and accumulate locally, limiting overall systemic adverse effects and improving the bioavailability of the drug. It has been suggested that sizes for chemotherapeutics should

be between 50 – 100 nm in diameter to prevent formulations from randomly intruding into healthy tissue vasculature. Furthermore, liposomes size can influence immune responses, rendering it a critical physical parameter in vaccine formulations. For example, it has been shown that increased sizes can induce cellular proliferation compared to their small counterparts [22], with sizes > 255 nm leading to increased levels of IL-12 and T_H1 while sizes < 155 nm produce increased T_H2 levels resulting from specific triggering of downstream cytokines [68].

1.3.3.2 Liposome surface charge

A further physicochemical consideration is the effect of liposome surface charge and its role in cellular interactions. The surface charge strongly influences liposomal fate when used *in vivo* or *in vitro* with cationic, anionic or neutral liposome eliciting different cellular effects. From studies, neutrally charged liposomes have poor cellular interactions resulting in poor uptake, causing limited drug efficacy as payloads become released in the extracellular space [74, 75]. However, the investigation into anionic liposomes found that due to their charge, they are less stable *in vivo* than their neutral and cationic counterparts brought about through their rapid uptake up into cells [76]. Of the differently charged liposomes, cationic liposomes were identified early for use in vaccine research [77, 78], resulting from specific immunostimulatory abilities with various differently charged lipids which can improve leading the stimulation of antigen-presenting cells [79]. Cationic liposomes have been a prime candidate for nucleic acid delivery due to their capacity to electrostatically bind to anionic portions of the nucleic acids at the liposome surface.

It has been shown that cationic liposomes can also protect entrapped DNA payloads (lipoplex), preventing enzymatic degradation allowing cellular transfection. However, there are limitations to such a system, primarily due to the toxicity *in vitro* and *in vivo*. This can be caused by lipoplexes changing cellular membranes such as reducing mitosis, vacuolisation of cytoplasm's and cell shrinkage [80]. However, toxicity can be reduced by selecting tertiary lipid headgroups over quaternary headgroups [81].

1.3.3.3 Bilayer fluidity and liposome adjuvant impact

The number and strength of Van der Waals forces within the bilayer have a distinct role in membrane fluidity and can be influenced by the chosen lipids. Lipids with a higher degree of saturation and alkyl chain can increase the intermolecular forces within the bilayer and, as such, impact the bilayer's physical states by increasing the transition temperature (T_m). Using body temperature as a reference point, liposomes with a Tm > 37 °C have a solid ordered state while phospholipids with a Tm < 37 °C are more fluid and disordered. Such an effect was tested to induce cellular immunity *in vitro*. Liposomes in a fluid disordered state composed of unsaturated phospholipids (DOPG):DOPC:DOPE:Chol were compared against liposomes consisting of saturated phospholipids (DSPE:DSPG):DSPC:Chol. It was found that liposome fluidity improved antigen delivery to MHC I compartments and aided in the induction of cellular immunity to a greater extent than their solid-ordered state counterparts [63, 82, 83].

It has also been demonstrated that cholesterol can improve bilayer packing efficiencies [84]. As such, the T_m of phospholipids is eliminated through studies by Moghaddam et al. It was shown through the addition of either 33 or 50 % the T_m for DSPC (54 °C) was no longer detectable [85], resulting in a more fluid bilayer. This abolishment of phospholipid T_m through the inclusion of cholesterol has been attributed to the cholesterol condensing the bilayer and improving the orientation order of hydrocarbon chains leading to decreased membrane permeability and increased membrane fluidity [86, 87]. The inclusion of cholesterol was also tested within dimethyldioctadecylammonium (DDA) and trehalose 6,6'-dibehenate (TDB), which is a known cationic liposome adjuvant in numerous studies [88-90], and can elicit high Th1 and cell-mediated responses. Research has shown that the inclusion of cholesterol can reduce the Th1 response and lower levels of IFN-γ, impacting the cellular uptake [86], highlighting differences in membrane fluidity and the effects on immune responses.

1.3.3.4 Circumventing transition temperatures

One of the most critical considerations in liposome formation is the Tm. This is defined as the temperature required to cause a change in the phospholipid bilayer from a tightly packed ordered gel phase where the hydrocarbon chains are tightly packed and rigid [91]. Above a specific temperature the hydrocarbon tails become disordered and more fluid in nature,

increasing membrane elasticity. Several factors affect the transition temperature, such as hydrocarbon length, charge and whether the hydrocarbon tail is either unsaturated or saturated. For example, increasing the hydrocarbon length leads to more Van der Waals forces interactions, requiring more energy to disorder the rigid packing. In addition, introducing double bonds with the hydrocarbon chain leads to links in the hydrocarbon tail, limiting the number of Van der Waal interactions and thus lower temperatures are needed to cause the physical bilayer change (table 1.2). It has been shown previously that using a microfluidic system, it is possible to circumvent transition temperatures [88], which were once a crucial part in liposome formation and caused potential adverse effects when loading biologics. It has been theorised that liposomes could be formed when lipids within the solvent phase come into contact with the aqueous stream, which causes individual monomers to self-assemble through a bottom-up process. It has also been theorised that flow rate ratio (FRR) can impact this by causing liposomes to undergo a continual cycle of assembly/disassembly due to aqueous and solvent mixing [92, 93]. It has been thought that by increasing the FRR (i.e. increasing the aqueous:solvent ratio), the solvent concentration is reduced, which reduces the number of assembly/disassembly cycles, leading to an overall reduction in liposome size as a result of this.

1.3.3.5 Bilayer surface modification

The biodistribution of liposomes can also be influenced through surface modification using polyethylene glycol (PEG; mentioned in section 1.2), which can be covalently attached to phospholipids to create "stealth liposomes". Stealth liposomes allow prolonged circulation in systemic circulation and avoid clearance by the reticuloendothelial system (RES) consisting of phagocytic cells, which eliminate foreign particles [94]. This is achieved by reducing opsonisation through PEG's ability to create a hydrophilic hydration barrier around the vesicles, preventing the liposomes from being 'tagged' for phagocytic cells and subsequent clearance [14, 94]. The effect of PEG on the adjuvants was investigated when combined with the cationic phospholipid DDA with known adjuvant properties [95, 96] and the immunostimulator TDB. It was found that increasing the percentage of PEG in the formulation from 10% to 20% blocked the formation of a depot commonly seen with cationic formulations due to electrostatic interactions with anionic protein at the site of injection (SOI) [71].

Furthermore, at 10%PEG, Kaur et al., demonstrated that rapid production of antibodies can be achieved along with a switch from a cell-mediated response to a humoral response, indicating that when PEG is used at different concentrations the immune response is modified along with the biodistribution of the formulation when PEG is used [71]. The previous results showing that PEG can affect the biodistribution of liposomes also aligned with results from Carstens et al., where PEGylation was investigated using phosphatidylcholine (PC), dioleoylphosphatidylethanolamine (DOPE) and 1,2-dioleoyl-3-trimethylammonium-propane (DOTAP) [97] and indicated that lymphatic draining was improved using PEGylated liposomes compared against non-PEGylated liposomes after subcutaneous injection delivering entrapped plasmid DNA [97].

Table 1.2. *Phospholipid transition temperatures as a result of saturation within the hydrocarbon tails*

Name	Structure	Charge	Tm (°c)
1,2-distearoyl-sn-glycero-3-phosphocholine (DSPC 18:0)		Neutral	55
Hydro Soy PC (HSPC 18:0)		Neutral	53
1,2-dimyristoyl-sn-glycero-3-phosphocholine (DMPC 14:0)		Neutral	41
1,2-dioleoyl-sn-glycero-3-phosphoethanolamine (DOPE 18:1 (Δ9-Cis))		Neutral	-16
1,2-dioleoyl-3-trimethylammonium-propane (chloride salt) (DOTAP 18:1)		Cationic	~-0
Dimethyldioctadecylammonium (Bromide Salt) (DDA 18:0)		Cationic	47
1,2-dipalmitoyl-sn-glycero-3-phospho-(1'-rac-glycerol) (sodium salt) (DPPG 16:0)		Anionic	41
1,2-dipalmitoyl-sn-glycero-3-phospho-(1'-rac-glycerol) (sodium salt) (DPPG 16:0)		Anionic	41
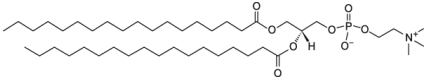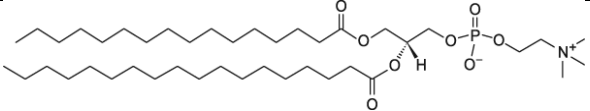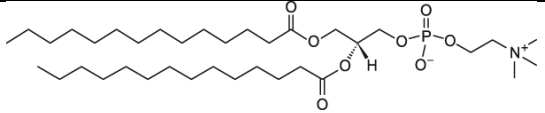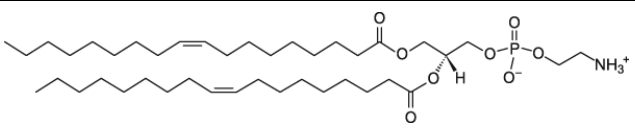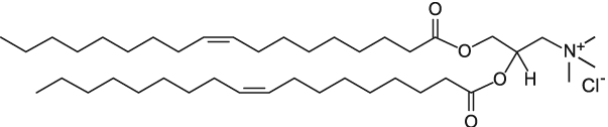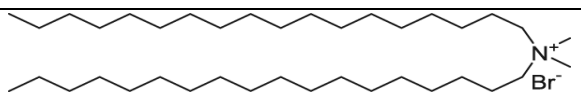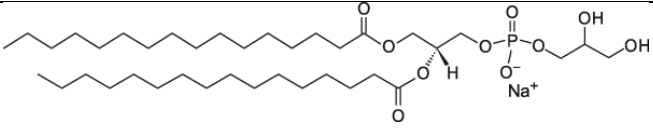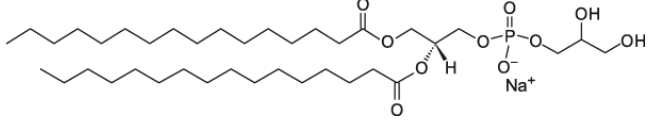
1.4 Traditional liposome manufacturing strategies

As liposome geometry is directed by the manufacturing method, a particular emphasis can be placed on the manufacturing methods for liposomes. While this is an essential consideration for production platforms to meet regulatory requirements, as discussed by Perrie et al., manufacturing methods directly impact liposomal attributes such as the vesicle size. [72] For liposomal systems, a common factor involved in their formation, regardless of manufacturing method used, is the mixing lipids with an aqueous buffer which typically lead to large liposomes, that are often multi-lamellar, being formed which would later require mechanical down-sizing strategies to meet formulation requirements.   This traditional approach to liposome production is typically described as a "top-down" manufacturing method.

1.4.1 Lipid Film Hydration

The Bangham method, or lipid-film hydration method [98, 99], involves the evaporation of the solvent (traditionally a mixture of chloroform and methanol), leading to film on the bottom of the flask. The lipids are then subsequently hydrated and swell using an aqueous buffer with a rotary evaporator under a vacuum to remove any residual solvents that were not previously evaporated. During the hydration of the lipids, the flask undergoes mechanical agitation (often performed above the lipid transition temperatures), leading to the formation of large multi-lamellar vesicles (LMVs). These vesicles commonly vary in size and dispersity, requiring further down-sizing strategies to improve formulation uniformity. For drug delivery purposes, the active pharmaceutical ingredient (API) is either added to the solvent phase containing the lipids or the aqueous buffer, depending on the drug's partition coefficient, leading to entrapment of the molecule either in the liposome bilayer or aqueous core. While an established and well documented that is already employed in products on the market, such as AmBisome® and Caelyx®, throughput is limited to batch-scale production, which can be costly with an additioanl complication of batch-to-batch variability [100]. By introducing a novel 'bottom-up' technology such as microfluidics (figure 1.3), many of these difficulties are circumvented by avoiding the need for downsizing techniques [101].
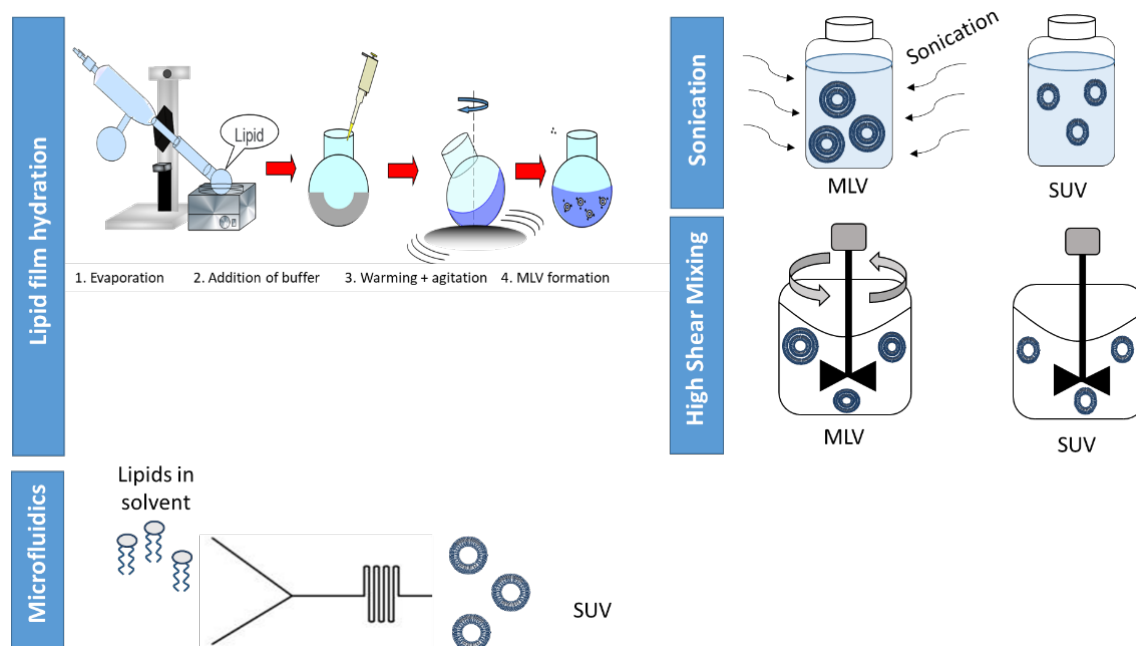
Figure 1.3 *Schematic overview of different manufacturing methods*

1.4.2 Reverse-phase evaporation

The Bangham method was a defining moment for the liposome field, which allowed a simple method of production to study membrane properties [98]. However, when used to produce drug delivery carriers and therapeutic candidates, there were poor entrapment capabilities of macromolecules [99], which has been attributed to the production of MLVs with reduced aqueous compartments due to the multiple internal lamellae [12]. To tackle this issue, Szoka and Papahadjopoulos described a production method where small volumes of aqueous buffer are added to dissolved lipids in an organic solvent and sonicated, leading to a water in oil emulsion. The solvent is then evaporated using a rotary evaporator, which after a critical point, a gel is formed, that in turn collapses to form suspended liposomes in an aqueous solution [12]. Using such a method produces high entrapment efficiencies of water-soluble compounds [12, 102]. However, the resulting liposomes are large (LUVs), and would need further down-sizing, impacting its scalability. Furthermore, if a molecule of interest is to be entrapped within the vesicle, it would first require the molecule to be immersed in the organic solvent meaning it would not be a suitable production method for biological compounds due to biological denaturing [102].

1.4.3 Injection methods

In contrast to the Bangham and REV methods described, the ethanol injection method was one of the first procedures adopting a "bottom-up" manufacturing approach which was first described in the 1970s by Katzi and Korn and allowed for the production of SUVs [103]. The described method is simple and involves the rapid injection of lipids dissolved in an organic solvent into an aqueous buffer, leading to the precipitation of lipids into SUVs. Using an ethanol injection method allows for high entrapment capacities for lipophilic drugs; however, as a result of the high aqueous volume used, entrapment efficiencies for hydrophilic drugs are low [12, 104]. Furthermore, a secondary step to remove the non-encapsulated drug and additional concentration of the final formulation is often required. To further aid in the scalability and provide greater control for manufacturing, an "inkjet method" was described by Hauschild et al., which uses an inkjet printer to inject the lipids SUVs within the range of 50 – 200 nm to be controlled [105] [102]. While the injection method has been further developed by Polymun and Alza [106, 107], the poor hydrophilic molecule entrapment, residual solvent removal, and the need for high final concentrations to be used remain an underlying issue.

1.4.4 Post synthesis downsizing

For the methods that produce MLVs, downsizing strategies need to be used after their formation to improve their size and dispersity. The most common methods used include extrusion, sonication and high-pressure homogenisation (HPH), which use mechanical forces to form SUVs by reducing their lamerallity. HPV is used to subdivide vesicles into smaller vesicles over several cycles by subjecting the formulations to high and controlled pressures (100 – 2000 bar), causing shear stress when the fluid is passed through small orifices [108], resulting in a homogenous formulation [109]. Similarly to HPH, using extrusion forces MLVs under low pressure through small orifices in meshes and filters with pore sizes that correspond to the required size [102]. The pressure and number of cycles can also be adjusted to control the size further if required [110]. Sonication can also be used as a downsizing strategy upon using a probe or sonication bath, and uses sound waves to produce vacuum bubbles that collapse in the solution known as cavitation, releasing large amounts of energy in the form of shockwaves. The shockwaves lead to reduced lamerallity in the MLVs, which in

turn cause reduced sizes [108]. The degree of particle size reduction can be influenced by the frequency, amplitude and sonication time and can be assisted by running the sonicator at temperatures higher than the transition temperature of the lipids used [111]. However, due to the large amounts of energy released from cavitation, this can affect thermos-sensitive compounds due to the heat produced from the shock waves [110, 112].

1.5 Novel and scalable liposomal manufacturing using microfluidic mixing

1.5.1 *Background*

While liposomes have been versatile in delivering APIs of varying partition coefficients, a significant bottleneck in their transition from the lab bench to the clinic is the convoluted and time-consuming conventional manufacturing methods that arise when scaling a manufacturing process. Microfluidics could offer a solution by providing a "bottom-up" approach to liposome or lipid-based nanomedicine production. The application of microfluidics relies on a nanoprecipitation principle that produces nanoparticles in a one-step process [113] through micro channels (1 – 1000 μm [114]). Microfluidics relies on mixing ratios between a solvent and aqueous phase. With the lipids dissolved in the solvent, once the two streams converge, a significant dilution in the solvent phase occurs, leading to nanoprecipitation reactions as the lipids hydrophobic chains become less soluble due to the increased polarity causing the formation of small unilamellar vesicles [91]. Providing that the solvent and aqueous phases are miscible with each other, various parameters can be altered to give desired physical properties such as the effect of buffer concentration [115] or influence polarity through solvent choice [116] in addition to changing the mixing ratio of the two phases to influence size [117]. Microfluidics offers improved control over production parameters allowing desired vesicle sizes and uniformity. Furthermore, the more efficient use of materials through reduced volumes, minimises costs and further experimentation during scale-up improves the overall throughput [118]. Within fluid mechanics, some of the process parameters which need to be described are microflows and dimensionless numbers that allow transport of particulates and mixing to be characterised and understood.

Table 1.3 *Established microfluidic process parameters for microfluidic production of nanoparticles*

Process Parameters	Factors to consider	References
Solvent selection	Suitability of solvent for large-scale production. Lipid(s) solubility in the given solvent. Polarity of the solvent can impact particle size.	[9]; [116]; [119]
Aqueous buffer	Aqueous buffer strength can be used to control particle size.	[115]
Lipid concentration	Initial lipid concentration can impact particle size.	[120]; [117]
Production flow rates	Flow rate can impact particle size	[121]; [93]
Aqueous to alcohol mixing ratio	Mixing ratio can impact on: • particle size, • drug loading, • drug release.	[117]; [119]; [101]; [122]
Operating temperature	Microfluidic production of liposomes does not need to be conducted above the transition temperature of lipids.	[117]

1.5.2 Mass transport and dimensionless numbers

1.5.2.1 Mass transport

Within laminar flow microchannels, there are generally three main types of mass transfer: molecular diffusion, Taylor dispersion, and advection [123]. Of the three, molecular diffusion and advection are notably the most important [92, 124], while Taylor dispersion typically refers to the dispersion of solute travelling in front of a microfluidic channel [125]. Molecular diffusion is expressed as the random movement of molecules from a high concentration to a low concentration region. Fick's first law can describe the degree of diffusion under a steady-state, where the diffusive flux is proportional to the concentration gradient. Under laminar conditions, advection describes solutes carried down a channel parallel to the bulk flow,

making it not an effective form of mixing. However, when advection is nonparallel chaotic advection occurs, which significantly improves mixing efficiencies [92]. This improves surface areas and leads to thinner fluid streams which enhances diffusion over shorter distances [126].

1.5.2.2 <u>Reynolds number</u>

The Reynolds number (Re) is often the most reported dimensionless number used to characterise a microfluidic system. The Re value represents the ratio of inertial forces to viscous forces. Both forces can be regarded as a measure of resistance; however, inertial forces directly refer to the change of motion of molecules occurring within the channels, while viscosity refers to resistance caused by shear forces between the molecules due to their flow through the channel. Fluid flow can be divided into laminar and turbulent regimens (figure 3.1). At low Re values, the fluid flow is laminar, with streams occurring in parallel layers with little disruption (figure 3.1A). When turbulent flow is compared to laminar, the fluid streams are highly disruptive and chaotic, resulting from internal forces domination over viscous forces (figure 3.1B). Turbulent flow differs from chaotic advection as within chaotic advection, as fluid flow remains constant over time while fluid flow under turbulent mixing fluctuates over time [114].

$$Re = \frac{Inertial\ forces}{Viscous\ forces} = \frac{V d_u \rho}{\mu} \qquad (1.1)$$

With   V   Fluid velocity

          d_u Channel diameter

          ρ Fluid density

          μ Dynamic fluid viscosity
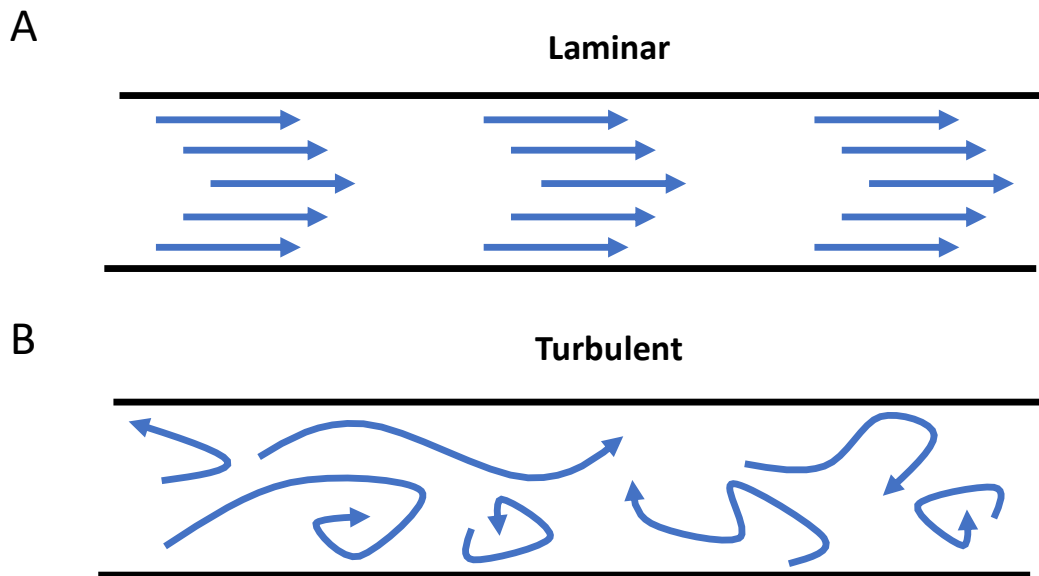
Figure 1.4 *Schematic representing fluid flow profiles characterized by Reynolds number. (A) laminar flows within channels (Re ≤ 2000) and (B) turbulent flow caused by high Reynolds number (> 2000).*

There has been discussion concerning the critical point when fluid flow becomes laminar, which is a crucial parameter when designing a microfluidic cartridge. Early researchers in the field derived transitions from laminar flows at Re = 300 to fully turbulent flows at Re = 1000 [113], while later researchers arrived at values ≤ 2000, where they subsequently attributed the lower values due to the roughness of the microchannels used in early studies [123, 127]. The mixing channel length within a micromixer is characteristically low, corresponding to a low Re value (< 100), meaning that fluid flow will fall into a laminar flow [128]. At Re values at this range, the mixing will be governed by diffusion, which without disruption will take a considerable time to achieve sufficient mixing of streams [124].

1.5.2.3 Péclets number

The Péclets number (Pe) describes the degree of molecular diffusion that occurs within microchannels by representing the ratio of convection/advection to diffusion, i.e. the ratio of passive transport of particulates in fluid against the random motion particulates from a high to a low concentration

$$Pe = \frac{advective\ transport}{diffusive\ tranport} = \frac{Lu}{D} \qquad\qquad (1.2)$$

With   L   Characteristic length

        u   Fluid velocity

        D   Diffusion coefficient

The Pe number is a valuable parameter for estimating a distance in channel width to achieve diffusive mixing with higher Pe values representing a higher degree of advection (equation 1.2). A linear relationship exists between mixing time and Pe, indicating that as channel length increases, the degree of molecular diffusion increases [127, 129]. Because of this, in systems where there is a lack of turbulent mixing, other forms of mixing (such as the introduction of transverse flows), must be investigated to minimise the channel lengths while increasing diffusive mixing [127].

1.5.3 Micromixer design

Micromixers can be categorised into active or passive categories (figure 1.5). Active micromixers use external forces such as temperature, pressure and acoustics to induce fluid mixing, making them complicated to fabricate and costly to run [130]. On the other hand, passive mixers require no external energy to run and instead relies on molecular diffusion or chaotic advection, which due to these principles makes passive micromixers easier to integrate within a manufacturing platform. Of the various mixing strategies listed in figure 1.5, chaotic advection with passive micromixers will be investigated as a micromixer to overcome fluid systems with a low Re value. One of the methods used to ensure sufficient mixing efficiencies with low Re values is to increase contact surface areas to improve diffusive mixing. While many approaches have been investigated, such as using external energy (active mixing) by ultrasonic pulses or thermal actuation to enhance mixing performances, however, these are hard to fabricate and often require external power sources making them difficult to integregate within a manufacturing platoform. An alternative is manipulating channel architecture (passive mixing) to facilitate fluid stream folding and increase contact surface area consequently. By precisely fabricating alternative geometries such as manipulation of channel width, shape, splitting of fluid paths, and use of grooves facilitates a wide range of

micromixers that can be used (table 2). Herein, passive micromixers have become easier to implement in manufacturing lines due to no need for additional power to improve mixing efficiencies.
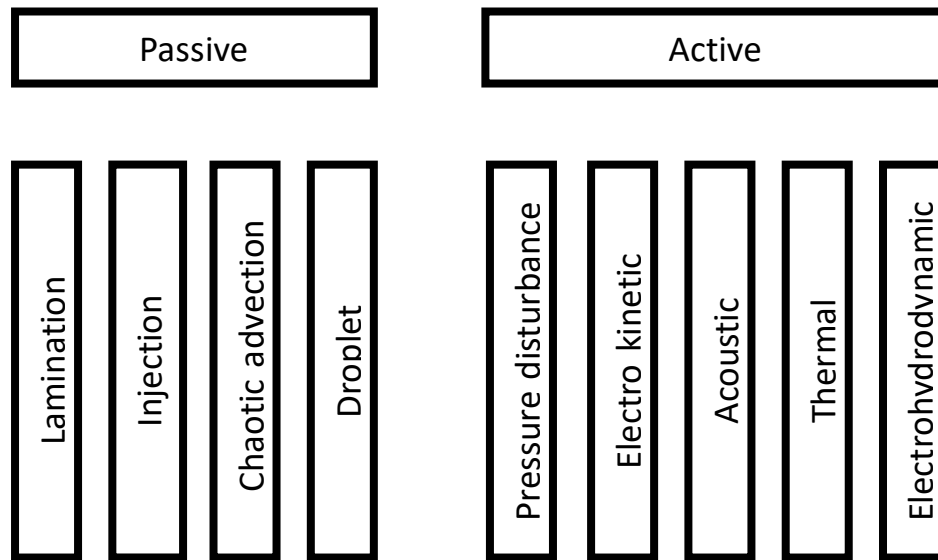
Figure 1.5 *Overview of various forms of microfluidic mixers*

As discussed, mixing in microflow is largely inefficient (Re < 100; Capretto et al., 2011), meaning such micromixers require adaptation. Channel geometry significantly affects diffusion and diverting the mixing path, and increasing contact surface areas by narrowing channel diameters have been found to improve fluid mixing [128]. To this effect, the channel geometry can be further modified to stretch, fold and break fluid streams. For example, using a staggered herringbone micromixer (SHM), repeating protruding herringbone structures cause transverse fluid vortices to be created by altering the position of the herringbone structures, which leads to the one-step production of size-controlled liposomes in a more refined manner.

1.5.3.1 Staggered herringbone micromixer

One of the ways mixing efficiencies can be improved in channels with low Re number is through manipulating micromixer design, such as the addition of embedded herringbone chevrons along the channel floor, as shown in figure 1.6. Facilitating such grooves leads to transversal chaotic flows causing helical mixing patterns when multiple streams converge [129]. As a result, mixing fluid paths have increased surface area and thinner streams,

improving diffusive mixing (figure 1.7). This principle was further examined by incorporating additional chevrons along either the sides or roof of the channel, causing paired vortices to be created on the horizontal and vertical axis [131]. This modification reduced the required channel length to achieve homogenous mixing by 50%; however, this further medication will lead to additional fabrication complexities [129]. Using an SHM has been found to act independently from the Re number allow for shorter channels to be used that the Re value would suggest [132]. Incorporating multiple asymmetric staggered herringbone structures across the channel leads fluid streams to be repeatedly folded and stretched, correlating to multiple mixing cycles, leading to chaotic advection and improved diffusive mixing. While the SHM has been used for a range of nanoparticles [121, 133, 134], there are some limitations for its further use. One of these limitations is the complex fabrication process for the micromixer itself, which is costly and time-consuming. In addition to this, the herringbone structures within the micromixer also limit the fluid throughput speeds, which hinder its use for good manufacturing practice (GMP) systems.
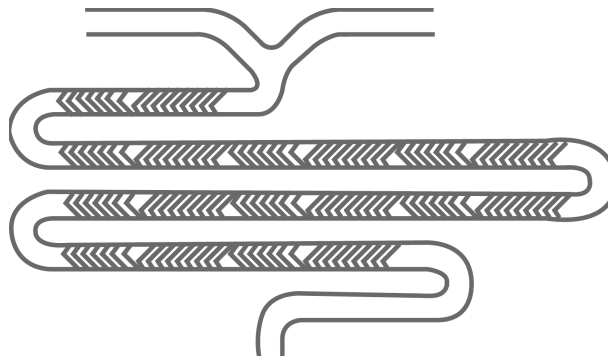
Figure 1.6 *Schematic of the staggered herringbone micromixer (SHM)*

A Lipids in solvent

Aqueous phase

Chaotic advection SHM
micromixer (low shear stress)

B

C (Stroock et al., 2002)

Position 1   Position 2

D
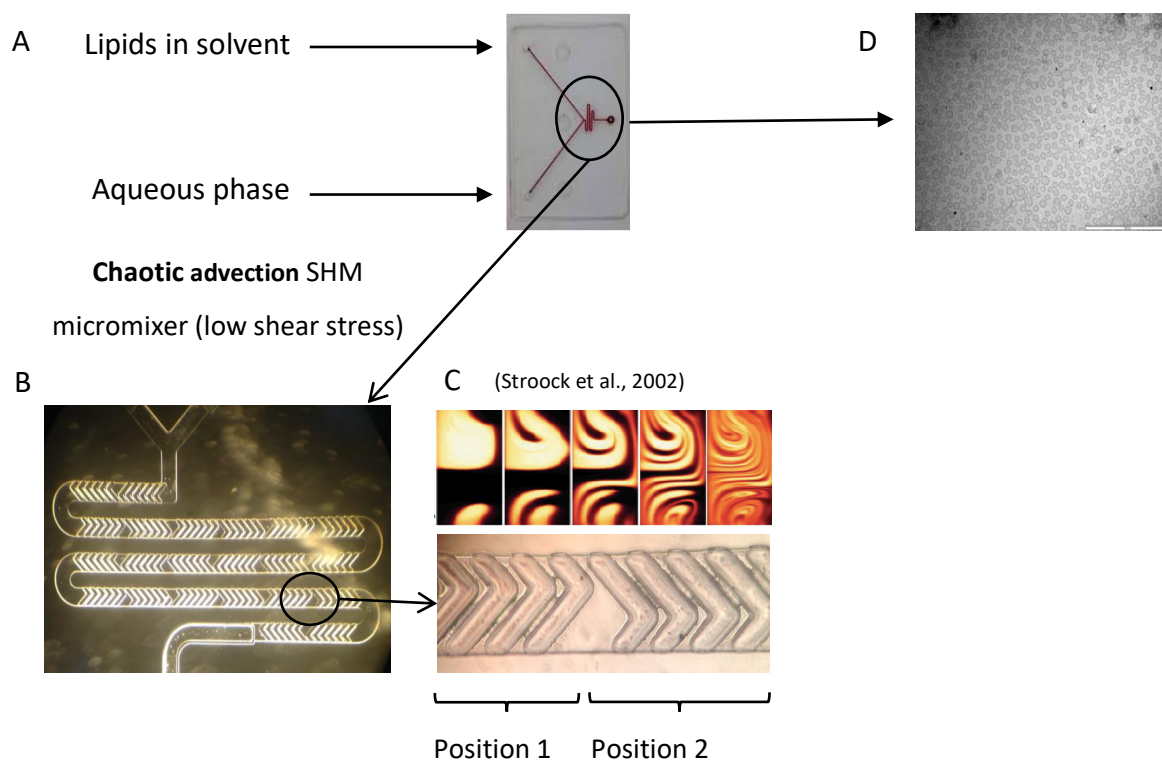
Figure 1.7 *Graphic representation of the SHM microfluidic chip (A) with the SHM architecture magnified illustrating herringbone grooves (B). Further magnification highlights the angular position changes of the grooves (C) and fluid mixing which occurs as a result of the geometry shown by Strook et al., (D) Cryo-TEM image illustrating the SUV liposomes that can be achieved using a microfluidic bottom up approach.*

1.5.3.2 Toroidal micromixers

To translate formulations from the lab bench to a large scale without changing process parameters, a novel microfluidic structure was implemented. As fluid flows through curved channels, fluid is forced against the outer channel walls at higher velocities than the fluid flowing by the inner walls due to no-slip boundary conditions (figure 1.8) [135]. This leads to the creation of rotational vortices perpendicular to the channel known as Dean vortexing. Using the micromixer manufactured by Precision NanoSystems Inc., they include repeating circular toroids within the channel path, causing varying fluid path flow volumes to occur depending on which path the fluid takes when split by the toroid. The bifurcation of fluid volumes when split by multiple toroid's results in improved mixing over fluid streams that are split repeatedly (figure 3.1A). The different fluid volume balance caused by fluids taking one of two paths around the toroids causes dean vortexing. The fluid streams then converge and

are split over several cycles causing the fluid streams to be folded and kneaded together, leading to increased fluid contact times and decreased mixing times.
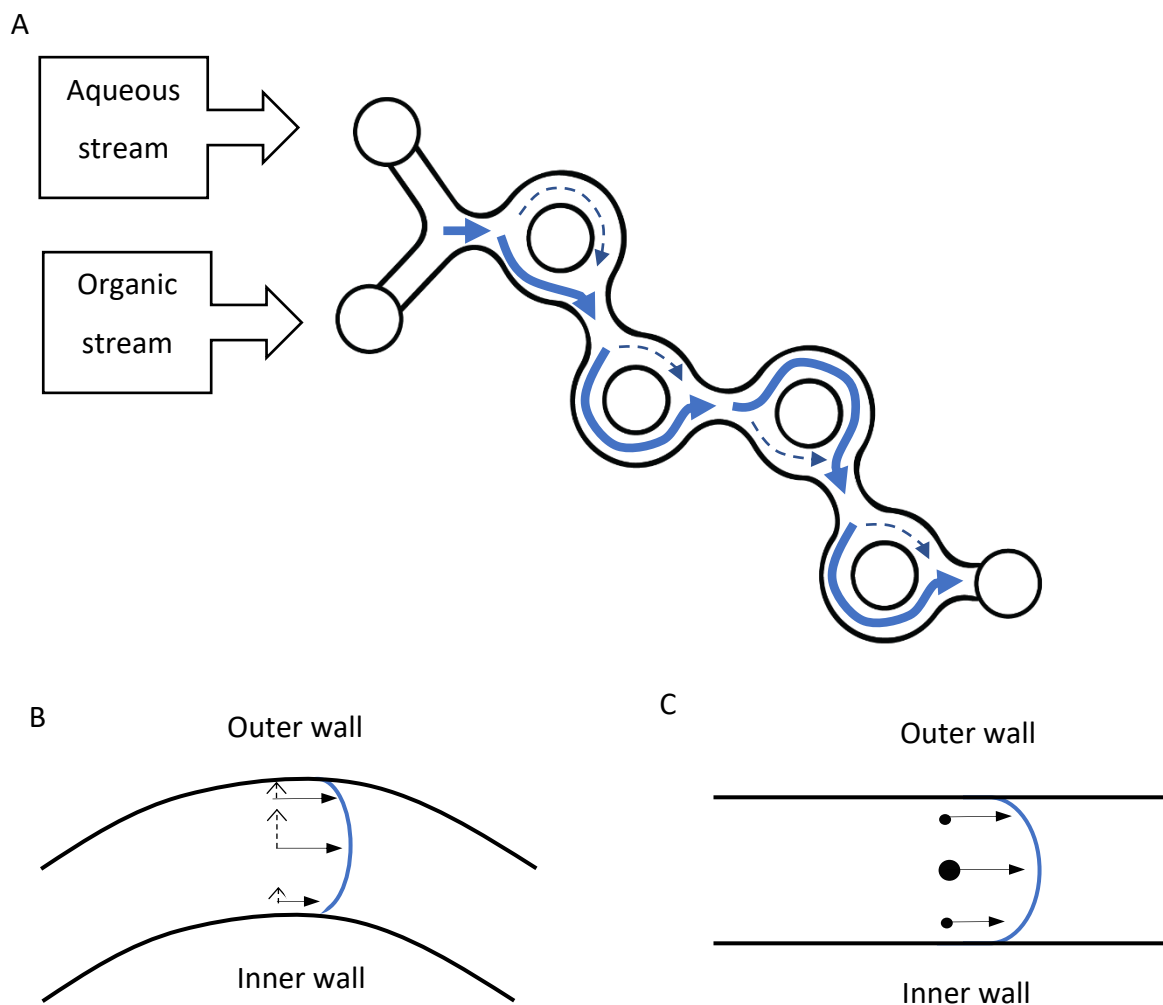
Figure 1.8 Schematic representing fluid flow paths through the toroidal micromixer. A) represents the fluid pressure distribution resulting from fluid streams passing through curved architecture with B) demonstrating the centrifugal forces of fluid paths within the centre of the channel and C) the parabolic pressure distribution of fluid down a straight channel.

Furthermore, compared to curved paths, when fluid flows through straight channels, the distribution of pressure is unidirectional, with fluid flowing fast down the centre of the column (figure 3.1C [135]). However, the fluid flowing down the centre in curved channels expresses greater centrifugal force as higher pressure will be forced against the outer wall (figure 3.1B [136]). This causes vortices to be formed resulting from fluid ejection from the centre to the exterior walls facilitating secondary mixing and improved homogenisation between the two streams [135].

Table 1.4 *Use of different microfluidic architectures to manufacture therapeutic nanomedicines*

Microfluidic architecture	Formulation	Entrapped material	Reference
Staggered herringbone mixer (SHM)	POPC	Doxorubicin	[101]
	DLinkE2-DMA:DSPC:Chol:PEG-c-DMA	Si-RNA	[137]
	DSPC:Chol	Metformin and Glipizide	[9]
	DMPC:Chol / DSPC:Chol	Atenolol and quinine	[121]
	Span80:Chol / Tween85:Chol	Curcumin	[133]
	Span60:Chol:Cremophor®(ELP or RH40) / Span60:Chol:Solutol®HS15	Cinnarazine	[138]
	PLGA / PEG - PLGA	Curcumin	[139]
	ATX*:DSPC:Chol:DMG-PEG:PEG2000	Si-RNA	[134]
T-mixer	Triolein:POPC:PEG-DSPE	Iron oxide	[140]
	PMMA:Cremophor:ELP	Ketoprofen	[141]
	PMMA:Eudragit S100:Pluronic F68	Paclitxel	[142]
	Chitosan Poloxamer 407:HMPC:SDS:Tween20	CRS 74	[143]
	PVPVA:Poloxamer 407:Poloxamer 188	Itraconazole	[144]
Y - type	Ethyl cellulose:Tween80	Losartan potassium	[145]
HPIMM	PMMA:Cremophor:ELP	Ketoprofen	[141]
K-M	PMMA:Cremophor:ELP	Ketoprofen	[141]
Hydrodynamic flow focusing	PLGA	Ribavirin	[146]
	PLGA	Dexamethasone	[147]
	DMPC:Chol:PEG2000-PE	Doxorubicin	[148]

1-palmitoyl-2-oleoyl-sn-glycero-3-phosphocholine (POPC); 1,2-distearoyl-sn-glycero-3-phosphocholine (DSPC); Chol (Cholestrol); 1,2-dimyristoyl-sn-glycero-3-phosphocholine (DMPC); Cremophor® ELP (purified polyoxyl 35 castor oil) [17]; Cremophor® RH40 (hydrogenated polyoxyl 40 castor oil); Solutol® HS15 (polyoxyl 15 hydroxystearate); poly(lactic-co-glycolic acid) (PLGA); Polyethylene glycol (PEG); ATX (proprietary ionizable amino lipids); DMG-PEG (1,2-Dimyristoyl-sn-glycerol, methoxypolyethylene glycol, PEG chain molecular weight: 2000; 1,2-distearoyl-sn-glycero-3-phosphoethanolamine-N-[amino(polyethylene glycol)-2000] (DSPE-PEG(2000)); Poly(methyl methacrylate) (PMMA); Pluronics F68 (Poloxamer 188, poly(ethylene oxide)–poly(propyleneoxide); hydroxypropyl methylcellulose (HPMC); Sodium dodecyl sulfate (SDS); Polyvinylpyrrolidone vinyl acetate (PVPVA);

1.6 Continuous manufacturing of liposomal products

1.6.1 Batch vs continuous production

Typically, GMP manufacturing processes have been batch-type, whereby bulk material is processed as one unit and can only proceed to the next manufacturing stage after the entire unit has been processed. In contrast, continuous manufacturing (CM) will have raw material continuously fed into the beginning of the system with the final product constantly discharged [100]. CM platforms offer considerable benefits over batch platforms such as improved formulation reproducibility, consistency, reduction in overall material costs and smaller manufacturing facilities (such as separate storage and production suites are not required) which offer significant financial benefits [149] and improved robustness overcoming poor product quality resulting in medicine shortages [150].

Batch manufacturing (BM) has been well established in the pharmaceutical industry; however, due to the multi-stage processing of materials, the transfer of materials to and from reactor vessels can be time-consuming, leading to increased risk of contamination and loss of material. To this end, additional testing and validation experiments need to be conducted to prove there are no differences between formulations tested during clinical trials made in smaller batches compared to the batch sizes required for mass production. This further increases time and monetary expenditure through additional validation experiments and regulatory pressures. In comparison, CM negates many of these disadvantages. The development of process analytical technology (PAT) allows for the real-time processing of data and permits new opportunities for continuous manufacturing platforms to be established mitigating batch-to-batch variation. Furthermore, the same equipment can be used from initial development through to production scale, which reduces further validation issues and saves between 9 – 40% on the raw materials and API by switching to CM from BM have been reported [149].

1.6.2 Formulation purification

After producing the vesicles, refinement of the formulation needs to occur to remove impurities such as non-encapsulated drugs or solvents. Such an operation can be achieved using tangential flow filtration (TFF), which can also concentrate formulations to desired strengths. The process occurs by continually circulating fresh buffer and the liposome formulation across a hollow fibre membrane and back into a central retentate vessel with the permeate (waste stream) leaving the system and into a waste vessel. Fresh buffer is added to the stream at the same rate the permeate leaves the system due to the constant-weight diafiltration, which facilitates buffer exchange leading to the subsequent dilution and elimination of solvent and other impurities. After the buffer exchange has been completed across the defined diafiltration cycle, the formulation can be concentrated to the required strengths by running the system but stopping the buffer addition. Such a purification system can also be monitored during the purification process, further facilitating the incorporation of TFF within a continuous manufacturing platform [117].

1.7 Aims and Objectives

To support the transition of liposomes from the lab bench into the clinic for the use as vaccine formulations, the overall aim was to explore how novel mixing strategies can be used to circumvent convoluted and complex production methods currently associated with liposome manufacturing. As liposome physical attributes are determined by their method of manufacture, various microfluidic methods are to explored by primarily altering known microfluidic process parameters, such as FRR, TFR and lipid concentration for producing neutral and cationic liposomes with entrapped or adsorbed antigen subunits respectively. The produced liposomes physical attributes are to be assessed primarily by DLS-measurements to record vesicle size, PDI and zeta potential. Using active antigens, the developed manufacturing methods and liposomal formulations are to be assessed within in *in vivo* muring models to explore formulation biodistribution and measure formulation immunogenicity by conducting vaccine studies.

To achieve this aim, various objectives were examined:

1. The impact of solvent polarity was to be assessed using microfluidics for the production of liposomes. Liposome size, PDI and charge will be measured against lipids solubilised in different water soluble solvents with varying degrees of relative polarities. For this objective, the solvents methanol (MeOH, 0.762 relative polarity), ethanol (EtOH, 0.654 relative polarity) and isopropanol (IPA, 0.546 relative polarity) will be used to solubilise the lipid mixture. The morphology of the vesicles produced using MeOH, EtOH and IPA will be examined by cryo-TEM to investigate if any geometric changes occur in the vesicle structure from using solvents with low and high relative polarities.

2. To investigate if two different laminar flow microfluidic cartridges, using either a staggered herringbone (SHM) or toroidal (TrM) micromixer design, can be interchanged to produce liposomes with the same vesicle size, PDI, charge, protein loading, protein release rates and liposome morphology. To achieve this, known SHM microfluidic process paramerers such as FRR, TFR and solvent polarity will be systematically tested to validate if the same process parameters apply to the TrM architecture. The vesicle size, PDI, charge and protein loading will be measured using DSPC:Chol (2:1 w/w) with entrapped OVA from liposomes produced at the laboratory scale (1 mL) through to GMP production volumes (> 200 mL) to ensure no physical changes in the vesicles and validate the scalability of microfluidics for the formulation.

3. To explore and develop and microfluidic manufacturing process for controlled adsorption of subunit antigen formulations allowing for reduced residual solvent concentrations (< 10% v/v). An inline microfluidic mixing method and procedure comprising of two manufacturing steps will be investigated to both form cationic liposomes (DSPC:Chol:DDA 10:5:4 w/w) and coat antigens onto the liposome surface to control antigen to liposome adsorption.

4. To examine *in vivo* biodistribution for cationic liposomes (DSPC:Chol:DDA 10:5:4 w/w) and protein individually using fluorescent tags over 9 days with a secondary objective to identify if liposomes and protein drain towards specific organs such as the kidneys and liver due to their roles in pharmacokinetics of compounds and the spleen and lymph nodes (inguinal and popliteal) for their important function in immunity and high concentrations of immune cells such as B and T cells.

5. Investigate antibody subtypes (IgG total, IgG1 and IgG2a) for cationic liposome formulations (DSPC:Chol:DDA 10:5:4 w/w) with adsorbed major outer membrane protein (MOMP) of *Chlymadia trachomatis* using different ratios of liposome:protein (L:P) and produce formulations with the controlled adsorption of antigens using microfluidic methods developed from objective 3. The results would elute if antibody subtypes can be stimulated to a greater extent by i) varying the L:P to assess if the ratio of adjuvant to protein leads to an increased immune response and if ii) the method of antigen adsorption plays a role in formulation immunogenicity.

6. Optimise and establish a potential microfluidic production method for the reproducible production of DDA:TDB (5:1 w/w) and a novel DDA:PHAD (5:1 w/w) formulation with controlled adsorption of antigen (developed from objective 3). This would provide an alternative microfluidic method to lipid film hydration as well as a new method of production for DDA:PHAD for use in future studies.

7. Conduct an *in vivo* vaccine study to evaluate and compare liposomal adjuvant formulations comprising of TDB and PHAD which have been manufactured by microfluidics and lipid film hydration using a spike protein from SARS-CoV-2. Assessment of IgG total, IgG1, IgG2a and neutralising antibodies from blood serum and cytokines from stimulated spleenocytes to assess and compare the humoral and cell mediated responses invoked my TBD and PHAD.

Chapter 2

Materials and Methods

Chapter 3	Chapter 4	Chapter 5	Chapter 6
Chapter 3	**Chapter 4**	**Chapter 5**	**Chapter 6**
DSPC, HSPC, DMPC and Chol	DSPC and Chol	DSPC, Chol and DDA	DDA, TDB, PHAD, DSPC and DMG-PEG(2K)
Ovalbumin	Ovalbumin	Ovalbumin, DQ-OVA, AF647-OVA or major outer membrane protein (*Chlamydia trachomatis*)	Ovalbumin or spike antigen (SARS-CoV-2)
Microfluidics	Microfluidics	Microfluidics	Microfluidics and lipid film hydration
Tangential flow filtration (100, 500 or 750 kD), dialysis (14 & 300 kD)	Tangential flow filtration (300 or 750 kD), dialysis (14 & 300 kD)	Dialysis (14 kD)	Dialysis (14 kD)
Physical vesicle characterisation (DLS, cryo-TEM, phospholipid assay)	Physical vesicle characterisation (DLS, NTA, cryo-TEM)	Physical vesicle characterisation (DLS, cryo-TEM)	Physical vesicle characterisation (DLS)
Protein quantification and protein release kinetics (RP-HPLC)	Protein quantification and protein release kinetics (RP-HPLC, micro-BCA)	Protein quantification (micro-BCA) and exposure to digestive enzymes (fluorescence and SDS-PAGE)	*In vivo* vaccine study (IgG subtypes and cytokines)
		In vivo biodistribution and vaccine study (IgG subtypes)	
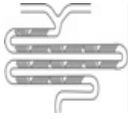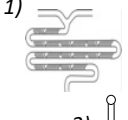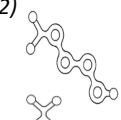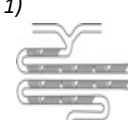
2.1 Materials

Table 2.1 *Materials used for data acquisition and suppliers*

Materials	Suppliers
1,2-dimyristoyl-*sn*-glycero-3-phosphocholine (DMPC)	Avanti polar lipid (Alabaster, AL, USA)
1,2-dioleoyl-*sn*-glycero-3-phosphocholine (DSPC)	Lipoid (Ludwigshafen, Germany)
3,3',5,5'-Tetramethylbenzidine	Sigma Aldrich Company Ltd., (Poole, UK)
96-well plates	Fisher Scientific (Loughborough, UK)
Biotin anti-mouse IFN-γ antibody	Biolegend (San Diego, USA)
Chicken egg ovalbumin (OVA)	Sigma-Aldrich (St. Louis, MO, USA)
Chloroform	Sigma-Aldrich (St. Louis, MO, USA)
Cholesterol (Chol)	Sigma-Aldrich (St. Louis, MO, USA)
Collagenase, Type I	Biolegend (San Diego, USA)
Colormetric phospholipid assay kit	Sigma Aldrich Company Ltd., (Poole, UK)
Concanavalin A from Canavalia ensiformis (Jack bean)	Sigma Aldrich Company Ltd., (Poole, UK)
DNase I	Sigma Aldrick Company Ltd., (Poole, UK)
Ethanol (EtOH)	Fisher Scientific (Loughborough, UK)
Gel Doc™ EZ Imager	Bio-Rad Laboratories (Hertfordshire, UK)
Goat anti-mouse IgG; IgG1 & IgG2a	Invitrogen, Thermo Scientific, Life Technologies Ltd (Renfrew, UK)
Hydrogenated soy phosphatidycholine (HSPC)	Lipoid (Ludwigshafen, Germany)
Ignite™	Precision NanoSystems Inc., (Vancouver, Canada)

Invitrogen™ Mini Gel Tank	Invitrogen, Thermo Scientific, Life Technologies Ltd (Renfrew, UK)
Isopropanol (IPA)	Fisher Scientific (Loughborough, UK)
Jupiter 5 µm C5 300A column	Phenomenex, UK
Krosflo Research Iii tangential flow filtration system (TFF)	Spectrum Inc., (Breda, The Netherlands)
LEGENDPlex™ Th MU cytokine panel	Biolegend (San Diego, USA)
Malvern Nano ZS	Malvern Panalytical Ltd., (Worcestershire, UK)
Methanol (MeOH)	Fisher Scientific (Loughborough, UK)
Microplate reader model 680	Bio-rad Laboratories Inc., (Hertfordshire, UK)
Modified polyethersulfene (mPES) hollow fibre columns (100 – 750 kD MWCO)	Spectrum Inc., (Breda, The Netherlands)
Mouse IL-1β DuoSet ELISA	Bio-Techne, R&D Systems (Minneapolis, USA)
NanoAssemblr GMP system	Precision NanoSystems Inc., (Vancouver, Canada)
NanoAssemblr® Benchtop	Precision NanoSystems Inc., (Vancouver, Canada)
NanoSight NS300	Malvern Panalytical Ltd., (Worcestershire, UK)
Novex™ WedgeWell™ 12% Tris-Glycine	Invitrogen, Thermo Scientific, Life Technologies Ltd (Renfrew, UK)
NxGen Blaze™	Precision NanoSystems Inc., (Vancouver, Canada)
Phosphate buffered saline tablets (PBS)	Oxoid Ltd,. Basingstoke, UK
Pierce™ Unstained Protein MW Marker	Invitrogen, Thermo Scientific, Life Technologies Ltd (Renfrew, UK)
Propofol	Sigma-Aldrich (St. Louis, MO, USA)

Purified anti-mouse IFN-γ antibody	Biolegend (San Diego, USA)
Purified streptavidin	Biolegend (San Diego, USA)
Recombinant SARS-CoV-2 D614G Spike, Active Trimer Protein CF	Bio-Techne, R&D Systems (Minneapolis, USA)
RPMI 1640 Medium, no glutamine	Sigma Aldrich Company Ltd., (Poole, UK)
SARS-CoV-2 Neutralising Antibody Detection Assay	AdipoGen Life Sciences (Liestal, Switzerland)
Shimadzu 2010-HT (RP-HPLC)	Shimadzu (Milton Keynes, UK)
Spark™	Precision NanoSystems Inc., (Vancouver, Canada)
Spectra-Por® dialysis tubing (MW 300000 Da)	Spectrum Labs (Breda, The Netherlands)
Tris-base	IDN Biomedical Inc. (Aurora, OH, USA)
VMR® Micro Star 20	VMR International (Leuven, Belgium)

2.2 Experimental methods

2.2.1 Liposome production

Lipids were dissolved in a water miscible solvent (table 2.2) and protein dissolved in either PBS or Tris (table 2.3) were injected into the respective cartridge inlets. Depending on the formulation, the total flow rate (TFR) and the flow rate ratio (FRR) were adjusted for each formulation. When required, a heating block was used to increase the lipid solubility above the transition temperature. Before production of the formulation, approximately 5% of the total sample volume is collected as waste with 70% collected as the main sample under steady-state. After the main sample has been collected, the remaining 25% of the total sample volume is discarded as waste.

Table 2.2 *Lipids used within empirical chapters with their respective solvents and initial concentrations required for solubilisation*

Lipid Compound	Organic solvent	Initial lipid concentration (mg/mL)	Temperature	Chapter
DSPC	Methanol	2.67		3, 4
	Ethanol	0.33 – 27		3, 4, 5, 6
	Isopropanol	2.67	RT & 60 °C	3
	Ethanol/Dimethyl sulfoxide (80:20 v/v)	4.8	60 °C	6
HSPC	Methanol	2.67		3
	Ethanol	2.67		3
	Isopropanol	2.67		3
DMPC	Methanol	2.67		3, 4
	Ethanol	2.67		3
	Isopropanol	2.67		3
Chol	Methanol	0.4 -1.33		3, 4
	Ethanol	0.16 - 13		3, 4, 5, 6
	Isopropanol	0.4 - 1.33	RT & 60 °C	3
SyntheChol™	Ethanol	1.33		4
DDA	Ethanol	5 - 20		3, 5, 6
	Chloroform/methanol *(9:1 v/v)*	5		6
TDB	Ethanol	4		6
	Ethanol/Dimethyl sulfoxide (80:20 v/v)	4	60 °C	6
	Chloroform/methanol *(9:1 v/v)*	1		6
PHAD	Ethanol	4		6
	Ethanol/Dimethyl sulfoxide (80:20 v/v)	4	60 °C	6
	Chloroform/methanol *(9:1 v/v)*	1		6
DMG-PEG2K	Ethanol	0.48		6
	Ethanol/Dimethyl sulfoxide (80:20 v/v)	0.48	60 °C	6

Table 2.3 *Antigens used within empirical chapters with their respective buffers and initial concentrations required for solubilisation*

Antigen	Buffer	Initial concentration (mg/mL)	Reference chapter
Ovalbumin (OVA)	PBS, pH 7.3	0.1 – 4	3, 4, 5
	Tris 10 mM (pH 7.4)	0.04 – 10	5, 6
Major outer membrane protein (MOMP)	Tris 10 mM (pH 7.4)	0.044 – 0.48	5
Trimeric SARS-COV-2 spike antigen (spike)	Tris 10 mM (pH 7.4)	0.04	6

2.2.2 Liposome production by lipid film hydration and microfluidic production methods

2.2.2.1 Microfluidic production using low, medium and high throughput platforms

2.2.2.1.1 *Small scale microfluidic production < 1 mL*

For initial rapid screening, the formulations were prepared using a Spark™ (Precision NanoSystems Inc., Vancouver, Canada). Disposable microfluidic chips were loaded with 31 µL lipid stock and 93 µL PBS or Tris buffer in the reaction chambers, respectively. The receiving chamber was filled with 124 µL PBS or Tris buffer (pH 7.4, 10 mM). With formulations prepared with entrapped OVA, the protein was added to PBS and made to a concentration of 1 mg/mL. The formulations were processed at setting 8–10, and the product was transferred to a glass vial and further diluted to 1000 µL of PBS or deionised water. All formulations were prepared at room temperature.

2.2.2.1.2 Bench scale microfluidic production < 20 mL

Microfluidic production of liposomes was achieved using either the NanoAssemblr® Benchtop or the Ignite™ (Precision NanoSystems Inc, Vancouver, Canada). In these systems, different microfluidic mixers were used: a staggered herringbone (SHM) or a toroidal mixer (TrM) (NanoAssemblr Classic or NxGen™ respectively). To administer the solvent and aqueous components, disposable syringes (1 – 5 mL, Luer Lock) were used to attach the syringes to separate inlets on the microfluidic cartridge. Depending on the formulations various FRR were used ranging between 1:1 to 20:1 with TFRs of 10 – 20 mL/min.

2.2.2.1.3 Pre-clinical microfluidic production < 1000 mL

A pre-clinical microfluidic platform was used to allow for faster throughput speeds and increased volume during one process which bridges the gap between bench-scale and GMP production. This was achieved using the NxGen Blaze™ (Precision NanoSystems Inc, Vancouver, Canada) which uses the same TrM micromixer design as the Ignite™. Lipids dissolved in solvent and protein dissolved in buffer are mixed in the microfluidic cartridge by independent sippers which draw up each independent phase separately into the microfluidic cartridge under continuous flow which can be precisely controlled to the desired FRR and TFR.

2.2.2.1.4 GMP microfluidic production > 1 L

For final GMP liposome production the same formulation from small scale < 1 mL all the way through to GMP scale the NanoAssemblr GMP system was used (DSPC:Chol 2:1 w/w) with modified HPLC pumps (Precision NanoSystems Inc, Vancouver, Canada) using the same TrM design. Single-use bioprocess containers are used to store lipids dissolved in ethanol and protein in PBS separately. A single-use fluid path was used to feed the separate phases into the TrM micromixer at a 3:1 FRR at 200 mL/min.

2.2.2.2 Manufacturing by lipid film hydration

Liposomes were prepared following an adaption of the Bangham method for producing liposomes [99]. Briefly, for the production of DDA:TDB and DDA:PHAD liposomes used in chapter 6, weighed quanities of DDA and TDB (5:1 w/w) or DDA and PHAD (5:1 w/w) were dissolved in a chloroform and methanol mixture (9:1 v/v) and transferred to a round bottom (figure 2.1). The organic solvent was then removed under vacuum using a rotary evaporator for 12 mins at 200 rpm. Once the solvent was evaporated, a thin lipid film was coated across

the wall of the flask which was hydrated with a volume to reach the appropriate total final lipid concentration of 6 mg/mL (5 mg/mL DDA and 1 mg/mL TDB or 1 mg/mL PHAD). The lipid suspension was then heated to 60 °C for 10 mins in a water bath with this process repeated until the lipids were no longer coating the wall of the flask. Spike protein was then mixed with liposomes at a 1:1 v/v ratio leaving a final liposome concentration of 3 mg/mL and 20 µg/mL (150 µg/50 µL liposome dose and 1 µg/50 µL spike protein dose for *in vivo* administration).
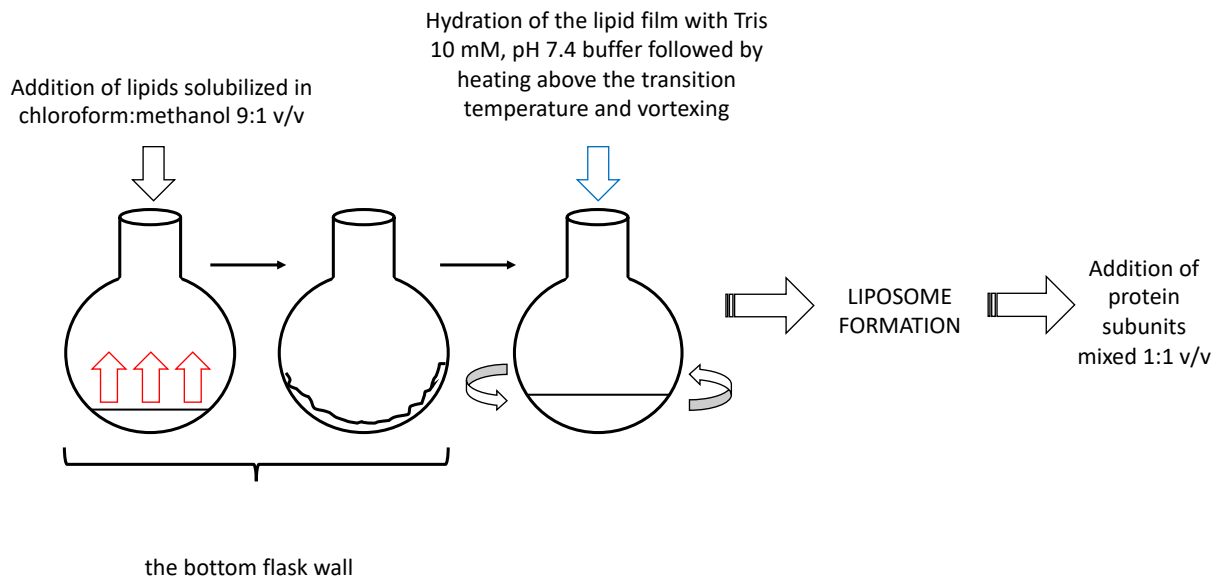
Figure 2.1 *Schematic of the lipid film hydration method for the production of liposomes*

2.2.3 Methods of loading of protein to liposomes

2.2.3.1 Entrapment of protein within neutrally charged liposomes

Protein was entrapped during liposome fabrication by adding a syringe loaded with OVA at 0.25 mg/mL solubilised in PBS to one inlet of the microfluidic chip and at the other inlet the lipids solubilised in either MeOH, EtOH or IPA (0.16 – 3.33 mg/mL initial lipid concentration). Liposomes loaded with OVA were produced at a 3:1 FRR and a 15 mL/min TFR. Liposomes were then subsequently purified using the TFF procedure described in section 2.5.2 before formulation analysis.

2.2.3.2 Adsorption of protein to cationics liposomes

2.2.3.2.1 *Microfluidic adsorption methodology for DSPC:Chol:DDA (10:5:4 w/w)*

Within chapter 5 different microfluidic operational methods were conducted to develop a controlled protein subunit absorption method using DSPC:Chol:DDA liposomes. Table 2.4 outlines the microfluidic parameters for the associated figures. For the 2-step method utilising a 1:1 FRR, dialysis was conducted immediately after liposome production using a 14 kD dialysis membrane against Tris 10 mM (pH 7.4) for 1 h to remove solvent. For other methods, the same solvent removal process was conducted after protein absorption.

Table 2.4 Microfluidic developmental operational parameters used within chapter 5. (*) denotes the same FRR used for both liposome production and controlled antigen adsorption

Manufacturing method	Solvent	Buffer	Inline dilution FRR (with antigen)	Mixing ratio (v/v) or FRR	TFR (mL/min)	Figure number
Vortex	Methanol	Tris	N/A	1:1	N/A	5.1; 5.2; 5.3
	Ethanol	Tris	N/A	1:1	N/A	5.11; 5.15
1 step	Methanol	Tris	N/A	9:1	15	5.19; 5.20; 5.21; 5.22; 5.23; 5.24; 5.25
	Ethanol	Tris	N/A	9:1	15	5.8; 5.9; 5.15; 5.16; 5.17; 5.18
1 step inline	Ethanol	Tris	9:1	9:1	15	5.8; 5.10
2 step	Methanol	Tris	N/A	1:1*	15	5.4; 5.18
	Ethanol	Tris	N/A	1:1*	15	5.4; 5.19; 5.20; 5.21; 5.22; 5.23; 5.24; 5.25
	Methanol	Tris	N/A	9:1*	15	5.5
	Ethanol	Tris	N/A	9:1*	15	5.5; 5.6; 5.7; 5.8; 5.9; 5.15; 5.17; 5.18

2.2.3.2.2 Protein subunit adsorption onto the surface of DDA:TDB

For liposomes prepared by microfluidics, a 2 step method from chapter 5 was adopted. DDA:TDB lipsomes were pre-formed at initial concentrations at 12 – 24 mg/mL using a 3:1 FRR and 10 mL/min suspended in either ethanol or ethanol/dimethyl sulfoxide (80:20 v/v). Further formulation refinement indicated that ethanol/dimethyl sulfoxide (80:20 v/v) was not a suitable solvent for these lipids and was only used within one experiment. Additional lipids were required for microfluidic preparation of DDA:TDB leading to the addition of DSPC (10 – 50% w/w) and DMG-PEG$_{2000}$ (2 – 5% w/w). After microfluidic production, liposomes were then dialysed using a 14000 D membrane against Tris 10 mM which was stirred for 1 h. At a 1:1 FRR and 10 mL/min TFR OVA was mixed with the pre-formed liposomes at an L:P of 60:1 or 150:1 L:P. For spike protein adsorption, the protein was mixed with liposomes composed of DDA:TDB (5:1 w/w) with the addition of DSPC (20%) and DMG-PEG$_{2000}$ (2%) at a 1:1 FRR and 10 mL/min TFR with a 150:1 L:P leaving a final liposome concentration of 3 mg/mL and spike concentration of 20 µg/mL. For spike adsorption onto DDA:TDB prepared by lipid film hydration, the method in section 2.2.1.2 was followed.

2.2.3.2.3 Protein subunit adsorption onto the surface of DDA:PHAD

The microfluidic production and protein adsorption onto DDA:PHAD followed a 2-step microfluidic adsorption method. Liposomes were pre-formed at an initial concentration of 24 mg/mL using a 3:1 FRR and 10 mL/min suspended in either ethanol or ethanol/dimethyl sulfoxide (80:20 v/v). Further formulation refinement indicated that ethanol/dimethyl sulfoxide (80:20 v/v) was the most suitable solvent for these lipids and was used for the majority of its formulation. Additional lipids were required for microfluidic preparation of DDA:PHAD leading to the addition of DSPC (10 – 50% w/w) and DMG-PEG$_{2000}$ (2 – 5% w/w). After microfluidic production, liposomes were then dialysed using a 14000 Da membrane against Tris 10 mM which was stirred for 1 h. At a 1:1 FRR and 10 mL/min TFR OVA was mixed with the pre-formed liposomes at an L:P of 150:1 L:P. For spike protein adsorption, the protein was mixed with liposomes composed of DDA:PHAD (5:1 w/w) with the addition of DSPC (20%) and DMG-PEG$_{2000}$ (2%) at a 1:1 FRR and 10 mL/min TFR with a 150:1 L:P leaving a final liposome concentration of 3 mg/mL and spike concentration of 20 µg/mL. For spike

adsorption onto DDA:PHAD prepared by lipid film hydration, the method in section 2.2.1.2 was followed.

2.2.4 Methods for quantification

2.2.4.1 Phospholipid quantification

For quantification of phospholipid concentrations a commercial colourimetric phospholipid assay (Sigma Aldrich Company Ltd., Poole, UK) the manufacturer's recommendations were followed. Briefly, a calibration curve was produced by diluting the included standard to 0.5 mM and adding varying standard volumes to a 96 well plate in duplicate to a final volume per well to 50 µL with deionised water. 50 µL of solubilised phospholipids were diluted 1:50 with purified water while liposome samples before and after tangential flow filtration were diluted 1:10 with purified water. 50 µL of reaction mix containing the assay buffer, enzyme mix, phospholipase D enzyme and dye reagent, as per manufacturers recommendations, was added to each sample which was then incubated at room temperature for 30 min. Absorbance was measured at 562 nm using a Bio-rad 680 microplate reader.

2.2.4.2 Protein analysis

2.2.4.2.1 Liposome solubilisation for neutrally charged liposomes

Before measuring protein entrapment with neutrally charged liposomes, they first need to be solubilised to release the encapsulated protein. This method was adapted based on published materials [117, 151] using a mixture of PBS/2-propanol 50/50 v/v. For each sample to be analysed, the solubilisation mixture is then added to the sample at a 50/50 v/v ratio and vortexed immediately after addition.

2.2.4.2.2 Protein quantification by the Pierce™ Micro BCA Protein Assay

For the detection of protein, the micro bicinchoninic acid (BCA) protein assay kit was used (Pierce™ micro-BCA Protein Assay Kit, Sigma Aldrich, Poole, UK) following the manufacturer's recommendations. Briefly, samples were incubated at 37 °C with 150 µL of the sample mixed 1:1 v/v with a working reagent comprised of reagent A, B and C (25:24:1 v/v) respectively. For the production of the calibration curve separate Eppendorfs's containing solubilised liposomes were mixed 50/50 v/v with dissolved OVA in PBS with the final protein

concentration ranging from 2 – 40 µg/mL and a final lipid concentration that matches the analysed sample. After 150 µL of the calibration curve standards and unknown samples are added to the microplate wells, 150 µL of working reagent is added to the wells and incubated at 37 °C with the absorbance measured at 562 nm using a Bio-rad 680 microplate reader.

2.2.4.2.3 Sodium dodecyl sulfate (SDS) polyacrylamide gelelectrophoresis (PAGE)

Gel electrophoresis was conducted to determine protein adsorption on cationic liposomes surface. Prior to loading the experiment, the samples of interest were mixed 1:1 v/v with sample buffer and heater to 90 °C for 3 mins to denature the proteins. After 3 mins, 40 – 60 µL of samples were added to lane 2 onwards, with the protein ladder containing native proteins of different molecular weights to lane 1 allowing for accurate protein size comparisons. A running buffer composed of Tris, glycine, SDS and d.H_2O was added to the Novex Mini Cell gel apparatus and ran until the dye reached the end of the gel by applying 30 mA across the gel. The gel was then stained overnight using Coomasie blue which was then detained using a mixture of H_2O:MeOH:CH_3COOH (50:40:10 v/v/v) and imaged using the Gel Doc™ EZ Imager.
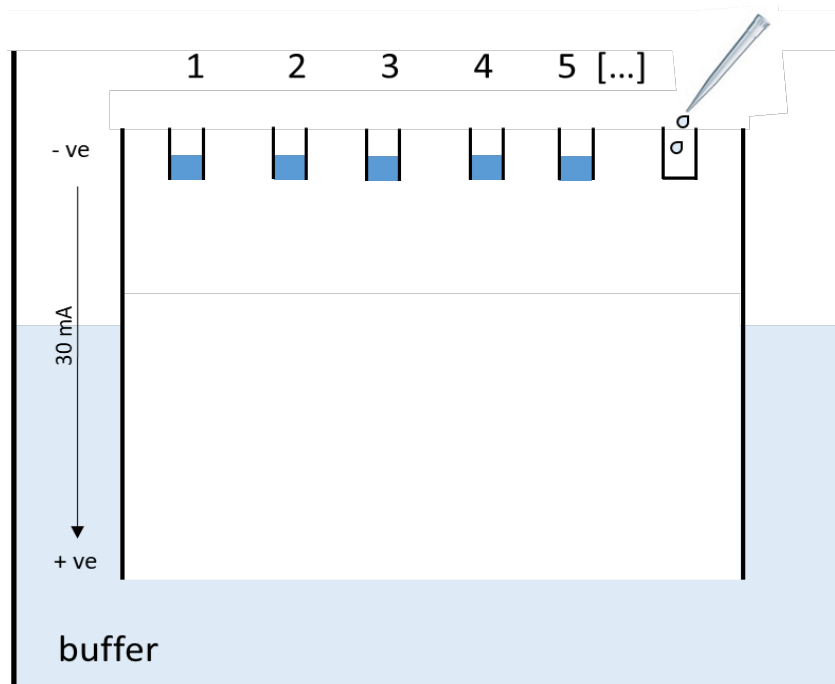
Figure 2.2 Simplified schematic of SDS-PAGE gel

2.2.4.2.4 *Protein quantification by liquid chromatography*

Protein quantification measured by reverse phase high-performance liquid chromatography (RP-HPLC) was performed using either a Jupiter 5 µm C5 300A column 4.6 mm i.d. x 250 mm length (Phenomenex, Macclesfield, UK). The ultraviolet (UV wavelength, flow rate, analysis time, the gradient was adjusted for each method (table 2.5). The flow rate for each method was 1 mL/min with an injection volume of 100 µL. The limit of detection (LOD) and limit of quantification (LOQ) was calculated using equation 2.1 with each curve assessed for linearity using the coefficitent of determination (R^2).

Table 2.5. *RP-HPLC methodology used to quantify ovalbumin entrapment*

Chapter	Retention time (min)	UV detector (nm)	Phase A	Phase B	Method		
					Time	A%	B%
					0	95	5
3	8 - 14	210 or 280	0.1% TFA + d.H20	0.1% TFA + ACN	10	95	5
					15	5	95
					20	95	5
					Time	A%	B%
					0	95	5
4	10 - 14	210 or 280	0.1% TFA + d.H20	0.1% TFA + ACN	20	35	5
					25	5	95

$$LOD = \frac{(\sigma \cdot 3.3)}{m} \qquad\qquad LOQ = \frac{(\sigma \cdot 10)}{m} \qquad (2.1)$$

σ = Standard deviation
m = gradient of slope

2.2.5 Liposome purification

2.2.5.1 Dialysis

Dialysis tubing (MW 14000 Da, Sigma Aldrich, Poole, UK) was used for solvent removal and was treated in a solution of 1 mM EDTA and 2% sodium bicarbonate at 80 °C for 2 h to remove sulphites and glycine from the membrane. The membrane was then washed with deionised water and stored in 20% ethanol with 1 mM EDTA. Solvent removal from samples using the 14000 Da tubing was undertaken using 1 mL of the sample and dialysed against 200 mL of either PBS or Tris buffer for 1 h. For protein removal, a 300000 Da MWCO (Spectra-Por®, Spectrum Labs, Breda, The Netherlands) was used and the manufacturers instructions were followed. Samples requiring free protein removal were loaded into the tubing and dialysed against 400 mL of Tris for 1 – 2 h followed by two additional buffer exchanges and left overnight at RT.

Table 2.6 *Dialysis methodology for the removal of residual solvent and 'free' protein*

Method	Membrane pore size (Da)	Duration	Volume of buffer (mL)	Buffer exchange
Solvent removal	<14000	1 h	200	None
Protein removal	300000	24 h	400	Buffer changed every for 1 – 2 h for first 4 h then buffer changed and left overnight at RT

2.2.5.2 Tangential flow filtration

Ovalbumin and solvent were removed from neutrally charged DSPC:Chol liposomes by using a Krosflo KR2i TFF system (Waltham, MA, USA) which was equipped with an mPES membrane with a pore size of 300, 500 or 750 kD membrane. Unless otherwise stated, the sample volume was 1 mL with a diafiltrate volume of 12 mL.

2.2.6 Liposome characterisation

2.2.6.1 <u>Dynamic light scattering</u>

The particle size (Z-average diameter) and polydispersity index (PDI) can be measured by dynamic light scattering (DLS) using a Zetasizer Nano ZS (Malvern Panalytical Ltd, Worcestershire, UK) equipped with a 4-mW 633 nm He-Ne laser and a detection angle of 173°. Unless otherwise stated, samples were measured at 25 °C diluted 1:10 (v/v) in deionised water and untaken in triplicate with the attenuation value between 6 and 9. The same dilution (1/10) was used for zeta potential measurement. The dispersant (water) refractive index and viscosity values were 1.330 and 0.8872 cP respectively. Zetasizer software v.7.11 (Malvern Panalytical Ltd.) was used for the acquisition of data.

2.2.6.2 <u>Nanoparticle tracking analysis</u>

Nanoparticle tracking analysis (NTA) measurements were performed with a NanoSight NS300 (Malvern Panalytical Ltd, Worcestershire, UK) equipped with a low volume flow cell (LVFC). The samples were injected into the LVFC with sterile syringes until the sample liquid had completely filled the LVFC. The samples were illuminated with a 488 nm blue laser, and the light scattered was visualized via a 20x magnification microscope onto which a high sensitivity sCMOS camera was mounted. All measurements were performed at room temperature with live monitoring of temperature fluctuations by the software. Samples were diluted 10,000 times in MilliQ ultra-pure water; thus, the viscosity of each sample was assumed to be that of water. The software used for capturing and analysing the data was the NTA 3.4 Build 3.4.003 (Malvern Panalytical, Worcestershire, UK). Five repeat measurements were performed on each sample with 60-second captures being carried out. Samples were measured underflow so that an individual particle would take between 7 to 10 seconds to cross the field of view. Manual shutter and gain settings of 1300 and 512, respectively.

2.2.6.3 <u>Cryogenic transmission electron microscopy</u>

Cryogenic transmission electron microscopy (Cryo-TEM) samples were prepared using a Gatan CP3 Cryoplunge by depositing liposomes (3 - 5 µL) onto a 300 mesh copper TEM grid (graphene oxide / holey carbon or holey carbon) held in tweezers in a controlled environment (~23 °C, 80% humidity), blotted for 1.5 s then plunged into liquid nitrogen cooled liquid ethane (-172 °C) to vitrify. Samples were maintained under liquid nitrogen until transfer to the TEM

(Gatan 926 cryo sample holder) and held at −176 °C during analysis (Gatan Smartset model 900 controller). Images of liposomes were recorded using a JEOL 2100 Plus operating at 200 kV (Gatan Ultrascan 100XP camera).

2.2.7 Liposome stability study

Neutral liposomes (DSPC:Chol 2:1 *w/w*) were produced using microfluidics at a 3:1 FRR and 15 mL/min TFR (4 mg/mL initial lipid concentration) in either MeOH, EtOH or IPA. Solvent was removed by TFF (12 mL wash cycle per mL of sample). Liposome suspensions were then stored at 2–8 °C in the fridge and their size and PDI was measured over 7 days with the Zetasizer Nano ZS (Malvern Instruments Ltd., Worcestershire, UK) using a 1/10 dilution with purified water.

Cationic liposomes (DSPC:Chol:DDA 10:5:4 w/w) were produced using microfluidics at 1:1 FRR and 15 mL/min TFR (4 mg/mL initial lipid concentration) in MeOH at the solvent inlet and Tris 10 mM used at the aqueous inlet. Solvent was removed by dialysis using a 14000 Da dialysis membrane over 1 h with 1 mL of sample dialysed in 200 mL Tris 10 mM. Liposomes were fed through the microfluidic for a second time in one inlet and in the other inlet, protein was added at various liposomes to protein ratios. A final lipid concentration of 1 mg/mL was used with the final protein concentrations at either 0, 5, 16.5, 33, 50, 100 or 125 μg/mL. Liposome suspensions were then stored at 2 – 8 °C in the fridge and their size, PDI and zeta potential was recorded over 14 days with protein loading calculated on day 0 and day 14 after dialysis with a 300000 Da membrane to remove free protein. DDA:TDB liposomes had size measurments recorded over the course of either 150 or 360 h using a 60:1 or 150:1 L:P ration with samples stored at 4 °C between measurements. Using the Zetasizer Ultra DDA:TDB and DD:PHAD liposomes were measured each hour for 12 h and then at 24 and 48 h from the first recorded to measure short term stability. Samples were cooled to 4 °C and measured at 25 °C.

2.2.8 Protein release study from neutral liposomes

Ovalbumin-loaded entrapped within DSPC:Chol liposomes were produced using microfluidics at a 3:1 FRR and 15 mL/min TFR (16 mg/mL initial lipid and 1 mg/mL initial Ovalbumin) using

MeOH, EtOH or IPA. These formulations were then purified via TFF (as previously described) with 1 mL of the purified formulation added into a 300 kD float-a-lyzer™ (Spectrum™, Breda, The Netherlands) in the presence of 20 mL PBS (pH 7.4 ± 0.2). The samples were incubated at 37 °C with agitation with 100 µL of sample removed and replaced with an equal volume of buffer at specific time points between 0 – 120 h. The protein content within the liposomes was quantified using the described RP-HPLC method.

2.2.9 Quantification of antigen protection by cationic liposomes against proteolytic enzymatic digestion by monitoring fluorescent emission

For results outlined in chapter 5, dry-quenched OVA (DQ-OVA) was challenged against trypsin to assess the degree of protection against proteolytic degradation by monitoring the fluorescence of DQ-OVA. 10:1; 30:1 and 60:1 liposome:DQ-OVA was manufactured either by vortex; 1 step or 2 step with solvent and free protein removed via a 300 kD membrane. Trypsin was added at a 1:1 v/v at a concentration of 20:1 w/w trypsin:DQ-OVA to ensure a sufficient and an aggressive challenge against DQ-OVA. To calculate the degree of protein protection provided by the formulation, 'free' DQ-OVA was added to trypsin (20:1 w/w trypsin:DQ-OVA) at the same protein concentrations used in the 10:1; 30:1, and 60:1 L:P formulations allowing for the percentage of protein 'protected' from trypsin to be calculated using equation 2.2. Formulations mixed with trypsin were left at room temperature (RT) or incubated at 37 °C for either 4 or 24 h. DQ-OVA fluorophores were measured using a fluorimeter (Polarstar Omega, BMG Labtech) at a fixed emission of 485 nm and excitation wavelengths of 520 - 590 nm. The excitation wavelength of 535 nm was idenitfed as the optimal filter.

$$\%DQ - OVA\ protected = 100 - \left[\left(\frac{(formulation\ fluorescence\ (+)trypsin\ - formulation\ fluorscence\ (-)trypsin)}{(DQ-OVA\ fluorescence\ (+)trypsin\ -\ DQ-OVA\ fluorescence\ (-)trypsin)} \right) * 100 \right] \quad (2.2)$$

2.2.10 In vivo biodistribuition and immunogencity studies

All *in vivo* studies conformed to guidelines outlined by The Home Office of the UK Government under the Animals [Scientific Procedures] Act 1986 (UK project license PP1650440). All experiments were carried out in a designated establishment in the animal facility at the

University of Strathclyde (Glasgow, UK) following guidelines from the Home Office of the UK government under the Animals [Scientific Procedures] Act 1986.

2.2.10.1 In vivo biodistribution studies

BALC/c mice (8-12 weeks old) were split randomly into groups of 1 or 5 across 7 cages. To track formulation biodistribution *in vivo* liposomes were dual labelled with the lipophilic dye and a Alexa Flour labelled OVA. The lipiophilic dye used was 1,1'-dioctadecyl-3,3,3',3'-tetramethylindotricarbocyanine iodide (DiR) at a 500:1 w/w total lipid:dye ratio following the method previously described [152]. Ovalbumin was substituted for the fluorescence conjugate Alexa Fluor 647 (AF647-OVA) allowing for fluorescent tracking. Mice imaging was carried out using an IVIS Spectrum (Perkin Elmer) with Living Image software used for data capture and analysis. The presence of DiR was detected using an excitation wavelength of 710 nm and an emission filter of 780 nm. AF647-OVA was detected using an excitation wavelength of 650 nm and emission filter of 680 nm. A medium binning and f/stop of 2 was used and an auto-exposure setting was used to calculate acquisition times. Mice were anaesthetized for imaging using 3% isoflurane. Anaesthesia was maintained during imaging at 1% isoflurane. Images were taken pre and post administration of formulations after 6, 24, 48, 72, 144 and 216 h post injection. Mice were terminated after the last time point following a schedule 1 method while still anaesthetised allowing for the spleen, liver, kidneys, popliteal and inguinal lymph nodes (draining and non draining) to be removed allowing for further data acquisition and analysis using the DiR and AF647 ex/em settings described. The total flux (p/s) was calculated at the injection site (region of interest) for each mouse.

2.2.10.2 In vivo assessment of immunogenicity

An *in vivo* study was carried out in chapter 5 to evaluate the induction of an antigen-specific antibody immune responses following immunisation of MOMP (without carrier); with liposomes manufactured by 1 step at a 10:1; 30:1 or 60:1 L:P or 2 step using either a 30:1 or 60:1 L:P. Female BALB/c mice aged 7-9 weeks were housed in 6 groups of 5 with free access to food and water. The mice were immunised i.m with 50 µL of formulation with 7.5 % w/v trehalose for isotonicity twice (day 0 and 21) into the right quadricep at a liposome concentration of 120 µg/dose and a MOMP concentration of either 2, 4, or 12 µg/dose with

blood taken from the tail (the day before immunisation and day 20) and stored at -20 °C for future analysis of antibodies. Mice were terminated on day 49 by cardiac puncture.

To evaluate immogencity of spike protein (chapter 6) 30 female BALB/c mice (7-9) weeks were house in 6 groups of 5 with free access to food and water. Each mouse was i.m injected with 50 μL of formulation in the right quadricep with either spike protein (no carrier), AddaVax (positive control), DDA:TDB:DSPC:DMG-PEG(2%), DDA:PHAD:DSPC:DMG-PEG(2%), DDA:TDB and DDA:PHAD. The mice would receive a final total spike concentration dose of 1 μg/50 μL and a total DDA:TDB/PHAD (5:1 w/w) concentration of 150 μg/50 μL. The prime injection on day 0 and booster injection was set at 21 days following the initial prime injection. On day 50, the objectives were to obtain blood serum via a cardiac puncture, isolate the spleen for restimulation and obtain muscle serum at the sight of injection. Any biological samples obtained during the study were stored at -20 °C for future analysis.

2.2.10.3 <u>Antibody response analysis</u>

For quantification of serum immunoglobulins, blood was collected via tail bleeds a day before the first injection and on day 20. On the final day of the study, blood was collected via a cardiac puncture. Blood was collected in an autoclaved Eppendorf and centrifuged for 10 mins at 10 000 x g allowing a serum supernatant to be separated and collected from blood cells. The serum for each mouse was then pipetted in a separate Eppendorf and stored at -20 ºC for later analysis.

A direct enzyme-linked immunosorbent assay (ELISA) was used to detect total IgG, IgG1 and IgG2a in the serum. The assay was carried out by coating the microtiter plates (Nunc Maxisorp) in carbonate buffer; 0.1 M pH 9.6 using the antigen concentrations and volumes outlined in table 2.7.

Table 2.7 *ELISA coating antigen and concentration used for immunoassays conducted in chapters 5 and 6*

Chapter	Sub-unit protein antigen	Concentration (µg/mL)	Volume per well (µL)
5	Major outer membrane protein (MOMP)	0.5	100
6	Recombinant SARS-CoV-2 Spike His-tag (spike)	2	50

The plates were incubated overnight at 4 °C and washed with PBS containing 0.05% v/v Tween20 and blocked to eliminate any non-specific binding with 2% w/v BSA in PBS for 1.5 h at 37 °C. The plates were then washed 3 times with the wells then filled with 100 µL of serum which was serially diluted in 1% w/v BSA in PBS (diluent buffer) and incubated at 37 °C for 2 h. After 3 washes, 100 µL of horseradish peroxidase labelled goat anti-mouse was diluted in diluent buffer to the desired concentrations (IgG total 1:2500; IgG1 and IgG2a 1:5000) and was added to the wells and incubated for 1 h at 37 °C. The plates were then washed 5 times with 100 µL TMB substrate (room temperature) and was added to each well and left in the dark for 30 mins at room temperature. The reaction was stopped by adding 100 µL of 0.2 M H_2SO_4 to each well with the plates then immediately read at 450 nm. Results were then calculated by the reciprocal endpoint value.
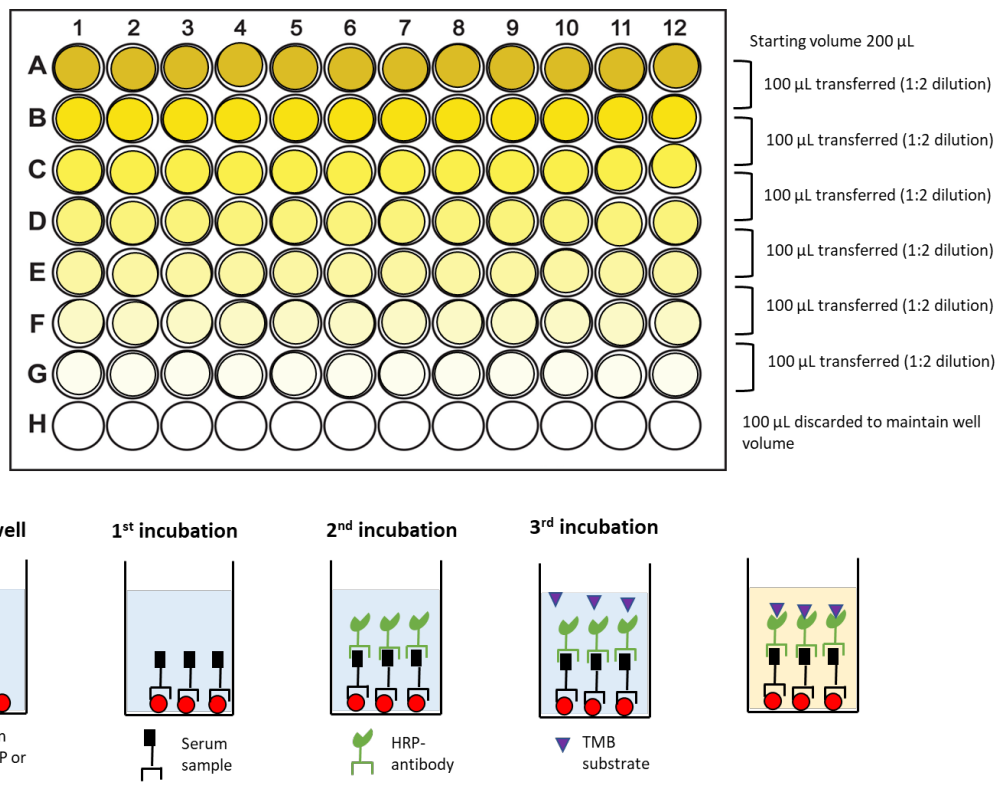
Figure 2.3 *A schematic for both the outline of the ELISA microplate set for analysing antibodies in the blood serum and representation of the direct ELISA method*

2.2.10.4 Neutralising antibody analysis

A direct ELISA was used to detect neutralising antibodies in the serum using a SARS-CoV-2 neutralising antibody detection assay from AdipoGen Life Sciences. The assay protocol was followed but briefly, SARS-CoV-2 spike (RBD) recombinant protein was precoated on a 96-well microtitre plate and stored at 4 °C. 100 µL of negative and positive control was added to the wells in duplicate with 100 µL of diluted (1:10) serum samples and incubated for 1 h at 37 °C. Wells were aspirated before the addition 300 µL of wash buffer (1x) to the wells. The process was repeated five times. 100 µL of ACE2-HRP was added to the wells and incubated at 37 °C for 1 h with the aspirate/wash step repeated five times as before. TMB solution was then added to the wells (100 µL) and left to develop in the dark for 15 mins before the addition of STOP solution (100 µL) to stop the development reaction and immediately read at 450 nm. The presence of neutralising antibodies is measured by a reduction in the optical density

indicating the inhibition of binding of SPIKE to ACE2 receptors. %inhibition was then calculated following equation 2.3.

$$\%inhibition = \left(1 - \left(\frac{OD \ of \ sample}{OD \ of \ negative \ control}\right)\right) * 100 \qquad (2.3)$$

2.2.10.5 Re-stimulation of splenocytes

On the day of the cull, spleens were removed aseptically and placed into universal tubes containing 5 mL of complete RPMI 1640 media and placed on ice until all spleens have been removed. Spleens there then forced through a cell strainer and collected in a 50 mL falcon tube with the cell strainer washed with an additional 5 mL of complete media. The samples were then spun at 300 x g for 5 mins at 4 °C. The supernatant was discarded and the pellet was resuspended with 3 mL of Boyles solution. The sample was left to incubate at room temperature for 5 mins before being added to the centrifuge at 300 x g for 5 mins at 4 °C. The pellets were then washed in 5 mL complete media and centrifuged at 300 x g for 5 mins and finally resuspended in 1 mL complete media. Viable cells were estimated by Trypan blue exclusion with cells diluted to 5 x 10^5 cells per 100 µL (5 x 10^6 cells/mL) and added to appropriate wells using a Nuclon 96-well plate (Fisher Scientific, Loughborough, UK). The cells were then stimulated by adding 100 µL of media (unstimulated control), concanavalin A (ConA; 10 µg/mL) as the positive stimulated control or 1 µg/mL spike protein as the investigated antigen. The cells were then incubated at 37 °C; 5% CO_2 and 95% humidity for 3 days which were then transferred to -20 °C storage for cytokine ELISAs at a later date.
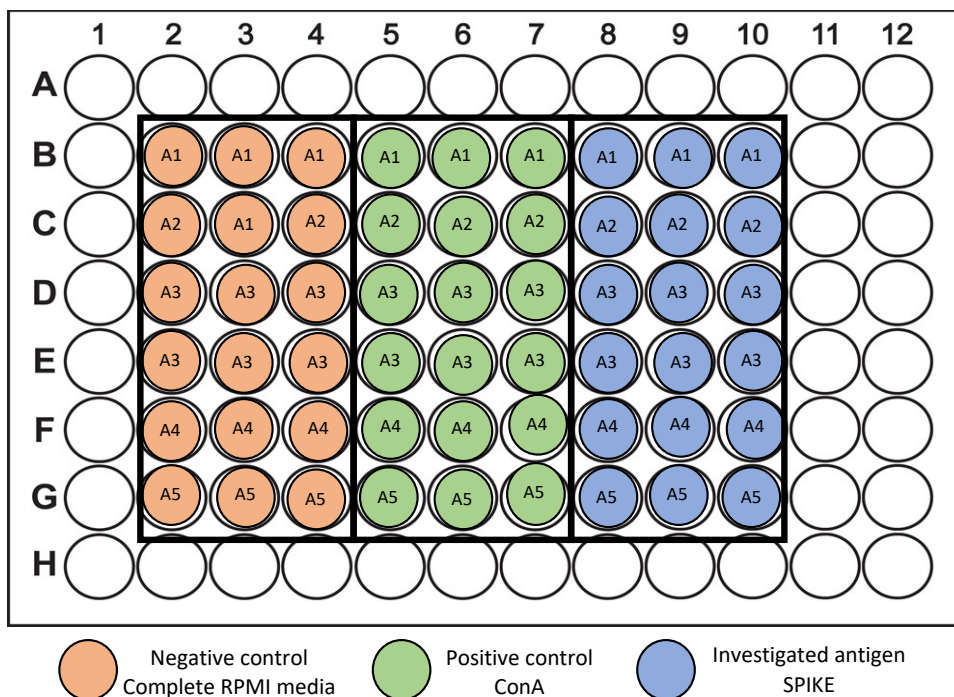
Figure 2.4 *A schematic of the ELISA microplate setup for the restimulation of splenocytes.*

2.2.10.6 Muscular tissue removal and digestion protocol

To quantify IL-1β at the site of injection the muscle at the site of injection (right leg) has to be digested to remove extracellular matrices and fibrous tissue allowing the collection of muscle cells. To achieve this, a digestion medium has to be produced composed of 100 µg/mL of DNAse-I (stored at – 20 °C) and 20 mg/mL per sample suspended in 1 mL of RPMI prepared with no FBS or HBSS with Ca^{2+}/ Mg^{2+} due to interactions with the collagenase and DNAse-I. On the day of the cull, muscular tissue is isolated from the leg, ensuring that popliteal nodes are removed, and placed into a 48-well plate immersed in 1 mL of RPMI (without FBS) which is then dab dried. The muscle is then transferred to a 12-well plate and minced with sterile scissors to obtain tissue sizes of approximately 2 mm. To this, 1 mL of the prepared digestion medium is added to the well with the tissue spread out of clumps to maximise the tissue surface area. The 12-well plate is then incubated at 37 °C and 5% CO_2 for approximately 30 – 40 mins. After incubation, the samples are then pipetted up and down at least 10 times or until most of the tissue has been disrupted. The digestion reaction is then stopped by adding

2 mL of PBS supplemented with 5 mM EDTA to each well. The cell suspension is then filtered directly into a 50 mL falcon tube through a 100 µm cell strainer and washed with 10 mL PBS supplemented with 5 mM EDTA allowing the collection of between 10 – 15 mL of cell suspension in total. The samples are then centrifuged at 400 x g for 10 mins at 4 °C after which the supernatant is discarded and the cell pellet is then resuspended in 1 mL of RPMI (without FBS). Groups are then pooled together and aliquoted into 1.5 mL Eppendorfs and stored at – 20 °C or later analysis.

2.2.10.7 IFN-γ from spleens and IL-1β at the site of injection analysis

For IFN-γ analysis, the supernatants from the restimulated spleens were quantified using a sandwich ELISA. Briefly, a day before the analysis date plates were coated with 50 µL/well of 2 µg/mL rat anti-mouse cytokine antibody in PBS, pH 9, and incubated at 4 °C overnight. On the day of the analysis, the plates were washed with wash buffer (PBS pH 7.4 containing 0.05 % v/v Tween-20) three times. The plates were then blocked with 200 µL/well using PBS pH 7.4 containing 10% v/v FCS (heat-inactivated) for 1 hour at 37 °C to eliminate any non-specific binding. Plates were then washed again in wash buffer three times before 30 µL/well of samples or IFN-γ standard diluted in 10 % v/v FCS in PBS pH 7.4 and incubated for 2 h at 37 °C. Again, plates were then washed three times using the wash buffer allowing 100 µL/well of rat anti-mouse biotin IFN-γ antibody to be added to the wells at a concentration of 1 µg/mL diluted in 10% v/v FCS in PBS pH 7.4 and incubated for 1 hour at 37 °C. Plates were washed three times in wash buffer with 100 µL/well of HRP-streptavidin (diluted 1:4000 in 10 % v/v FCS in PBS pH 7.4) to the wells and incubated for 1 hour as before. The plates were then washed three times in wash buffer with 100 µL/well of TMB (room temperature) applied to the wells. The plates were then kept in the dark for 20 mins and were stopped by adding 100 µL/well of 0.2 M H_2SO_4.

A comparable method to the one used for the IFN-γ analysis ELISA method was used for IL-1β. The only change to the method was that for coating 100 µL/well of the diluted capture antibody was required with 300 µL/well of the blocking reagent added the following day to eliminate non-specific binding sites.
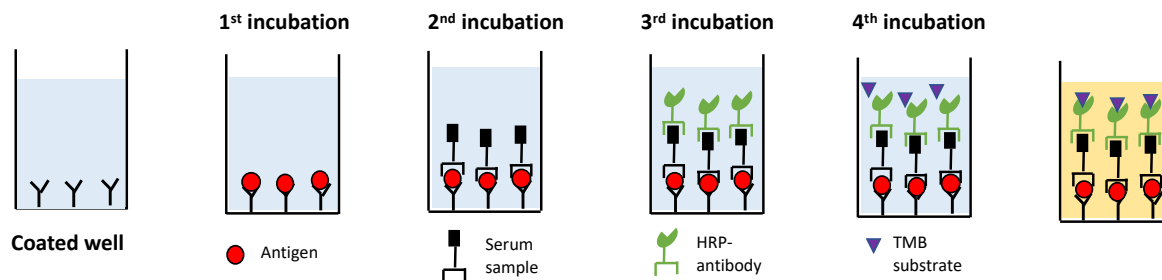
Figure 2.5 *A schematic of the sandwich ELISA used for quantifying IFN-γ in stimulated splenocytes and IL-1β within muscle serum.*

2.2.10.8 Bead-based immunoassay for re-stimulated splenocytes

Using the LEGENDplex™ Mouse Th Cytokine panel, multiple cytokines can be screened to gain an understanding of the immune responses stimulated by adjuvanted formulations. The principle of the assay relies on the differences in bead size and fluorescent intensity. A specific antibody that serves to capture specific analytes, when mixed with the sample, are conjugated onto different beads. Following the addition of biotinylated detection antibodies and streptavidin-phycoerythrin a fluorescent signal is emitted proportional to the amount of bound analytes. Using a flow cytometer, the beads are then differentiated by size allowing specific populations of differently sized beads to be separated and quantified using a standard curve for each particular analyte. The cytokines IL-2, 4, 5, 6, 9, 13, 17A, 17F, 22, IFN-γ and TNF- α were quantified following the manufacturer's recommendations.

Briefly, all reagents and samples were left to warm to room temperature. The standards were then prepared by reconstituting the Th Panel Standard cocktail with 250 µL of assay buffer which serially diluted 1:4 to obtain 7 concentrations with straight assay buffer used as the 0 pg/mL concentration. Using a V-bottom plate, 25 µL of assay buffer was added to all wells of the V-bottom plate with 25 µL of the standard to the standard wells and 25 µL of sample to the sample wells, the plate was then sealed and vortexed on a plate shaker for 30 s. Following this, 25 µL of mixed beads were added to each well. During the addition of the beads, the beads were shaken intermittently to prevent bead settling. The plate was then sealed and covered with aluminium foil and secured onto a plate shaker for 2 h at 800 rpm. After 2 h, the plate was centrifuged at 1050 rpm (approximately 250 g) using an microplate adapter. Immediately after centrifugation, the supernatant was dumped into the sink with a quick

inversion in one continuous and forceful movement to ensure beads remain at the tip of the V-plate. 200 μL of 1x wash buffer was then added to each well and aspirated with the step repeated an additional two times. After blotting excess wash buffer, 25 μL of biotinylated detection antibodies were added to each well with the plate then sealed and wrapped in aluminium foil which was secured onto a plate shaker set to 800 rpm for 1 h. After 1 h, without aspirating, 25 μL of streptavidin-phycoerythrin was added to each well directly and placed onto a plate shaker set to 800 rpm for 30 mins ensuring the plate is sealed securely and wrapped in foil. The plate was then centrifuged at 1050 rpm (approximately 250 g) using a microplate adapter with supernatant removed following a quick and forceful downward motion into the sink. The plate was then washed and aspirated with 200 μL of 1x wash buffer twice. The beads were suspended with 150 μL of 1x wash buffer before being read on the flow cytometer. Results were then analysed using BioLegend's LEGENDplex™ data analysis software.
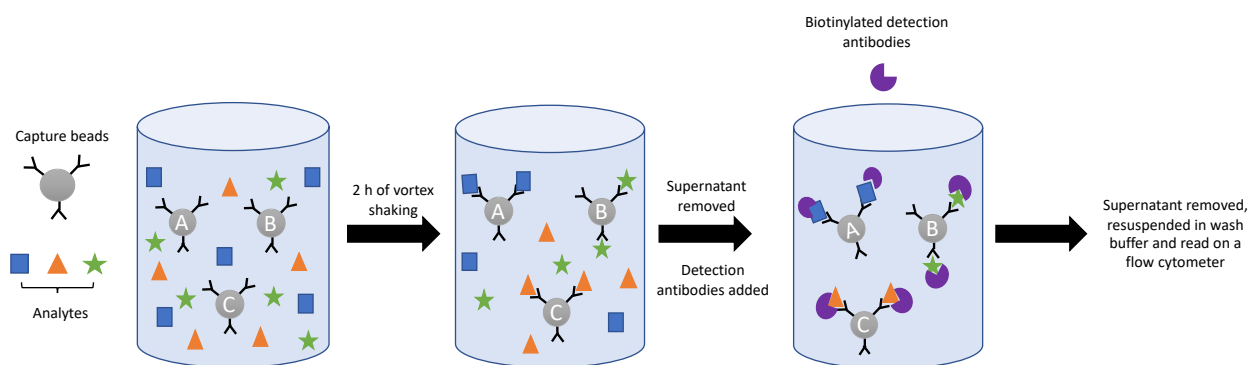
Figure 2.6 *A simplified schematic of the bead-based immunoassay used to screen for multiple analytes*

2.3 Statistical analysis

The mean ± standard deviation (SD) was calculated for all experiments with n = 3 independent batches unless otherwise stated. Statistical analysis was tested by one- or two-way analysis of variance (ANOVA) with Tukey's post adhoc test to compare the mean differences in the results. Statistical significance are noted on the graphs by: $p > 0.05$ (ns), $p < 0.05$ (*), $p < 0.01$ (**), $p < 0.001$ (***). Where appropriate the similarity or difference between protein release profiles of different formulations was assessed using an f_2 similarity test.

Chapter 3

Implementation of a novel microfluidic manufacturing parameter: Exploiting organic solvent polarities to fine-tune vesicle physical properties
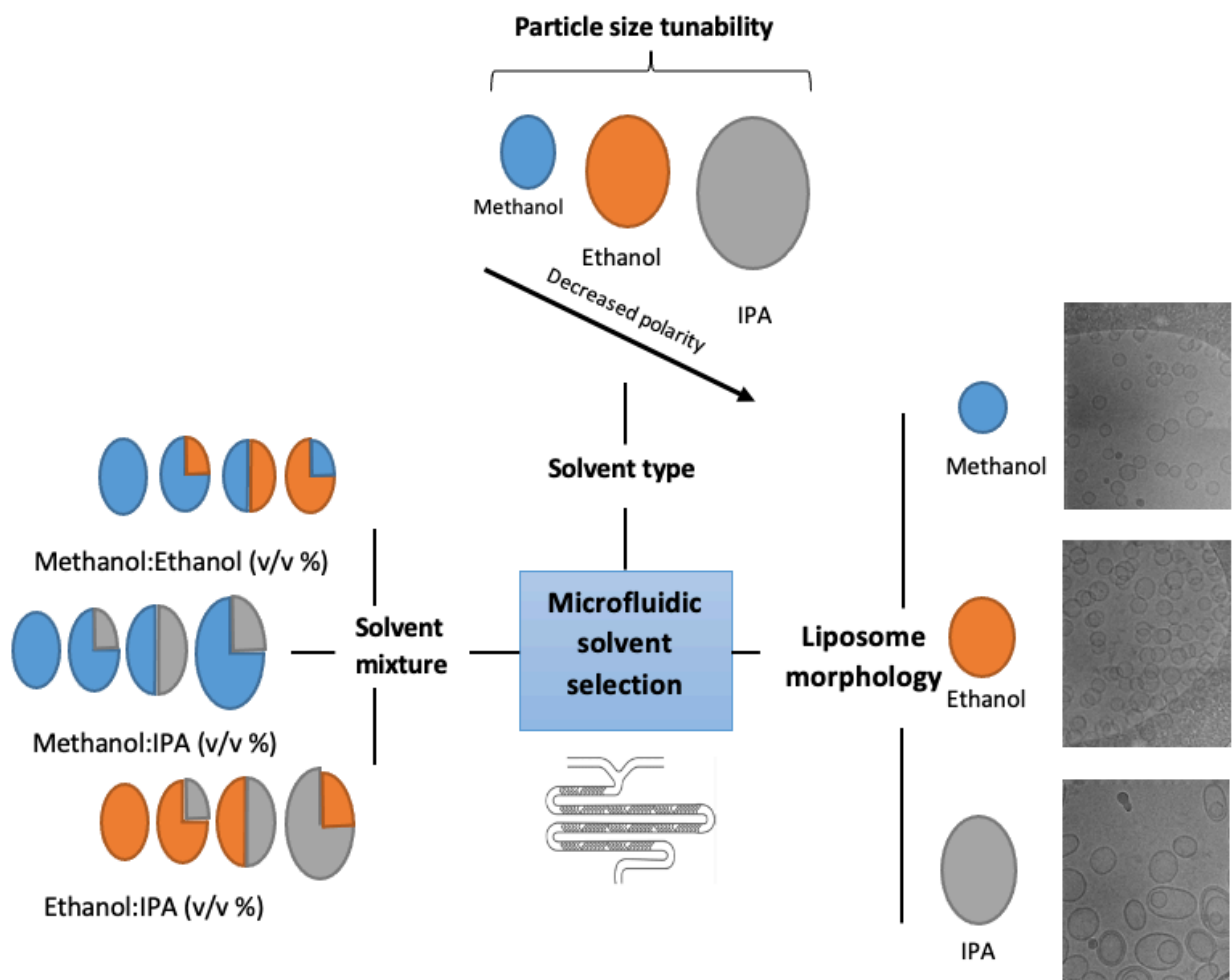
The work presented in this chapter has been published in:

3.1 Introduction

As the research volume involving microfluidics increases, various process parameters have been identified to improve liposome production of which which circumvents multi-stage manufacturing processes. Such parameters include flow rate ratio (FRR) [153], total flow rate (TFR) [119], lipid concentration [117] and buffer selection [115]. However, an area that requires further investigation is the impact of solvent selection that is used to dissolve the lipids and the effect this has on liposome physical properties. A variety of solvents can be used for this purpose; however, their use within pharmaceutical products needs to be carefully assessed. Some pose more significant toxicological concerns than others [154]. Solvents can be grouped into three classes. Class 1 solvents, such as benzene and carbon tetrachloride, should be avoided as they are known carcinogens, respiratory depressants and cause a variety of environmental hazards. Class 2 solvents are grouped into solvents that can cause other toxicities such as neurotoxicity or teratogenicity and are limited to doses of 0.1 mg/mL (10 ppm) (i.e. methanol, chloroform). Class 3 solvents (i.e. ethanol and IPA) are primarily regarded as the least toxic, with concentrations in pharmaceutical manufacturing deemed safe with no health hazard. However, this advice governs short term use as there is limited long-term analytics to show potential safety concerns. Solvent levels of 50 mg/day (corresponding to 5000 ppm [154]) are acceptable for class 3 solvents during manufacturing with no additional justification with higher levels permitted, providing they are in line with GMP requirements [154].

As part of the microfluidic manufacturing process, water soluble solvent streams mix with aqueous fluids allowing nanoprecipitation and self-assembly of vesicles [155]. The degree of solvent solubility in the aqueous phase is governed by carbon chain length. Orangic solvents with low molar masses (such as methanol, 32.04 g/mol) are more miscible due to many dipole-dipole interactions occurring through hydrogen bonding between the respective hydroxyl groups. Solvent polarity and the impact of mixing during microfluidics were investigated by Zook and Vreeland [91], where it was hypothesised that higher polarity solvents caused a reduction in lipid solubility. This is due to fewer intermolecular molecular forces driving lipids to self-assemble into planar lipid bilayers resulting in the increased size

of planar lipid bilayers. To reduce the surface areas of hydrophobic chains in contact with the polar solvent, they bend to form spherical liposomes (figure 3.1).

a) Disc growth due to aggregation of lipids into bilayer planar discs

b) Lipid discs begin to bend

c) Rapidly close

d) Spherical vesicles form
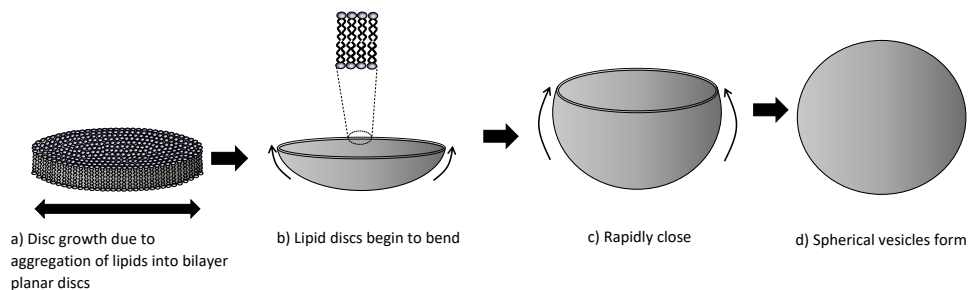
Figure 3.1 The hypothesised mechanism for liposome formation (adapted from Zook and Vreeland [1]. (A) The growth of lipid discs following (B) the bending of discs to reduce surface area of exposed hydrophobic chains to the water-miscible solvent leading to (C) rapid closure and (D) spherical liposome formation.

3.2 Aim and Objectives

This chapter aimed to investigate the effect of solvent polarity on the physical and chemical characteristics of the microfluidic production of liposomes. To achieve this, the objectives were:

- Perform an early screening study using a high throughput system for manufacturing DSPC:Chol (2:1 w/w) liposomes in either methanol (MeOH, 0.762 relative polarity), ethanol (EtOH, 0.654 relative polarity), and isopropanol (IPA, 0.546 relative polarity) to investigate if the vesicle size, PDI or zeta potential changes post microfluidic mixing as a result from solubilising DSPC and Chol in solvents with different relative polarities.
- Exploring if liposome size can be precisely controlled by adjusting solvent polarity when manufactured by microfluidcs.
- Evaluating if MeOH, EtOH or IPA can be used to solubilise lipid mixtures impacts on protein entrapment efficiencies post microfluidic mixing and if protein release kinetics are either increased or decreased as a result from the use of the either of the three solvents during microfluidic mixing.
- To identify if the liposomes morphology of lipsoomes (DSPC:Chol 2:1 w/w) using either MeOH, EtOH or IPA is altered as a result of the changes in solvent polarity by utilising

cryo-TEM. Such results would provide an insight towards the geometry of the liposomes produced by MeOH, EtOH and IPA and if the morphology of the vesicles is maintained across the three solvents.

3.3 Results and Discussion

3.3.1 Liposome characterisation by dynamic light scattering

3.3.1.1 Z-average diameter and uniformity

The particle size (Z-average diameter) and polydispersity index (PDI) can be measured by dynamic light scattering using a Zetasizer Nano ZS equipped with a 4-mW 633 nm He-Ne laser and a detection angle of 173 ° and has been used extensively within this thesis. The non-destructive measurement of samples records the velocity of the particles within the sample under Brownian motion, which is defined as the random movement of particles resulting from collisions with adjacent particles. Using the Stokes-Einstein equation (equation 3.1), the translation diffusion coefficient (D) can be converted to the particle size [156].

$$d_H = \frac{kT}{3\pi\eta D}$$

(3.1)

d_H = hydrodynamic diameter

k = Boltzman constant

T = temperature (K)

η = solvent viscosity

D = Translational diffusion coefficient

The translational diffusion coefficient function relies on various parameters such as the choice of diluent buffer, diluent buffer viscosity and analyte concentration in addition to the assumption that the particles are spherical [157]. The particle size recorded by the DLS measurement is known as the "hydrodynamic diameter", and the diameter gathered from the measurement is the diameter of the vesicle that is equal to the "translation diffusion coefficient" of the particle. The translational diffusion coefficient depends on factors such as media viscosity, which directly impacts the size measurement. Therefore, samples have been

suspended in d.H2O at a 1:10 dilution factor for consistency throughout this thesis. A detector analyses the scattered light and plots a correlation curve examining the diffusion of the particles to light fluctuations over time, with smaller particles (figure 3.2A) moving at higher velocities indicating faster changes than larger particles (figure 3.2B). These measurements can then be used to form a correlation function that describes the duration a particle remains within a fixed location within the sample. In the beginning, the correlation function (figure 3.2C and D) is linear (known as baseline), suggesting that the particle remains at the exact location. However, an exponential decay later occurs, suggesting that the particle is moving. The decay function represents the time it takes a particle to move from its relative positions. Smaller particles move faster, causing a quicker decay (figure 3.2C), and larger particles move slower, leading to a slower decay (figure 3.2D). The start of decay can be used to determine the Z-average diameter of the formulation with the steepness of the decay gradient used to indicate the polydispersity of the formulation [156, 157]. The most accurate measurement from DLS is known as the Z-average diameter, which is the average intensity of the particle diameter.
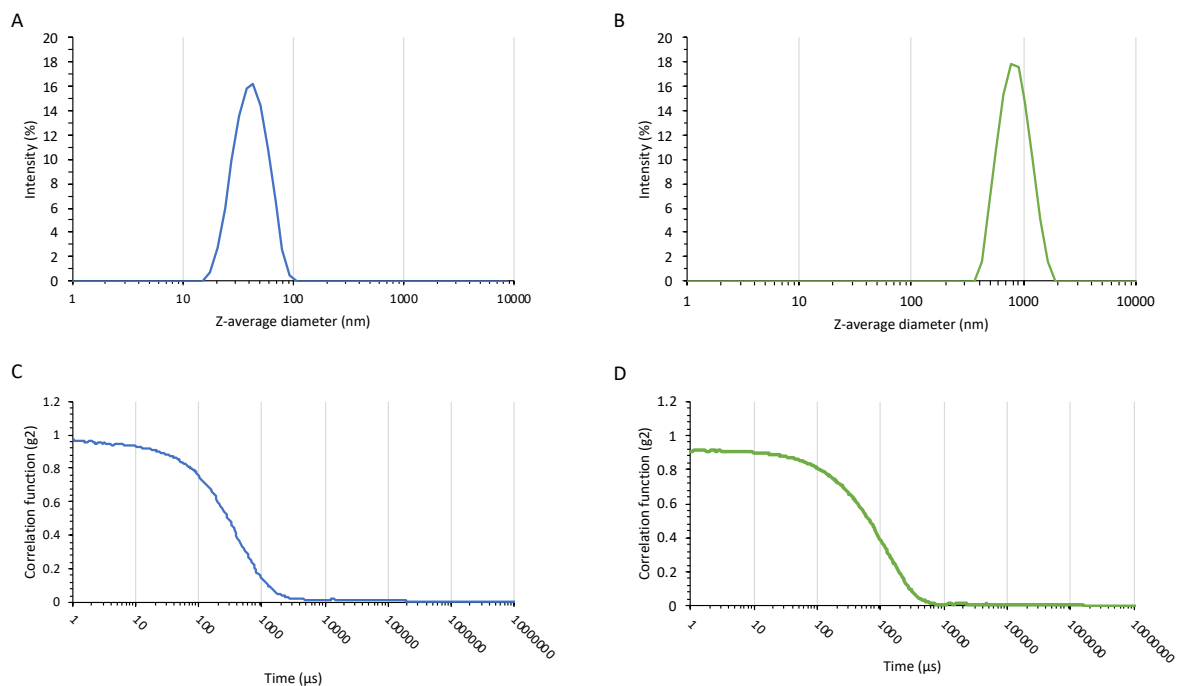
Figure 3.2 *Impact of particle size on intensity and correlation curve functions. Empty DDA:TDB (5:1 w/w) liposomes were prepared by microfluidics (approximately 100 nm in size) were measured by DLS and had their intensity distributions (A) and correlation function (C) recorded. Likewise, the same formulation was manufactured using lipid film hydration (approximately 600 nm in size) and had the intensity distribution (B) and correlaction function (D) plotted. A final concentration of 6 mg/mL was used for both samples prepared by microfluidics and lipid film hydration. Liposomes prepared using microfluidics had lipids dissolved in EtOH using a FRR of 3:1 and TFR of 10 mL/min. Liposomes prepared by lipid film hydration had lipids dissolved in chloroform:mEtOH (9:1 v/v).*

The Z-average diameter is a recognised ISO standard [158] and unless otherwise stated has been used as a measurement of vesicle size throughout this thesis. However, it cannot be compared to number-based size (such as sizes by microscopy) because it is an intensity-based calculated value. In addition, the measurement is sensitive to aggregates which can dramatically affect the calculated value [157]. Vesicle uniformity can also be calculated during particle size measurements, reported as the polydispersity index (PDI) with a value of 1 indicating a very heterogenous formulation. Berne and Pecora described PDI's exceeding 0.7 representatives of a highly dispersed formulation and cannot be accurately measured by DLS measurements. However, it has been shown with microfluidic manufacturing that formulations with tight size distributions can be achieved; therefore, a PDI criterion for formulations achieving PDIs < 0.2 was set within this thesis which would indicate a narrow a size distribution for liposomes

.

3.3.1.2 Zeta potential measurements

The zeta potential of particles is calculated through the development of a particle charge when a solid surface comes into contact with liquid through either the adsorption of ionic species onto the vesicle surface or ionisation of groups on the particle surface. An electrical double layer is formed comprising of a fixed and diffuse layer where an equilibrium is established between the two layers. Counterions become highly associated onto the surface of the particles and remain so within the fixed layer, creating the surface of shear that separates the fixed layer from the diffuse layer. In the diffuse layer, oppositely charged ions exist in equilibrium with the bulk solution but do not remain fixed to the particle. Measuring the charge at specific layers is difficult to accomplish; however, the closest approximation of the actual charge at the particle surface can be achieved by recording the charge at the surface of shear by electrophoresis.

However, some factors affect the zeta potential during measurement, such as the electrolyte concentration, as shown in figure 3.3. This is due to the equilibrium that exists between the double layer and the bulk solution. As the concentration of electrolytes increases, so does the concentration of electrolytes within the double layer. This will cause a significantly greater

proportion of electrolytes to exist within the diffuse layer and so will cause more electrolytes to be attracted onto the fixed layer. Due to an increased electrolyte concentration within the fixed layer, the particles actual charge becomes effectively masked which in turn will reduce the potential at the surface of shear. This is demonstrated in figures 3.3A and B, where diluting buffer concentrations causes an increase in the zeta potential due to the reduced electrolyte concentration to a point where an eventual plateau of the zeta potential is created. In addition, the salts' valency within the bulk also affects the zeta potential as more ionic species have greater attractive possibilities than less ionic particles. This can be demonstrated when Tris and PBS are used as buffers to record the zeta potential. When Tris is used (figure 3.3A), there is a significant difference between 0 and 10 dilution factors.
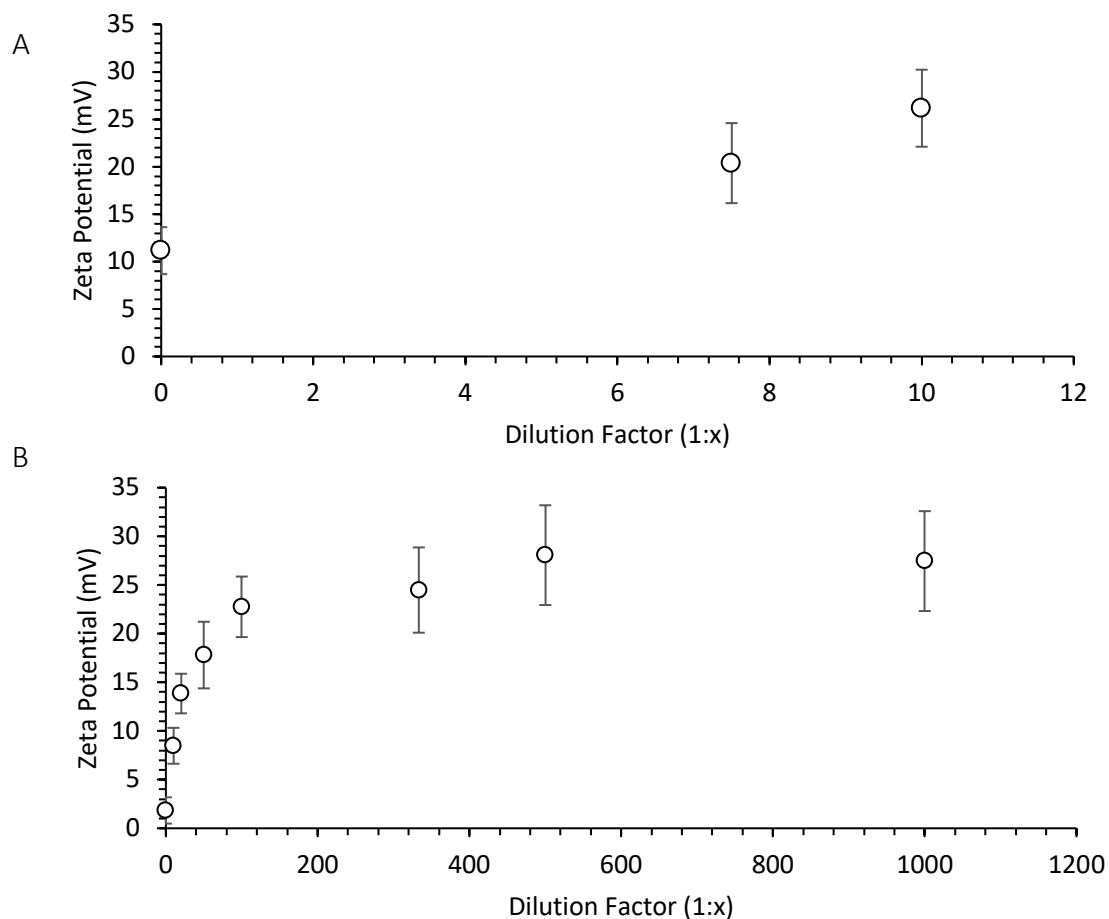
Figure 3.3 *Effect of buffer salts on zeta potential measurements. (A) Use of PBS as a diluent and (B) Tris 10 mM pH 7.4. Each was diluted to the desired dilution factor with d.H$_2$O. An initial concentration of 4 mg/mL HSPC:Chol:DDA (2:1:1.5 w/w) liposomes produced using a FRR of 2.5:1 and 12 mL/min TFR was used for the production of the liposomes used. Results represent mean ± SD from three independent batches.*

In contrast, when PBS (figure 3.3B) is used, a more gradual increase in the zeta potential arises as the PBS buffer becomes more diluted, indicating PBS to be a more ionic species requiring higher dilution factors to reach an eventual plateau of the zeta potential. When Tris is used (figure 3.3A), there is a significant difference between 0 and 10 dilution factors. From these results, all zeta potential recordings were measured using d.H$_2$O as a dilutent (1/10 dilution factor) to improve the consistency of the results and minimise the influence of the buffer on measurements.

3.3.2 High throughput screening studies demonstrate solvent polarity influences liposome physical characteristics

To investigate if using different solvents influenced the production of the vesicles, a high-throughput, low volume microfluidic manufacturing process was used to screen a range of formulations. Using a high throughput screening platform (Spark™; Precision NanoSystems Inc.), three formulations containing phospholipids with varying transition temperatures and cholesterol were selected.

Unlike other microfluidics cartridges that require syringes to force the fluid streams through the cartridges, the Spark™ utilises pressure for controlled low-volume and high-throughput manufacturing. Briefly, formulation buffer (PBS) was added to the outlet well with an aqueous solution pipetted into one inlet well with the lipids dissolved in either MeOH, EtOH, or IPA into the other inlet well. Lipid concentrations for each formulation were maintained at an initial 4 mg/mL using a combination of DPSC:Chol, DMPC:Chol and HSPC:Chol dissolved in either MeOH, EtOH or isopropyl alcohol (IPA).
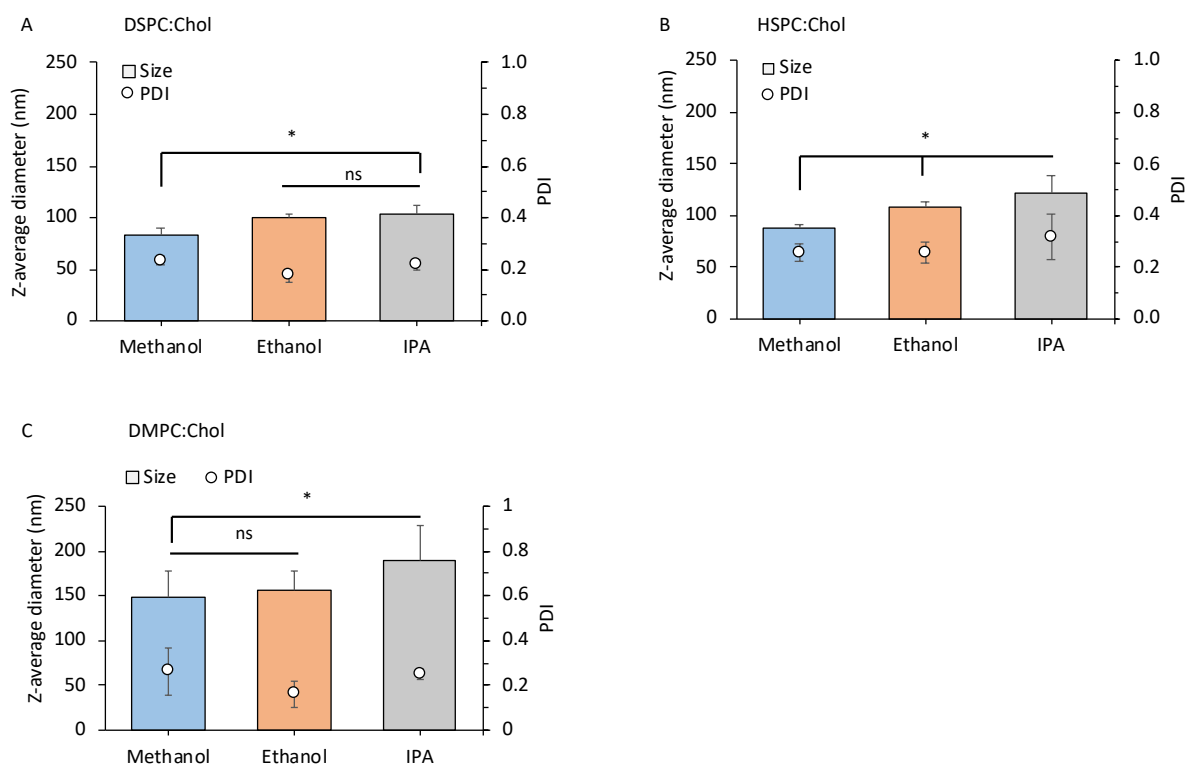
Figure 3.4 *Use of a low volume, high-throughput screening platform for liposome production in different solvents. Liposomes were manufactured using the Spark™ in different solvents (MeOH, EtOH or IPA) and mixed with PBS within the micromixer. Using (A) DSPC:Chol (2:1 w/w); (B) HSPC:Chol (2:1 w/w) and (C) DMPC:Chol (2:1 w/w). Liposomes are produced at a 3:1 FRR using a 4 mg/mL initial lipid concentration. Columns represent size of the liposomes and open circles represent PDI. Results represent mean ± SD from 3 independent batches. Statistical significance for vesicle sizes was calculated: (*) $p \leq 0.05$*

Across the three neutral liposomes tested, there was a steady increase in vesicle size moving from MeOH to EtOH to IPA. Using DMPC:Chol highlighted the largest difference in liposome size when IPA was compared to MeOH and EtOH. Using DSPC:Chol and HSPC:Chol (figure 3.4A and B), there was less impact when solvent polarity decreased (MeOH to IPA). With DSPC:Chol, there was an increase in size from approximately 83 ± 7 nm to 104 ± 8 nm, with significant differences between MeOH and EtOH. For HSPC:Chol, statistically significant size differences were obtained as solvent polarity increased, i.e. vesicle sizes increased progressing from MeOH < EtOH < IPA, with sizes of 88 ± 3 nm, 108 ± 5 nm, and 122 ± 16 nm for MeOH, EtOH, and IPA respectively with the PDIs across the thee solvents using the two formulations between 0.2 to 0.25. Using DMPC:Chol (figure 3.4C), which has a shorter phospholipid tail length than DSPC and HSPC (14C compared to 18C), the liposome sizes were larger across each respective solvent compared to the other two formulations. In MeOH, the size was 149 ± 7nm, which increased to 156 ± 20 nm and 190 ± 40 nm when dissolved in EtOH

106

and IPA, respectively. Results also show that DMPC:Chol was less uniform when compared to the formulations prepared using phospholipids with a phospholipid tail of 18C with PDIs between 0.2 – 0.3 (figure 3.4C).

The initial work in figure 3.4 used a low volume and high-throughput microfluidic platform to investigate if solvent polarity can impact the particle size with a tendency towards increased liposome sizes with reduced solvent polarity. It can be proposed that during the mixing process between the solvent and buffer streams that an increase in polarity results in the formation of lipid disks (figure 3.1). As solvent polarity is reduced (going from MeOH to IPA), the rate of change in polarity during the mixing process will be reduced, resulting in larger discs being formed, which subsequently close into larger liposomes [116] as observed in figure 3.3. The effect of phospholipid chain length on liposome particle size is in-line with other studies [117]. It was also shown that as the phospholipid tail length increases, a reduced vesicle size is observed. This may be due to a more significant number of Van der Waals interactions causing a more rigid lipid bilayer, resulting from a stronger cohesion [159]. This promotes closely packed chains within the bilayer explaining why DMPC:Chol liposomes are larger than DSPC:Chol and HSPC:Chol. Furthermore, DMPC:Chol liposomes lead to an increased PDI, which is also comparable to the work by Zook and Vreeland, where it was also shown that larger liposomes led to a more dispersed formulation [91]. The authors' summation for this effect was due to the PDI's dependency on median liposome size, with liposomes being more polydisperse as their median size increases as the measurement is the width of particle size distribution compared to the median size.

3.3.3 Cholesterol modifies lipid bilayer elasticity and influences solvent impact

While liposomes have been demonstrated to be a versatile formulation in permitting the incorporation of hydrophilic and lipophilic molecules within liposomes [13, 14], one of the physical chemical factors affecting their use is their physical and chemical stability. Within the phospholipid bilayer, chemical and physical degradation reactions can occur in terms of ester bonds becoming hydrolysed and phospholipid oxidation in unsaturated acyl chains [160, 161]. Furthermore, liposome aggregation, flocculation and coalescence [162, 163] can further

hinder liposome use as a therapeutic formulation by reducing shelf-life. Although early studies demonstrated that the inclusion of cholesterol 50% mol/mol (2:1 w/w) within the formulation improved liposome stability [84], it was found that molar concentrations between 20 to 50% allowed cholesterol to dissolve within the liposome bilayer improving packing densities [164]. In contrast, concentrations greater than this led to crystallised regions [165]. However, a significant hurdle in developing liposomal drug delivery carriers is the requirement to prolong circulation time. This allows vesicles to reach target tissues through prevention of macrophage interception in the liver and spleen, commonly known as either the mononuclear phagocyte system or reticuloendothelial system (MPS or RES respectively). This limitation was noted early on in 1973 by Gregoriadis and theorised the desire to direct liposomes to cells other than the liver or spleen by specific formulation manipulations [166-168]. In 1980, the same author published findings addressing this concern, where it was discovered that the incorporation of cholesterol (equimolar to the phospholipid) within the bilayer permitted greater half-life of liposomes within the circulating blood [169]. The improvements phospholipid packing density that cholesterol promotes within the bilayer [170, 171] also resisted the destabilising impacts of lipoproteins [167, 168] leading to a reduction in drug loss [169].

It has been demonstrated that the inclusion of 50% mol/mol cholesterol allows for gel-to-liquid transitions to be abolished, permitting the use of thermo-sensitive compounds to be incorporated during the manufacturing process and broadening phase transition temperatures. This effect has been proven using a variety of techniques, including differential scanning calorimetry [172], temperature scanning x-ray diffraction [173] and more recently Langmuir studies [85]. This phenomenon was further investigated using microfluidics, and it was found that regardless of cholesterol percentage within the formulation, liposome formation could occur below lipid transition temperatures [117]. Interestingly, what was found in this study [117] was that as the cholesterol content increased, vesicle size was reduced.

To investigate membrane elasticity further and the impact solvent selection has on liposome formation, cholesterol concentrations ranging from 11% to 33% were used with DSPC. The size and PDI measurements were recorded at each cholesterol concentration using either

MeOH, EtOH, or IPA as the solvent (Figure 3.5). At 11% cholesterol concentration, only liposomes formulated in MeOH could be sized (~100 nm). Large aggregation of the lipids was noted when EtOH and IPA were used and subsequently resulted in high PDIs across the three formulations. At a cholesterol concentration of 33% (2:1 w/w lipid:cholesterol), the sizes for MeOH, EtOH, and IPA were 45 ± 1 nm, 55 ± 3 nm, and 95 ± 1 nm, respectively (Figure 3.5), which were lower than the results obtained in figure 3.4A. This can be attributed to the more controlled TFRs (15 mL/min) that can be achieved using a syringe pump (figure 3.5) instead of the fluid rates through the microchannels driven by pressure (figure 3.4). For the formulations incorporating 18, 25, or 33% cholesterol, the PDI (figure 3.5B) remained below 0.2 across the three solvents indicating good uniformity in the vesicles produced. However, the PDIs at 18% (8:1 DPSC: Chol w/w) when formulated in IPA and EtOH could not be accurately recorded.
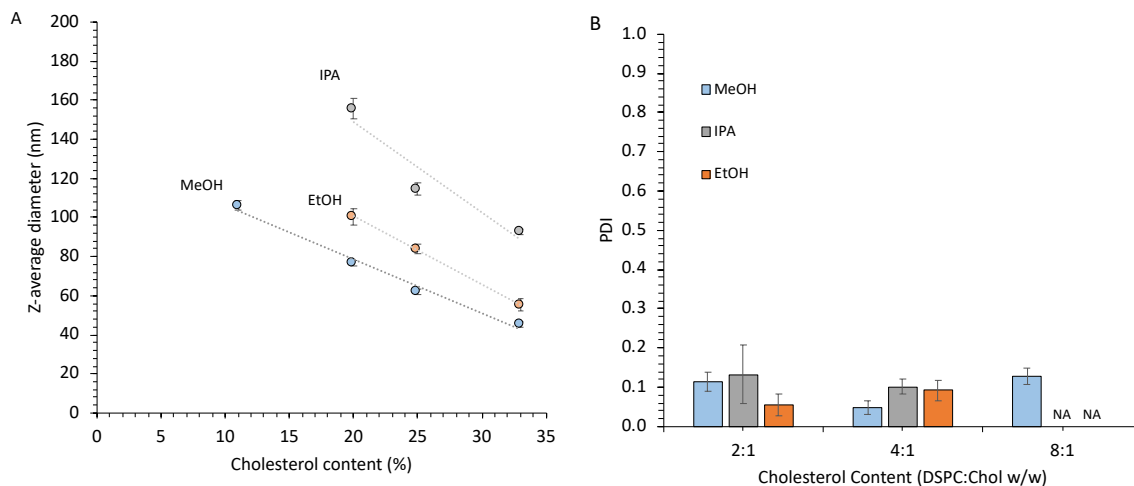
Figure 3.5 *Effect of cholesterol content on liposomes manufactured using microfluidics. Cholesterol was increased from 11 to 33% using DSPC:Chol and DMPC:Chol using a 3:1 FRR, 15 mL/min and 4 mg/mL initial lipid concentration with liposome size (A and C) and PDI (B and D) investigated. Results represent mean ± SD from 3 independent batches.*

Results published by Genova et al., found that increasing cholesterol percentage from 0 to 50% within 1-stearoyl-2-oleoyl-*sn*-glycero-3-phosphocholine:Chol lead to a significant increase in membrane bending elasticity [174] resulting from improved lipid packing arrangements around the cholesterol molecule [171]. Whilst there were no liposome sizes reported within this study, it was surmised that as a result of higher cholesterol concentrations, there is an increase of bending elasticity within the bilayer, permitting smaller

vesicle sizes with additional evidence that cholesterol can function as a cavity filler within the lipid bilayer further improving packing densities [175]. From the results in figure 3.5, it has been demonstrated that cholesterol does affect lipid bilayer physical characteristics and at higher cholesterol concentrations can reduce the impact of solvent polarity against liposome size. This suggests that the ordered packaging of lipids to form liposome bilayer supersedes the effect of solvent polarity in terms of vesicle size.

However, it has been desmonstrated that solvent selection is an important characteristic which can be used to control vesicle size. Such a mechanism can be described within microfluidics in terms of the hydration of the solvent, governed by molecular diffusion, at the interface where the aqueous and solvent phases meet. For a more polar solvent, such as MeOH with has a relative polarity of 0.762, there is a smaller rate of change between the polar aqueous phase and polar solvent accelerating lipid discs closure. Conversely, it could be theorised that for a less polar solvent like IPA (relative polarity of 0.546), lipid disc closure is prolonged due to increased duration to hydrate the solvent leading to enlarged lipid discs and subsequently larger vesicles, as shown in figure 3.6. Additionally, the authors' Shah et al., investigated lipid nanoparticle formation mechanisms during microfluidic production using EtOH and attributed mixing rates to be a crucial parameter [176].

Solvent	Relative polarity
Water	1.00
Methanol	0.762
2-propanol	0.546
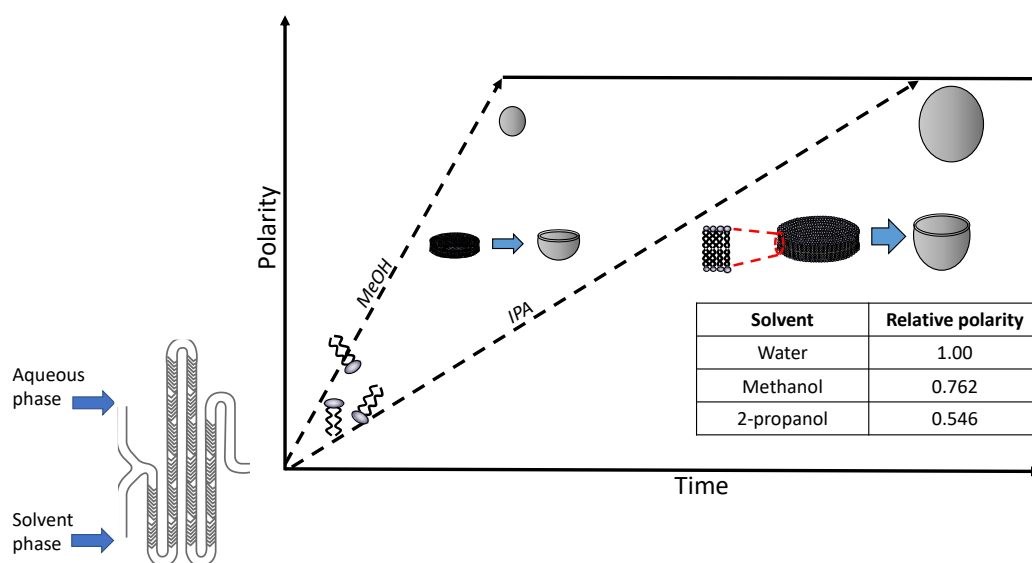
Figure 3.6 *A schematic highlighting the liposome formation process within the microfluidic cartridge. Depicting time differences of MeOH and IPA to achieve vesicle closure leading to the formation of larger lipid discs and thus larger liposomes.*

3.3.4 Effect of temperature on liposome formation using IPA

From previous findings by Jahn et al., it has been shown that applying microfluidics for liposome production makes it possible to form liposomes through self-assembly, allowing the formation of liposomes below the associated phospholipid transition temperatures, which supports the results in figure 3.4 and 3.5 [92, 177]. To further investigate this effect, the temperature was precisely controlled using a heating block, allowing a temperature of 25 °C and 60 °C to be used, permitting the production of liposomes both below and above the transition temperature of DSPC (55 °C).

Figure 3.7 showed a significant increase ($p < 0.05$) in vesicle size when the liposomes were formulated in IPA at 20 °C compared to 60 °C. At 25 °C, the sizes were consistent with the results in figure 3.5 (where the liposomes were formulated at room temperature without temperature control). From Figure 3.7, it is shown that at 20 °C, a vesicle size of 91 ± 4 nm was obtained, which was significantly smaller than the 148 ± 11 nm vesicles produced at 60 °C. Despite the significant size variances, there was no statistically significant difference in the PDI of the respective vesicles, with each good demonstrating uniformity with values < 0.2.
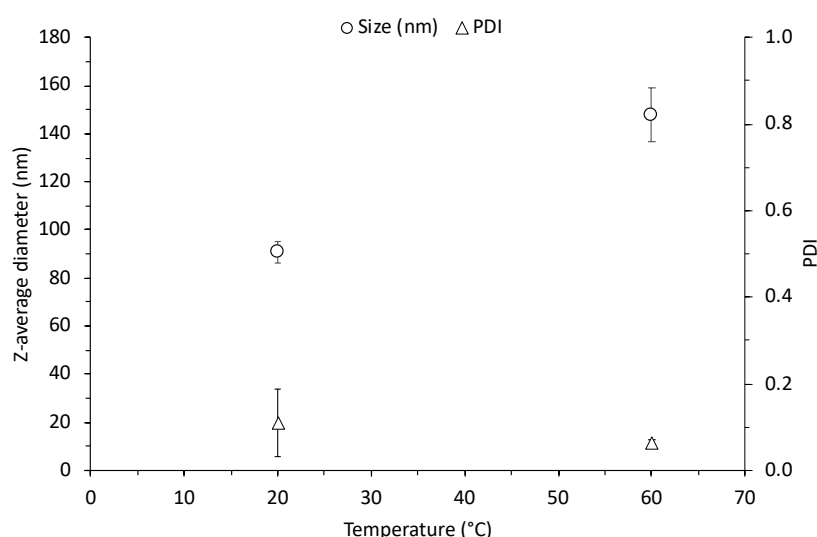
Figure 3.7 Working above transition temperatures and the effect on liposome size. DSPC:Chol (2:1 w/w) liposomes were manufactured in IPA at a 3:1 FRR; 15 mL/min TFR and initial lipid concentration of 4 mg/mL at ambient room temperature (plotted at ~20 °C) or 60 °C. Sizes are plotted as open circles (○) and PDI as open triangles (△). Results represent ± SD from 3 independent batches.

Similar temperature-dependent size changes have also been observed in other studies using EtOH as a solvent [178]. A similar experiment using microfluidics was conducted by Forbes et al. using MeOH and DSPC:Chol (10:5 w/w) with temperatures ranging from 17 to 60 °C, and it was found that the liposome sizes remained consistent at approximately 50 nm [117]. Furthermore, the results in figure 3.7 are also well aligned with Zook et al.'s observations, using DSPC liposomes within IPA. The authors hypothesised three possible ways in which temperature affects growth rate and closure time using a microfluidic system but concluded that in their microfluidic system, that changes in the membrane elasticity led to the observed changes as it affects the bending elasticity modulus to the line tension (the tension of exposed hydrophobic tails). It has been demonstrated that at temperatures below the transition temperature of the phospholipid that the elasticity of the membrane is 2 – 5 times higher ("stiffer") compared to the bending elasticity above the transition temperature [91], allowing smaller liposomes to be formed which is in line with the trend in the results seen in figure 3.7 and also Forbes et al [117]. A further explanation for the increase in size observed in figure 3.7 could be due to the improved solubility of the lipids in IPA. Tran et al., found that using differential scanning calorimetry, there is a decrease in the phase transition temperature when EtOH is heated [179], causing the lipids to change from an ordered (gel) arrangement to a disordered state (liquid crystalline). This can lead to the mobility of the lipid head groups to increase with the lipid tails able to move more freely, making the lipid bilayer less rigid causing the vesicle size to increase.

The ability for microfluidics to operate below lipid transition temperatures could be owed to the fact that alcohols are known modulators of bilayer properties [180]. Within this chapter, the solvent has been removed by TFF after liposome production, however, the influence of alcohol on bilayer properties is a factor to consider during microfluidic production. Studies have highlighted that water-soluble solvents can promote bilayer disorder, and in particular short-chain alcohols, such as MeOH, scales linearly with their bilayer partitioning [180, 181]. The bilayer packing is distributed due to the way alcohols sequester within the layer as the hydroxyl group is within the interfacial region, while their methyl heads are towards the hydrophobic core of the bilayer [182]. As the chain length of the alcohol increases, the additional methyl groups raise the alcohols partition coefficient within the bilayer increases up a carbon chain length of ≥ 6 where the chain is long enough to diminish the influence of

the alcohol's disruptive effects on the bilayer [180]. Therefore, during the production of liposomes, using the investigated miscible solvents MeOH, EtOH and IPA permits bilayer disruption of the bilayer discs allowing vesicle formation to occur below the transition temperature.

3.3.5 Varying solvent composition to tailor liposome size

From figures 3.4, 3.5, and 3.7, solvent polarity has been shown to influence liposome Z-average diameter leading to a causative effect to their respective sizes. To further investigate this and track liposome size attributes with changing polarity, solvent mixtures were made, allowing liposomes to be formulated from DSPC:Chol (2:1 w/w). The solvent mixtures were composed of 0 – 100 % of either MeOH/EtOH, MeOH/IPA, or EtOH/IPA, all formulated at a 3:1 FRR at 15 mL/min with an initial lipid concentration of 4 mg/mL.

The results in figure 3.8 allowed for an in-depth analysis of solvent mixture refinement that can be employed to meet precise size criteria using the investigated formulation. Figure 3.8A demonstrates that MeOH and EtOH can be precisely mixed to allow significant variances in liposome size, with particle sizes increasing from 45 ± 1 nm to 53 ± 2 nm. Likewise, when investigating the most polar and least polar solvents of the three investigated (i.e. MeOH and IPA, respectively), the sizes obtained from each solvent mixture was highly significant ($p < 0.001$) when compared against other mixtures. The largest size differences observed when 100% MeOH and 100% IPA was used with a similar trend also observed when an EtOH and IPA mixture was used with significant differences observed between each solvent mixture. Across all solvent mixtures, the PDI was low (< 0.2) with good uniformity, as shown from the intensity-weighted size distribution plots in figures 3.8B, D, and F.

The empirical solvent polarity (ESP) can be calculated from molecule dielectric constants and refractive indices of each solvent [183]. The ESPs are calculated relative to water (1.00), of which the relative values for MeOH, EtOH, and IPA are 0.762, 0.654, and 0.546. The slight difference in ESP between MeOH and EtOH can account for the moderate size increase transitioning between MeOH and EtOH but the smaller ESP for IPA relative to the other two

solvents can provide further rationale for the larger size differences observed. To explain the larger sizes observed using less polar solvents, a model proposed by Zizzari et al., could be used to describe the findings [184]. Their hypothesis was used to explain why at lower FRRs, larger liposomes are formed due to increased time for lipids to assemble lipid discs. The model could be extrapolated further to account for the improved stability of suspended lipids resulting from the increased solubility when more non polar solvents are used (i.e. IPA). This, in turn, will prolong the time lipid discs are allowed to grow, resulting in larger vesicle sizes. When more polar solvents are used, such as MeOH, there is reduced lipid solubility, which reduces the stability and the time lipid discs are allowed to grow, resulting in smaller liposomes. While the direct mechanism behind liposome formation, whether disc growth or rate of disc closure [1], could be further defined in future studies. It has been demonstrated that it is possible to manipulate liposome size by controlling solvent mixtures finely.
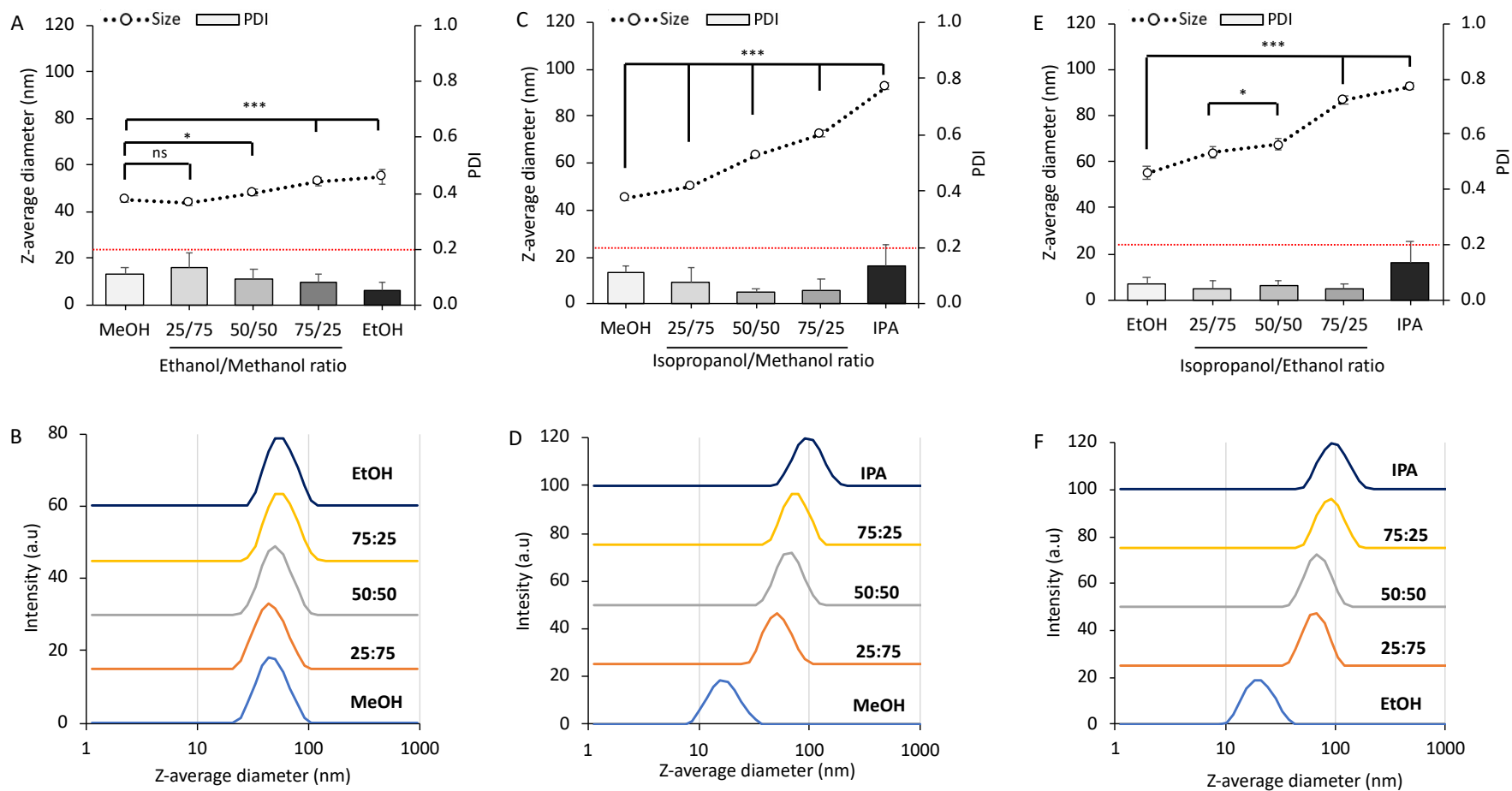
Figure 3.8 *Investigating solvent mixtures liposomal size and uniformity. DSPC:Chol (2:1 w/w) liposomes were manufactured at 4 mg/mL and dissolved in (A) MeOH:EtOH 0-100 %; (C) MeOH:IPA 0-100% and (E) Ethanol:IPA 0-100% with intensity-weighted size distribution for each solvent mixture (MeOH:EtOH (B); MeOH:IPA (D) and EtOH:IPA (E)). Liposomes were manufactured at a FRR of 3:1; 15 mL/min TFR and initial lipid concentration of 4 mg/mL. Results represent mean ± SD from 3 independent batches. Statistical significance: (*) p ≤ 0.05; (***) p ≤ 0.001*

3.3.6 Effect of solvent selection on liposome stability and protein encapsulation

3.3.6.1 <u>Downstream purification: Tangential flow filtration</u>

Tangential flow filtration (TFF) is a rapid and scalable method for purifying liposomes, allowing for solvent removal and non-incorporated ('free') protein removal by appropriate selection of TFF pore sizes. Unlike traditional liposomal production methods such as lipid film hydration, where the solvent is evaporated, microfluidic preparation contains residual solvent within the formulation post-production. Techniques such as dialysis can remove the solvent; however, this is often time-consuming and not scalable. Therefore, utilisation of a scalable method such as TFF would allow both the purification of the sample by 'washing' out the residual solvent and allow for the separation of 'free' particulates such as unentrapped proteins through the selection of specific pore sizes, which would retain the larger liposomes and remove small particulates through the pores within the membrane. Briefly, samples are passed across the membrane surface, and moieties smaller than the pore size pass through the membrane and leave the system (permeate; figure 3.9A). At the same time, the remainder (retentate) is recirculated back through the system. The solvent was removed from liposomal samples in a KR2i TFF (Lab spectrum) using a modified polyethersulfone (mPES) column with a pore of 100, 500, or 750 kDa. The process rate is primarily governed by transmembrane pressure (TMP), which accounts for the differences in pressure at the feed inlet against the permeate outlet, which can correspond to the degree of "shear" a formulation experiences during the process. To determine the optimum number of wash cycles for neutral formulations to remove free protein, 1 mL of neutral liposomes consisting of DSPC:Chol (2:1 w/w; 4 mg/mL initial lipid concentration) with OVA (0.25 mg/mL initial protein concentration) incorporated by microfluidics was washed with a 12 mL diafiltrate volume of PBS from results obtained in figure 3.9B. Using the Nanodrop 2000, 1 mL of Tris containing 200 µg/mL OVA was passed through the TFF with 1 mL aliquots of permeate collected and absorbances measured separately. From this, it was found that 12 wash cycles were required to altogether remove 1 mL 'free' OVA in a solution while maintaining liposomal characteristics both before and after purification. To examine physical changes in the liposomes after TFF, neutral liposomes composed of DSPC:Chol (2:1 w/w) were solubilised in EtOH and mixed with OVA in PBS at a 3:1 FRR with size measurements taken both before and after TFF. From figure 3.9C, there was

no impact on the size before and after TFF, 87 ± 2 nm and 85 ± 2 nm, respectively, with PDIs remaining below 0.2, indicating good sample uniformity as shown in the respective intensity plots. On a separate day, using the same formulation and production parameters as figure 3.4C pressure measurements were recorded at the feed and outlet inlet, allowing the transmembrane pressure to be extrapolated in figure 3.9D. Using a diafiltrate volume of 12 mL/1 mL of sample, a total volume of 22 mL of buffer was used to purify the formulation with slight increases in the pressure recordings at both the feed and outlet sensors. The TMP pressure was maintained between 2 – 5 PSI which was within the operational boundaries set from the current literature [185, 186].

TFF is a well-documented technique that has a developed history initially within the non-pharmaceutical industry before progressing into pharmaceuticals [100]. This technique has also been proven to be an established method within the laboratory with Forbes et al., reporting that solvent removal can be achieved within 12 washes using MeOH and was below the ICH recommended solvent level for MeOH of 3000 parts per million (0.3% v/v) [117]. As EtOH was used for the results in figure 3.4, the solvent levels are well below the recommended concentration of 5000 parts per million (0.5 % v/v) which the ICH has suggested [154]. In terms of downstream liposomal purification, the purification process is well placed over other techniques such as dialysis or gel filtration given its proven implementation within a continuous manufacturing setting and additional advantages to concentrating samples to desired concentrations that could benefit formulations involving lipids with poor solubility profiles.
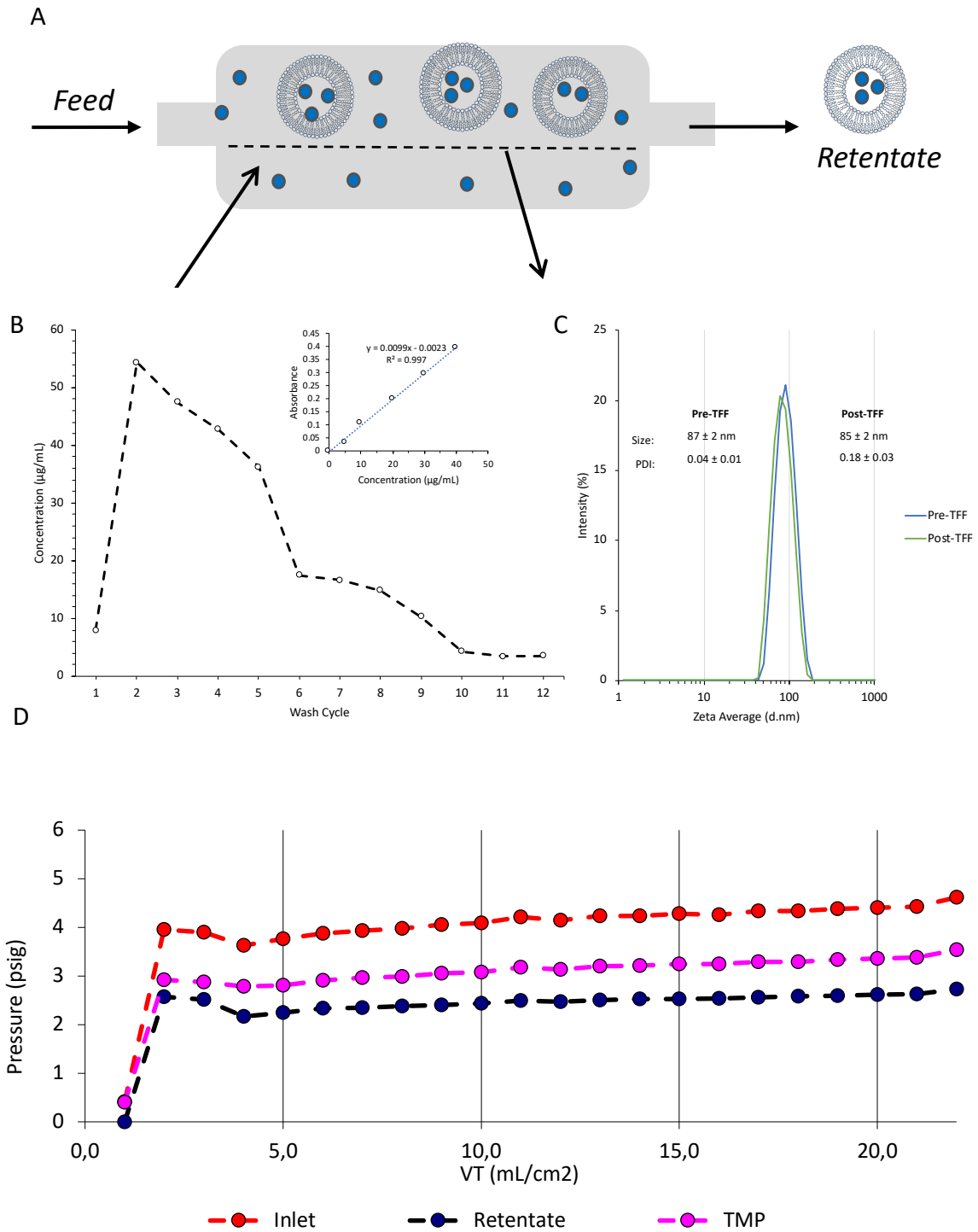
Figure 3.9 *Determination of "wash cycles" required to purify unentrapped protein while maintain vesicle characteristics. (A) 12 washes was determined by removing 1 mL of 300 µg/mL "free" OVA from the column suspended in Tris 10 mM. (B) DSPC:Chol (2:1 w/w) liposomes were sized both before and after 12 washes of TFF to ensure vesicle characteristics were maintained. On a separate 2 mL samples, the pressure obtained at inlet and outlet sensors was measured against volumetric throughput (D).*

3.3.6.2 Solvent selection does not influence liposomal stability or protein release kinetics

To investigate if the choice of solvent impacted short-term liposome stability, the stability of DSPC:Chol (2:1 w/w) liposomes formulated in MeOH, EtOH, or IPA was assessed over 7 days with liposomes refrigerated at 4 °C. A 2:1 w/w lipid/cholesterol ratio or 1:1 molar ratio was selected to maintain formulation continuity throughout the experiments and other literature stating that 50 % mol/mol for lipid and cholesterol lead to the most stable liposomes [84, 169]. The encapsulation efficiency of OVA was also investigated with a 5-day release study to identify if solvent selection had any impact on the liposomes' ability to entrap and release protein. Liposomes were prepared using a 3:1 FRR at 15 mL/min TFR with a 4 mg/mL lipid concentration and an initial protein concentration of 250 µg/mL. The formulation was then purified using TFF with a 12 mL diafiltrate volume. Protein entrapment was quantified using RP-HPLC. For the protein release study, concentrations for both lipid and protein were produced at a 4-fold higher concentration (i.e. 16 mg/mL initial lipid concentration and 1 mg/mL initial protein concentration).

From the stability study in figure 3.10A, the only significant size ($p \leq 0.05$) variances occurred when EtOH was used as a solvent, with significantly different sizes occurring between days 1 – 5 and between days 5 and 7. This was primarily due to do the mean sizes recorded on day 5 being greater than 60 nm while comparatively the sizes recorded on each other respective day were ≤ 55 nm. IPA and MeOH were both shown to produce highly stable liposomes across the days with no significant sizes variances between the days of each respective solvent. Again, using DSPC:Chol as a formulation, IPA produced the largest liposomes are were approximately 90 nm whilst the more polar solvent MeOH produced the smallest liposomes of the solvents investigated at approximately 45 nm in size. When PDI was studied in figure 3.10B, all formulations started at a PDI of < 0.2; however, after day 1, liposomes produced in MeOH were the least uniform with PDIs exceeding 0.2. Liposomes made in EtOH and IPA were able to maintain good uniformity with PDIs < 0.2 across the 7 days. An RP-HPLC calibration curve (figure 3.10C) was built using empty DSPC:Chol liposomes (2:1 w/w) with a solubilisation mixture (IPA:buffer 50:50 v/v) with increasing ovalbumin concentrations at a final concentration of 0 – 1 mg/mL, the RP-HPLC method has been described in section 2.4.2.3. In figure 3.10D, the loading values for MeOH and EtOH were 36 ± 1%, 38 ± 2%, and when IPA was used, entrapment efficiency was 24 ± 1%. There was no significant difference

between MeOH and EtOH ($p > 0.05$). Still, there was a significant reduction in the liposomes' ability to entrap OVA when IPA was used compared to the other two solvents ($p \leq 0.001$).
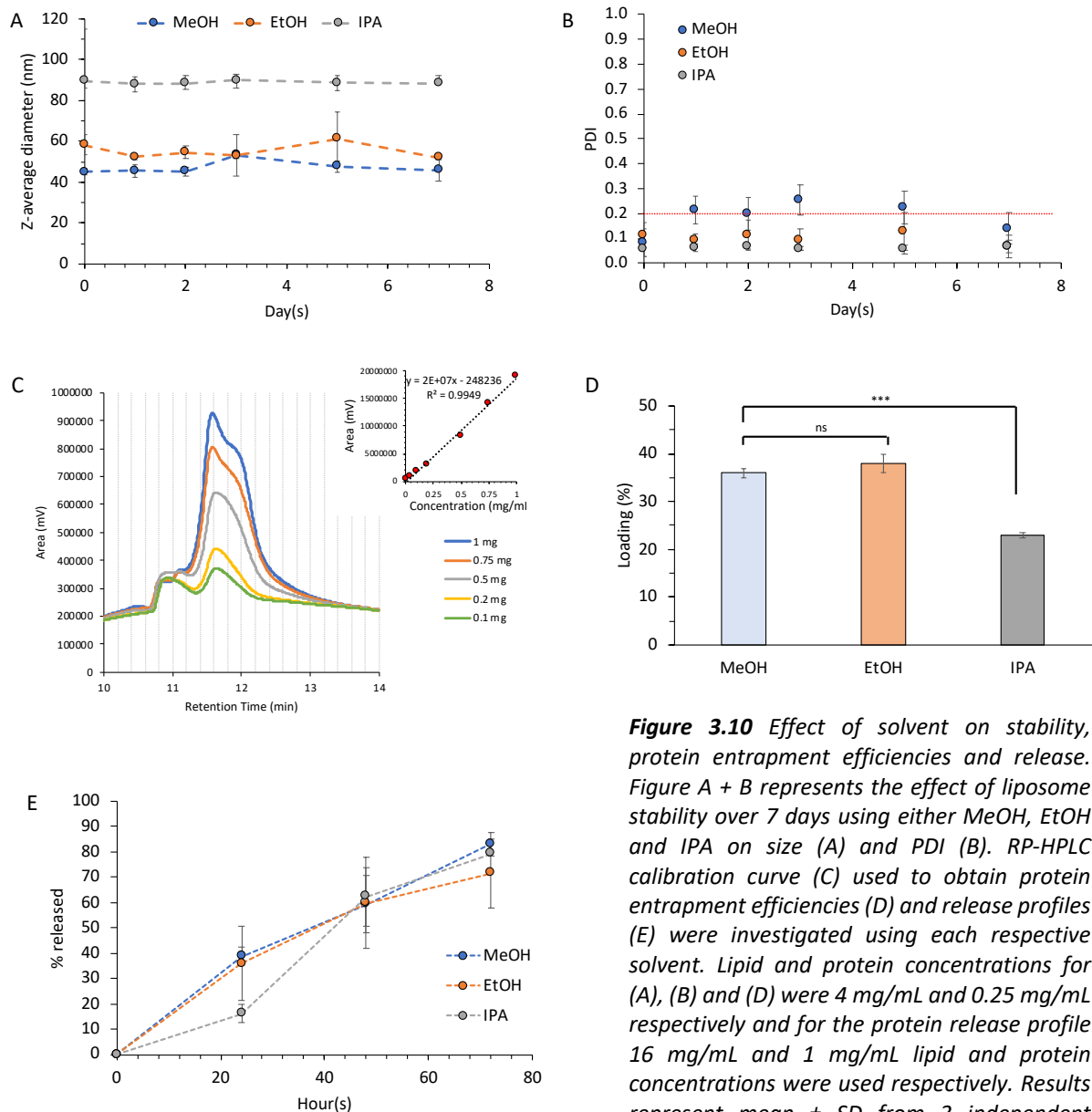
Figure 3.10 *Effect of solvent on stability, protein entrapment efficiencies and release. Figure A + B represents the effect of liposome stability over 7 days using either MeOH, EtOH and IPA on size (A) and PDI (B). RP-HPLC calibration curve (C) used to obtain protein entrapment efficiencies (D) and release profiles (E) were investigated using each respective solvent. Lipid and protein concentrations for (A), (B) and (D) were 4 mg/mL and 0.25 mg/mL respectively and for the protein release profile 16 mg/mL and 1 mg/mL lipid and protein concentrations were used respectively. Results represent mean ± SD from 3 independent batches. Statistical significant: (ns) p > 0.05; (*) p ≤ 0.05 (***) p ≤ 0.001.*

The protein release rates (figure 3.10E) were then compared to analyse if solvent affected the protein release profiles. An f_2 similarity factor calculation was carried out between the curves to establish if there is a statistical similarity in release profiles. A public standard of f_2 value between 50-100 indicated similarity between the two release profiles. From the results it was found that the three release profiles had strong similarities in protein release rates as values

were all >50 (MeOH + EtOH = 0.80; MeOH + IPA = 0.88; EtOH + IPA = 0.71) with results reaching ~ 80% after 72 hrs.

All the formulations demonstrated good stability across the 7 days tested in figure 3.10A and agree with published studies using the identical lipids and molar or weight ratios. Webhe., et al used a comparable formulation and extended a study for an additional 7 days; despite some statistically significant results using EtOH during some of the study (figure 3.10A), the sizes obtained on day 0 and day 7 were not statistically significant [178]. This could be attributed to the cholesterol within the formulation providing formulation stability. Incorporating cholesterol within the bilayer improves packing efficiencies and densities [164] by filling empty pockets within the bilayer, making it more compact [165] and improving vesicle bilayer stability. The destabilising effects of solvents can be further seen in the PDIs for each mixture tested in figure 3.10B. During the stability study, it was found that the higher polarity solvents caused higher PDIs indicating greater heterogeneity compared to more non-polar solvents such as IPA, which were more homogenous.

Interestingly, this refutes the point made by Zook and Vreeland, who indicated that larger liposomes produced greater PDIs as they noted that PDI is a measurement of the width of the size distribution compared to median size [91]. However, as noted by both Ingólfsson et al., and Zeng et al., shorter chain solvents promote greater disorder within the layer and so could extend the size distribution of vesicles leading to elevated PDIs as observed in figure 3.8B [180, 181]. Using the calibration curve obtained in figure 3.10C the protein encapsulation was investigated (figure 3.10D), with the results indicating no significant effect in using MeOH or EtOH, with results in line with previous publications [187]. Lower protein encapsulation results ($p \leq 0.001$) were seen when using IPA, highlighting possible incompatibilities using IPA with the protein.

Interestingly, the release profiles in figure 3.10E across all three solvents were similar, as shown by their f_2 values. Alcohols can modulate bilayer properties by influencing bilayer packing disorder and their partitioning [180] by inserting their hydroxyl group within the bilayer and hydrophobic carbon groups sandwiched within the hydrophobic core [182], leading to disorder. This effect was also exploited in terms of drug loading by Wehbe et al.,

where the authors were able to passively load carboplatin (a chemotherapeutic agent) across the lipid bilayer and equilibrate using EtOH combined with heat that was found to act as a permeability enhancer without affecting the liposome structure [178]. From the results, it has been demonstrated that stable formulations can be manufactured using solvents of varying polarity.

3.3.6.3 Solvent selection influences liposome morphology

The liposome morphology for each formulation manufactured in MeOH, EtOH, and IPA was accomplished using cryo-TEM. Using cryo-TEM would allow a detailed insight in the geometric structure and offer a potential rationale for the increased sizes observed. The same protein-loaded formulation used throughout the chapter was manufactured using DSPC:Chol (2:1 w/w; 4 mg/mL initial lipid concentration) and 0.25 mg/mL initial OVA concentration, which was then purified via TFF using a diafiltrate volume of 12.

Methanol   Ethanol   IPA
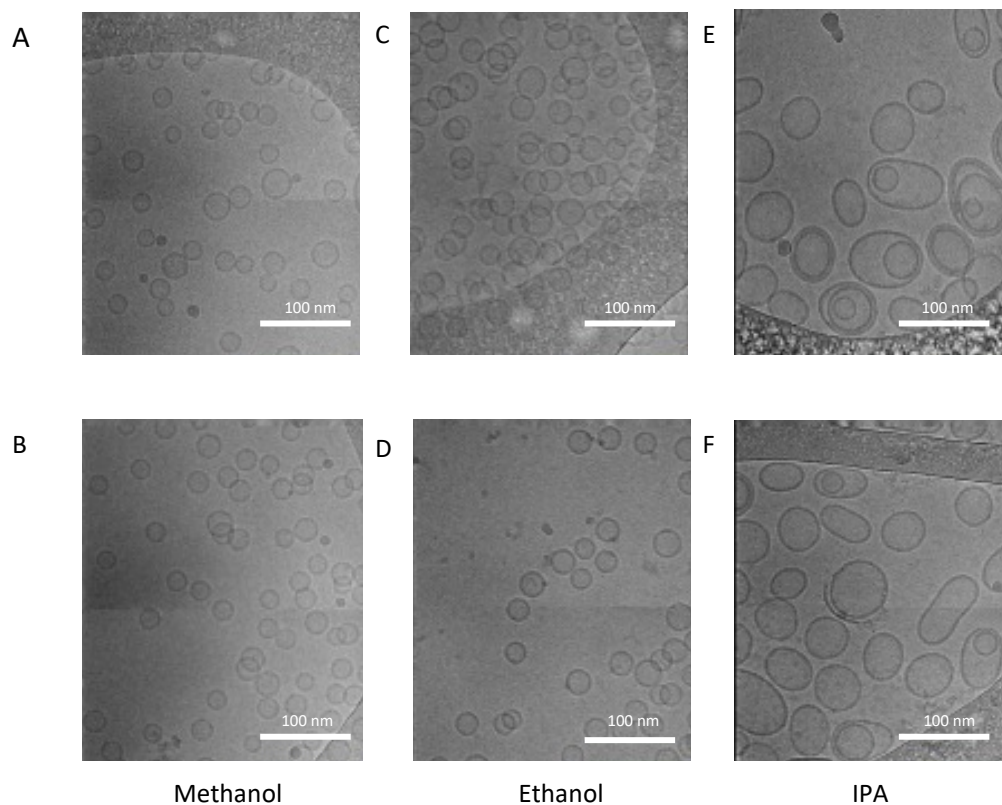
Figure 3.11 *Structural changes in liposomes as a result of solvent selection. Cryo-TEM images were recorded in MeOH (A+B); EtOH (C+D) and IPA (E+F). Liposomes were manufactured at a 3:1 FRR; 15 mL/min and initial lipid and protein concentrations of 4 mg/mL and 0.25 mg/mL.*

From the images, both MeOH (figure 3.10A+B) and EtOH (figure 3.10C+D) lead to small unilamellar vesicles (SUVs), which have been observed in previous publications [153] while liposomes manufactured in IPA (figure 3.10 E+F) lead to vesicles with multiple bilayers. The cryo-TEM further validates the DLS recordings as liposomes were within the range of previous size measurements for each formulation. It can be postulated that SUVs can form due to small lipid discs, as previously discussed when solvent polarities are high. However, as a result of larger lipid discs forming using a more non-polar, which improves lipid solubility during vesicle bending, larger discs begin to engulf smaller lipid discs leading to liposomes with multiple bilayers. Interestingly, it could have been expected due to the larger size of the vesicles that the hydrophilic core would have a larger aqueous compartment allowing for improved protein loading efficiencies. However, this was found not to be the case in figure 3.9C, where a significant decrease in loading efficacies (p ≤ 0.001) was observed, possibly perturbed. However, the optimised solubilisation method has been developed for SUVs and not liposomes with multiple bilayers; therefore, it could mean that the solubilisation procedure would need to be refined further to ensure that all vesicles were lysed.

3.4 Conclusion

From these studies, it has been shown that solvent selection is a critical process parameter that can be used to manipulate and control liposome characteristics. It was also demonstrated that by using precise solvent mixtures would allow the fine-tuning of liposomes to desired sizes. Additionally, of the two-class 3 solvents investigated (IPA and EtOH), the experiments have shown EtOH to be the most effective solvent in terms of the liposome size, production of SUVs (liposome geometry verified by cryo-TEM) and higher protein entrapment efficiencies. The results from this chapter have indicated that a class 3 solvent can be used for the effective production of liposomes allowing improvd safety profiles compared to if other solvent classes were used [154]. Therefore, during the development of a microfluidic process, solvent selection should be investigated along with other identified microfluidic process parameters as it has been demonstrated that physical characteristics of liposomes are affected.

Chapter 4

Bench to GMP: Systematic mapping analysis of microfluidic geometries to permit scale-up production of liposomal drug delivery systems
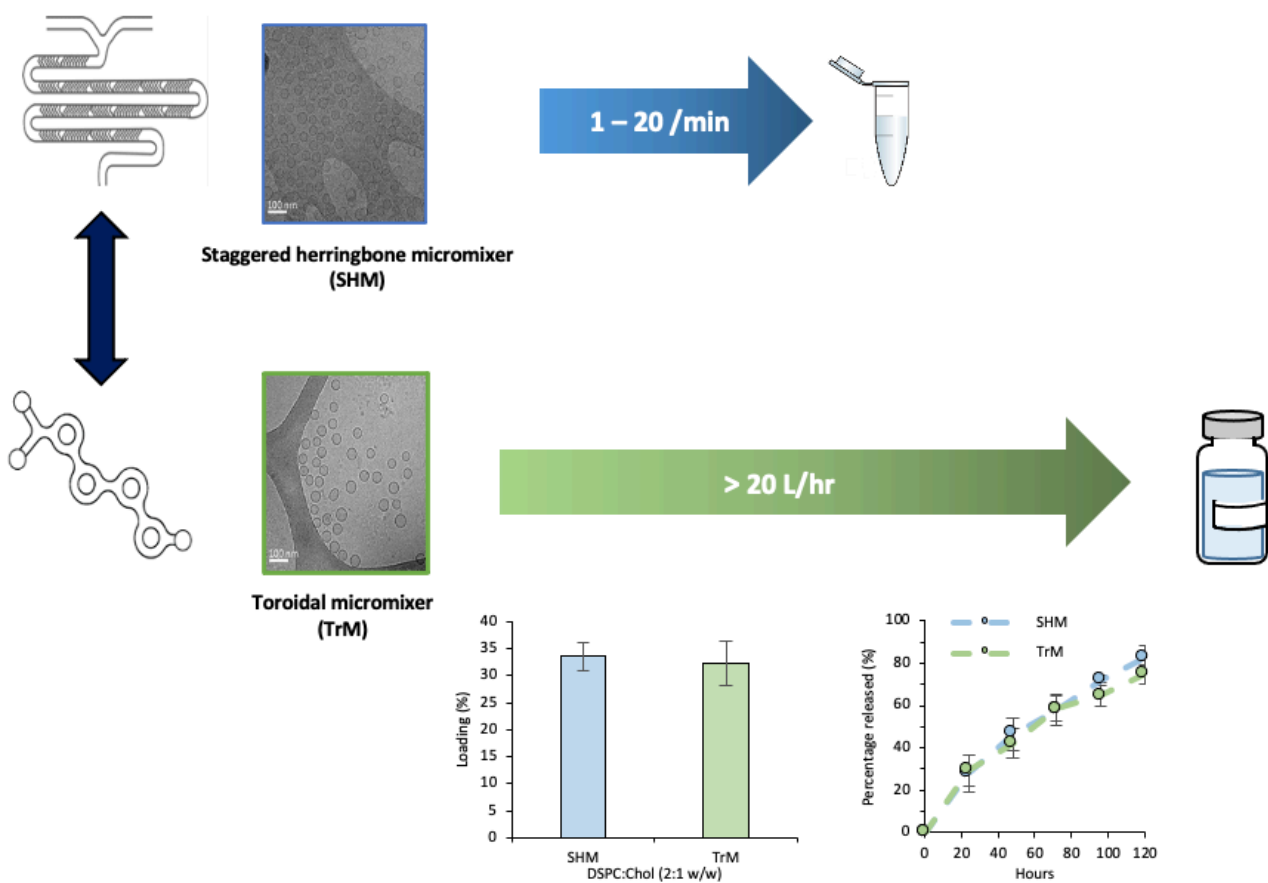
The work presented in the chapter has been published in:

4.1 Introduction

The manufacture and regulatory space of nanomedicines have entered an interesting period resulting from the ongoing COVID-19 pandemic. Despite liposomes known benefits for drug delivery, scaling conventional bench-scale manufacturing methods have hindered their translation into commercialised products with less than 50 reaching the market [188]. However, in December 2019 the emergence of a novel severe acute respiratory syndrome-coronavirus-2 (SARS-CoV-2) rapidly spread globally to become a pandemic in March 2020. Following the genetic sequencing of SARS-CoV-2 on Janurary 2020 a international response was with a focus on accelerating the development of a vaccine. This lead to the rapid effort to understand the mechanism of infection for the development of novel treatments and vaccines [189]. Of the hundreds of potential vaccines in development [190], lipid-based formulations were the first to progress to clinical trials for the delivery of mRNA [191] which allowed the protection of mRNA structure and improved cellular delivery of the antigen to APCs producing both humoral and innate immune responses [192]. The urgency created by the need for a vaccination program also prompted the BioNTech-Pfizer candidate along with those from Imperial College London and Arcturus to use LNPs for mRNA delivery [193-195]. The BioNTech-Pfizer mRNA vaccine was approved first by the MHRA on the 2nd of Dec 2020, and subsequently, the EMA and FDA followed with their approval. The MHRA approved the Moderna vaccine shortly after on the 8th of January, 2021. For these mRNA vaccines, LNPs' ability to physically protect encapsulated mRNA cargo, improve cellular uptake to antigen presenting cells and allow for sustained mRNA expression [196] led to an interesting regulatory GMP challenge to ensure that formulation efficacy and physical-chemical consistency is maintained during the scale-up production process.

The advancement of microfluidic mixing techniques [197] for the production of lipid medicines has revolutionised the lipid nanomedicines production space by offering a scalable, robust and highly reproducible manufacturing strategy. To streamline the process of formulation development, working with Precision NanoSystems Inc., microfluidic process parameters were systematically trialled using the novel toroidal microfluidic architecture (TrM) and compared against results obtained from the established staggered herringbone micromixer (SHM) using the the same microfluidic parameters, to demonstrate that the new

microfluidic architecture has no impact on the liposomes produced. The development of the TrM using centrifugal mixing would permit higher flow rate speeds (> 200 mL/min) which was previously unobtainable using the staggered herringbone mixer (1 – 20 mL/min) employing chaotic advection utilising staggered chevrons.

To ensure that the microfluidic process attributes identified within chapter 3 and previous publications [61, 115, 116, 198] apply to the TrM architecture without any impact on the liposomes produced, both the SHM and TrM were be compared and mapped against each other from a range of liposome formulations. In addition to this, the concept of bench to GMP was challenged using the model formulation (DSPC:Chol 2:1 w/w) with an entrapped protein subunit testing formulation production at GMP-scale without altering microfluidic process parameters used at the bench.
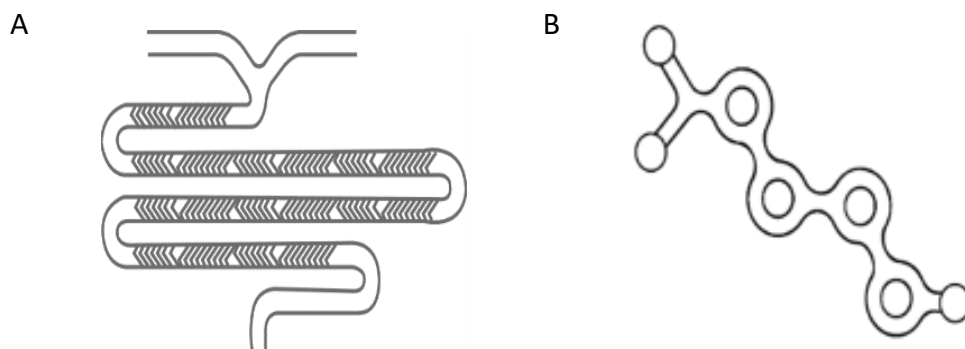
Figure 4.1 *Schematics of the investigated microfluidic mixers. The staggered herringbone micromixer (A) utilises embossed chevrons to promote chaotic advection promoting stream folding and mixing, while the toroidal micromixer (B) employs centrifugal forces to mix fluid steams.*

4.2 Aim and Objectives

The work within this chapter aimed to compare and validate two different laminar flow microfluidic cartridges by challenging them against known critical process parameters and manufacturing a protein sub-unit loaded liposome formulation to GMP-scale. To achieve this the following objectives were:

1. Evaluate and compare the size, PDI and charge of liposomes with entrapped protein (OVA) produced using the SHM and TrM cartridges using DLS-measurements, the liposome morphology by cryo-TEM and protein release

kinetics via RP-HPLC were used to validate if the two cartridges can be used to produce vesicles with the same physical characteristics.

2. Understand if the same microfluidic process attributes such as FRR, TFR and selection of water-soluble solbent, known to affect the liposome physical characteristics produced by chaotic advection (SHM cartridge) also impacts the vesicles formed by centrifugal mixing (TrM cartridge) or if difference microfluidic process parameters apply to the TrM cartridge.

3. Test the robustness of microfluidc manufacturing and downstream purification methods by calculating lipid recovery to ensure that there is no lipid loss as a result of manufacturing using the SHM and TrM cartridges.

4. Check the manufacturing reproducibility using the SHM and TrM cartridge to produce protein loaded liposomes (DSPC:Chol 2:1 w/w) and for each cartridge to meet pre-defined formulation specifications set at: size 50 – 70 nm, PDI < 0.2, zeta potenial -5 to -10 mV and a protein encapsulation efficiency of 26 – 36%.

5. Verify if protein subunit liposomal formulations with the same physical attributes (50 – 70 nm, PDI < 0.2, zeta potenial -5 to -10 mV and a protein encapsulation efficiency of 26 – 36%) can be produced at the lab bench (< 1 mL) and scaled to GMP (> 200 mL/min) without changes to microfluidic manufacturing process parameters such as lipid concentration, solvent choice or FRR.

4.3 Results and Discussion

4.3.1 Initial effect of bench-scale cartridge design on liposomes pilot study

The staggered herringbone micromixer is a well-documented micromixer that has enabled numerous publications to arise from the production of novel formulations to investigations of critical manufacturing parameters (table 4.1). While the SHM is routinely used for bench-scale research and development, a limitation of its use is the micromixer's complex architecture. This makes it costly to fabricate and reduces fluid stream velocities preventing its use for larger-scale manufacturing. To surmount this limitation the microfluidic

architecture was simplified which allowed streams to mix by dean vortices which would also permit greater throughput speeds.

Table 4.1 *Identified microfluidic operational parameters identified to impact liposome physical characteristics.*

Process Parameters	Factors to consider	References
Solvent selection	Suitability of solvent for large-scale production. Lipid(s) solubility in the given solvent. The polarity of the solvent can impact particle size.	[9]; [116]; [119]
Aqueous buffer	Aqueous buffer strength can be used to control particle size.	[115]
Lipid concentration	Initial lipid concentration can impact particle size.	[120]; [117]
Production flow rates	Flow rate can impact on particle size	[121]; [93]
Aqueous to alcohol mixing ratio	Mixing ratio can impact on: • particle size, • drug loading, • drug release.	[117]; [119]; [101]; [122]
Operating temperature	Microfluidic production of liposomes does not need to be conducted above the transition temperature of lipids.	[117]

To investigate the novel TrM architecture, the initial study purpose was to establish if there were any physical differences in vesicle sizes by assessing variances in vesicle size, PDI, and zeta potential by DLS measurements. In addition to this, any destructive forces arising from microfluidic mixing was also investigated through a phospholipid assay which would quantify phospholipid recovery both before and after microfluidic mixing. Throughout these studies, it was decided that the same DSPC:Chol (2:1 w/w) formulation, used in chapter 3, was to be used. This would allow differences in the produced liposomes to be identified by systematic experimentation by altering microfluidic process parameters.

For the pilot study, an FRR and TFR of 3:1 (aqueous:solvent) and 15 mL/min respectively was used with an initial lipid concentration of 4 mg/mL; this led to the production of significantly smaller liposomes when the TrM architecture was used ($p < 0.05$). Using the SHM cartridge liposomes were 41 ± 2 nm while liposomes manufactured using the TrM architecture were 37

± 1 nm (figure 4.2A). Both cartridges produced uniform liposomes with a PDI of less than 0.2 with near-neutral zeta potentials (-6 ± 1 and -5 ± 1 for SHM and TrM respectively). When investigating phospholipid recovery (figure 4.2B) after microfluidic production there was shown to be no loss in phospholipid concentration with values post-manufacture remaining at 100% indicating that both microfluidics and TFF are non-destructive techniques.
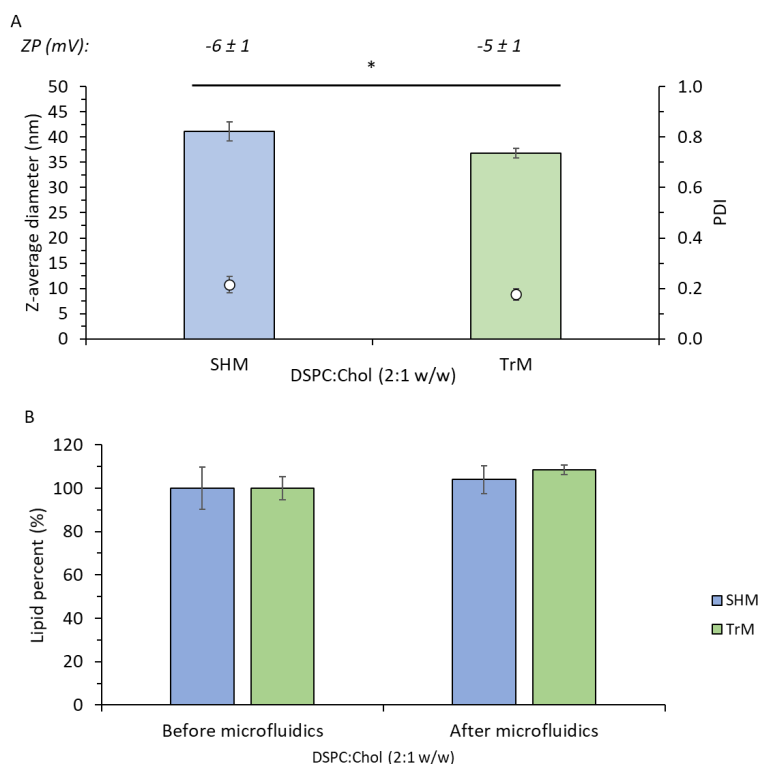
Figure 4.2 Comparison of micromixer design on physical attributes of liposomes. Liposomes were prepared using either a staggered herringbone micromixer (SHM) in the NanoAssemblr® or toroidal mixer (TrM) in the Ignite™ and their sizes and PDI compared using DLS measurements (A) Phospholipid recovery was assessed by each mixer before production and after microfluidic production and purification using tangential flow filtration (B). DPSC:Chol (2:1 w/w) was prepared at a FRR of 3:1 at 15 mL/min which was later purified immediately after using TFF. All formulations had an initial lipid concentration of 4 mg/mL in MeOH. Results represent mean ± SD of 3 independent batches. Statistical significance for vesicle sizes was calculated: $p < 0.05$ (*).

Based on these initial physicochemical characteristics, which were mapped across both cartridges, it suggests that liposome production can translate across the two cartridge designs with both cartridge architectures producing SUVs with no phospholipid loss. Using empty neutral liposomes, the centrifugal mixing used within the TrM architecture permits significantly smaller liposomes to be manufactured compared to those produced with the SHM cartridge. This could be due to the effectiveness of asymmetric fluid splitting and recombination to enhance mixing performance which has been shown to permit higher Reynolds numbers from the unbalanced collision of fluid streams, allowing the formation of dean vortices [199-201]. Despite this, the significant difference in the sizes is less than 5 nm and therefore would unlikely elicit any noticeable effect on cellular size-dependent mechanisms [202-204].

4.3.2 Impact of microfluidic architecture on protein entrapment

It has been demonstrated using empty neutral liposomes (figure 4.2) that it is possible to fabricate liposomes with comparable physical properties. To progress from this, the next phase of the mapping study was to identify if the different cartridge geometries can produce liposomes of equivalent size, PDI and zeta potential from mixing a neutrally charged lipid mix (DSPC:Chol) with 0.25 mg/mL of OVA. Again, this formulation and the incorporated ovalbumin concentration have been well documented allowing a robust comparison of the produced formulations. Finally, much like the experiment in figure 5, the same FRR and TFR were used with the same lipid concentration of 4 mg/mL allowing an analysis to be carried out investigating 1) the effect of ovalbumin loading on liposome physicochemical properties and 2) to further map the effect of cartridge design on liposome production.

4.3.2.1 Method validation for quantifying protein by colourimetric analysis

4.3.2.1.1 Linearity of solubilised ovalbumin

To quantify entrapped protein within the liposomes and to identify if solvent influences entrapment efficiencies (EE%), the entrapped OVA must be released by first lysing the liposomes and then quantified. Using the micro-BCA assay, calibration curves first need to be produced using OVA to assess the linearity across intraday and interday variances in distilled water and PBS. For intraday results, three separate curves were created on the same day (figure 4.3A and D), while for interday precision, five calibration curves were produced on separate days (figure 4.2B and E) using deionised water and PBS to identify differences with the inclusion of buffer. Using both water and PBS to solubilise the OVA allowed for high degrees of linearity ($R^2 > 0.99$) with the LOD and LOQ for the intra- and interday curves falling between 2.1 μg/mL and 7.1 μg/mL respectively when water was used (figure 4.2C). These values were slightly elevated when PBS was used for the intra- and interday samples which were between 3.4 μg/mL and 10.2 μg/mL (figure 4.3E); however, despite this the values fell within the acceptable parameters as concentrations greater than 10 μg/mL of OVA would be quantified.
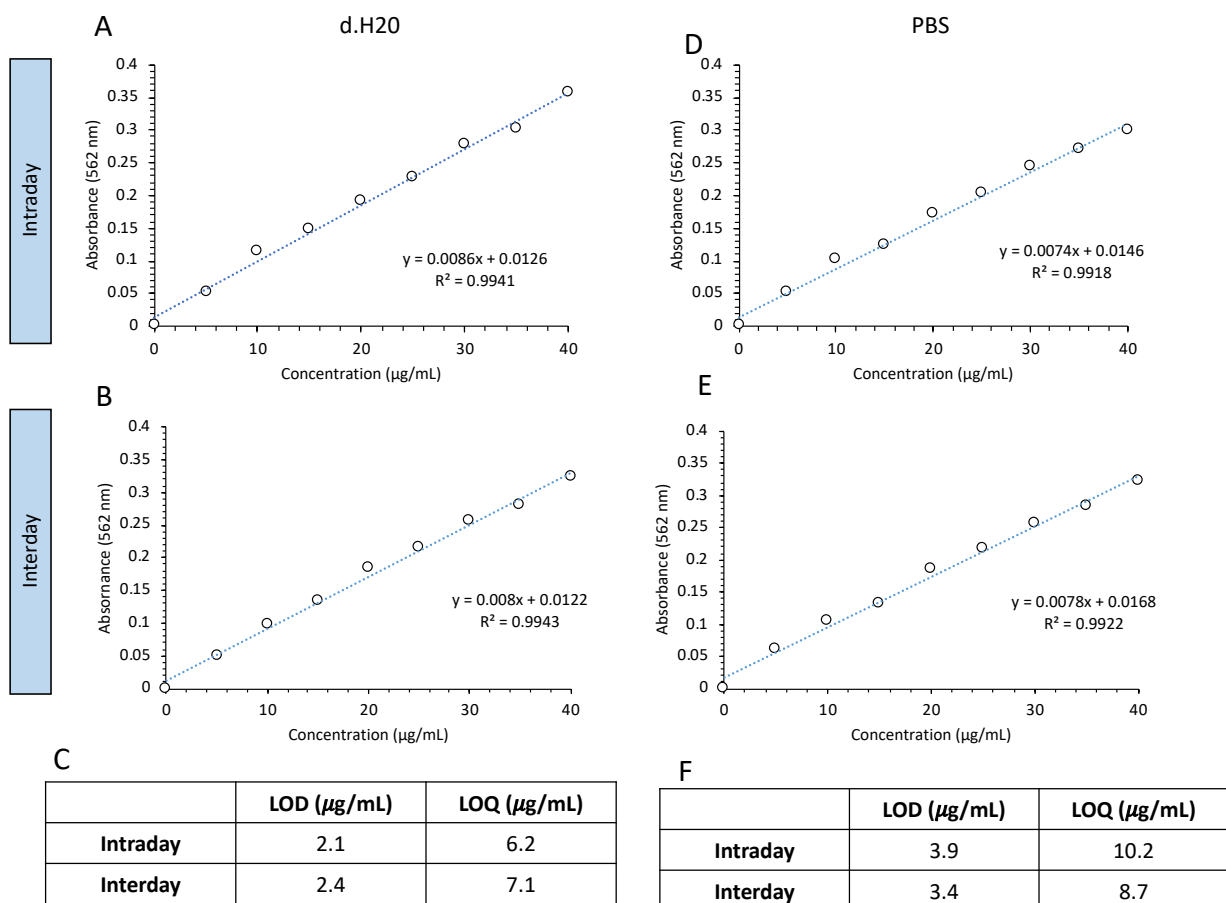
Figure 4.3 *Calibration curves to assess linearity with ovalbumin solubilised in d.H₂O and PBS. Three calibration curves were produced on the same day to produce intraday calibration curves allowing the average to be taken for ovalbumin solubilised in d.H₂O (A) and PBS (D). Interday curves were then produced for d.H₂O (B) and PBS (E) generated over separate days allowing the LOD and LOQ to be calculated for ovalbumin in d.H₂O (C) and PBS (F).*

4.3.2.1.2 Influence of liposome inclusion and solubilisation on protein quantification

Solubilising protein in either water or PBS allowed for a robust linear relationship upon increasing concentrations ($R^2 > 0.99$). The next step was to include liposomes to examine the effect of lipids and a solvent mixture (buffer:IPA 50/50 v/v) which was used to lyse the liposomes to release the entrapped OVA. Extensive work conducted by Hussain et al. has highlighted the assay and solubilisation mixture can be used effectively to quantify protein when liposomes are manufactured in MeOH. However, it has not been conducted in EtOH [187]. Kessler and Fanestil have also indicated that lipids can interact with the linearity of the assay at high concentrations [205]. Using DSPC:Chol (2:1 w/w) manufactured in EtOH highlights that across the concentration range tested (0.1 – 4 mg/mL) leads to minimal impact on the absorbance values.
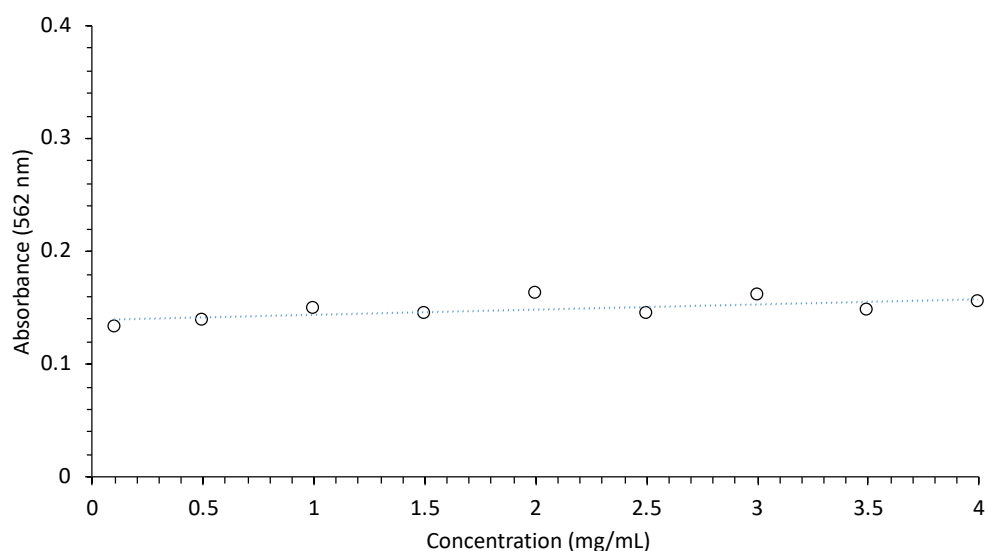
Figure 4.4 *Impact of lipid concentration with solubilisation mixture. Lipsosomes were manufactured at a FRR of 3:1 using DSPC:Chol (2:1 w/w) and solubilised at a 1:1 v/v of IPA:Buffer (50:50 v/v). Results represent n = 3 of independent batches.*

The results in figure 4.4 highlight that between a liposome concentration of 0.1 – 4 mg/mL the liposomes are compatible with the assay and the solubilisation mixture that lyses the liposomes also has minimal impact. However, there was an elevation in the absorbance (approximately 1.4; figure 4.4), meaning that liposomes would need to be included in the standard curve and the solubilisation mixture to measure protein concentrations accurately.

4.3.2.1.3 *Impact of isopropanol on ovalbumin linearity*

Figure 4.4 indicated the assay's capability to produce a standard curve to a high degree of linearity and was compatible with the solubilisation mixture IPA/buffer 50:50 v/v. However, to ensure that ovalbumin linearity is maintained before moving onto the quantification of entrapped protein within liposomes, verification that calibration curves can be produced in the presence of the solubilisation mixture which has been mixed 1:1 v/v with the ovalbumin to reach a final concentration range of 0 – 40 μg/mL. In addition, ovalbumin solubilised in water and PBS was tested to identify if any changes were a result of the buffer choice.

The intraday and interday measurements for both buffers with protein in the presence of solubilization mixture were shown to maintain ovalbumin linearity to a high degree ($R^2 > 0.99$; figure 4.5A, B, D, and E). Low LOD and LOQ values were obtained when the ovalbumin was

solubilised in water with LOD intra- and interday values of 2.3 μg/mL and 2.2 μg/mL respectively and LOQ values of 6.9 μg/mL and 6.8 μg/mL respectively (figure 4.5C). These values were slightly elevated which matches the observation in figure 3.7 when PBS was used to solubilise the ovalbumin. The LOD values for the intra- and interday measurements were calculated to be 2.7 and 3.5 μg/mL respectively with a LOQ of 9.7 μg/mL and 8.2 μg/mL for the intraday and interday respectively (figure 4.5E). Again, these values fall within the acceptance criteria as ovalbumin concentrations greater than 20 μg/mL will be used.

	LOD (μg/mL)	LOQ (μg/mL)
Intraday	2.3	6.9

	LOD (μg/mL)	LOQ (μg/mL)
Intraday	3.5	9.7
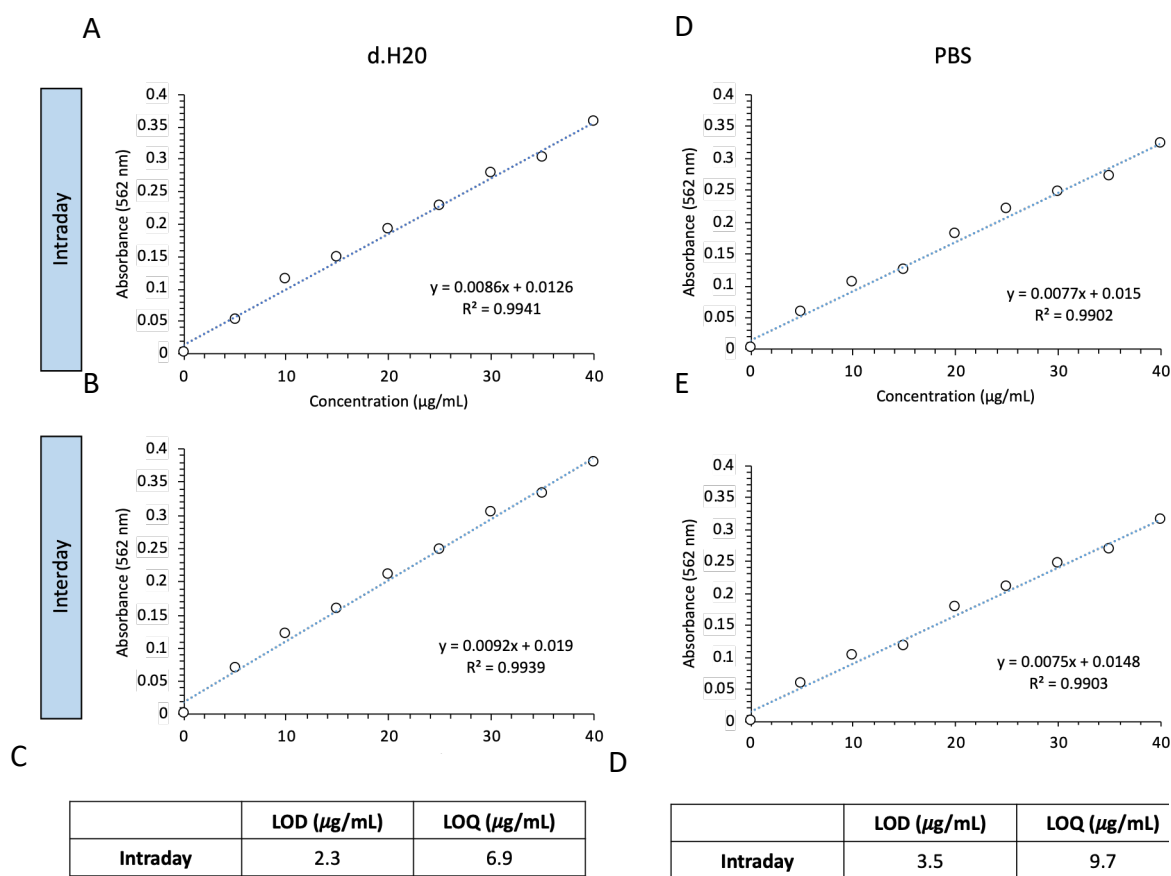
Figure 4.5 Calibration curves to assess linearity with ovalbumin in the presence of solubilisation mixture. Three calibration curves were produced on the same day to produce intraday calibration curves allowing the average to be taken for ovalbumin solubilised in d.H$_2$O (A) and PBS (D) which had been mixed 1:1 v/v with IPA:Buffer (50:50 v/v). Interday curves, with ovalbumin with the solubilisation mixture 1:1 v/v, were then produced for d.H$_2$O (B) and PBS (E) generated over separate days allowing the LOD and LOQ to be calculated for ovalbumin in d.H$_2$O (C) and PBS (F).

4.3.2.1.4 *Ovalbumin calibration curve production in the presence of liposomes and solubilisation mixture*

Following the systematic assessment of variables that could impact the linearity of ovalbumin calibration curves, the results have successfully demonstrated from the variables investigated that buffer, presence of lipids, and solubilisation mixture does not impact the degree of linearity which can be produced. Therefore, to examine whether the protein concentrations are affected in the dual presence of liposomes and solubilisation mixture protein concentrations were added along with DSPC:Chol liposomes and solubilisation mixture (IPA/PBS 50:50 v/v) to result in a final ovalbumin concentration range of 0 - 40 μg/mL and 1 mg/mL of liposomes.

The results in figure 4.6 indicated that ovalbumin was not affected in the presence of both liposomes and solubilisation mixture with both the intraday (figure 4.6A) and interday (figure 4.6C) curves demonstrating a high degree of linearity (R^2 > 0.99). Futhermore, the LOD for both the intraday (figure 4.6B) and interday (figure 4.6D) was low (3.5 μg/mL and 2.8 μg/mL respectively) with LOQs for both the intra- and interday also low (10.7 μg/mL and 8.4 μg/mL respectively) falling within the acceptable parameters and remaining consistent with the LOD and LOQ values obtained when ovalbumin without lipids or solubilization was measured.
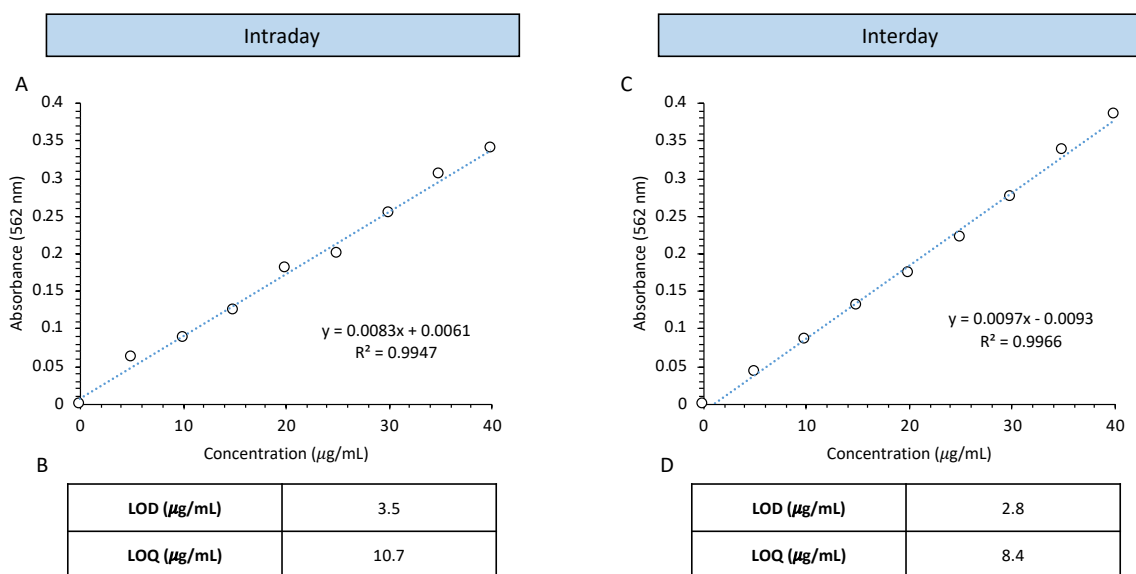
Figure 4.6 *Calibration curves to assess linearity with ovalbumin in the presence of liposomes and solubilisation mixture. Ovalbumin in PBS was mixed with DSPC:Chol (2:1 w/w) liposomes and solubilisation mixture (IPA/buffer) allowing three calibration curves to be produced on the same day allowing an average to be taken to produce intraday (A) and interday (C) calibration curves which were recorded on separate days. with ovalbumin in the presence of DSPC:Chol (2:1 w/w) liposomes and solubilisation mixture (IPA:Buffer 50:50). The LOD and LOQ was also measured for intraday (B) and interday (D) measurements.*

4.3.2.2 <u>Quantifying entrapped protein in liposomes produced by microfluidics</u>

Using the SHM cartridge and loading liposomes with 0.25 mg/mL of ovalbumin led to vesicle measurements of 56 ± 6 nm and using the TrM cartridge produced liposomes that were 57 ± 7 nm were formulated (figure 4.7A). Using both microfluidic architectures allowed for vesicles that were uniform in size and had a PDI of < 0.2. Upon comparison to unloaded liposomes manufactured by their respective cartridges (figure 4.7A), protein-loaded liposomes made by either SHM or TrM were statistically larger than their 'empty' liposome counterparts (manufactured by SHM: 56 ± 6 nm vs 41 ± 2 nm; manufactured by TrM: 57 ± 7 vs 37 ± 1 nm). There was no impact on the zeta potential with either cartridge or if they are unloaded or loaded as shown in figure 4.6A. In addition, the effect of cartridge design had no direct influence on protein loading with the liposomes formulated from the SHM and TrM cartridge entrapping 33 ± 3 % and 32 ± 4 % respectively (figure 4.7B).
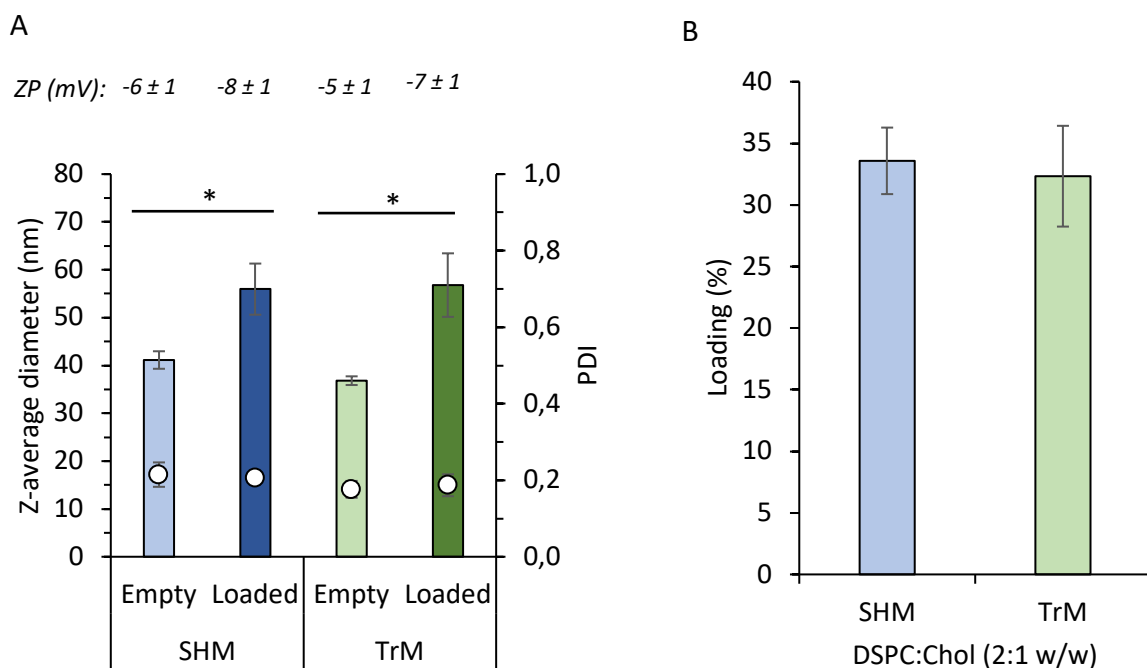
Figure 4.7 *Comparison of micromixer design on physical attributes of protein loaded liposomes. Liposomes (DSPC:Chol 2:1 w/w) were produced at a 3:1 FRR, 15mL/min TFR and an initial lipid concentration of 4mg/mL (dissolved in MeOH) and an initial ovalbumin protein concentration of 0.25mg/mL (dissolved in PBS pH 7.4) using either a staggered herringbone micromixer (SHM) in the NanoAssemblr® or toroidal mixer (TrM) in the Ignite. Formulations were later purified using TFF. The liposome size (column); PDI (open-cirlces) and zeta potential was characterised by DLS (A). Ovalbumin entrapment efficiencies were calculated using a microBCA assay (B). Results represent mean ± SD of 3 independent batches. Statistical significance for vesicle sizes was calculated: p < 0.05 (*).*

By investigating the impact of liposome physical properties and ovalbumin loading using different microfluidic cartridge designs there was no significant difference in vesicle size, PDI, zeta potential (figure 4.7A) or protein entrapment efficiencies (figure 4.7B). This further builds on the previous findings when the unloaded formulations were investigated that cartridge geometry does not affect liposome physical properties. However, for each cartridge, there was a significant impact on the formulation size when protein was entrapped compared to when there was no protein cargo within the liposomes. This effect was also observed by Forbes et al., from the investigation using DSPC:Chol (10:5 w/w) and DSPC:Chol:PS (10:5:4 w/w) which a neutral and negatively charged liposome formulations respectively [117]; it was found that increasing ovalbumin concentrations from 0.1 to 2 mg/mL led to an overall size increase from 60 to 80 nm due to the increased protein cargo concentration. This effect was not observed with anionic liposomes with liposomes of approximately 100 nm regardless of protein concentration used being produced. This could be a stabilising effect arising from the electrostatic repulsion between polar phospholipid head groups and the overall peripheral

anionic charge of the ovalbumin [206] at physiological pH which results from the arginine and lysine amino acid domains (pKa of 12.5 and 10.5 respectively). This prevents microfluidic manipulation of protein orientation [207] into the liposome bilayer affecting phospholipid-packing densities as protein concentrations increase leading to larger vesicles. These results indicate that the production of DSPC:Chol liposomes can be effectively mapped across microfluidic cartridges with different architectures in either an unloaded or loaded state with no impact on encapsulation efficiencies. The next step to take this work forward was to identify the effect of using lipids with different Tm and test if liposome attributes continued to map across between the two micromixers.

4.3.3 Circumventing glycerophospholipid transition temperatures using microfluidics

It has been previously shown by Forbes et al., using a SHM cartridge design that lipid transition temperatures can be negated because of the liposome self-assembly which takes place due to the fluid mixing within the micromixer allowing liposomes to form at ambient temperatures [117]. To test if a similar reaction takes place using the TrM cartridge 3 different glycerophospholipids were tested which included 14:0 PC (DMPC) that has a low Tm of 24 °C was compared against 18:0 PC (DSPC) and 18:0 PC (HSPC) which both have a higher transition temperature of 55 °C. From these results, it will be possible to ascertain if using a cartridge design encompassing centrifugal mixing impacts liposome formation at ambient temperatures and the effect of hydrocarbon tail length on vesicle size.
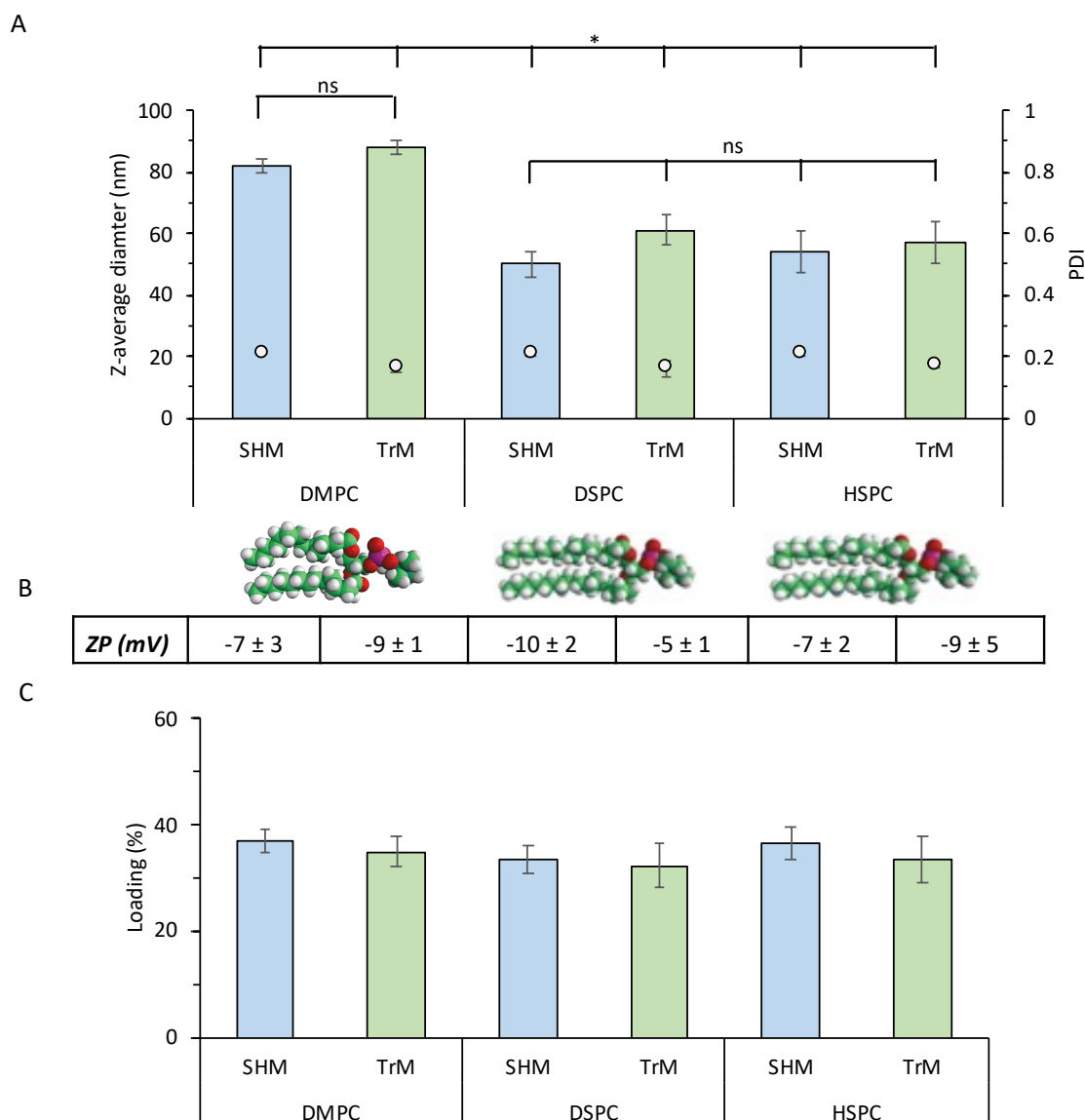
Figure 4.8 *Production of liposomes working below transition temperatures. DSPC:Chol; HSPC:Chol and DMPC:Chol (2:1 w/w) liposomes were manufactured using either a SHM or TrM micromixer with their size, PDIs and zeta potentials analysed using DLS measurements. Protein loading were quantified with RP-HPLC. Liposomes were produced at a 3:1 FRR, 15mL/min TFR and an initial lipid concentration of 4mg/mL (dissolved in MeOH) and an initial ovalbumin protein concentration of 0.25mg/mL (dissolved in PBS pH7.4) which was quantified by RP-HPLC after TFF. All liposomes were produced at an ambient room temperature. The liposome size (columns) and PDI (open circles) (A), loading (B) and zeta-potential (C) were compared. Results represent mean ±SD of three independent batches. Statistical significance for vesicle sizes was calculated: p < 0.05 (*).*

From the results in figure 4.8A, DMPC:Chol liposomes were 82 ± 2 nm and 88 ± 3 nm for liposomes formed using the SHM and TrM cartridges respectively with PDIs below 0.2, the differences in sizes were not significantly different (p > 0.05). When DSPC:Chol and HSPC:Chol were investigated, there were no significant differences between the cartridges or between the two different formulations that produced liposomes of 50 – 60 nm in sizes that also had

PDIs below 0.2. When DMPC:Chol liposomes were compared against DSPC:Chol and HSPC:Chol liposomes manufactured by their respective cartridges there was shown to be a significant difference in the vesicle size ($p < 0.05$). The zeta potential for all formulations was not influenced by lipid choice or cartridge with values between -9 to -12 (figure 4.8B). However, despite their size differences, there was no significant effect on the EE% between either formulation or when SHM or TrM cartridge designs were used with EE% of $30-36\%$ attained (figure 4.8C).

From these results, when the individual formulations are compared against the cartridge used there was no significant change in size or zeta potential which further adds to mounting evidence that the TrM micromixer maps across to the SHM cartridge. It has also been previously shown that phospholipid alkyl chain length affects vesicle chain length whereby longer unsaturated chains can form small vesicles due to the improved ability to create Van der Waal forces, ergo leading to improved membrane packing [117]. From these findings, it was expected that DMPC:Chol liposomes would be larger than both DSPC:Chol and HSPC:Chol and as such was found to be the case as shown in figure 4.8A. Similarly, the same paper also tested the ovalbumin EE% of a range of liposomes including PC:Chol; DMPC:Chol; DPPC:Chol, and DSPC:Chol with EE% of $30-40\%$ which is also in line with findings in figure 4.8C. These results also demonstrate that using the TrM cartridge liposomes could still be formed at ambient temperatures while working below transition temperatures following the self-assembly theory [117, 208]. Interestingly, vesicle size and rigidity did not influence EE%.

4.3.4 Impact of microfluidic operating parameters

To further explore microfluidic geometry and its impact on liposomal physical characteristics, the model formulation of DSPC:Chol was tested against established critical process parameters which have been shown to influence vesicle size [117, 177, 209]. Conducting these additional experiments would allow for a more complete comparison between the two cartridges and identify if liposomes formed by centrifugal forces by the TrM design are different from those mixed by chaotic advection.

4.3.4.1 Fluid mixing ratios on vesicle size

One of the benefits of microfluidics over other liposomal production platforms is that various manufacturing parameters that can be employed to alter the vesicle physical charactersitics as outlined in table 4.1. One of these, is the mixing ratio between the aqueous and solvent phases which has been found to influence the vesicle size [92, 210]. One of the earliest and arguably one of the most influential operating parameters identified is the aqueous to solvent ratio. To map liposome production between the two cartridges flow rate ratio was recognised as one of the operational parameters to test due to its influence on particle size, drug loading and drug release ratio [101, 117, 119, 122].

Figure 4.9 focuses on the liposomal formulation DSPC:Chol (2:1 w/w) manufactured at an FRR of 3 or 5:1 at an initial concentration of 4 mg/mL in PBS pH 7.4. From figure 4.9A where vesicle size and PDI were investigated, the vesicle size from the 3:1 FRR was 53 ± 3 and 54 ± 2 nm for the SHM and TrM cartridge respectively with PDIs for both cartridges below 0.2. When compared against the 5:1 FRR there was no significant difference in vesicle size or PDI when liposomes produced by each cartridge were compared against their 3:1 FRR counterparts producing sizes of 51 ± 2 and 45 ± 2 nm from the SHM and TrM cartridges respectively. Protein loading (figure 4.9B) was analysed using RP-HPLC by initially lysing the liposomes using a 50:50 v/v mix of 2-propanol/buffer (50:50 v/v solubilisation mixture/liposomes) to release the protein cargo. By comparing protein entrapment at a 3:1 FRR there was no significant difference in the entrapment efficiencies (EE%) (35 ± 2 % and 36 ± 1 % for the SHM and TrM micromixer respectively; figure 4.9). Again, no significant difference was observed when either cartridge was used to produce protein-loaded liposomes; when made at the 5:1 FRR protein loading was 27 ± 1 % and 31 ± 3 % for the SHM and TrM respectively. A significant difference ($p < 0.05$) in the EE% for liposomes produced at 3:1 FRR and 5:1 FRR using the SHM cartridge was observed which was not seen when the TrM cartridge was used.
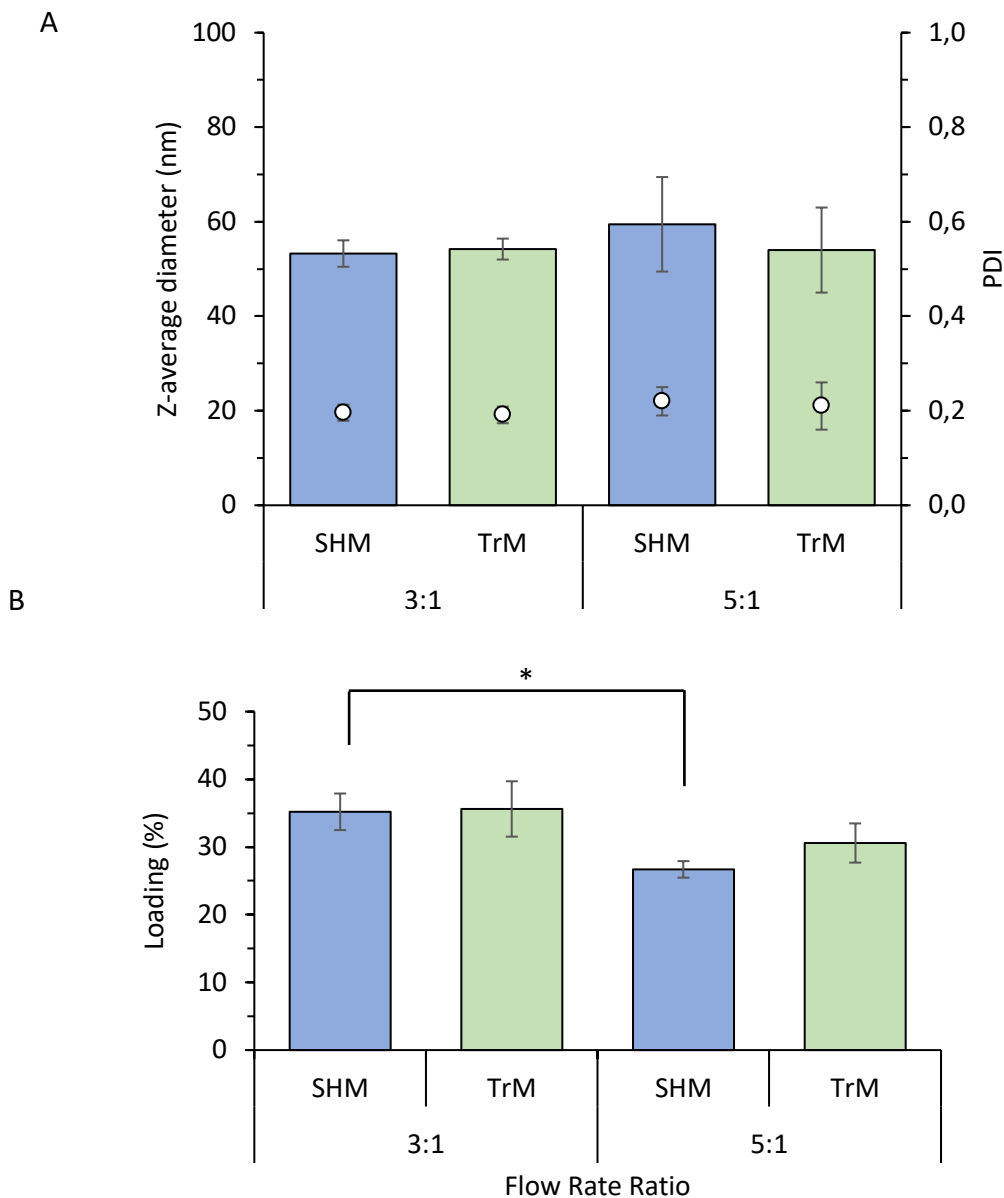
Figure 4.9 *Altering fluid mixing ratios and its effect on vesicle size and protein loading capacity. DSPC:Chol liposomes were manufactured using either a SHM or TrM micromixer with their size, PDIs analysed using DLS measurements. Protein loading were quantified with RP-HPLC. Liposomes were produced at a 3:1 or 5:1 FRR, 15mL/min TFR at an initial lipid concentration of 4mg/mL (dissolved in MeOH) and an initial ovalbumin protein concentration of 0.25mg/mL (dissolved in PBS pH7.4) which was quantified by RP-HPLC after TFF. All liposomes were produced at an ambient room temperature. The liposome size (columns) and PDI (open circles) (A), loading (B) were compared. Results represent mean ±SD of three independent batches. : p < 0.05 (*)*

The results in figure 4.9 further indicate that regardless of the microfluidic structure used the two cartridges continue to map well and produce liposomes of comparable sizes and EE%. Furthermore, upon investigation into microfluidic parameters by Forbes et al., also using

DSPC:Chol (2:1 w/w) produced similar findings whereby both the 3:1 and 5:1 FRR led to liposomes of between 50-60 nm using the staggered herringbone micromixer [117]. Larger size variances were observed from Kastner et al., where a 1:1 FRR was used to produce liposomes above 200 nm with liposomes below 50 nm when a 5:1 FRR was used [211]. From using a 1:1 FRR the solvent percentage upon meeting the aqueous stream and the channel convergence is 50% v/v %; this leads to a cascade of liposome assembly and disassembly because the liposomes are exposed to fluctuating solvent concentrations which are above and below the critical alcohol content. The changing solvent concentrations can also explain why at higher FRRs the liposomes have a reduced vesicle size. At higher FRRs, such as 3:1 and 5:1, the solvent content is reduced (25 and 16.6 % v/v% respectively) due to a decrease in the fluctuating solvent concentration range reducing the assembly and disassembly cycles [92, 177]. This observation can be used to explain why liposomes produced in figure 4.9A and those observed by Kastner et al., and Forbes et al., are between 50 – 60 nm when a 5:1 FRR is used [117, 211]. What was not examined by Jahn et al., but published by Phapal and Sunthar is that above certain FRRs there is a plateau in liposome sizes that can be achieved [212] which is in line with figure 4.9A where there were no significant differences in vesicle sizes when the 3:1 and 5:1 FRRs were compared. The researchers have attributed the phenomenon to the limitation of channel geometry where maintaining a stable flow can be challenging to obtain at high FRRs [212]. From this research, liposome physical characteristics can change due to microfluidic geometry. This demonstrates the requirement for systematic microfluidic mapping studies between cartridges to ensure no unexpected physical changes in liposomal properties when transiting between an established micromixer towards a more novel form.

4.3.4.1.1 *Effect of a synthetic cholesterol derivative*

SyntheChol™ was initially developed to overcome the limitations of animal-derived cholesterol due to its auxotrophic nature and the fact that supplementation is required for its use in cell lines due to its lipophilicity [213]. As a result, animal-derived cholesterol used in large-scale manufacturing is hindered which in turn led to the development of the synthetically fabricated form known as SyntheChol ™. As there are no molecular differences in SyntheChol™ and cholesterol this provides a useful non-animal derived option.

From figure 4.10A, at both 3:1 and 5:1 FRRs, no significant differences were observed when SyntheChol™ was used instead of cholesterol. Focusing on DSPC:SyntheChol™ (sizes and PDI for DSPC:Chol were stated in section 4.3.4.1) using the SHM cartridge the liposome sizes when a 3:1 and 5:1 was used the vesicle size was 53 ± 4 nm and 55 ± 3 nm respectively. When the TrM cartridge was used the vesicle sizes were 54 ± 2 nm and 55 ± 2 nm when a 3:1 and 5 :1 FRR was used. Again, vesicle uniformity was not influenced by the use of SyntheChol™ or when different microfluidic architecture was used with PDIs below 0.2. Furthermore, as expected, there was no impact on the zeta potential leaving a relatively neutral charge of -6 to -12 mV when cholesterol was substituted for SyntheChol™ as shown in figure 4.10B. In terms of loading capabilities, whilst previously shown in figure 4.9B, there was a significant difference in EE% when the 3:1 and 5:1 FRR were compared against each other; this was not the case when SyntheChol™ was used (figure 4.10B). Using DSPC:SyntheChol™ at a 5:1 FRR with the cartridges the EE% was 33 ± 5 % and 35 ± 5 % which is not significantly different from DSPC:Chol using the TrM cartridge at a 5:1 FRR which was 31 ± 3 %.

The use of a synthetic form of cholesterol has no impact on the physical properties of the liposome allowing for reproducible sizes of between 50 – 60 nm when either a 3:1 or 5:1 FRR was used, which was also seen when animal-derived cholesterol was used. There was also no significant difference in EE% using Synthechol™ which was different from the use of cholesterol at a 5:1 FRR where a significant difference ($p < 0.05$) was observed when compared against a 3:1 FRR. There were no other significant differences observed between the other FRRs or when SyntheChol™ was used with the different cartridges leading to the expectation that we can estimate ovalbumin EE% between 25 – 35% for this formulation tested.

ZP (mV)   *-12 ± 4*   *-9 ± 2*   *-9 ± 3*   *-7 ± 1*   *-7 ± 4*   *-6 ± 2*   *-8 ± 2*   *-8 ± 3*
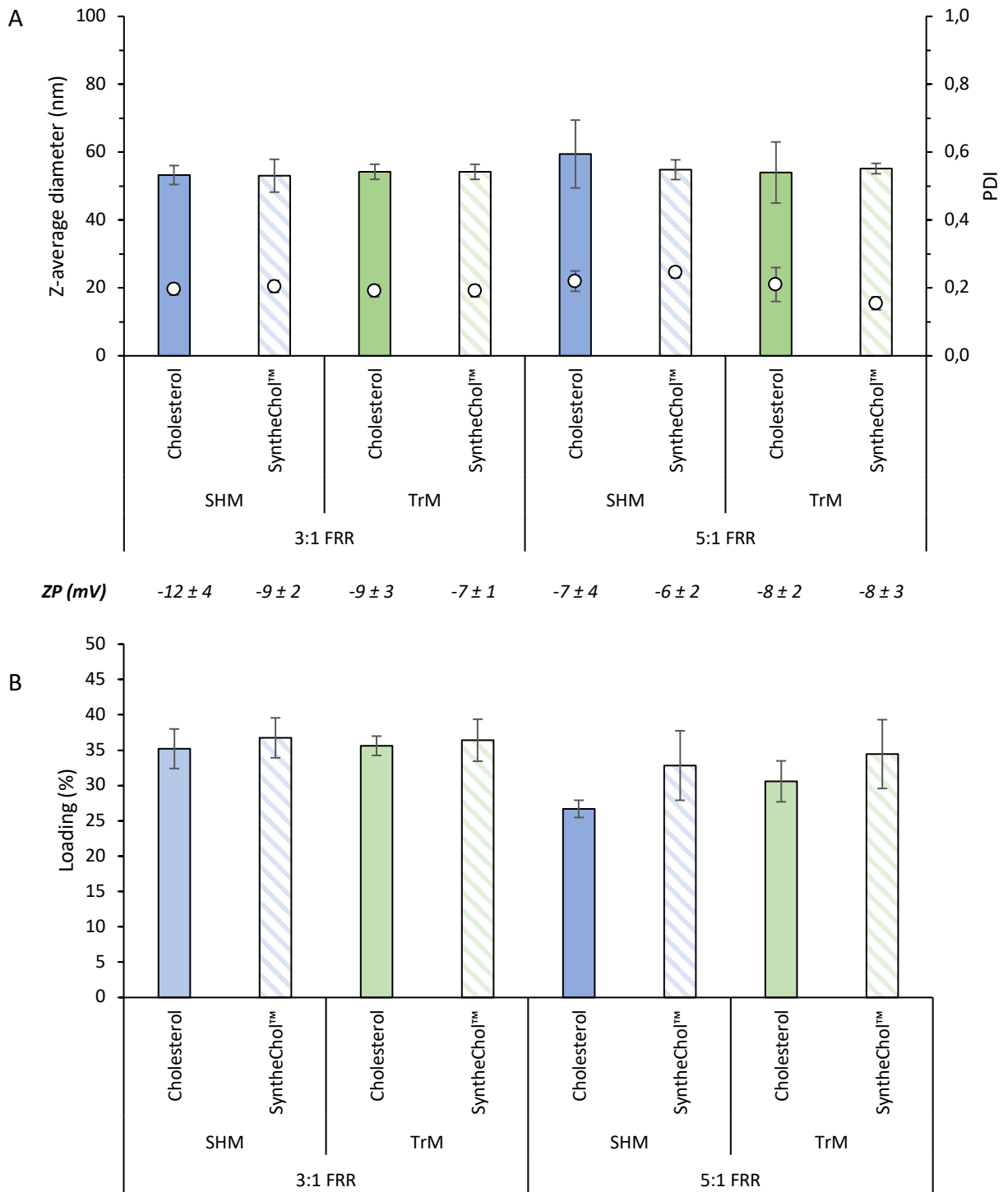
***Figure 4.10** FRR investigation and the effect of a synethetic form of cholesterol on liposome characteristics. Liposomes were manufactured using either a SHM or TrM micromixer with their size and PDI analysed using DLS measurements (DSPC:cholesterol 2:1 w/w). Protein loading was quantified by RP-HPLC. Liposomes were produced at a 3:1 or 5:1 FRR, 15mL/min TFR at an initial lipid concentration of 4mg/mL (dissolved in MeOH) and an initial ovalbumin protein concentration of 0.25mg/mL (dissolved in PBS pH7.4) which was quantified by RP-HPLC after TFF. All liposomes were produced at an ambient room temperature. The liposome size (columns) and PDI (open circles) (A), zeta potential (B) loading (C) were compared. Results represent mean ±SD of three independent batches.*

4.3.4.2 Altering fluid velocity to address GMP throughout speed requirements

An additional parameter that can be altered is the total flow rate (TFR) which can be described as the fluid velocity passing through the cartridge. This parameter was an important one to test as the end goal of this study was to take a formulation developed on the lab bench and scale it through to GMP. Therefore, bench-scale experimentation investigating the impact of fluid mixing velocities on formulation characteristics was a crucial attribute to test and understand before moving to "pre-clinical" and GMP volumes requiring larger volumes and greater speeds.

The model formulation of DSPC:Chol was chosen using a 3:1 FRR with the same initial concentrations and solvent used to ensure any differences observed resulting from the TFR. Operating speeds between 12 - 20 mL/min were used with 20 mL/min being the maximum operating speed that can be used using the NanoAssemblr®. Across the speeds tested there was no statistical difference ($p > 0.05$) in either the vesicle sizes or polydispersity index (figure 4.11A) with sizes remaining between 50 – 56 nm and PDI values between 0.15 and 0.19. Fluid mixing speeds also had no significant impact on formulation EE% with protein loading remaining between 34 – 36% (figure 4.11B).

The TFR was not shown to impact liposomal diameter, PDI or EE%. In terms of vesicle size, Kastner et al., performed a design of experiments (DoE) to determine the effects of FRR and TFR on liposome physical characteristics using DOPE:DOTAP (8:8 µmol). From their findings, TFR was not shown to correlate with vesicle size and that model predicted the FRR to be highly significant in terms of its impact on the size, PDI and cell transfection efficiencies [211]. An additional DoE also concluded that again FRR had the greatest effect on vesicle size ($p < 0.001$) while TFR above 8 mL/min had no impact on vesicle size or PDI with the results in figure 4.11 fitting this predicted statistical model [214].
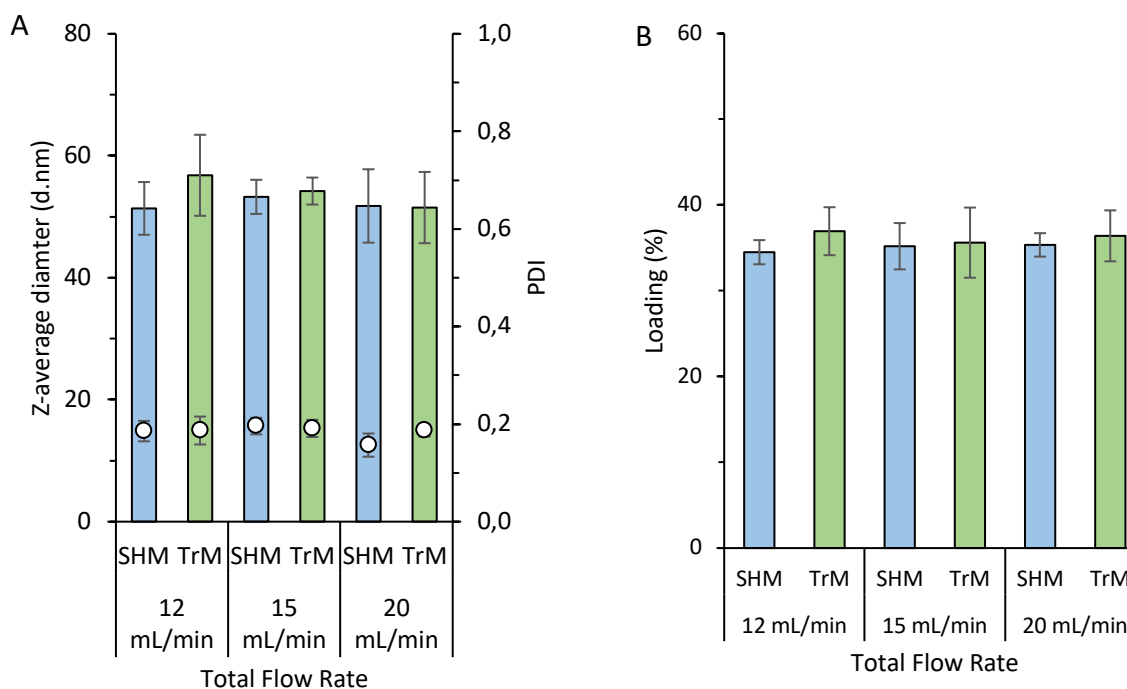
Figure 4.11 *Fluid mixing speeds and impact on vesicle size and EE%. Liposomes were manufactured using either a SHM or TrM micromixer with their size, PDIs analysed using DLS measurements (DSPC:cholesterol 2:1 w/w). Protein loading were quantified with RP-HPLC. Liposomes were produced at a 3:1 FR using either 12, 15 or 20 mL/min TFR at an initial lipid concentration of 4mg/mL (dissolved in MeOH) and an initial ovalbumin protein concentration of 0.25mg/mL (dissolved in PBS pH7.4) which was quantified by RP-HPLC after TFF. All liposomes were produced at an ambient room temperature. The liposome size (columns) and PDI (open circles) (A), loading (B) were compared. Results represent mean ±SD of three independent batches.*

4.3.4.2.1 *Impact of SyntheChol™ substitution*

To further develop the formulation characterisation and the effect on TFR has on its physical properties, SyntheChol™ was used to substitute cholesterol with the same range of TFR used in figure 4.6 with the same solvent and lipid concentrations used. The results in figure 4.12A highlight that regardless of TFR with use of SyntheChol™ or cholesterol there is no effect on the vesicle size or PDI (sizes between 51 – 57 nm and PDI of 0.16 – 0.19). In addition, there was no profound effect on the zeta potential which remained between -6 and – 12 mV, as shown in figure 4.12A. Comparable results between the EE% existed when both the synthetic and animal-derived forms of cholesterol were used from quantification with RP-HPLC. From these results in figure 4.12B, varying the TFR from 12 – 20 mL/min had no significant impact on EE% with loading capacities between 30 – 35 %.
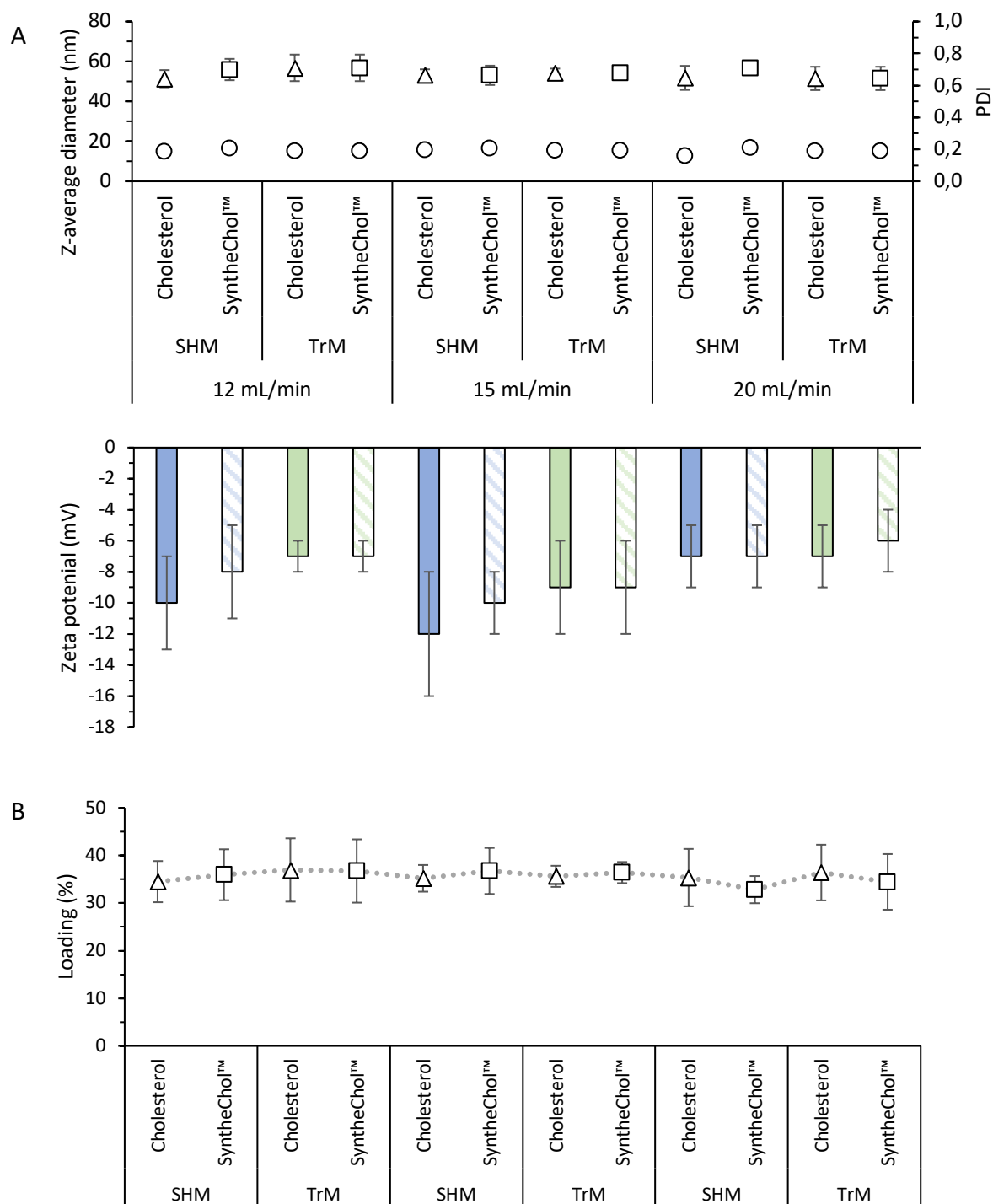
Figure 4.12 *Fluid mixing speeds and incorporation of synthetic cholesterol. Liposomes were manufactured using either a SHM or TrM micromixer with their size, PDIs analysed using DLS measurements (DSPC:Cholesterol 2:1 w/w). Protein loading were quantified with RP-HPLC. Liposomes were produced at a 3:1 using either a 12, 15 or 20 mL/min TFR at an initial lipid concentration of 4 mg/mL (dissolved in MeOH) and an initial ovalbumin protein concentration of 0.25mg/mL (dissolved in PBS pH 7.4) which was quantified by RP-HPLC after TFF. All liposomes were produced at an ambient room temperature. The liposome size, PDI, zeta potenial (A) and loading (B) were compared. Results represent mean ± SD of three independent batches. : $p < 0.05$ (*)*

The results in figure 4.12 show a robust analysis investigating the use of synthetic cholesterol and the influence of TFR. The results led to two conclusions to be formed: 1) the use of synthetic cholesterol can be used as an alternative to animal-derived products and, 2) fluid mixing velocities has no impact on vesicle size, PDI, zeta potential or loss of protein entrapment efficiencies. This provides a valuable set of results and understanding for the progression towards "pre-clinical" and GMP platforms with the expectation that fluid velocities can be increased with minimal impact on liposomal properties.

4.3.5 Mapping solvent selection across different micromixer architectures

As previously demonstrated in chapter 3, solvent polarity can influence liposome physical properties, particularly the size, making understanding organic solvents' influence on formulation characteristics a critical attribute to consider when mapping across different cartridges. Furthermore, as the overall goal of this chapter was a demonstration of taking a bench-scale formulation all the way through to GMP moving away from the class 2 solvent which has been used up to this point (MeOH) and transition to a less toxic class 3 solvent, in this case, EtOH was the next logical step to make [154]. Therefore, it was essential to test if EtOH produces larger vesicles than MeOH due to solvent polarity, as shown in the previous chapter with the new micromixer.

Figure 4.13 shows the average vesicle size of DSPC:Chol (2:1 w/w) liposomes manufactured using either the SHM or TrM cartridge in EtOH or MeOH. The results showed no significant differences in the formulation manufactured in EtOH or MeOH using either the SHM or TrM. However, similarity to chapter 3, significant differences were observed when the solvents were compared against each other using the same cartridge with liposomes made in MeOH and EtOH using the SHM reporting sizes of 53 ± 3 nm and 59 ± 2 nm respectively and using the TrM sizes of liposomes produced sizes using MeOH and EtOH of 54 ± 2 nm and 60 ± 1 nm respectively. There were no significant differences in the PDI (all < 0.2) or zeta potential (between -6 to -10 mV). Using RP-HPLC protein EE% was also investigated with no significant differences observed with loading values between 32 − 35%.
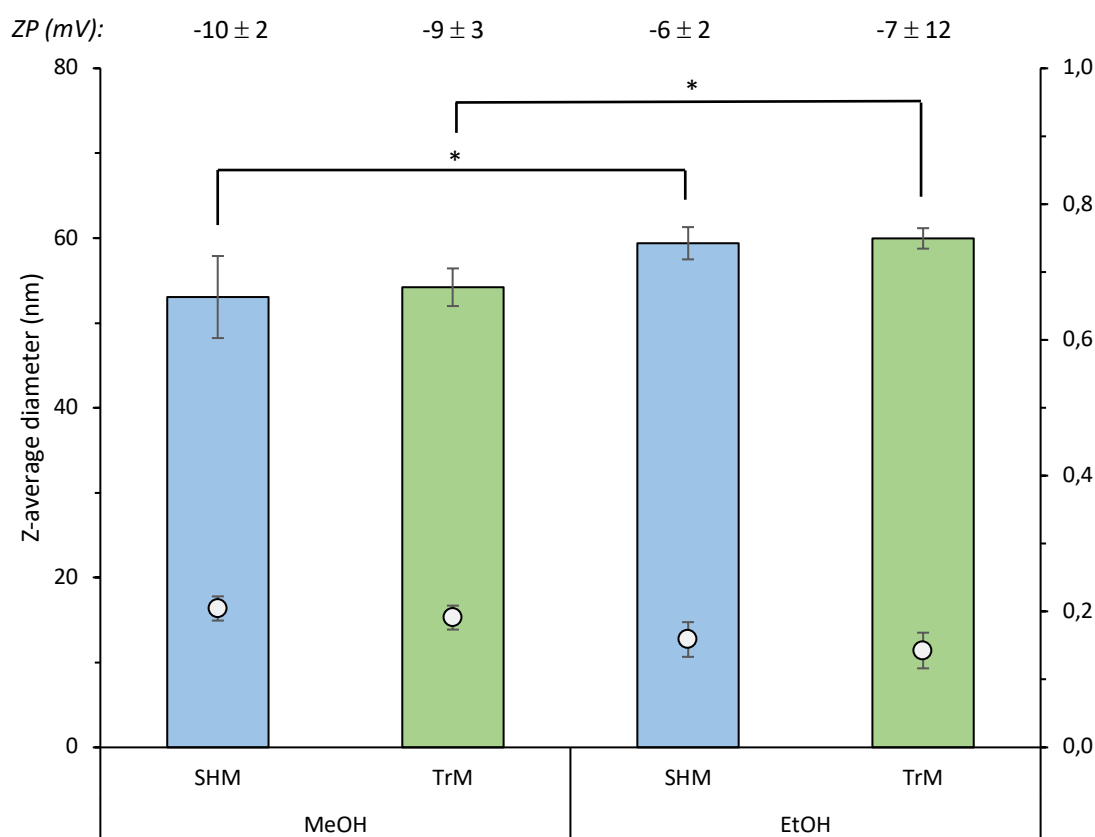
Figure 4.13 *Impact of solvent selection on liposome physicochemical characteristics. Liposomes (DSPC:Chol 2:1 w/w) were produced with entrapped with an initial OVA concentration of 0.25 mg/mL. Lipids at a concentration of 4 mg/mL were dissolved in either MeOH or EtOH and manufactured using either a SHM or TrM mixer at 3:1 FRR and 15 mL/min. Liposome size (columns); PDI (circles) and zeta potenial (A), PDI (B) and zeta potential (C) were recorded using DLS measurements while protein entrapment efficiencies (D) was quantified by RP-HPLC. Liposomes were purified by tangential flow filtration. Results represent mean ± SD of 3 independent batches. Statistical significance for vesicle sizes was calculated: p < 0.05 (*).*

From this study, additional observations were made similarly to that already explained in chapter 3 regarding larger lipid discs forming using lower polarity solvents (e.g. EtOH) due to reduced polarity changes during mixing with the aqueous phase allowing for longer disc expansion before bending into liposomes [116]. The findings in figure 4.13 also demonstrate that the same principles observed in chapter 3 using the SHM cartridge can be applied using the TrM design and that larger discs also expand using centrifugal mixing as a result of reduced polarity.

4.3.6 Lipid concentration vs. liposome characteristics vs. micromixer geometry

So far, various production parameters have been investigated including FRR, TFR and solvent selection. In addition, the effect of lipid concentration and liposome production from chaotic advection has been investigated [9, 117]. However, to understand further understand the effect of lipid concentration using a novel microfluidic mixing method, initial lipid concentrations of 4 to 40 mg/mL were used at a 3:1 FRR manufactured in EtOH to investigate the effect of lipid concentration in terms of liposome size, PDI, zeta potential and EE%.

The results in figure 4.14A highlight lipid concentration as an influencing factor for both the SHM and TrM cartridge. There was shown to be a significant decrease in liposome sizes manufactured at 0.5 and 2.5 mg/mL which were 62 ± 1 nm and 55 ± 1 nm respectively (61 ± 3 nm and 54 ± 1 nm when manufactured using the TrM cartridge). There was then a steady significant increase in size from 55 ± 1 nm to 76 ± 3 nm when measured at 2.5 mg/mL to 10 mg/mL using the SHM cartridge and 54 ± 1 nm to 76 ± 3 nm using the TrM cartridge. In terms of PDI (figure 4.14B) across all concentrations, excluding 10 mg/mL when the SHM cartridge was used, all were below 0.2. As expected, there was no influence on the zeta potential as no charged lipids were used within this study with values between -1 and -7 mV (figure 4.14C). The EE% indicated significant differences in protein loading at different final liposome concentrations (figure 4.13D). There was no significant difference between the lowest and highest concentration used 26 ± 3 % and 29 ± 2 % at 0.5 and 10 mg/mL using the SHM and 31 ± 5 % and 29 ± 1 % with the TrM. The final liposome concentration of 1 mg/mL led to the highest EE% using both the SHM and TrM at 35 ± 1 % and 35 ± 2 % respectively.

The results show that varying lipid concentration maps across different cartridges with no significant differences, but what was observed was the effect of varying lipid concentrations on vesicle size. This effect was also observed by Mijajovic et al., using POPC liposomes in IPA and manufactured using a hydrodynamic focusing production method [210]. Similarly, they also observed a drop in vesicle moving between 2.5 mg/mL and 5 mg/mL which then significantly increased progressing to 10 and 20 mg/mL which is also in line with the behaviour observed using other phosphatidylcholine lipids using injection methods [215, 216].
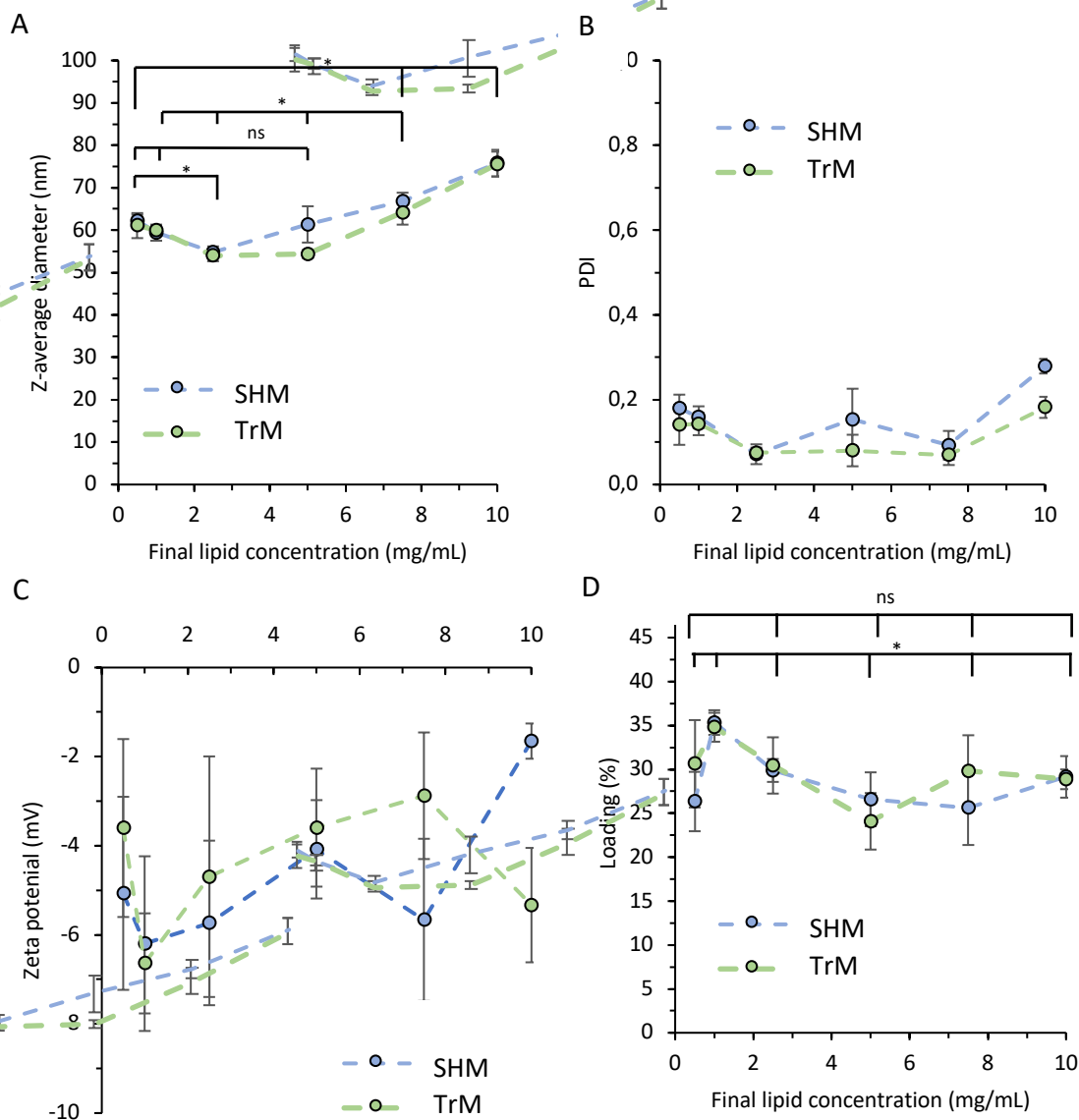
Figure 4.14 *Investigating lipid concentration using different microfluidic architectures. DSPC:Chol (2:1 w/w) liposomes were produced with and initial concentration of 0.25 mg/mL entrapped OVA with the lipids dissolved in EtOH and manufactured using either the SHM or TrM micromixer. Liposomes were manufactured at a 3:1 FRR with a TFR of 15 mL/min and final lipid concentration ranging between 0.5 to 10 mg/mL. Liposome size (A), PDI (B), zeta potenial (C) was measured using DLS measurements while protein entrapment (D) was recorded with a combination of RP-HPLC and micro-BCA. Liposomes were purified using tangential flow filtration. Results represent mean ± SD of three independent batches: p > 0.05 (ns), p < 0.05 (*)*

The size increase at concentrations greater than 7.5 mg/mL could be attributed to poor lipid solubility within the EtOH at higher concentrations leading to aggregates in the final concentration which coincidently caused an increased PDI to be observed across the two micromixers (> 0.2 PDI; figure 4.14B). It could be of interest in later studies to use a less polar

solvent such as IPA, which would improve solubility, and lead to more stable sizes with less variability across the increased lipid concentrations. Figure 4.14D was produced using a mixture of micro-BCA and RP-HPLC using the described procedures in sections 2.4.2.2.2 and 2.2.4.2.4. It was found that using a mixture of the two methods produced loading values that were within the acceptable ranges which have been previously obtained using the formulation which also highlights the interchangeability of the analytical method used for calculating EE% developed during this study and previous work [116, 187, 209]. This result also validates each technique as a quantification technique as no significant differences were observed when using either procedure for a given lipid concentration. From this set of results, there is now a mounting body of evidence that microfluidic geometry between the two cartridges tested has no impact on the physical properties of the liposomal formulation due to the non-significant results observed when the two cartridges are compared against each other. The liposomes produced by each cartridge are comparable when challenged against critical microfluidic parameters such as lipid concentration and FRR.

4.3.7 Liposome morphology and entrapped protein release kinetics

By conducting the physical characterisation work, the next stage was to check if there were any morphological changes due to the different microfluidic processes and examine potential differences in protein release rates from the formulation. From the work thus far, a great focus on the physical characterisation of vesicles have been conducted to try and best map the two microfluidic cartridges and gain a deeper understanding of the produced liposomes. An outstanding question in terms of the liposome morphology remains and whether the two cartridges produce liposomes with different physical geometries. To gain an insight towards this, cryo-TEM was employed as a direct and precise method to show any differences without the need for dehydration, cutting and staining, unlike other microscopy techniques that can be used to visualise the formulations produced from each cartridge.

Figure 4.15 A-B depicts liposomes formulated using the SHM cartridge while figure 4.15 C-D highlights the liposomes achieved using the TrM micromixer and upon closer inspection both appear visually the same in terms of uniformity and lamellarity. Furthermore, from these images, the opportunity to record additional size measurements using cryo-TEM was

conducted and compared against those from previous DLS results and nanoparticle tracking analysis (table 4.2) with a SHM cartridge in MeOH and EtOH. Nanoparticle tracking analysis (NTA) was used as an additional characterisation technique and allowed for the robust comparison of each analytical technique. From table 4.2 using NTA comparable sizes were obtained to that of the expected DLS results for both MeOH and EtOH. However, reduced sizes were observed when Cryo-TEM images were compared against DLS results for both methanal (57 ± 7 nm and 47 ± 5 nm for DLS and cryo-TEM respectively) and EtOH (70 ± 7 nm and 48 ± 5 nm).

Table 4.2 *Liposome sizes validated across different solvents using different analytical techniques. Liposomes (DSPC:Chol 2:1 w/w) entrapping OVA were produced using either MeOH or EtOH to dissolve the lipid using a SHM cartridge. Liposomes were then sized using either dynamic light scattering, nanoparticle tracking or based on CryoTEM images (ImageJ). Results represent mean ± SD of 3 independent experiments.*

	DPSC:Chol entrapping OVA formulated in MeOH			DSPC:Chol entrapping OVA formulated in EtOH		
Method	**Mean**	**Median**	**Mode**	**Mean**	**Median**	**Mode**
Dynamic light Scattering (Malvern Zetasizer)	57 ± 7 nm	60 nm	60 nm	70 ± 7 nm	72 nm	72 nm
Nanoparticle Tracking Analysis (Nanosight NS300)	53 ± 3 nm	NA	37 nm	65 ± 11 nm	NA	50 nm
Cryo-TEM	47 ± 5 nm	47 nm	44 nm	48 ± 5 nm	47 nm	44 nm

While cryo-TEM has clear advantages in terms of visualising possible morphological differences it has differences as an analytical sizing technique. One of these is that a 2D image is obtained from a 3D structure meaning various reconstructing techniques need to be employed to gain more information about a 3D shape [217]. In addition to this, as mentioned previously, the hydration layer of the liposomes is not taken into account which can explain the reduction in sizes seen compared to DLS measurements.

Figure 4.15E depicts the results of a protein release study over the course of 120 h to identify potential differences in the release rates from the formulations manufactured by each cartridge. For the release study, as RP-HPLC was being used to calculate the EE% there was a concern that during a 120 h experiment, protein concentration could dip below the LOD (50 µg/mL) of the calibration curve produced, ergo both lipid and protein concentrations were

scaled 4-fold to an initial lipid concentration of 16 mg/mL and initial protein concentration of 1 mg/mL. Before the study started, loading values of 215 µg/mL and 220 µg/mL concentrations were obtained from the SHM and TrM cartridges to ensure that protein concentrations were starting from the same point. Native OVA, 250 µg/mL (in PBS), without a liposome carrier was also analysed to identify if liposomes reduced protein release rate. Samples were maintained at 37 °C in a 300 kD dialysis bag with 100 µL of the sample removed and replaced with an equal volume of PBS at 0, 24, 48, 72, and 120 h.

From figure 4.15E there was a rapid release of free protein when a liposome carrier was not used after the 1st hour with 55% of the initial protein released and after 24 h there was no protein remaining. Using both the SHM and TrM cartridge there was a reduced release in protein from the formulation and after 24 h there was 76 and 73% of protein remaining in the liposomes made by the SHM and TrM respectively. After 120 h, 75 – 80 % of entrapped ovalbumin was released from the liposomes with no significant differences in the resulting concentrations from either cartridge. A similarity factor (f_2) was applied for the entire course of the study to identify the degree of release rate similarity between the two cartridges. From the analysis, a value of 65 was obtained (> 50 indicates good similarity) highlighting the lack of statistical difference between the two cartridges which is in line with the findings thus far.

The results concluded from this study suggest that there is now enough evidence to move forward with the scale-up to GMP and fully move on to using the TrM design which is used within the GMP mixer. The cryo-TEM results prove the ability of the TrM to manufacture comparable SUVs to those from the SHM cartridge. It could be argued that at 72 h the liposome produced by the SHM and TrM begin to diverge; however, this was not found to be significant, and at which point the protein concentrations start to become less than the LOQ at which point they cannot be accurately quantified. In addition to this, there was also a high degree of similarity in release rate kinetics from formulation produced by each cartridge producing the expected sustained release that can be achieved using this formulation and cholesterol concentration from increased lipid bilayer rigidity as shown through numerous pioneering studies [1, 84, 164]. The protein release study follows a first-order kinetic release profile and the performance of the formulation correlates to results produced within chapter 3 and previous publications using the SHM [116, 117].
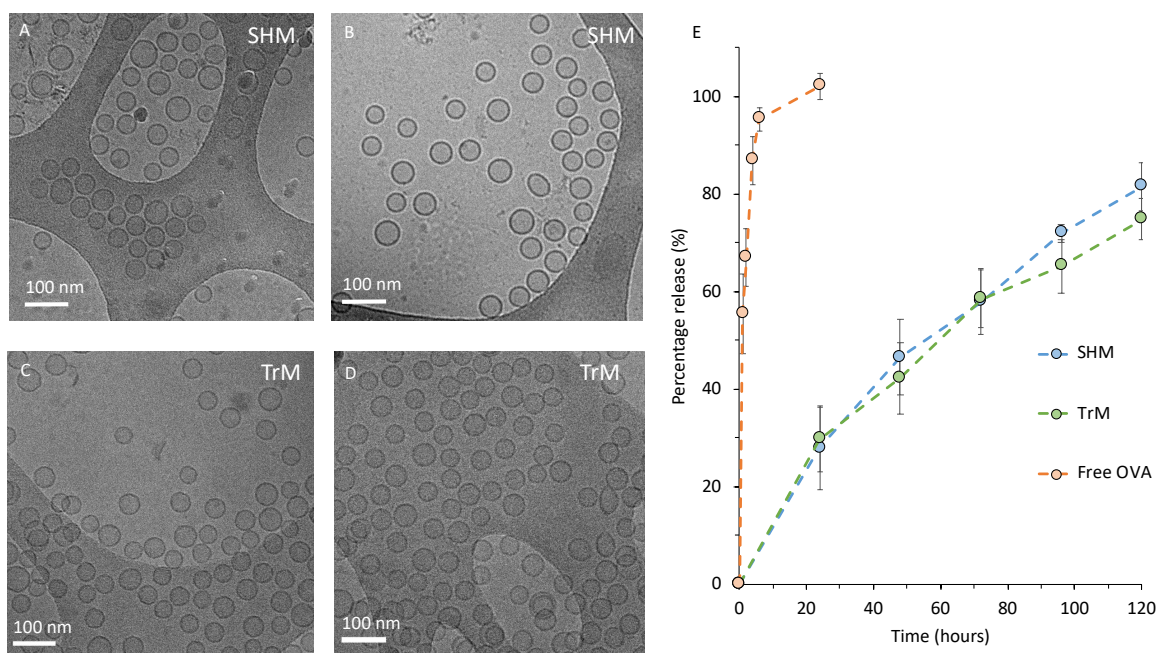
Figure 4.15 *Liposome morphology and protein release kinetic profiles using different microfluidic architecture. Liposomes were produced using DSPC:Chol (2:1 w/w) with entrapped OVA and manufactured with either a SHM or TrM architectures. Cryo-TEM images (A-D) show liposome morphology of liposomes produced using the SHM (A-B) and TrM (C-D). Protein release profile studies (E) produced by the different microfluidic mixers was conducted over 3 days with samples incubated at 37 °C and agitated. DSPC:Chol liposomes were produced using a FRR of 3:1 and TFR of 15 mL/min. Initial lipid concentration of 4 mg/mL in MeOH and an initial OVA concentration of 0.25 mg/mL in PBS was used. For the protein release studies concentrations for both lipids and protein were 4-fold higher (initial lipid concentration of 16 mg/mL and initial OVA 1 mg/mL). Protein concentration and release kinetics was calculated using RP-HPLC. Results represent mean ± SD of 3 independent batches.*

4.3.8 GMP manufacturing of protein loaded liposomes

It has been shown that liposomes can be effectively manufactured on the lab bench using a novel microfluidic architecture and map seamlessly across to the established SHM cartridge when known critical microfluidic process parameters have been challenged. From earlier experiments, bench-scale flow rate speeds did not affect the formulation when 12, 15, and 20 mL/min (figure 4.11 and 4.12) were trailed. In theory, based on these results it gives an early indication that suggests that higher throughput speeds could be achieved without affecting formulation characteristics. This is an important parameter to test as the final total flow rate within the GMP is 200 mL/min which is 10x faster than what has been used on the bench. To progress from these findings and test the bottom-up manufacturing strategy, different microfluidic platforms were used to obtain faster speeds and greater volumes using

the TrM geometry. Figure 4.16 follows the microfluidic manufacturing map from the start of the study using the bench-scale microfluidic platform (A and D) and subsequent translation to "pre-clinical" volumes permitting scale optimisation experiments allowing for 60 mL/min to be trialled (B and E). This would then enable the final progression to the GMP system all using the same protein-loaded model formulation of DSPC:Chol (2:1 w/w) without any alteration to lipid concentrations or FRR. This final portion of work surmounts this study's overall goal, which was trying to mimic a theoretical development and optimisation of a formulation from the primary R&D steps through to GMP which would further underpin microfluidics as a bottom-up manufacturing solution.
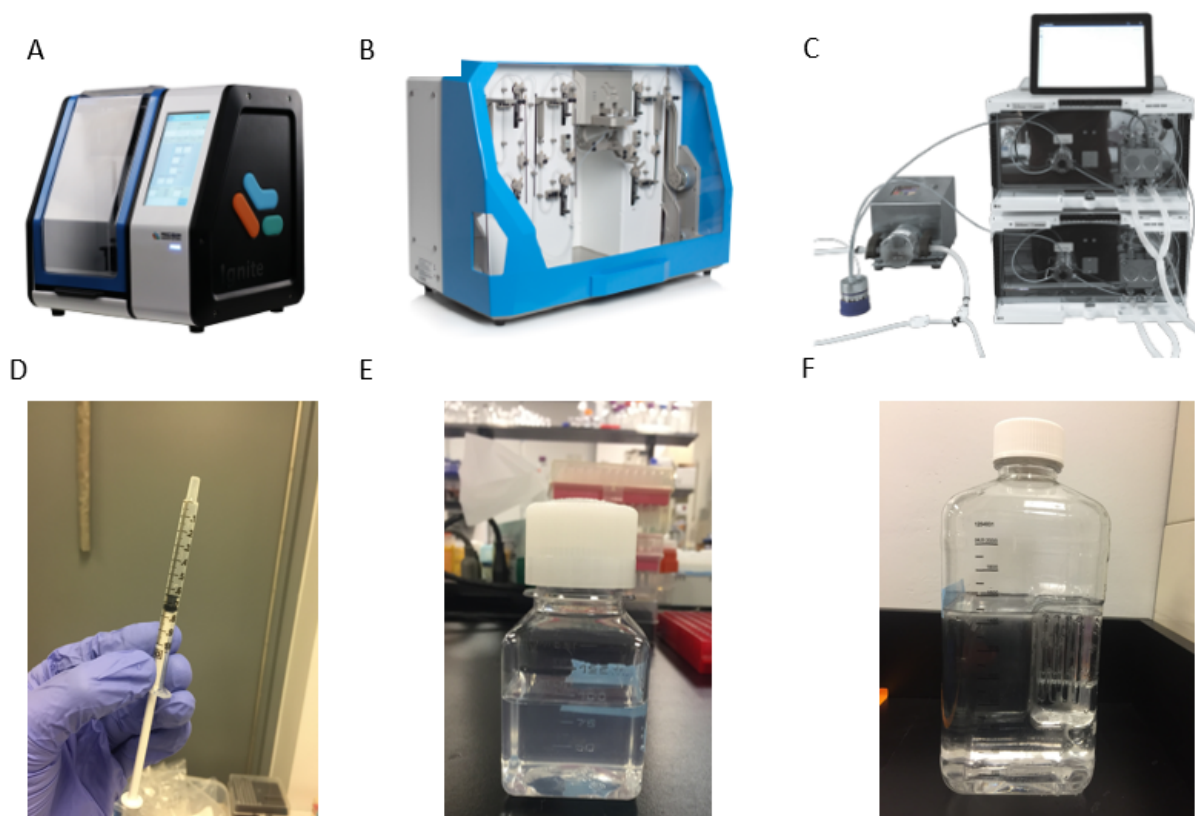
Figure 4.16 *Scalable microfluidic manufacturing map. A, B and C depict the equipment used to manufacture the liposomes allowing formulation progression from the lab bench using the NanoAssmblr® (A) to pre-clinical using the Blaze™ (B) and GMP production (C). Images D, E and F represents the starting lipid volumes for production with (D) for the NanoAssmblr®, (E) for the Blaze™ and F for GMP. Images obtained from Precision Nanosystems (A, B and C).*

4.3.8.1 <u>Optimisation studies for pre-clinical liposome manufacturing</u>

To allow for the systematic progression towards the GMP system, a "pre-clinical" system called the Blaze™ to be used which would allow for higher flow rates to be achieved. This would allow for an early insight into whether liposome physical characterisitcs would be effected by higher throughput speeds before moving to a costly GMP run. Using the Blaze™ two cartridges were trailed, these were the MF60 and MF80 (figure 4.17), of which the MF80 has a larger channel diameter and allows for a higher throughput of 90 mL/min compared to the 60 mL/mL which can be achieved using the MF60 cartridge. By conducting this experiment, it would also demonstrate the effect of either increased or decreased fluid pressure as a result of smaller or larger channel diameters (MF60 and MF80 respectively) and the effect this has on liposome production.
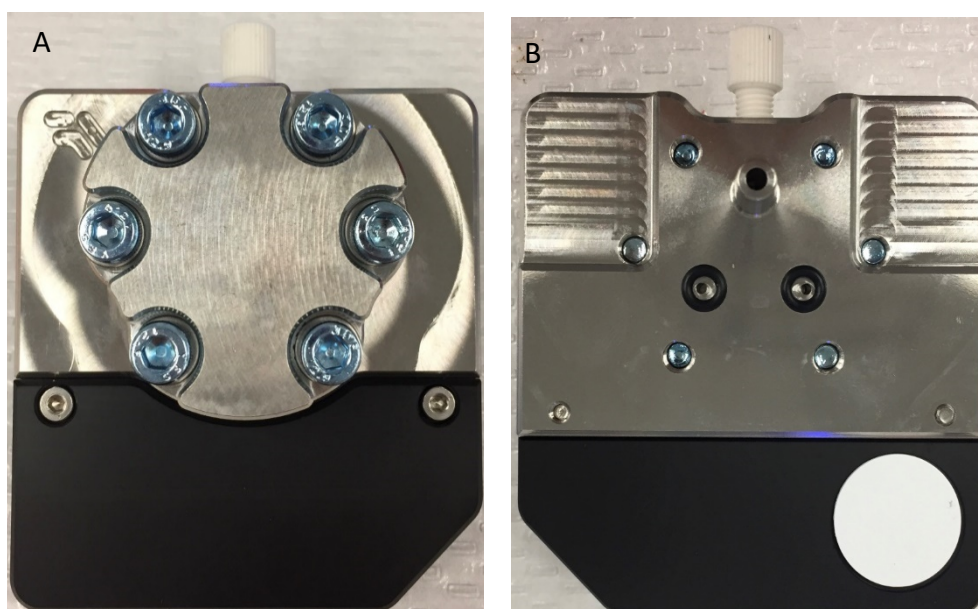
Figure 4.17 *Pre-clinical microfluidic manufacturing. Front (A) and back (B) profiles of the MF60 and MF80 cartridges using the TrM architecture used with the Blaze pre-clinical system.*

For "pre-clinical" manufacturing methods to be validated, a pre-set liposome size criteria of 60 nm were created based on results produced using the Ignite™ at 12 mL/min. Any results significantly larger than this value were deemed an ineffective method. Using these criteria, size measurements were taken at 12 mL/min and 60 mL/min with the MF60 cartridge and 12, 60, and 90 mL/min using the MF80 cartridge. Using a TFR of 12 mL/min in figure 4.18A a significant increase in size was observed using both the MF60 and MF80 cartridges (97 ± 1 nm

and 114 ± 11 nm respectively) when compared against sizes produced from the Ignite™ which was also run at 12 mL/min (61 ± 5 nm). When speeds were increased to 60 mL/min a decrease in size was observed because of the increased velocity and pressure. Using the MF60 at 60 mL/min the Z-average diameter was 61 ± 1 nm while using the MF90 the size was 84 ± 1 nm. Using the MF90 the speed could be increased further to 90 mL/min resulting in a reduced size of 77 ± 2 nm (figure 4.18A). Regardless of the TFR used on either cartridge, there was no effect on the PDI which remained below 0.2.
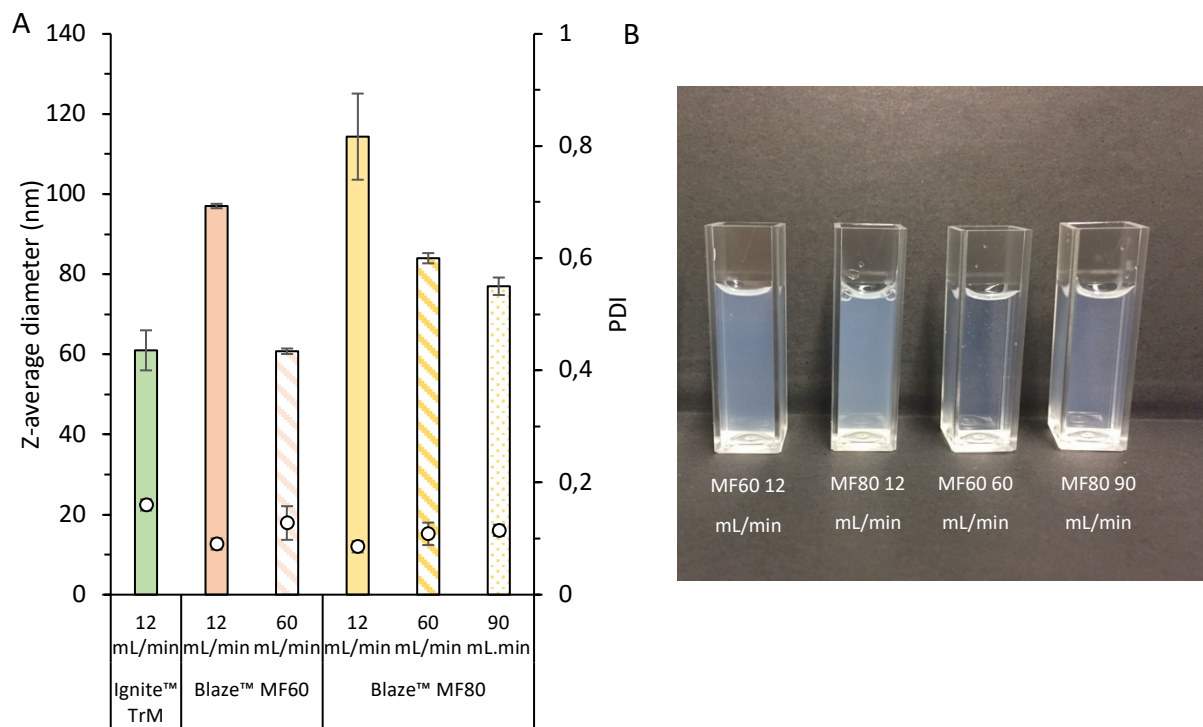
Figure 4.18 *Effect of microfluidic channel diameter and fluid velocity on liposome physical characteristics. Liposomes (DSPC:Chol 2:1 w/w; 4 mg/mL) with entrapped OVA (initial concentration 0.25 mg/mL) was used and manufactured at different fluid velcocites with the increasing channel diameters permitting higher flow rates to be used. Liposomes were produced using the Ignite™ at 12 mL/min; Blaze™ MF60 at 12 and 60 mL/min and Blaze™ MF80 at 12, 60 and 90 mL/min. Size and PDI (A) measurements were recorded using with DLS measurements and formulation turbidity for the MF60 and MF80 taken at the lowest and highest achievable speeds (B). Results represent mean ± SD of 3 independent batches.*

From figure 4.18, there is a clear indication of additional complexities when systems are scaled from the lab bench due to the size variances observed at different throughput speeds. Interestingly the findings contradict previous studies where channel width has been altered. In studies carried out by Jahn et al., different mixing channel widths (10 µm and 65 µm) were

used and found minimal changes in the liposome size distributions [92]. However, the results show that as channel diameter increases, throughput speeds need to be increased to maintain consistent pressure during liposome production for sizes to be directly mapped across from the bench scale to larger volumes. These results further illustrated that it would be possible to move to GMP scale as the formulation was not found to be affected by the throughput speeds so long as the optimised throughputs are used for the given cartridge.

4.3.8.2 Liposome performance at GMP throughput speeds

To finalise this body of work, the in-house GMP system (figure 4.19) at Precision Nanosystems (PNI), Vancouver, Canada was used with the assistance of PNI engineers to manufacture DSPC:Chol liposomes with entrapped protein. The results in 4.3.8.1 highlighted that when dealing with larger microfluidic structures the TFR needs to be increased in relation to the channel diameter to ensure that constant pressure is maintained within the channel. From this, the maximum speed of 200 mL/min was selected from these results as TrM cartridge diameters for the GMP system were optimised to run at these velocities, ergo allowing for maintained pressure across the microfluidic process using this high speed. Again, to verify the scalable production of the formulation, the size, PDI and protein loading was compared to the bench-scale and values obtained in figure 4.20. After microfluidic manufacturing TFF was used to purify the formulation was a further demonstration of a scalable manufacturing solution.
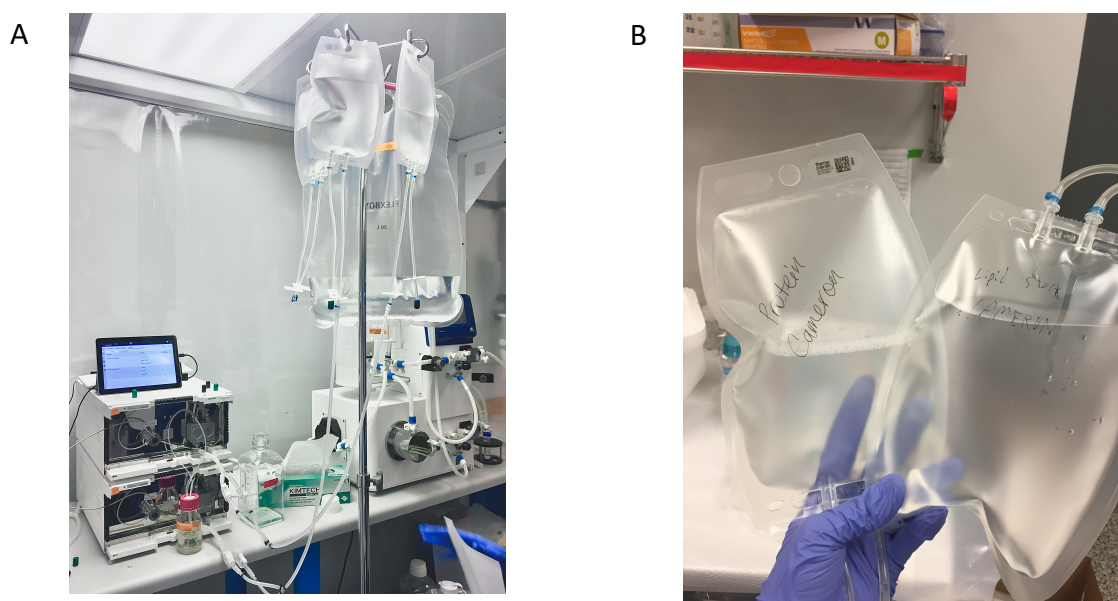
Figure 4.19 *Clinical GMP manufacturing setup. (A) The test run set up for 200 mL/min formulation run and (B) the bioprocess containers holding lipid stocks and protein stocks.*

Following the results, figure 4.20A, there was an increase in liposome size from 61 ± 5 nm to 69 ± 1 nm when the throughput speeds were increased from 12 to 200 mL/min. In terms of vesicle uniformity when manufactured at the higher speeds, a similar story to the previous work within this chapter was obtained where it was found that TFR did not influence PDI with values below 0.2 and similar distribution plots to vesicles manufactured at 12 and 60 mL/min (figure 4.20B). Furthermore, across the three throughput speeds, there was no significant change in the entrapment efficiencies, with loading capacities between 25 – 35 % (figure 4.20C) which also corroborates with previous loading measurements obtained throughout this body of work. Finally, to examine the effect of TFF size measurements were recorded both before and after TFF to check if the purification methods used had any detrimental impact on the produced formulation. The results demonstrate that both before and after TFF the liposome sizes were 69 ± 1 nm and 68 ± 1 nm (figure 4.19D) following the described TFF procedure in chapter 3. This indicated the robustness of the purification method developed had no impact on liposome physical characteristics even when mPES pore size was adjusted from that used within the lab 500 kD to that used at PNI 100 kD.

The toroidal micromixer microfluidic geometry results have demonstrated the premise it is possible to achieve a scale-independent production method allowing the complete progression from the lab bench to a GMP scenario. These results highlight the uniqueness of this manufacturing strategy as no additional critical manufacturing criteria other than the total flow rate needed to be adjusted to replicate results obtained at the lab bench. This also avoids the need to scale out a process through parallelisation by using multiple micromixers in parallel to meet GMP speeds which can additional technical complexities in terms of requiring multiple individual pumps that require individual pressures for each pump to be monitored. In contrast, scaling up allows for a proportional enlargement of the microfluidic system meaning that the same operational parameters are used, as demonstrated in figure 4.19. However, it is crucial that the correct mapping of liposomal physical attributes must be maintained across the micromixers regardless of the channel diameters [218] which underpins the mapping of the two cartridges and the purpose of this chapter. Furthermore, TFF can be used to support the role of microfluidic production by providing a scalable downstream purification method. From this work a single TFF column composed of multiple

mPES hollow fibres was used, however, by placing TFF columns in series it is possible to increase processing volumes reducing purification times and improving simplicity when large volumes need to be processed [219].
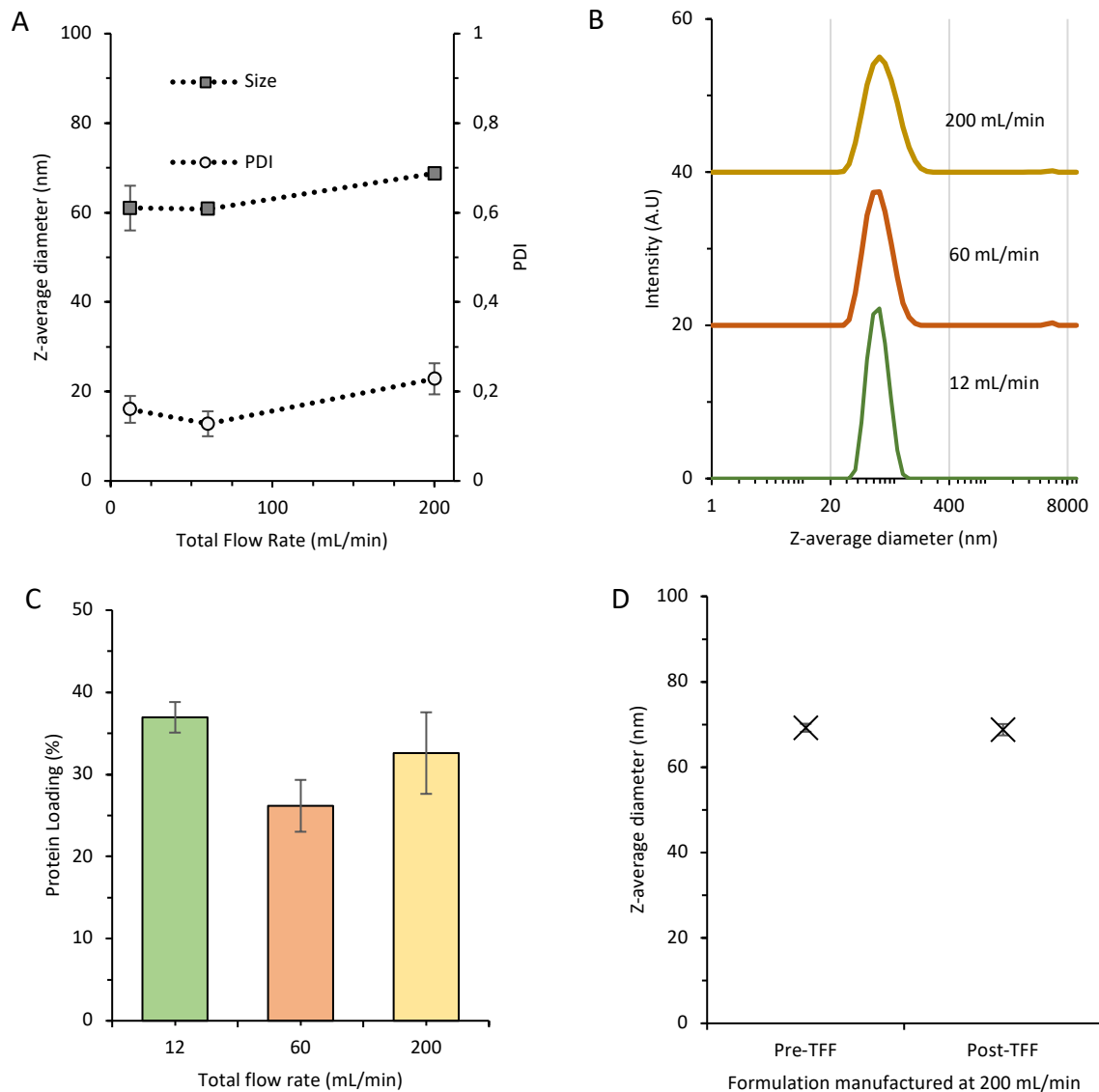
Figure 4.20 *Liposomal physiochemical characteristics impacted by progressing from the lab bench, to pre-clinical through to GMP. (A) highlights size and PDI changes as a result of manufacturing at different throughput speed with intensity plots (B) to show formulation distribution and protein loading against total flow rates (C). DSPC:Chol (2:1 w/w) liposomes were used with an initial concentration of 4 mg/mL with 0.25 mg/mL initial OVA concentration. (D) compares liposome sizes before and after TFF putifiaction. Liposomes manufactured at 12 mL/min used the Ignite™ with a TrM cartridge; at 60 mL/min the Blaze™ system was used and at 200 mL/min the NanoAssemblr GMP system. A TrM microfluidic architecture was used throughout. Results at 12 and 60 mL/min represent mean ± SD of three independent batches and for measurements at 200 mL/min results represent mean ± SD of two independent batches.*

4.4 Conclusion

The data compiled in this chapter has demonstrated a robust, high-throughput and scalable bottom-up manufacturing solution producing suitable particles for a clinical application [154]. From the results, microfluidics is a flexible manufacturing platform that allows for different microfluidic geometries to be used to produce vesicles with no significant differences. By completing a mapping study between the SHM and TrM mixers it ensures that nanoparticles can be produced with the same quality attributes using the same production parameters which provides validation for the new TrM mixer to be used with previous formulations manufactured with the SHM mixer. In the case of critical process parameters, flow rate ratio, lipid concentrations and the solvent polarity was found to have the greatest influence on vesicle formation with the trends observed in one cartridge also observed in the other. This indicates that the liposome self-assembly reaction principles apply regardless of fluid streams mixed by chaotic advection or centrifugal mixing. Most importantly, the planar geometric design of the TrM microfluidic mixer design fabrication complexities and practical limits on flow rate spending and channel enlargement affecting nanoprecipitation conditions is circumvented. This provides a direct and scalable manufacturing path for formulation development and optimisation ensuring that nanoparticles can be produced using the same process production criteria across a range of production speeds allowing transition from the lab bench to a commercial product.

Chapter 5

Development of microfluidic manufacturing processes for liposomal subunit antigen systems

Microfluidic method development
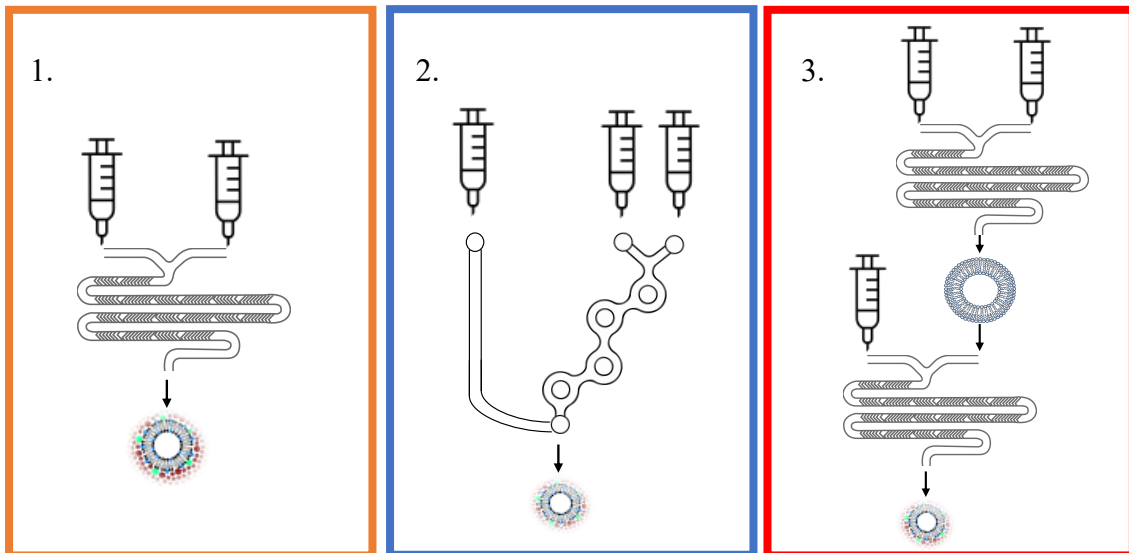
In vivo assessment
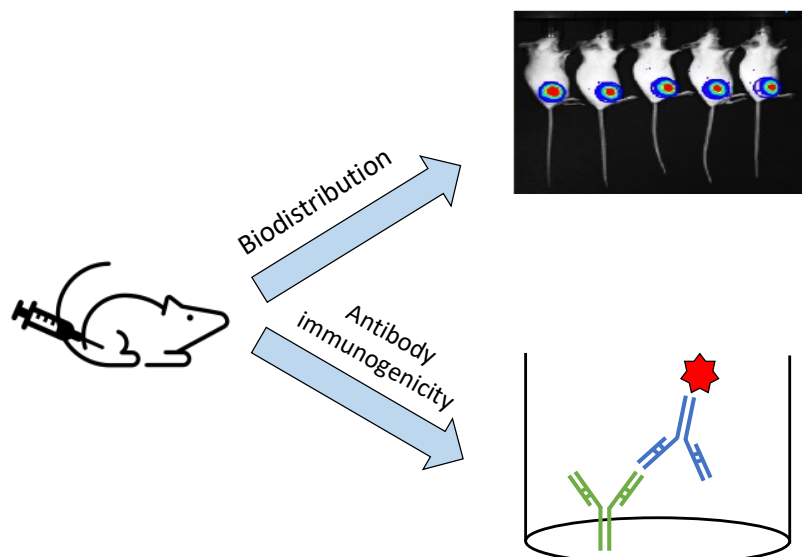
5.1 Introduction

During data collection for this chapter, a novel coronavirus emerged resulting in the World Health Organisation declaring the outbreak an international concern on the 30th of Janurary 2020 and later a pandemic on the 11th of March 2020. The pandemic challenged and advanced the biopharmaceutical industry tremendously, with lipid nanoparticles (LNPs) revolutionising the vaccine landscape [220, 221]. Liposome research and development are a cornerstone of LNP vaccine advancement and have shown to be effective vaccine carriers for inactivated with hepatitis vaccines [222] and protein subunit influenza vaccines [223]. Liposomes are still extensively studied and used as vaccine adjuvants [63] with the liposomal adjuvant CAF09b (Staten Serum Institut, Copenhagen, Denmark) used in phase 1 trials against prostate cancer (NCT03412786) and a neoepitope-based peptide cancer vaccine (NCT03715985). For lipid-based vaccines, a hindering factor in their continued success and global accessibility is the requirement for streamlined and controlled manufacturing, allowing for rapid distribution and reduced costs. Microfluidics adopts such an approach by permitting scale-independent processes with the proven capability to precisely control nanoparticle sizes compared to other methods, thus avoiding the requirement for downstream size reduction strategies [117].

The requirement for controlled consistent production of liposomes is crucial due to immune responses being dependant on physical attributes for liposomal formulations such as vesicle size [22, 67], charge [69, 224], vesicle fluidity [225] and composition [226]. With this shown to be vital for vaccine performance [227], controlling subunit protein adsorption through electrostatic attraction is the next step in the microfluidic manufacturing of cationic liposomal subunit vaccines. Traditional top-down methods of liposome production require the hydration of a lipid film with an aqueous buffer with downstream size reduction processes such as high shear mixing to produce liposomes within the nanoscale to desired sizes [177, 228]. This limits manufacturing to multiple batch-scale production platforms, leading to low to medium throughput with high cost [209]. Furthermore, the absence of precise critical manufacturing criteria for protein subunit adsorption (such as mixing speeds and volumes) hinders scalability.

In contrast, microfluidics uses a bottom-up approach [112]. Microfluidics promotes rapid mixing of two phases: an organic phase (lipids dissolved in a water-soluble solvent) and an aqueous phase (buffer) through a micromixer [117], enabling the production of vesicles without further size reduction and low polydispersity, which can help with formulation stability and performance [108, 153]. Vesicle sizes can be precisely controlled and modulated with high reproducibility using operational parameters [209, 229], as supported by chapters 3 and 4. The increased production speeds with microfluidics (up to 200 mL/min) [209] and elimination of downstream downsizing methods allow reduced operational times and costs. Microfluidics can address a crucial manufacturing area regarding liposomes' consistent and controlled production. However, the adsorption of protein subunits onto the surface of cationic liposomes adds an additional step after liposome production and can impact vesicle size, PDI, and zeta potential.

5.2 Aim and objectives

Therefore the aim of the work within this chapter was to introduce and develop different a controlled microfluidic protein adsorption to cationic liposomes method and to align current continuous manufacturing trends [230, 231] for future use when developing liposomal protein subunit vaccines. To achieve this, the objectives were to:

- Develop three different manufacturing methods to control antigen adsorption by either i) mixing lipid streams containing DSPC, Chol and DDA (10:5:4 w/w) to a buffer stream containing OVA or ii) preform liposomes within the microfluidic cartridge and inline mix with OVA to the formed liposomes or iii) preform liposomes and pass the liposomes through the microfluidic cartridge again and mix the liposomes with the OVA within the micromixer.

- Assess and evaluate various operational parameters such as FRR, TFR solvent choice, and liposome:protein (L:P) ratio for the three mixing methods by measuring physical characterisitics such as vesicle size, PDI, zeta potential and vesicle stability. The methods will be evaluated between each other to identify a lead manufacturing method that allows for stable SUV vesicles with adsorbed OVA to use in *in vivo* immunogenicity experiments.

- Assess antigen protection against proteolytic enzymes provided by cationic liposomes (DSPC:Chol:DDA 10:5:4 w/w) by the quantitative assessment developed to measure fluorescence emission from fluorescently tagged OVA to measure protein degradation. The novel method will be verified against results from SDS-PAGE to visually verify if liposomes provide a degree of protection.

- Explore individual liposome and antigen *in vivo* biodistribution after injection by dual labelling lipids and OVA with fluorescent dye. Using the IVIS *in vivo* imaging system, will track the movement of liposomes and protein within the same mice over 9 days and allow for the quantitative assessment of accumulation of liposomes and antigen at the injection site or within key organs involved with pharmacokinetics (liver, kidneys) or adaptive immune responses (spleen, popliteal and inguinal lymph nodes).

- Analyse IgG total, IgG1 and IgG2a antibody subtype responses uscing the active antigen "major outer membrane protein" (MOMP) of Chlymadia trachomatis on selected L:P ratios and manufacturing methods following i.m. injections to understand if i) antibody responses are affected by adjuvant:antigen ratios or ii) if using different manufacturing methods can be used to stimulate specific antibody subtypes

5.3 Results and Discussion

5.3.1 Microfluidic mixing controls antigen surface adsorption reducing vesicle sizes while improving vesicle homogeneity

A key factor to drive formulation development is the requirement to control the product characteristics through the manufacturing process. Initial experiments investigated a microfluidic protein adsorption method that would allow the controlled production of liposomes and aid in the controlled adsorption of protein subunits for use within vaccine manufacturing and development. To examine this further, empty liposomes (DSPC:Chol:DDA (10:5:4 w/w)) were manufactured using a FRR of 1:1 with a final lipid concentration of 2 mg/mL and purified by dialysis for 1 h to remove residual solvent. Purified liposomes were then mixed 1:1 *v/v* with ovalbumin (OVA) at various liposome to protein ratios (L:P w/w) using a manual "uncontrolled" method by simply pipetting the protein onto the liposomes. A manual "controlled" process involved slow vortex mixing while pipetting the protein onto the liposomes [232]. The microfluidic method involved feeding the liposomes through the microfluidic cartridge in one inlet with the OVA at the other inlet at a flow rate ratio of 1:1 and TFR of

15 mL/min. Table 5.1 outlines the liposome and protein concentrations for each of the L:P ratios investigated using the uncontrolled, controlled and microfluidic adsorption methods.

Table 5.1 Liposome and protein concentrations for respective L:P ratios before and after mixing

	Before mixing		After mixing (1:1 v/v or 1:1 FRR)	
L:P ratio	Liposome concentration (mg/mL)	Protein concentration (mg/mL)	Liposome concentration (mg/mL)	Protein concentration (mg/mL)
60:1	2	0.03	1	0.016
15:1	2	0.13	1	0.06
10:1	2	0.20	1	0.10
7:1	2	0.29	1	0.14
5:1	2	0.40	1	0.20
3:1	2	0.67	1	0.33
1:1	2	1.0	1	1.0
1:3	2	6.0	1	3.0
1:10	2	20.0	1	10.0

Figure 5.1 shows that the initial size and PDI of purified liposomes were 47 ± 3 nm and 0.19 ± 0.05, respectively. Using the uncontrolled manual method (figure 5.1A), vesicle size steadily increased between 60:1 to 3:1 L:P starting at 110 ± 3 nm and rising to 4415 ± 1482 nm. The vesicle size subsequently dropped to 734 ± 301 nm when a 1:1 L:P ratio was used and decreased further to 219 ± 11 nm at 1:3 L:P. Across all the L:P investigated in figure 5.1A, excluding the empty liposomes, the PDI remained between 0.4 – 0.7. As the protein concentration increases relative to the cationic liposomes, the zeta potential decreases from approximately 50 mV (with no protein added) to 10 mV at a 3:1 L:P ratio. This near-neutral zeta potential also co-insides with the high degree of particle aggregation observed at this L:P. With further increases in protein concentration, the zeta potential drops to approximately -20 mV suggesting a complete reversal of the liposome charge and a subsequent reduction in particle size again (figure 5.1A).

Figure 5.1B depicts the next step of the protein adsorption process where a vortex mixer was used to create a stable mixing motion with OVA that was pipetted directly onto the spinning liposomes using different concentrations of OVA. Again, a similar effect to figure 5.1A was observed with increasing sizes moving between 60:1 and 3:1 LP (99 ± 4 nm and 4001 ± 360 nm, respectively). The liposome PDI decreased because of increasing protein concentrations, as shown by the particle PDI between 60:1 and 3:1 L:P. The liposome size in figure 5.1B decreased between 1:1 and 1:3 L:P with the particle PDI remaining high between 0.4 and 0.9. Furthermore, the zeta potential profiles in figure 5.1D and E closely matched the empty vesicles displaying a zeta potential of +50 mV, which dropped to -20 mV

at the 1:1 and 1:3 L:P. From using the two protein adsorption methods in figure 5.1A and B, there were no notable differences in the size, PDI, and zeta potential profiles.

To develop a more controlled mixing process, microfluidics was introduced to promote consistent mixing. The microfluidic mixing in figure 5.1C demonstrated that particle size was reduced for all mixing ratios except at the lower 5:1 and 3:1 L:P ratios (figure 5.1). For example, improvements and control afforded by microfluidics from the start of formulation manufacturing methods have led to observations of liposomes being more uniform with smaller particles sizes than those produced by lipid film hydration and extrusion [233]. The formulation without any adsorbed protein was highly cationic with a charge between 60 – 70 mV. This was reduced to approximately 30 mV at 60:1 L:P, which was steadily reduced to 10 – 15 mV, in figure 5.1D, E and F, at a 3:1 L:P. As a result of the increased protein loading, it was possible to flip the zeta potential at a L:P of 1:1 to approximately -20 mV for all manufacturing methods with < 30 mV obtained for 1:3 and 1:10 L:P. More importantly, using the microfluidic method, PDI was reduced across all L:Ps compared to the other complexation methods with PDIs ranging between 0.1 – 0.4 due to improving the control over the manufacturing process. The zeta potential followed a similar trend in figures 5.1D, E and F for all production methods.
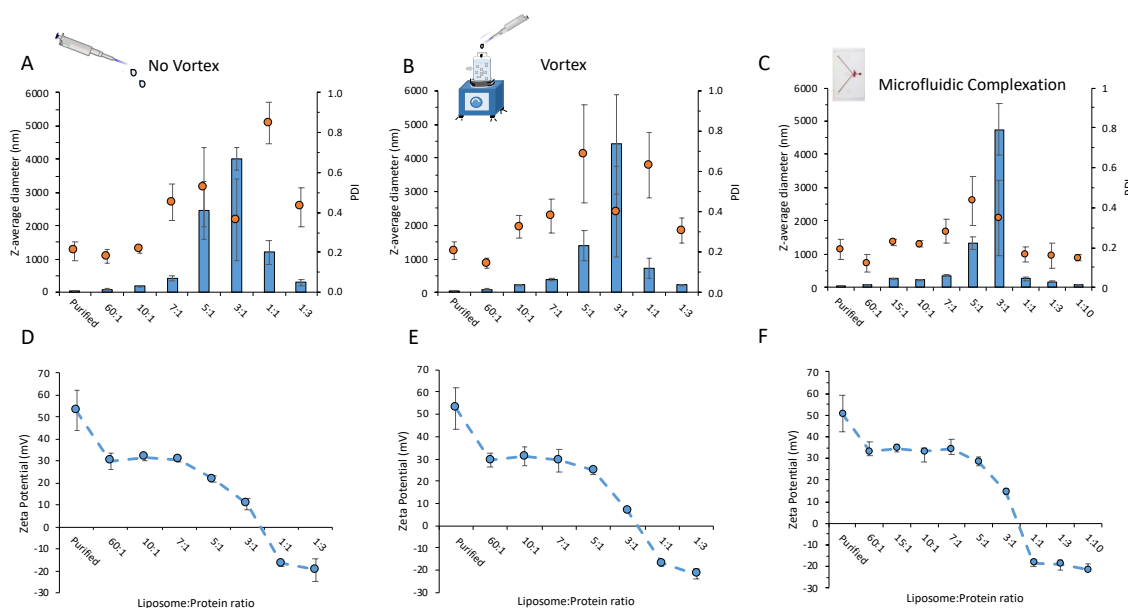
Figure 5.1 *Steps to refine size and liposomal uniformity upon protein sub-unit adsorption by altering adsorption methods for controlled adsorption. To investigate controlling protein adsorption a cationic liposomal formulation of DSPC:Chol:DDA (10:5:4 w/w) was manufactured by microfluidics at a FRR of 1:1 and 15 mL/min in MeOH (solvent phase) and Tris 10 mM (aqueous phase) which was purified by dialysis method (14 kD membrane) immediately after leaving a final liposome concentration of 2 mg/mL. Sizes were then measured by suspending OVA Tris 10 mM and either pipetted directly onto the liposomes (1:1 v/v) (A); vortexed while pipetting (1:1 v/v) (B) or mixed with liposomes via microfluidics (C) at a FRR of 1:1 and zeta potentials recorded for the respective methods (D, E and F). The final liposome concentration after OVA adsorption was 1 mg/mL with OVA concentrations between 0.016 – 10 mg/mL depending on the investigated L:P ratio. Results represent mean ± SD from 3 independent batches.*

This study aimed to control anionic protein adsorption with the cationic liposomes and improve formulation consistency between the batches produced. By initially looking at the overall size trend in figure 5.1, regardless of the manufacturing strategy used, the liposome size increases with increased protein adsorption starting from 60:1 with liposome size reaching their largest at a 1:3 L:P. This effect resembles strong similarities to "re-entrant condensation" of cationic liposomes [234], with similar findings observed using DOTAP liposomes [235]. The results in figure 5.1A - C show liposomes with the highest Z-average when the surface charge of the vesicles is near neutral (figure 5.1D -F). At this point, Van der Waals's attractive forces supersede the Coulomb forces, leading to the observed large aggregates [234, 236]. As the protein concentration increases further, the electrostatic repulsive forces favour smaller vesicles. At higher protein concentrations, the zeta potential of the formulation flips from a cationic to anionic charge (figure 5.1D, E and F) as a result of protein saturation neutralising the cationic nature of the DDA lipid. The researchers Hamborg et al., also observed this effect from investigating BSA adsorption onto DDA:TDB liposomes and its impact on membrane fluidity and found that as protein concentration increases, the DDA lipid charge is neutralised [237].

5.3.2 Increasing protein concentrations destabilises liposomes allowing for the identification of lead formulations

From figure 5.1, it was shown that microfluidics could achieve high concentrations of protein adsorption without compromising vesicle uniformity or large vesicle sizes. To refine the formulation selection further, a two-week stability study was conducted using seven formulations between 60:1 and 8:1 L:P to evaluate colloidal stability, vesicle uniformity and zeta potential. The same microfluidic operating parameters were used in figure 5.2 (FRR of 1:1 and TFR of 15 mL/min to mix liposomes and then coat the liposome surface with protein).

The results in figure 5.2 show that 'empty' cationic liposomes (no protein) and cationic liposomes at a low L:P ratio of 200:1, 60:1 and 30:1 tended to be more stable in terms of size, PDI, zeta potential and protein loading over the 14-day study period. However, as the protein

concentrations increase in the formulation, there is a general trend of large increases in size and PDI as a function of time indicating poor stability resulting in vesicle aggregation. For example, at 10:1 LP and 8:1 L:P, the particle at day 0 was 260 ± 22 nm and 522 ± 85 nm, respectively. These increased to 484 ± 37nm and 1055 ± 310 at day 14, respectively (Figure 5.2A). In contrast, for 200:1; 60:1 and 30:1 L:P there was < 20% relative size increase over the 14-day study. Vesicle uniformity was also investigated, and from figure 5.2B, an additional trend was observed whereby the PDI for each of the formulations tested increased with antigen concentration (i.e. the PDI for empty particles < 200:1 < 60:1 < 30:1). Despite the increased PDI, the 'empty' liposomes (200:1 and 60:1), had PDIs < 0.2 over the 14 days. The remaining formulations were ≤ 0.3 after 14 days, excluding the 10:1 and 8:1 L:P, which were 0.36 ± 0.07 and 0.45 ± 0.13, respectively.

Figure 5.2 *Assessing the influence of L:P ratios by microfluidic adsorption on liposomal stability and loading efficiencies. The effect of liposomal stability was measured over 14 days with size (A), PDI (B), zeta potential (C) and loading efficiencies (D) recorded at specific time points to plot the degree of change as a result of L:P ratios. DSPC:Chol:DDA (10:5:4 w/w) liposomes were manufactured at a 1:1 FRR and 15 mL/min at a final liposome concentration of 2 mg/mL using MeOH (solvent phase) and Tris 10 mM (aqueous phase) with solvent removed by dialysis (14 kD membrane). OVA, suspended in Tris 10 mM (pH 7.4) was then adsorbed to liposomes at a FRR of 1:1 and TFR of 15mL/min leaving a final liposome concentration of 1 mg/mL and OVA concentrations between 0.005 - 0.125 mg/mL. Samples were stored at 4 °C between time points. Results represent mean ± SD from 3 independent batches.*

In figure 5.2C, the zeta potential across the seven L:P remained between 25 – 35 mV and above 40 mV for the empty vesicles. This result was expected due to the shielding of the liposome surface with similar electrostatic interactions also observed in previous studies [224, 238]. The stability study was further expanded by examining antigen loading after day 14. Initially removing any excess protein on day 0 after protein complexation (using the dialysis procedure explained in 2.2.5.1) and again removing any dissociated protein after day 14 allowed a percentage loss to be calculated (figure 5.2D). Encouragingly, protein loading remained > 85% for all the L:P tested, which could be credited to the sustained positively charged zeta potential throughout the study supporting the electrostatic adsorption.

Protein adsorption onto lipid surfaces is driven by electrostatic interactions and Van der Waals forces [239]. The adsorption of protein onto lipid surfaces has been shown to impact vesicle size, charge and vesicle aggregation [240, 241], with the degree of adsorption influenced by the vesicle size, charge composition and exposure time [241-243]. A suspension of nanoparticles, such as liposomes, are prone to agglomeration due to physical instability, which can be affected by vesicle size, charge, concentration and adsorbed compounds [244]. In addition to the surface charge of the vesicle being crucial for protein electrostatic adsorption [245], the surface area of vesicles has also been shown to be essential for encouraging protein adsorption. Such experiments demonstrated this effect by using gold nanoparticles. It was found that spherical nanoparticles permit three times higher protein adsorption than branched shape gold nanoparticles with a similar size of 50 – 70 nm [246].

Furthermore, vesicles with a large radius of curvature could improve protein binding and allow for stronger interactions between the vesicles and protein which was demonstrated using silica nanoparticles [247] and gold nanoparticles [248]. Lipid-protein interactions are a complex relationship with many formulation attributes that can impact the degree of protein adsorption. However, the results in figure 5.2 highlight that using an unloaded vesicle of < 100 nm and a cationic surface charge allow for a high degree of lipid-protein interaction. Such lipid-protein interactions promoted good vesicle stability at higher L:P ratios with high protein loading (close to 100%) after 14 days regardless of the L:P used.

To further investigate the short-term stability, the size and PDI were measured every hour over a 14 h period using the 10:1 (figure 5.3A), 30:1 (figure 5.3B), and 60:1 L:P (figure 5.3C) formulations. The results show that whilst the 60:1 and 30:1 L:P formulations (Figure 5.3B and C) remain relatively stable over the 14 h period, the 10:1 L:P (Figure 5.3A) shows a rapid increase in the size and PDI within 4 h. Similarly, with the 10:1 L:P formulation, the vesicle PDI increased, indicating a more polydisperse system. The rapid increase in vesicle size also occurred using a slightly larger protein, streptavidin (66 kDa). Loughrey et al. coupled streptavidin to liposomes, with a vesicle size of 100 nm, at 100 µg protein/µmol lipid [249] and over 12 h the vesicle size approximately doubled, and an increase in the polydispersity of the vesicles was recorded [250]. This demonstrates that conditions that increase the degree of liposome to protein interaction, such as the lipid concentration, impacts the degree of aggregation due to the increased crossing-linking between protein molecules [249, 251].
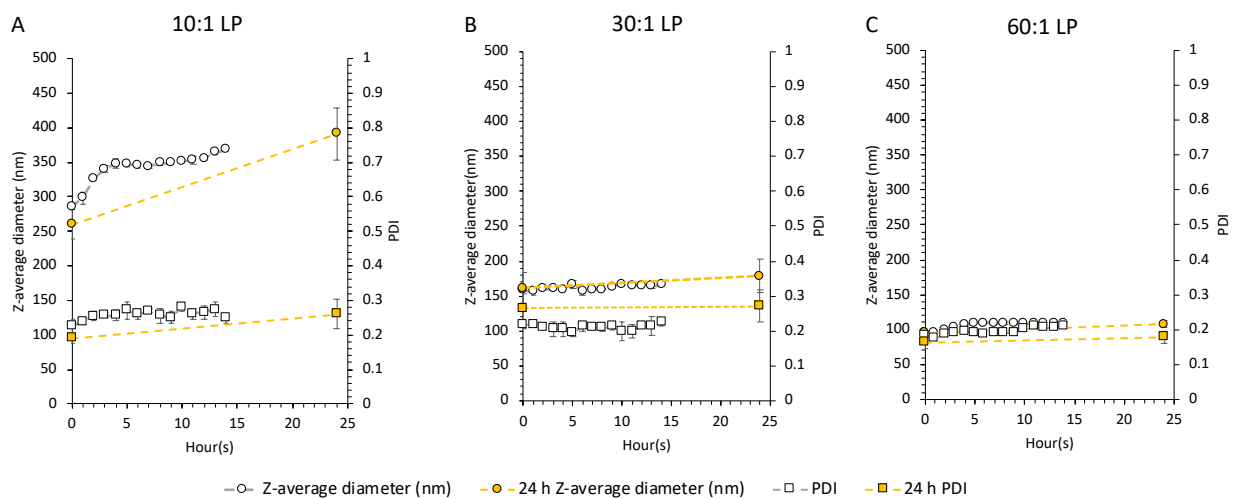
Figure 5.3 *Tracking liposome stability over 14 h. Liposome size and PDI was measured for 10:1 L:P (A); 30:1 L:P (B) and 60:1 L:P (C) over 14 h recorded at each hour. A method was set up to cool samples to 4 °C between measurements to simulate the storage conditions in figure 5.2 with samples heated at to the required 25 °C during the measurement. The same method of liposome production, purification and protein adsorption used in figure 5.2 was used to obtain figure 5.3.*

5.3.3 The selection of flow rate ratios controls the influence of solvent selection and allows early insight for a reduced solvent production method

To further refine the 60:1 L:P formulation, the FRR and choice of water soluble solvent were considered to identify if liposomes could be produced with low residual solvent concentrations to allow inline protein adsorption with minimal biological denaturing. The solvents trialled in figure 5.4 were MeOH and EtOH as both are organic and water-miscible and therefore applicable for use within a microfluidic system. MeOH was used to suspend the lipids in figures 5.1 - 5.3. However, transitioning to EtOH would be preferred due to its reduced toxicity profile [154].

Figure 5.4 presents various FRRs using either MeOH or EtOH to analyse the influence of mixing ratios and solvent selection while maintaining a final lipid concentration of 2 mg/mL. Figure 5.4A shows that vesicle sizes between 45 – 55 nm and PDIs of < 0.25 were achieved using an FRR of 1:1, 3:1, and 5:1. However, increasing the FRR to 19:1 meant the initial lipid concentration had to be increased to 40 mg/mL to achieve a final liposome concentration of 2 mg/mL. This led to significantly ($p < 0.05$) increased sizes (138 ± 50 nm and 183 ± 93 nm respectively) and PDIs (0.43 ± 0.1 and 0.57 ± 0.09 respectively; figure 5.4A). Figure 5.4B examined the formulations zeta potential for each FRR investigated; all formulations were cationic (> 30 mV), and there were slight variances in the results across the different FRR examined. However, as the purpose was to reduce vesicle size while maintaining a uniformity, the larger particle size & PDI obtained using the 9:1, and 19:1 FRR did not fall into our formulation criteria. Therefore this was not further investigated but may result from different lipid solubilities in MeOH at these high lipid concentrations. The next step was to repeat this experimental setup using EtOH to dissolve the lipids; in figure 5.4C, the 1:1 FRR led to the largest vesicle sizes at 121 ± 7 nm and the most uniform PDI of 0.03 ± 0.01. The vesicle sizes were then shown to plateau across 3:1, 5:1, and 9:1 FRR with a size range between 50 – 56 nm and a low PDI of < 0.25. This size increased marginally to 74 ± 23 nm at an FRR of 19:1 but was more heterogeneous with a PDI of 0.33 ± 0.14. From figure 5.4D, the zeta potential across all the FRRs tested was more consistent with values of 40 – 55 mV.

From chapter 3 and supporting literature, the organic solvent has been shown to influence the liposomal formation [116, 252] and was identified as a important microfluidic process parameter that can be used to alter liposome physical characterisitics. This is confirmed for this cationic liposomal adjuvant formulation (figure 5.4). However, this effect was only observed up to a 5:1 FRR. Above this FRR, it was found that by switching to EtOH, which is a less polar solvent compared to MeOH (polarity index: 5.2 vs 6.6 respectively), maintained vesicle at approximately 50 nm while in the case of MeOH at this FRR, the size and PDI increased significantly to 138 ± 50 nm and 0.43 ± 0.1 (figure 5.4). At 19:1 FRR, the size increases further to 183 ± 93 nm in the case of MeOH, while for EtOH, the size increase was 74 ± 23 nm (figure 5.4).
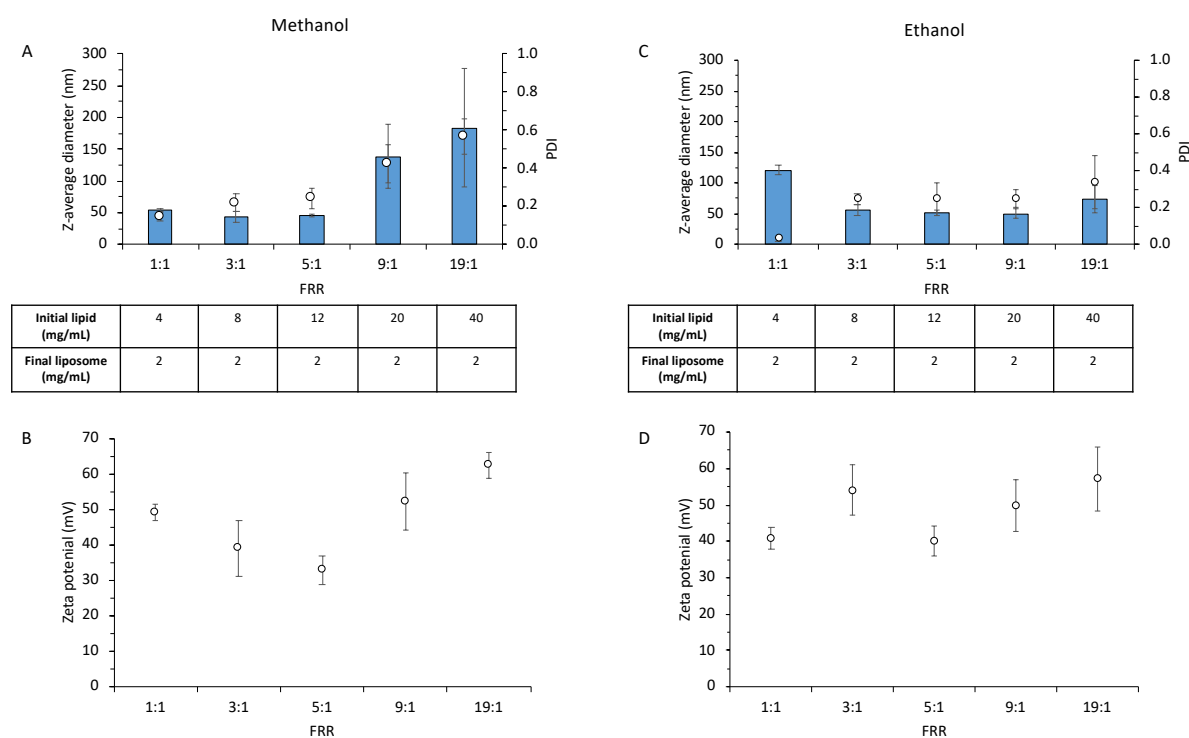
Figure 5.4 *Effect of flow rate ratios on liposome physical characteristics and influence of solvent selection. The impact of solvent on liposomes size and PDI for MeOH (A) and EtOH (C) in addition to zeta potential for MeOH (B) and EtOH (D) were investigated along with FRR to refine optimal liposomal manufacturing parameters for DSPC:Chol:DDA (10:5:4 w/w) liposomes. A TFR of 15 mL/min was used with Tris 10 mM used for both the aqueous phase at the respective FRRs and the dialysis buffer. Results represent mean ± SD from 3 independent batches.*

This could be due to the solubility of the lipids in each solvent at the concentrations required to keep a final fixed concentration of 2 mg/mL. At 9:1 FRR a lipid concentration of 20 mg/mL is required and for 19:1, a 40 mg/mL initial lipid concentration is needed. At these concentrations, a less polar solvent would be more advantageous to create a uniform solution due to the non-polar nature of the lipids used (namely DSPC with 18C acetyl chain) allowing more intermolecular forces to occur between the lipids and solvent, improving solubility. As MeOH is more polar than EtOH, fewer intermolecular attractions can occur, causing lipids to fall out of solution at higher initial lipid concentrations. When considering liposome geometry, Ali et al. [253] demonstrated that the introduction of lipids containing unsaturated double bonds leads to protruding alkyl chains inducing steric hindrance resulting in a less condensed monolayer caused by larger distances between molecules. Therefore, for larger vesicles, it could be that a poorly dissolved lipid mix results in uneven vesicle self-assembly during microfluidic mixing, as described by Forbes et al., [117]. As a result, uneven packing densities and a more polydisperse formulation with less condensed bilayer packing densities would result in larger vesicles. A key observation from this finding was that by using EtOH and applying a 9:1 FRR (which produced liposomes within the critical criteria) a residual solvent percentage of 10 % v/v could be obtained. Thus a low solvent microfluidic protein mixing strategy can be used, allowing antigen adsorption with a reduced risk of protein denaturing. Ergo, the next step was to identify a microfluidic mixing ratio permitting uniform vesicle formation with sizes of < 100 nm.

5.3.4 Controlled antigen adsorption permits SUV formation with reduced solvent volume

Using the 60:1 L:P, the next step was to develop further a microfluidic mixing strategy to improve the controlled adsorption while simultaneously allowing the operation at reduced solvent concentrations. Figure 5.5 outlines the development of a novel mixing method to reduce solvent concentrations with the size, PDI, zeta potential and loading efficiencies measured to identify if changing the protein adsorption mixing ratios leads to alterations in the physical characteristics.

A simplified schematic of the mixing strategy in figure 5.5A outlines the method used to control protein adsorption while simultaneously diluting out the residual solvent and

exposing the protein to lower solvent levels. Using this method, the results in figure 5.5B highlight a size increase between the empty vesicles (47 ± 1 nm) and the pre-dialysis formulation (83 ± 1 nm, 86 ± 4 nm, and 89 ± 3 nm at FRR 1:1, 3:1 and 9:1 respectively; statistical significance (p ≤ 0.01) was only observed between the 1:1 and 9:1 FRRs). Given that there was now protein in the aqueous phases, the final protein concentrations increased from 16.7 μg/mL to 25 μg/mL and 30 μg/mL using the 1:1, 3:1, and 9:1 FRRs, respectively.

Interestingly, following protein adsorption, the vesicle PDI decreased from 0.27 to < 0.2 in all FRRs tested, indicating a high degree of uniformity in the formulations. These liposomal-protein formulations were then subjected to dialysis to remove the solvent. After dialysis, the vesicle size increased to between 100 – 105 nm for each FRR with no significant difference (Figure 5.5B), and the PDI of < 0.2 was maintained for all three FRRs. In figure 5.5C, antigen loading was calculated from the theoretical antigen adsorption efficiencies. From the results, there were no significant differences in antigen adsorption used at the three FRRs tested; using the 1:1 FRR, the antigen loading was 108 ± 13 %, while for the 3:1 and 9:1 FRR, the degree was antigen loading remained high at 81 ± 18 % and 83 ± 13 % (figure 5.5C).

A

9:1 FRR
(Aq:solvent)
15 mL/min

Lipids +
EtOH

X:1 FRR (L:P)
15 mL/min

Tris 10 mM;
pH 7.4

OVA + Tris

B

ZP (mV)	52 ± 8	39 ± 9	40 ± 5	39 ± 4	35 ± 8	37 ± 5	40 ± 6

C

	1:1 FRR	3:1 FRR	9:1 FRR
Final lipid (mg/mL)	1	1.5	1.8
Final protein (µg/mL)	16.7	25	30
Final solvent % (v/v)	5	7.5	9
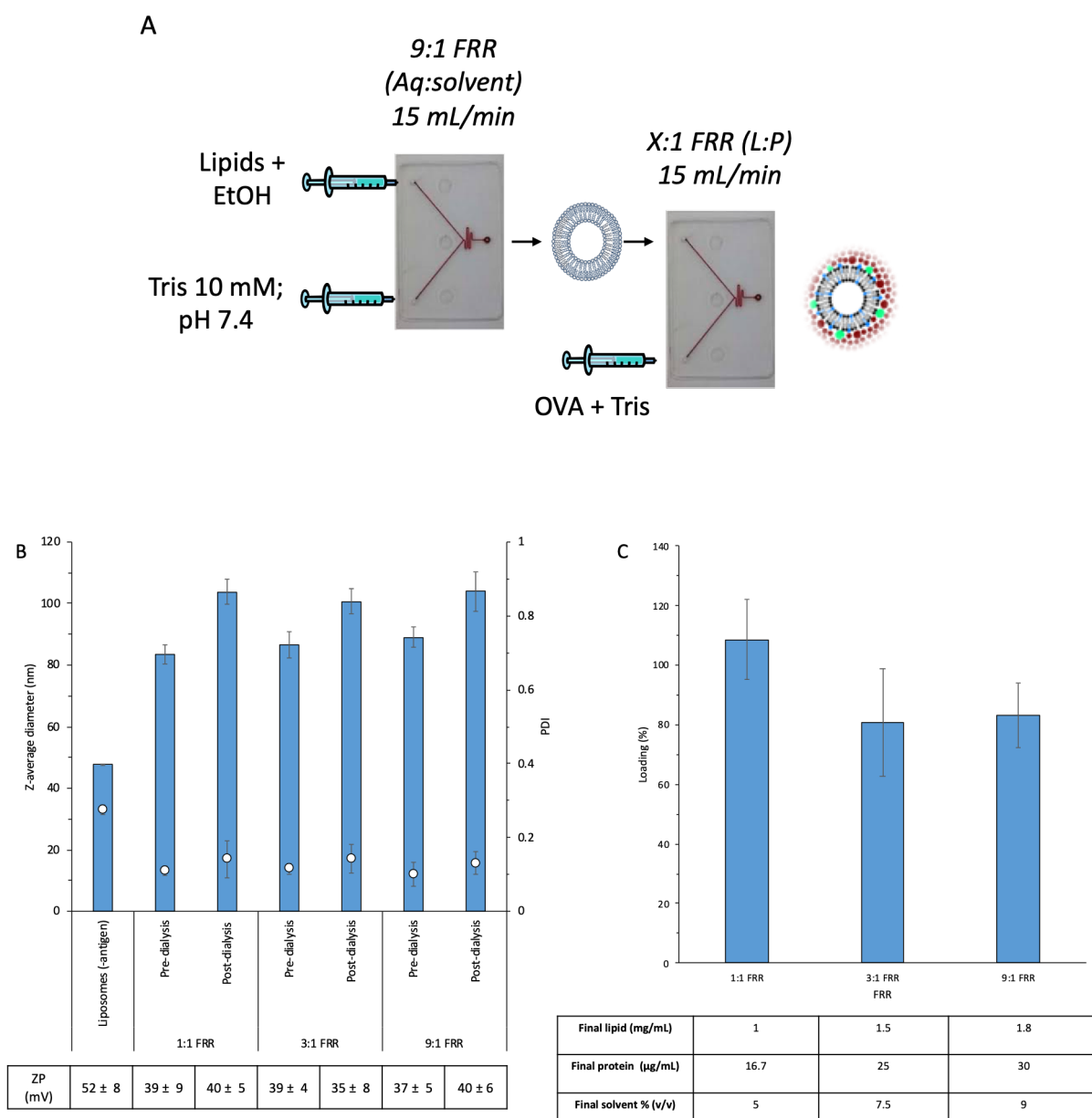
Figure 5.5 *Investigation towards reducing residual solvent concentrations by altering adsorption mixing ratios through the introduction of a two step mixing strategy. (A) provides a schematic of the proposed mixing strategy by initially making the liposomes at a 9:1 FRR and then feeding the liposomes through the chip and mixing with OVA (60:1 L:P) at a FRR of either 1:1; 3:1 or 9:1 with size, PDI and ZP measured (B) and loading efficiencies calculated (C). Results represent mean ± SD from 3 independent batches. Statistical significance: (**) p ≤ 0.01.*

The aim was to further control antigen adsorption and outline a new reduced solvent production method. Focusing on the vesicle properties after antigen adsorption showed that vesicle size increased due to protein adsorption. This could be due to either surface coating of the liposomes, structural re-organisation of the lipids into new constructs, or controlled aggregation of the liposomes. It has been previously shown that smaller unilamellar

liposomes had a greater capacity to adsorb protein resulting from a greater surface area. This is not seen in larger multivesicular vesicles with a smaller surface area, therefore reducing possible protein binding sites [254].

Interestingly, following protein adsorption, the PDI was reduced and lead to a more uniform system suggesting that the formulation is stabilised by electrostatic repulsions created by the liposomes, balanced by attractive forces between bound protein and surrounding liposomes. More importantly, there was no significant difference in loading values across the different FRRs used which was expected as the same lipid:protein ratio (60:1) was used for all three FRRs. By now focussing on the solvent volume percentage within each formulation, all FRRs allow for < 10% v/v within the final formulation. Even though the 1:1 FRR would permit < 5% v/v solvent percentage, there was no difference in vesicle size or loading efficiencies. Progressing with the 9:1 FRR would allow for greater protein concentrations, which would benefit *in vivo* tests [255].

5.3.5 Investigating the impact of altering DDA content with the liposomal system

DDA is a synthetically derived amphiphilic compound with two 18C alkyl chains and a positively charged dimethylammonium headgroup. Gall et al. were the first innovators for its use and described its potential as an adjuvant from immunological responses elicited in guinea pigs against diphtheria toxoid [256]. Since then, it has long been established to be highly effective at inducing cell-mediated immunity [257] and extensively evaluated as adjuvants within a range of vaccines [257-260]. Additionally, it is a valuable component within a liposome system for delivering subunit proteins [260-262]. However, in general, a hindrance towards its use and cationic formulations is its association with the cytotoxicity [263, 264] because of its headgroup. Due to the positive charge, it can activate cellular pathways, such as the pro-inflammatory cascade, which can restrict its use for potential new formulations [81, 265, 266]. Therefore, the investigation into appropriate DDA concentrations was conducted as up to this point 21% w/w DDA has been used within DSPC:Chol:DDA (10:5:4 w/w) with the aim to identify if varying DDA concentrations would permit high degrees of

loading and if reduction of DDA percentages would help reduce the zeta potential while maintaining a high degree of loading efficiencies.

The results in figure 5.6A indicate that within DSPC:Chol:DDA, as the percentage of DDA increases from 12 to 21 and 35%, the size increases significantly ($p \leq 0.05$) with the PDI remaining below 0.2. At a DDA% (w/w) of 12 and 21%, after overnight dialysis to remove free protein, the liposome size remains below 100 nm at 74 ± 2 nm and 100 ± 4 nm, respectively. However, as the DDA% is increased to 35% (w/w), the vesicle size increases to 145 ± 9 nm. As expected in figure 5.6B, as the DDA% within the liposomal system increases, so does the zeta potential. The zeta potential recorded in liposomes with 12% w/w was 26 ± 3 mV which was a significantly different value ($p \leq 0.001$) when compared against liposomes with 21 and 35% (w/w) DDA, which were recorded at 37 ± 4 mV and 39 ± 6 mV. The protein loading was also investigated, and using 12% w/w DDA within the formulation led to a significant reduction ($p \leq 0.05$) in OVA adsorption (64 ± 6 %) when compared to formulations that contained 21 and 35 % w/w which had loading efficiencies of 83 ± 10 % and 80 ± 5 % respectively.
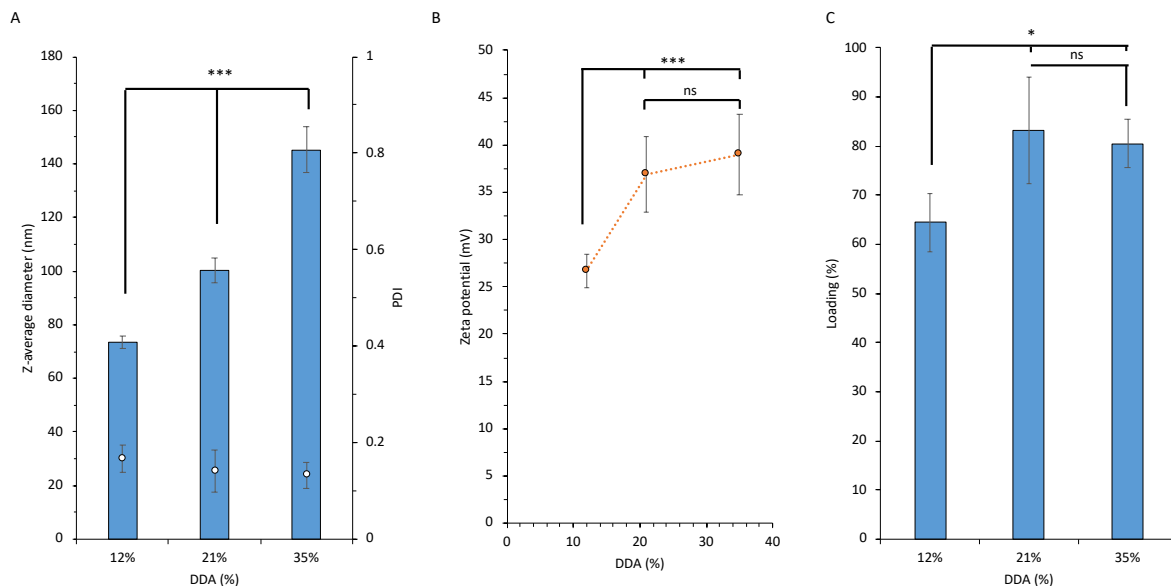
Figure 5.6 *Impact of increased DDA content on liposome size and PDI and the affect on liposome zeta potential and loading efficiencies. A DSPC:Chol (2:1 w/w) was used with the cationic lipid incorporated at concentrations of either 12; 21 or 35% w/w. The size and PDI (A) was investigated along with the zeta potential (B) and OVA loading efficiencies (C) to identify the impact DDA had on these attributes. Lipids were solubilised in EtOH with liposomes were produced at a 9:1 FRR and OVA adsorbed also at 9:1 FRR. Results represent mean ± SD from 3 independent batches. Statistical significance: (ns) p > 0.05; p ≤ 0.05 (*); (***) p ≤ 0.01.*

It is possible for DDA to spontaneously form bilayers assemble into bilayers when exposed to an aqueous environment, as described by Gall et al.. However, additional lipids are required due to their physical instabilities when used solely on their own [256, 267]. For this reason, a helper lipid such as DSPC and stabilising lipid (such as Chol) can help form a stable formulation and address such stability issues allowing DDA to be used as an effective adjuvant. Using these lipids, a significant size increase was observed as DDA% increased ($p \leq 0.01$; figure 5.6A). The literature is limited when investigating changes in cationic lipid concentrations while simultaneously adsorbing protein; however, using 'empty' liposomes, previous research suggests that increasing cationic concentrations within liposomes reduces vesicle size by increasing bilayer rigidity [268, 269]. The increased vesicle size observed at higher DDA% concentrations could result from electrostatic attractions between neighbouring particles with negatively charged surface-bound OVA. The zeta potential of the liposomes also increased significantly from 12 to 21% DDA % (w/w); however, there was no significant increase in zeta potential from 21 to 35% DDA% (w/w). Interestingly, there was no difference in the loading capabilities between 21 to 35 % DDA% w/w suggesting that the degree of OVA adsorption is achieved between 35 – 40 mV is 80 to 90%, which is in line with publications using the cationic lipid DDA and OVA antigen [270]. From these results, there was no benefit in reducing the DDA% from 21%, which has been used in figure 5.1 – 5.5 as the drop in cationic charge from reduced DDA% leads to a significant reduction in the loading efficiency of the liposomes, which could reduce immunological responses upon transitioning toward *in vivo* studies [238, 271].

5.3.6 Introduction of a 1-step mixing strategy incorporating either direct or post-production inline antigen coating

As a high FRR was identified earlier in figure 5.4 using EtOH as a solvent, two different manufacturing methods were also considered using one production step instead of the two steps to simplify the manufacturing process. From sections 5.1 to 5.5, a 2-step strategy has been investigated, allowing for reduced solvent in post-production formulation (< 10%) and remaining compatible within a continuous manufacturing platform. Studying and effectively demonstrating alternative production methods would provide a foundation for future

method development and allow greater flexibility in delivering different manufacturing methods for the effectively controlled production of lipid nanomedicines, aligning with current "Industry 4.0" trends [272]. Schematics of the two new one-step production methods are shown in figure 5.7, with (A) representing a direct method of formulation production where the antigen, suspended in Tris 10 mM, is mixed directly with the lipid steam. Figure 5.7B uses a new cartridge design using the TrM geometry; as discussed in chapter 4, liposomes are produced, and protein adsorbed inline after liposome production.
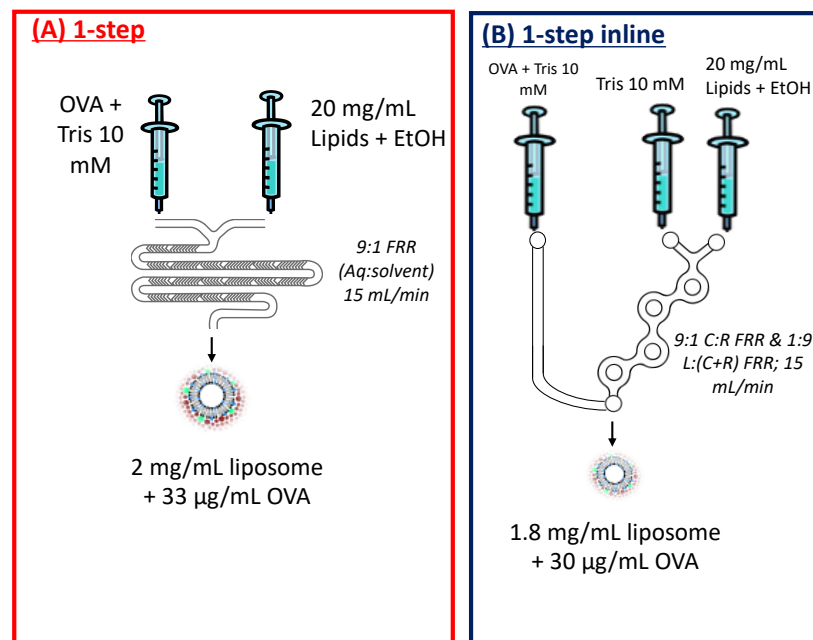
Figure 5.7 Schematic representation of the two new manufacturing methods allow direct OVA adsorption with reduced solvent. (A) Represents direct mixing of protein with lipid streams while (B) uses an inline adsorption approach with liposomes manufactured first before protein adsorption.

5.3.6.1 Physical characteristic assessment

To establish any physical changes immediately after manufacturing, a stability study was conducted to assess vesicle changes by measuring the size, PDI and zeta potential without removing solvent over 2 h. This purpose of the experiment was to investigate if residual solvent within the formulation creates a destabilising effect on the vesicles. Furthermore, this

would identify the suitability of the two microfluidic methods shown in figure 5.7 as one-step protein adsorption production methods.

By initially measuring the empty vesicles produced in figure 5.8A from liposomes manufactured at a 9:1 FRR in EtOH at 0 h, the sizes were 55 ± 14 nm and a high PDI of 0.5 ± 0.17. However, after 1 h, the formulation was more homogenous with sizes of 46 ± 1 nm and a PDI of 0.29 ± 0.04, and after 2 h, the size and PDI were 49 ± 2 and 0.23 ± 0.05, respectively. These findings can also be corroborated with figure 5.8B intensity plots with comparable peak formations between the 1- and 2-hour time points. The 1-step production method produced the largest vesicles stable between 0 to 2 h with sizes between 100 - 105 nm and low PDIs of < 0.11 across the 2 h for the protein-loaded formulations. The 2-step production method, as previously shown, was also stable across the 2 h. Post-production, the vesicles were measured at 94 ± 3 nm and after 2 h, 98 ± 4 nm with PDIs of 0.12 ± 0.02 and 0.13 ± 0.02. The stability of 1 and 2-step formulations can also be observed from the the intensity plots in figures 5.8C and D, respectively. The 1-step inline method allowed the smallest protein-loaded vesicles to produce the investigated processes. At a time point of 0 h, the size of the vesicles was recorded at 76 ± 3 nm with a PDI of 0.33 ± 0.07, indicating a greater degree of heterogeneity when compared against the other two production methods. However, after 1 and 2 h, the PDI dropped to 0.17 ± 0.01 and 0.16 ± 0.01 respectively, with sizes recorded at 73 ± 2 nm and 74 ± 2 nm for 1 and 2 h respectively and was shown to be highly significant ($p \leq 0.001$) compared to two other production methods across the 2 h. Figure 5.8E highlights this time-dependant stabilising effect as a broad peak can be shown at 0 h, indicating highly dispersed formulations. In contrast, after 1-hour, narrower peaks are formed of similar shapes, indicating comparable sizes and uniformity between the vesicles at these time points. The zeta potential was also investigated to evaluate further the manufacturing strategy on the vesicle characteristics (figure 5.8F). From comparison against the empty formulation, there was no statistical difference using the 1-step method. The same can be said for the 2-step approach other than the measurements made at 0 h, which were statistically significant post-production ($p \leq 0.05$). The 1-step inline method liposomes had a reduced zeta potential of between 30 – 35 mV across the 2 hour measuring period with statistical differences between the empty vesicles observed after 0 and 2 h ($p \leq 0.01$).

Investigating the liposome size (figure 5.8A) due to altering the manufacturing method highlighted some interesting observations regarding colloidal stability. Large variances in the vesicle PDI (figure 5.8A) and size distribution (figure 5.8B) were observed from initially looking at the empty liposomes. This could be a result of the high FRR used for liposome production (9:1 FRR), causing a large change in polarity between mixing of the organic and aqueous phase leading to a high degree of liposomal deformation and reformation post-manufacture, which requires a 'settling' time of > 1 h for the liposomes to equilibrate and form stable vesicles [229, 237]. A more stable and uniform formulation can be produced by incorporating OVA onto the liposome surface. Hamborg et al. studied this effect using low L:P ratios, comparable to those L:P concentrations used in figure 5.8A. They observed that using smaller vesicles increased vesicle surface area, permitting greater protein adsorption capacities and possibly permitting an increase in intermolecular bonds between protein molecules leading to liposome complexes, and as such increased vesicle sizes [237]. The high liposome concentrations relative to protein concentration also allow the vesicles to remain positively charged, as shown from figure 5.8F, thus increasing stability as repulsive forces between the vesicles still prevail within the colloidal system.
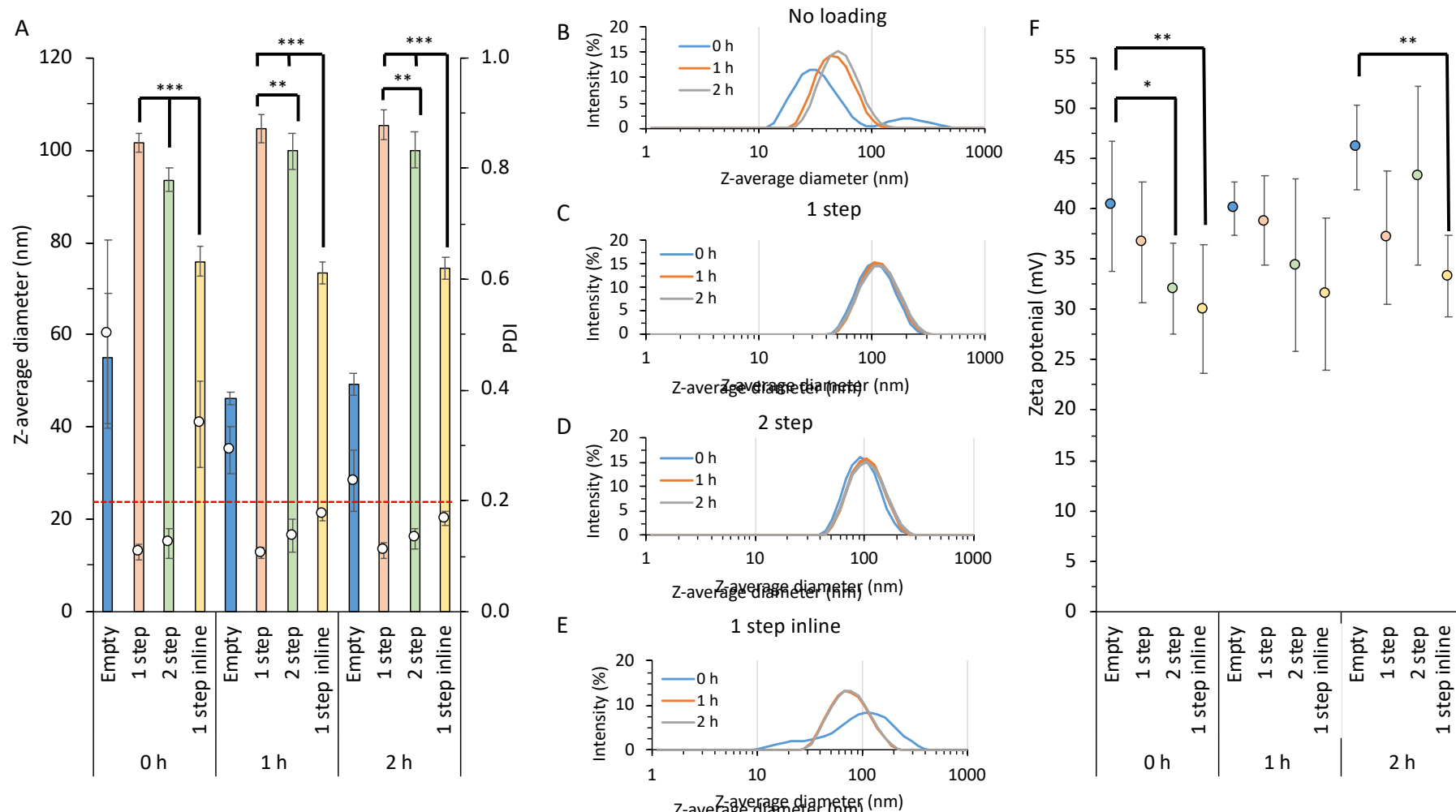
Figure 5.8 *Short term stability of liposomes using different manufacturing methods. Liposomes were manufactured at an initial lipid concentration of 24 mg/mL using either 1-step; 2-step or 1-step line with their size and PDI measured over 2 h at hour intervals (A). Intensity plots for empty (B); 1-step (C); 2-step (D) and 1-step in line (E) were also obtained to identify sample changes over time. Zeta potential measurements were also collected at hourly intervals (F). Initial lipid concentrations were 24 mg/mL suspended in EtOH. Results represent mean ± SD from 3 independent batches. Statistical significance: $p ≤ 0.05$ (*); (**) $p ≤ 0.01$; $p ≤ 0.001$ (***).*

5.3.6.2 <u>Inline dilution of protein as a mixing method to coat cationic liposomes</u>

Liposomes produced from each manufacturing method proved to be significantly different from each other, as explicitly demonstrated in terms of vesicle sizes from 5.8A. Interestingly, while the 1 and 2-step manufacturing methods allow for the formation of vesicles between 90 – 110 nm, the 1-step inline adsorption method led to liposomes that were significantly smaller than both vesicles (figure 5.8A) with reduced zeta potentials (figure 5.7F) when compared to the two manufacturing method. To examine this further, the two critical production steps were individually investigated to identify at what point the formulation physical attributes deviate from the 1 and 2-step manufacturing methods. As the 1-step inline method uses a TrM geometry to produce the liposomes, while the 1 and 2-step methods use an SHM architecture, the first step was to compare the SHM against the TrM architectures using a cationic formulation using similar microfluidic bridging studies as carried out in chapter 4. Secondly, as the 1 and 2-step methods adsorb protein to the liposomes within the microfluidic mixer itself, the inline method was then compared to a protein-loaded formulation produced without mixing to assess the differences and identify If mixing within microfluidic architecture is a crucial parameter to be considered.

5.3.6.2.1 Microfluidic manufacturing bridging studies following protein adsorption using the cationic formulation DSPC:Chol:DDA

To assess the potential impact and influence microfluidic architectures have on protein adsorbed cationic formulations, the 1-step and 2-step manufacturing methods were be used with both cartridges and the physical vesicle properties assessed. The results in chapter 4 have highlighted using DSPC:Chol that SHM and TrM architectures can be successfully interchanged with no impact on formulation attributes. However, the incorporation of DDA with simultaneous loading of protein both following direct mixing with the fluid streams (1-step) and adsorption immediately after production (2-step) is yet to be assessed and validated. Furthermore, these bridging studies can provide greater insight into whether

cartridge design could be responsible for differences in size and zeta potential results observed in figure 5.8 when 1-step inline mixing was introduced.

Using the 1-step method of production, there were no significant differences ($p > 0.05$) when the TrM or SHM cartridges were compared before or after dialysis (figure 5.9A). With the SHM cartridge, the size and PDI results were 107 ± 4 nm and 0.1 ± 0.02 before dialysis and 112 ± 3 nm and 0.09 ± 0.02 after dialysis. This is comparable to the TrM cartridge with measurements of 112 ± 2 and 0.1 ± 0.02 pre-dialysis and 111 ± 1 and 0.08 ± 0.01 post-dialysis. Furthermore, the zeta potential (figure 5.9B) for both cartridges was not significantly different with charges for formulations made with either cartridge remaining between 30 – 40 mV before and after dialysis. The loading for the formulation was also compared for the two cartridges (figure 5.9C). It again was not shown to be significant ($p > 0.05$) with the loading efficiency for liposomes produced using the SHM cartridge being 67 ± 6 %, while for vesicles manufactured using the TrM cartridge, the loading efficiency was measured at 73 ± 5 %. The same studies were carried out using the 2-step method of production, as shown in figure 5.9D, and again no significant differences between the formulations manufactured using the SHM or TrM cartridge ($p > 0.05$) when compared before or after dialysis. The measurements obtained with the new TrM mixer was 98 ± 5 nm and 0.1 ± 0.02 before dialysis for the Z-average diameter and PDI respectively, and 107 ± 3 nm and 0.12 ± 0.01 for the Z-average and PDI respectively post-dialysis. The results were comparable when the pre-dialysis and post-dialysis results were compared to the SHM measurements. In figure 5.9E, much like the 1-step results in figure 5.9B, the zeta potentials were cationic and again maintained between 30 – 40 mV between the two cartridges, both pre and post-dialysis. There were no significant differences in the liposomes produced by either cartridge (figure 5.9F) in terms of loading efficiency (83 ± 10 % and 82 ± 7 % for the SHM and TrM, respectively) and no significant difference when the results in figure 5.9C and F were compared in terms of both cartridges and manufacturing methods.
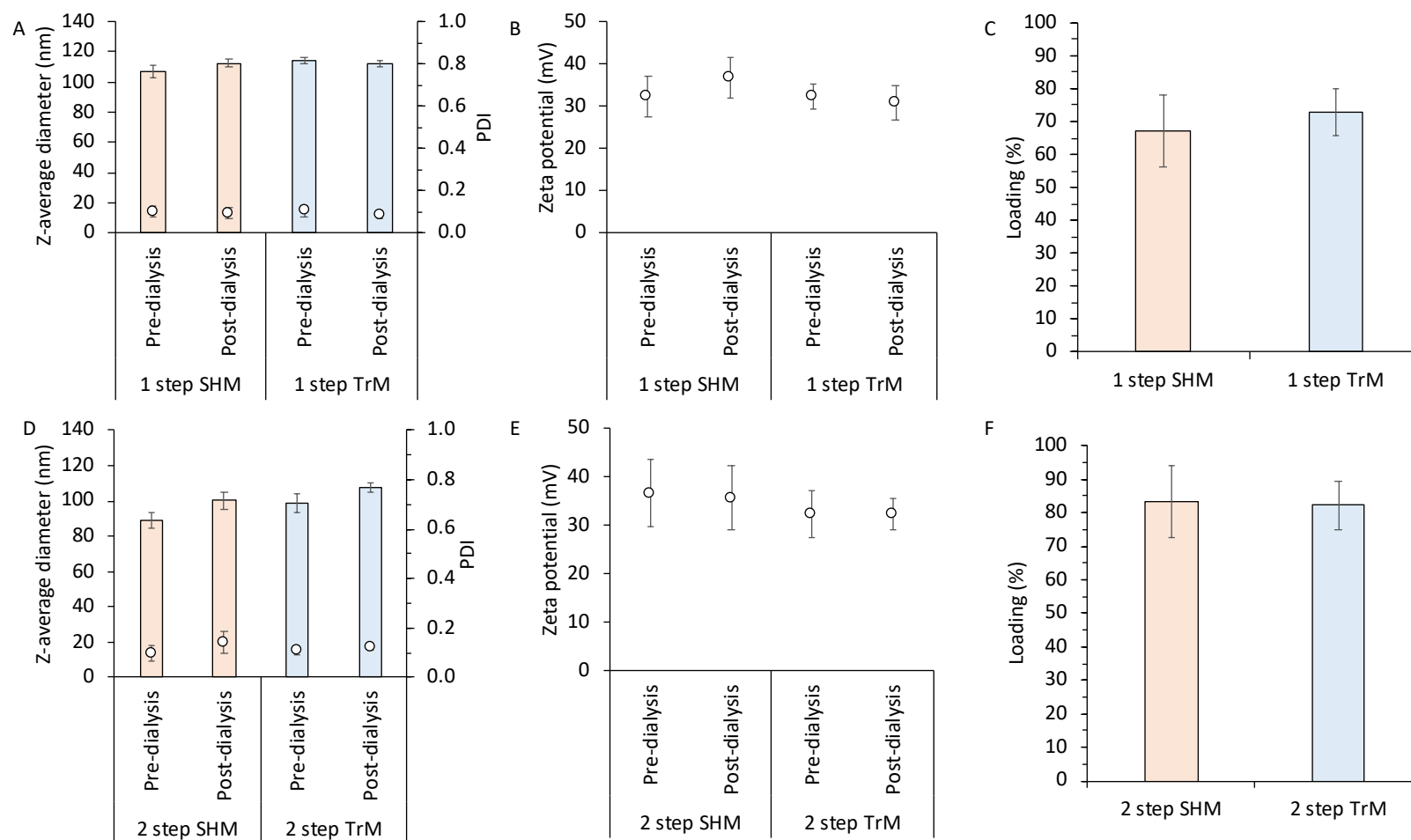
Figure 5.9 *Manufacturing method bridging studies between microfluidic cartridges using the cationic formulation DSPC:Chol:DDA following protein adsorption. Size and PDI measurements were measured both before and after dialysis for the 1-step method (A) and 2-step method (B) with zeta potential measurements recorded for the respective manufacturing methods (B and D). Loading efficiencies for the 1-step (C) and 2-step (D) method was also calculated using a Bradford assay. For the 1-step a FRR of 9:1 was used at 15 mL/min, while for the 2-step a 9:1 FRR for liposomes production was utilised along with a 9:1 FRR for protein adsorption also at 15 mL/min. Lipids were suspended in EtOH prior to production at an initial concentration of 24 mg/mL with a final liposome concentration of 2 mg/mL and 1.8 mg/mL with a final L:P ratio of 60:1. Results represent mean ± SD from 3 independent batches. Statistical significance: (ns) $p > 0.05$*

The results in figure 5.9 build on chapter 4 and further expand the use of the TrM cartridge design to produce liposomes and adsorption of subunit proteins onto the liposomal surface. Within chapter 4, the neutral formulation DSPC:Chol was successfully manufactured to a high degree of comparability using different cartridge architectures by bridging liposomal attributes such as size, PDI, charge, and entrapped protein release kinetics. However, figure 5.8 indicated some differences between formulations manufactured by 1 and 2-step (SHM) and 1-step inline (TrM). To validate that the TrM cartridge design had no hindrance to liposome production or protein adsorption, recorded measurements were compared to the benchmark measurements from the SHM cartridge for each manufacturing method. From figure 5.9A and D using the 1-step and 2-step methods, respectively, there were no significant differences between the two cartridges when either manufacturing method was used. From the 2-step process, though the data is not shown for the empty liposomes manufactured, if the empty liposomes were significantly affected by the cartridge design, there would most likely be significant differences between the formulations, which would warrant a deeper investigation. As expected from the result obtained up to this point, there were no differences in the zeta potential in figures 5.9B and E as factors influencing the zeta potential such as buffer concentration or lipid concentration were not altered.

With the 1-step method, the protein is exposed (although briefly) to a higher percentage of EtOH than the 2-step method. This could cause concern if the solvent phase leads to protein instabilities and issues with the protein structure integrity and affect the hydrophobic bonds within the protein. Researchers have demonstrated this effect using human serum albumin and reported that using EtOH > 30 % v/v completely transforms the protein's secondary structure [273]. The impact of solvent exposure on protein structure (ovalbumin) during microfluidic production was investigated by Forbes et al. using circular dichroism. The authors investigated protein integrity after microfluidic mixing in the presence of MeOH at an FRR of 3:1 (25% v/v MeOH) [117]. The researchers compared the ovalbumin in the presence of 25% v/v MeOH to that suspended in formulation buffer. They concluded that the MeOH percentage the ovalbumin would be exposed to did not alter the secondary structure of the protein, which is also in line with the findings of other researchers [117, 274]. These publications support the rationale that as EtOH is replaced with MeOH (which is more polar) along with the reduced solvent method (< 10% v/v residual solvent), the protein structural

integrity is maintained. These results also confirm that SHM and TrM can be successfully mapped across, allowing for potential scale-up and demonstrating that liposome production is unaffected by switching to a planar toroidal design, suggesting that the vesicle size differences using the 1-step inline method results from the adsorption step.

5.3.6.2.2 *1-step inline mixing leads to insufficient antigen adsorption eliciting the observed physical differences*

Results in figure 5.9 show cartridge design has no impact on physical attributes using DSPC:Chol:DDA (10:5:4 w/w). Therefore to examine the vesicle differences with the 1-step inline cartridge, liposomes were manufactured and immediately added to a falcon tube containing protein at a ratio of 9:1 liposomes protein to match the flow rate ratio and end liposomes/protein concentrations from the 1-step inline mixing. This experiment could identify if the adsorption step using the 1-step inline method leads to vesicle differences.

From figure 5.10A, using the 1-step inline mixing method, the size was maintained between 70 to 75 nm across all time points. However, using the non-mixing method, there was a large increase in liposome size immediately after the addition of the liposomes to the protein with a size of 167 ± 2 nm, this size reduced down to 95 ± 3 nm and 97 ± 2 nm for the 1- and 2-hour time points respectively. The PDIs in figure 5.10B were largest for each manufacturing method at 0 h with a PDI of 0.34 ± 0.01 and 0.45 ± 0.01 for the inline mixing and no mixing method, respectively. Yet, these decreased over the remaining 2 h of the experiment to 0.17 ± 0.01 and 0.33 ± 0.01 for the inline mixing and no mixing methods, respectively, at the 2-hour time point. In figure 5.10C for the no mixing method, the intensity plot indicates that after 2 h, the vesicles are at a steady state due to elimination of the double peak; in figure 5.10D, the vesicles are dispersed at 0 h, which the PDI also confirms. After an hour, the vesicles are shown to be monodisperse due to the singular peaks shown after this point. The zeta potentials for both the methods were unchanged across the 2 h and were between 30 – 40 mV, which agrees with figures 5.8 and 5.9. When the loading efficiency was calculated (figure 5.10F), the inline method had a loading efficiency of 54 ± 4 %, while the no mixing method allowed for 81 ± 6 %.
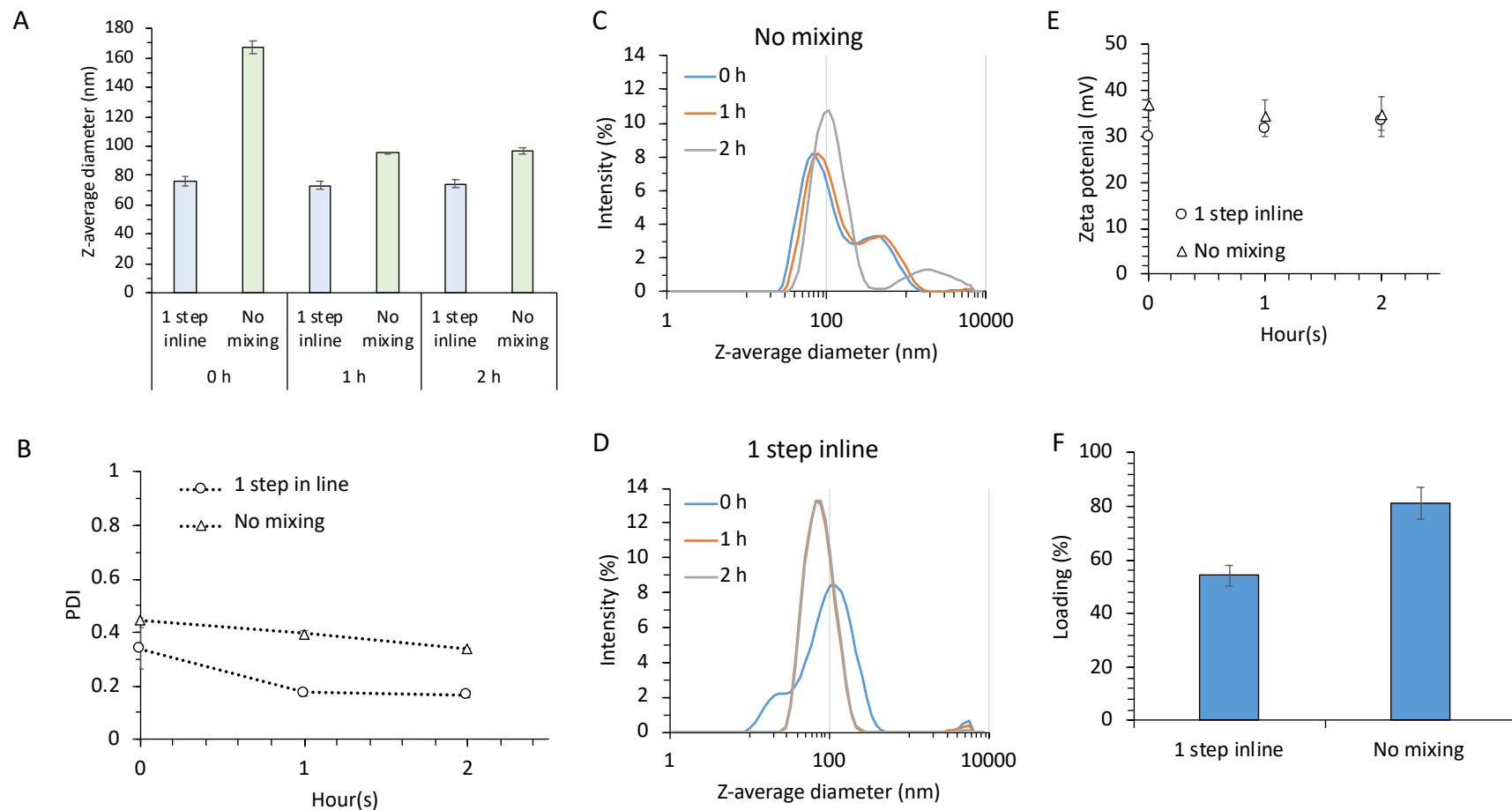
Figure 5.10 *1-step inline mixing vs no mixing. Size (A) and PDI (B) measurements were measured at 0, 1 and 2 h after production with intensity plots recorded for both the no mixing (C) and 1-step inline mixing (D). The zeta potential (E) and loading efficiencies using a Bradford assay were also measured after free protein removal by dialysis (F). For the 1-step inline method a FRR of 9:1 was used at 15 mL/min and a 9:1 FRR liposome:protein also at 15 mL/min. For the "no mixing" method a 9:1 FRR was added to a falcon tub at a ratio of 9:1 v/v. Both methods had a final concentration of 1.8 mg/mL and 30 μg/mL OVA. Lipids were suspended in EtOH before production. Results represent mean ± SD from 3 independent batches.*

This experiment assessed the role mixing plays in effectively coating the liposome with antigen. The results in figure 5.10A using the no mixing method can be directly compared to the 2-step mixing since the same concentrations, and mixing ratios are used; apart from that, a microfluidic mixer is not used at the adsorption step. By comparing figure 5.10A to 5.8A, the large size increase observed at 0 h is wholly negated with a microfluidic mixer allowing for stable sizes and reduced PDIs. After 1 h with no mixing, the sizes are comparable to the 2-step. However, the PDI is greater than > 0.2, which is not experienced using the 2-step microfluidic method. Yet, the inline process produces liposomes of reduced size with a more polydisperse population, as shown through figure 5.10B and D. It is clear from figure 5.10F that using the 1-step inline method is not an effective method of protein complexation. Using this method, the point of protein convergence is perpendicular to a continuous flow of liposomes pressure changes could be affecting protein stability [275]. However, this is hard to conclude, given the lack of literature within this specific area. It should also be considered that if incomplete mixing was achieved, the liposomes were left suspended with the protein for 2 h. This was enough time for the 'no mixing' method to achieve 81 ± 6 %, suggesting that the root cause is either protein stability or morphological changes with the liposomes.

5.3.6.3 Manufacturing methods have no impact on short term liposome stability

From figure 5.2, the impact of L:P on liposome stability has been investigated, and it was clear from using 60:1 L:P that liposomes were stable at 4 °C for across the 14 days testing with loading also remaining unchanged from the measurements at day 0. A short-term stability assessment was conducted to build upon this work and validate the investigated manufacturing methods. In figure 5.11 with liposome size, PDI, ZP (data not shown), loading and morphology investigated where measurements were taken at both pre/post solvent removal and pre/post "free" protein removal to track the possible physical changes which could occur at each step. A "vortex" method was also introduced as control and manufactured in the same fashion as the formulations used in figure 5.2 with EtOH used instead of MeOH to keep in line with the EtOH used for the 1-step, 1-step inline, and 2-step manufacturing methods.

Between days 0 and 7 using the vortex method, there was no significant difference in the vesicle size in figure 5.11A, and after free protein removal on day 7, the Z-average diameter was recorded at 151

± 3 nm with a uniform PDI maintained between 0.05 – 0.08 across the 7 days. Again, in terms of stability, for both the 1 and 2 manufacturing methods, there was no significant change in their size or PDI between day 0 (pre-solvent removal) and 7 (post solvent removal). For the 1-step at day 0, the size was 110 ± 6 nm, and on day 7, it was 107 ± 3 nm. For the 2-step process, comparable sizes were obtained as shown in previous figures 5.8A and 5.9D, with recordings of 107 ± 3 nm and 107 ± 3 nm for day 0 and day 7, respectively. The PDI for both the 1 and 2-step was below 0.2 across the 7 days, highlighting a high degree of uniformity within the formulations. For the 1-step inline results in figure 5.11, the sizes remained unchanged when measured after "free protein" removal on day 7 at 77 ± 4 nm. There were significant differences ($p < 0.05$) for the PDI measurements on day 0 between the pre-solvent and after solvent removal, however, after 7 days, this settled to an end PDI of 0.2 ± 0.04 after free protein removal. The loading in figure 5.11B was also reported after 7 days to identify any protein loss during this period. The results were well aligned with previous figures showing that the 2-step method closely matches the non-microfluidic adsorption method (vortex) with 83 ± 8 % and 77 ± 12%, respectively. These were significantly different ($p < 0.05$) from the 1-step inline measured at 57 ± 3 %. Despite the 1-step method vesicles measuring less than the vortex and 2-step method, this was found not to be statistically significant with a loading efficiency of 65 ± 5%. By obtaining cryo-TEM images, it is possible to identify any morphological changes between the control (vortex) adsorption method and those where microfluidics achieved protein adsorption. The vortex method in figure 5.11C-D produced liposomes composed of a similar bilayer with a uniform shape. The same shape and uniformity applied are similar to the 1-step (figure 5.11E-F) and 2-step (figure 5.11G-H). The 1-step inline vesicles in figure 5.11 I-J were not as uniform or concentric and instead appeared to have a more globular morphology.

Liposome stability is a crucial concern, and a fundamental challenge of liposomal formulations as their physical degradation can lead to adverse events and a reduction in efficacy due to their instability when suspended in an aqueous environment [276]. Of the causes that can impact stability, hydrolysis of the ester bonds and oxidation of the alkyl chains are the two primary causes of chemical instability of phospholipids [277]. However, the primary focus of this work is the physical stability that can arise from aggregation, such as the surface-bound protein (which was the purpose for investigating stability in figure 5.11), membrane bilayers and encapsulated compounds that can impact the physical stability of liposomes [278, 279].
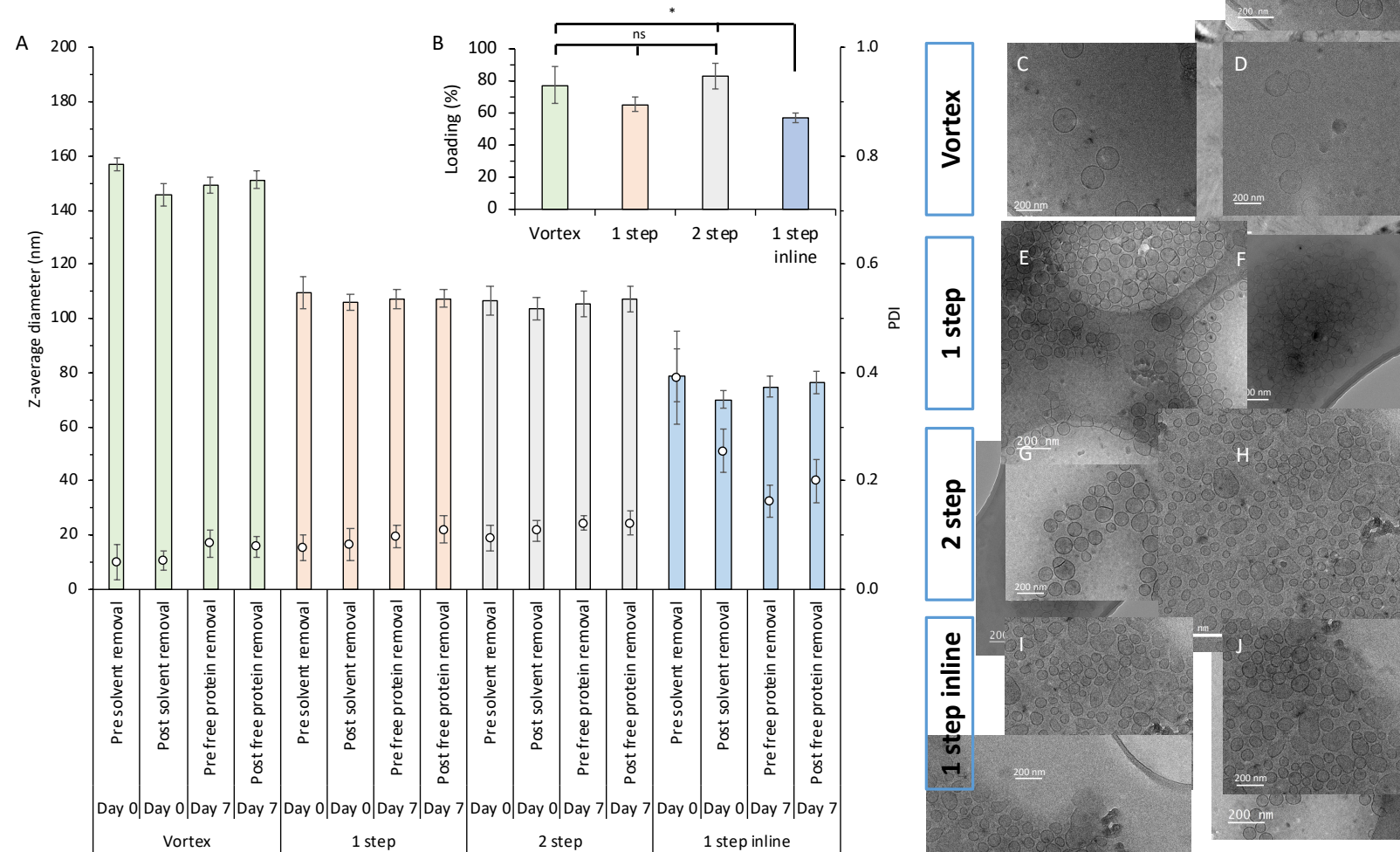
Figure 5.11. *Physical characteristic monitoring over 7 days with vesicle morphology. Liposomes were m[...]ing 24 mg/mL initial lipid concentration with DSPC:Chol:DDA solubilised in EtOH. Size and PDI measurements were recorded both before and afte[...]nd before and after free protein removal on day 7 (A). Cryo-TEM images were also obtained for vortex samples (C+D); 1-step (E+F); 2-step (G+H) and 1-step inline (I+J) methods. Results represent mean ± SD from 3 independent batches. Statistical significance: p > 0.05 (ns); p ≤ 0.05 (*)*

If physical liposomal stability was a concern and desired for the product to achieve long-term stability, freeze-drying (lyophilisation) could be a practical solution to prepare samples and reconstitute the formulations when required. By lyophilising a liposomal suspension, water is removed from the product in a frozen form under low pressure, preventing hydrolysis of the phospholipids and producing a freeze-dried product with improved physical stability through reducing molecular mobility [112, 280]. A well designed freeze-dry process encompasses three distinct stages. The first is the initial freezing of the liposomal formulation, the primary dry phase where water is removed by sublimation without the intermediate liquid phases. Finally, the secondary dry phases remove residual water, such as adsorbed water on the vesicles. However, without the introduction of cryoprotectants, the formulation can be damaged, resulting in aggregation and fusion [280], which can be overcome by adding saccharides [281]. The addition of saccharides could replace the adsorbed water at the polar lipid head group, which is known as the water replacement hypothesis [281] or an alternative method is by altering the gel-to-fluid transition temperature of the vesicles during the primary drying phase through the formation of a vitreous layer (glass layer formation) [282] at a specific temperature. The formation of a vitreous layer inhibits movement of the vesicles and, in turn, helps prevent aggregation [283]. Of the saccharides, trehalose is preferable to use as a cryoprotectant. It is less hygroscopic and more flexible as it lacks intermolecular hydrogen bonds and low chemical reactivity, making it a compatible saccharide with liposomal formulations [283-285]. Evaluating liposomal protective properties against proteolytic degradation

5.3.7 Evaluating liposome protective properities against proteolytic enzymatic degradation

While it is accepted that liposomes can entrap protein cargo and function as a physical barrier against circulating enzymes, it has also been shown that adsorbed antigens can stimulate a more robust immune response than entrapped antigens [286, 287] which has also been demonstrated for non-immunogenic molecules [288, 289]. From this, developing a formulation that offers protection against proteolysis is a crucial characteristic due to proteases present in the bloodstream and tissue, leading to irreversible denaturing and loss of biological function and rapid clearance by the liver or kidneys [290]. Studies have shown that using other biocompatible inorganic nanoparticles such as silica and gold that the size of the particles can have a profound effect on the delivery of antigens [291], and using polymer delivery systems can delay the degradation of fluorescently labelled protein against proteolytic enzymes using polymer shells [292]. Therefore, to quantitatively assess if

liposomes can reduce protein degradation when challenged against proteolytic, a ovel method was developed to quantiatively determine protective adsorption (i.e. reducing protein by proteolytic enzyme [%protected]) was developed using dry-quenched OVA (DQ-OVA), which would monitor fluorescence and thus track the degree of protein degradation by exposing the manufactured liposomes to the proteolytic enzyme trypsin.

5.3.7.1 Method development for a fluorescent quantitative liposomal protection protocol

5.3.7.1.1 Identification of a trypsin concentration based on fluorescence

DQ-OVA is a self-quenched conjugate of OVA that allows for green fluorescence from hydrolysis by proteolytic enzymes. Previous methods using DQ-OVA and proteolytic enzymes have been shown to have a long lengthy experimental procedure [292]. Therefore, to address this, the incubation time and the trypsins:DQ-OVA ratios were investigated along with instrument parameters such as "gain" to determine sample excitation times.
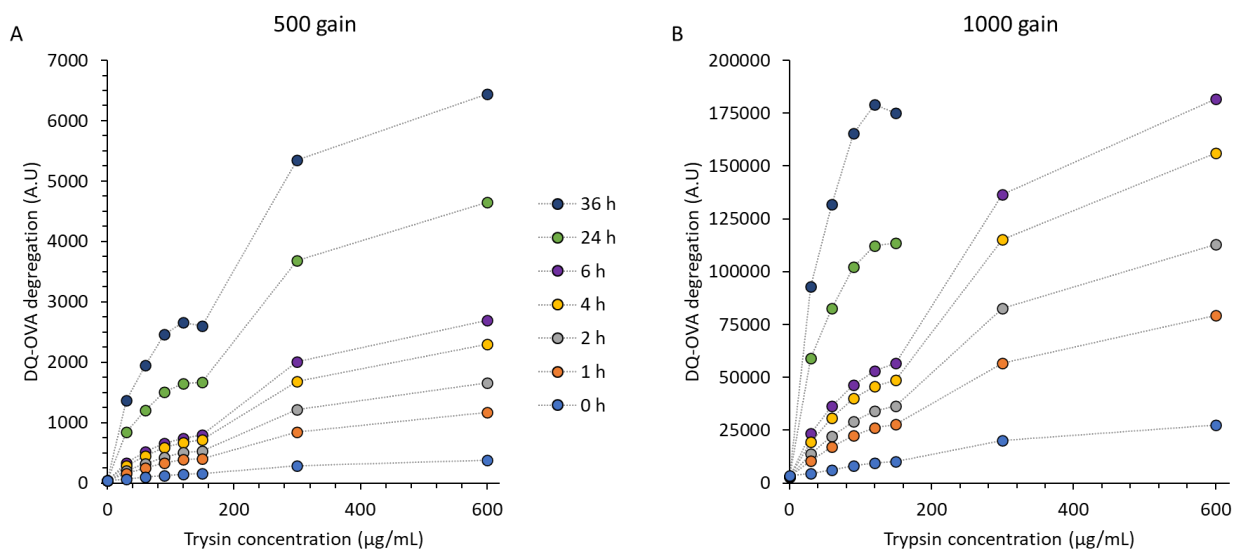
Figure 5.12 *Investigating trypsin:DQ-OVA ratios. Using DQ-OVA, 30 µg/mL was mixed 1:1 v/v with 0 – 600 µg/mL of trypsin and emission intensity measured at specific time points over 36 h. A gain setting of either 500 (A) or 1000 (B) was used on the instrument to optimise experiment protocols. The excitation and emission wavelengths were 505 and 520 nm respectively.*

A fixed DQ-OVA concentration of 30 µg/mL was selected based on the final protein concentration within a 60:1 L:P formulation, which would be used to assess the degree of liposome protein. The protein was then dissolved in PBS and exposed to increasing levels of

trypsin with fluorescence recorded at various time points over a 36 h period to track fluorescence intensity as a function of exposure time. Using trypsin:DQ-OVA ratios of 0; 1; 2; 3; 4; 5; 10 and 20:1 w/w (figure 5.12) it was shown that as the concentration of trypsin increased DQ-OVA degradation (as measured by fluorescence) increased. However, when a 1000 gain setting was used, the emission intensities were far greater for each respective trypsin:DQ-OVA ratio when compared to the 500 gain setting used (figure 5.12). At a trypsin concentration greater than 150 µg/mL and exposure to the protein after 24 h, the emission intensity was too great for the instrument to capture. Therefore, progressing with the method, a gain of 500 was used to prevent intensities beyond the range of the instrument.

5.3.7.1.2 *Refinement of trypsin ratios and selection of emission wavelengths*

The results in figure 5.12 highlighted that exposure time and trypsin concentration contribute to quantifying protein degradation using DQ-OVA. There was no indication that an emission plateau was reached from the exposure times investigated. Consequently, to further optimise and establish a standard assay further and ensure the emission maxima is captured by the instrument, an emission filter wavelength range between 520 – 590 nm was measured.

One of the first initial observations in figure 5.13 was that across the wavelength emission filters used (A-E), a filter wavelength of 535 nm was used in subsequent studies as it allowed for greater intensities to be captured than the 520 nm wavelength filter, which was used previously in figure 5.12. Furthermore, a trypsin:protein exposure time of 4 h (figure 5.12D) and (figure 5.12E) was investigated further as using the ratio of 10:1 w/w (figure 5.12F) allowed for a clear separation between digested and undigested (no trypsin). It would be a high ratio to provide sufficient aggressive digestion of protein and challenge the potential protective properties of the liposomes by the investigated manufacturing methods.
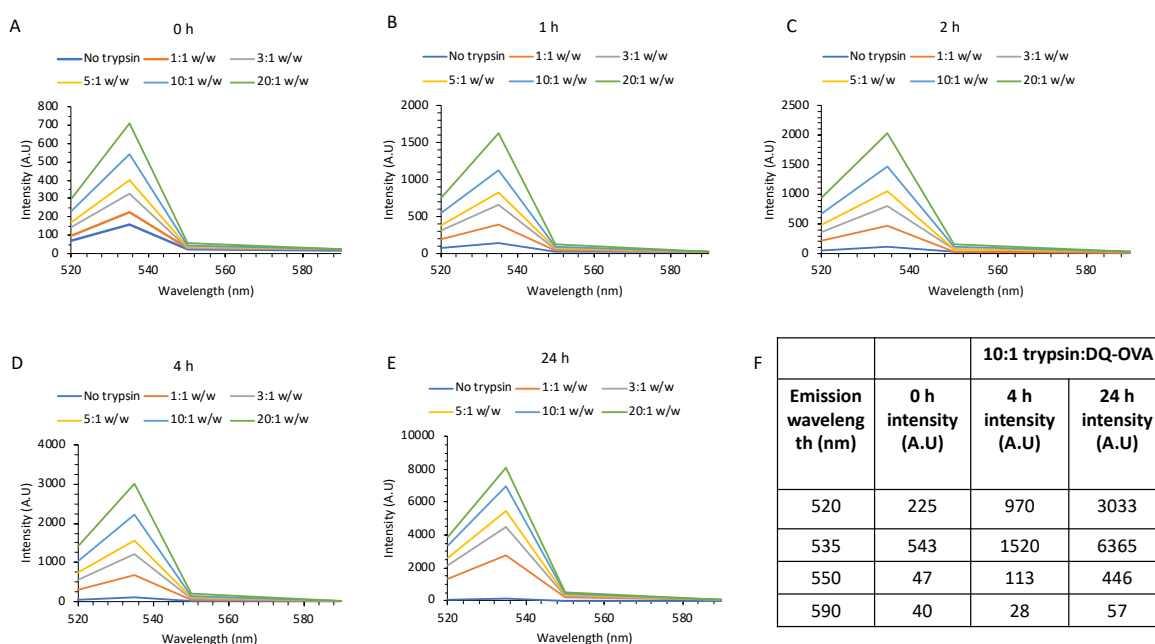
Figure 5.13 *Refinement of emission wavelengths and selection of trypsin:DQ-OVA ratio with incubation times. Trypsin:DQ-OVA ratios of either 0; 1:1; 3:1; 5:1; 10;1 and 20:1 w/w were selected and incubated at RT for 0 h (A); 1 h (B); 2 h (C); 4 h (D) or 24 h (E) with excitation filter of 505 nm and emission filters of 520 nm to 590 nm used to further optimise instrument settings. A raw data read of the 10:1 w/w with intensity values are shown for the 0 h; 4 h and 24 h incubation times.*

5.3.7.2 Effects of microfluidic mixing and ethanol has no impact on DQ-OVA degradation

Before running the experiment with liposomes, a final control test was conducted to ensure that EtOH had no influence on DQ-OVA degradation upon microfluidic mixing during liposome production and protein adsorption. The experimental objectives were to identify if i) microfluidic mixing led to DQ-OVA degradation and ii) if EtOH promoted DQ-OVA degradation. To test this, DQ-OVA mixed with PBS without and with 10:1 w/w trypsin were tested, and to investigate if microfluidic mixing affected protein degradation, DQ-OVA was mixed with PBS at a 9:1 v/v ratio by addition of PBS using a pipette or at a 9:1 FRR with the solubilised DQ-OVA at the aqueous inlet and PBS at the solvent inlet.

The results in figure 5.14 confirm that fluorescence is only detected in the presence of trypsin and that microfluidic mixing of DQ-OVA did not result in degradation and subsequent fluorescence. From figure 5.14, it can be seen that there are only background levels of

fluorescence for DQ-OVA mixed either by pipetting or by microfluidics (with intensity values of 176 ± 2 and 170 ± 4 A.U respectively; figure 5.14). Likewise, there was no significant difference when EtOH was introduced, which again was mixed at a 9:1 v/v DQ-OVA:EtOH using the pipette or at a 9:1 FRR by microfluidics with values of 167 ± 3 and 164 ± 5 A.U when protein was mixed by pipette or microfluidics respectively. The method validation results acquired in sections 5.7.1.1 – 5.7.1.3 allowed the identification of trypsin concentrations, the selection of the correct emission filter for the instrument, and evidence that microfluidics and EtOH have no impact on the degree of the DQ-OVA degradation, which allows the progression towards testing with liposomes and assessment of protein protection.
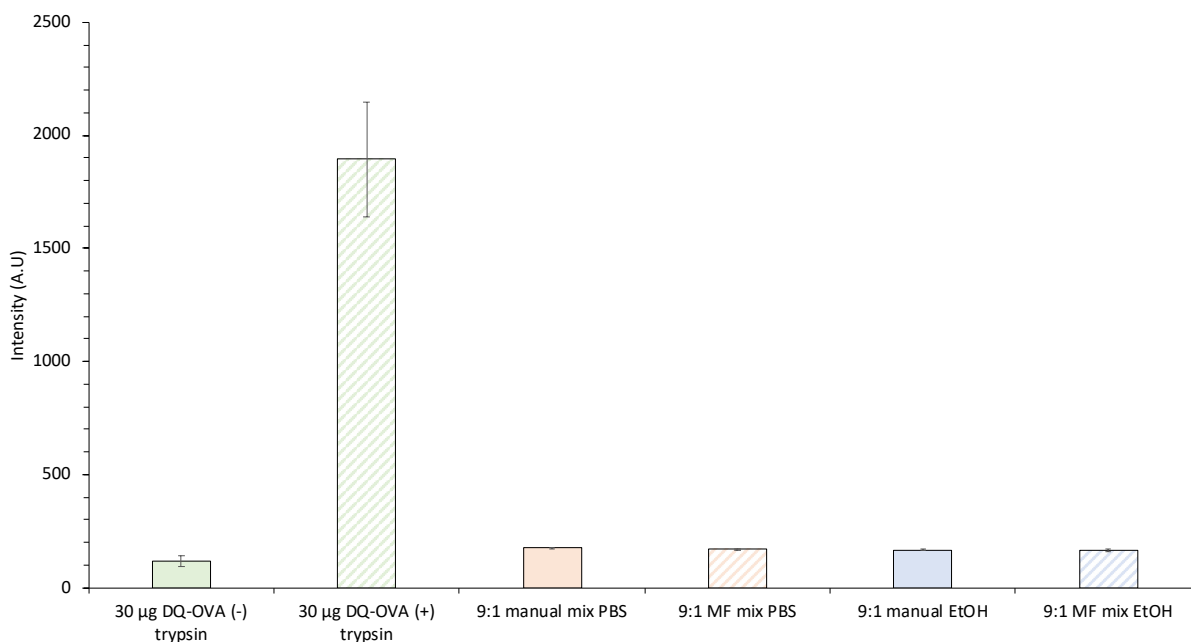
Figure 5.14 *Impact of solvent and microfluidic mixing on DQ-OVA degradation. DQ-OVA fluorescent intensities (ex/em 505/535 nm) were measured and compared against a negative control (DQ-OVA (-) trypsin) and a positive control (DQ-OVA (+) trypsin). DQ-OVA was mixed either by pipette (9 parts DQ-OVA and 1 part PBS) or within the microfluidic mixer (9:1 FRR protein:PBS) to assess degradation as a result of microfluidic mixing and also by mixing with EtOH by pipette (9 parts protein and 1 part EtOH) or by microfluidics (9:1 FRR protein:EtOH). Results represent mean ± SD from 3 independent batches*

5.3.8 DSPC:Chol:DDA liposomes reduces proteolytic digestion towards DQ-OVA

Following the method development outlined in sections 5.7.1.1 to 5.7.1.4, liposomal formulations with adsorbed DQ-OVA were manufactured using either a vortex adsorption strategy or the 1 or 2-step manufacturing methods using microfluidics. The experiment aimed to quantitatively assess the degree of protection liposomes brought by exposing the formulation, after the free protein has been removed, to a 10:1 w/w trypsin:protein for 4 h at either room temperature or 37 °C.

Without using a liposomal carrier, the results show increased fluorescence at both room temperature (RT) and 37 °C, which were 1058 ± 145 and 2828 ± 282 A.U, respectively (figure 5.15A). In contrast, when the DQ-OVA is electrostatically bound to cationic liposomes (DSPC:Chol:DDA 10:5:4 w/w), there was a marked decrease in the fluorescence intensity values both at RT and 37 °C irrespective of the manufacturing method used to prepare the formulations (Figure 5.15A). From the values, the percentage protection was calculated (figure 5.15B). Across all the manufacturing methods, there was no significant difference between conducting the assay at RT or 37 °C for each respective method. There is no notable difference between the manufacturing methods, with the cationic liposomal adjuvants offering between 40 to 55% protection to the electrostatically bound DQ-OVA.

It is evident from the results in figure 5.15A that using liposomes and loading DQ-OVA onto its surface reduces the fluorescent intensity when the investigated manufacturing strategies are compared against "free OVA", suggesting that the liposomes were protecting the protein against enzymatic degradation resulting in reduced fluorescent intensities when compared to the DQ-OVA without the liposome carrier. As expected, the fluorescent intensities of samples incubated at 37 °C were greater than those at RT due to the increased enzymatic reaction rates. However, incubation temperatures had no impact ($p > 0.05$) on each respective manufacturing method's level of protection.
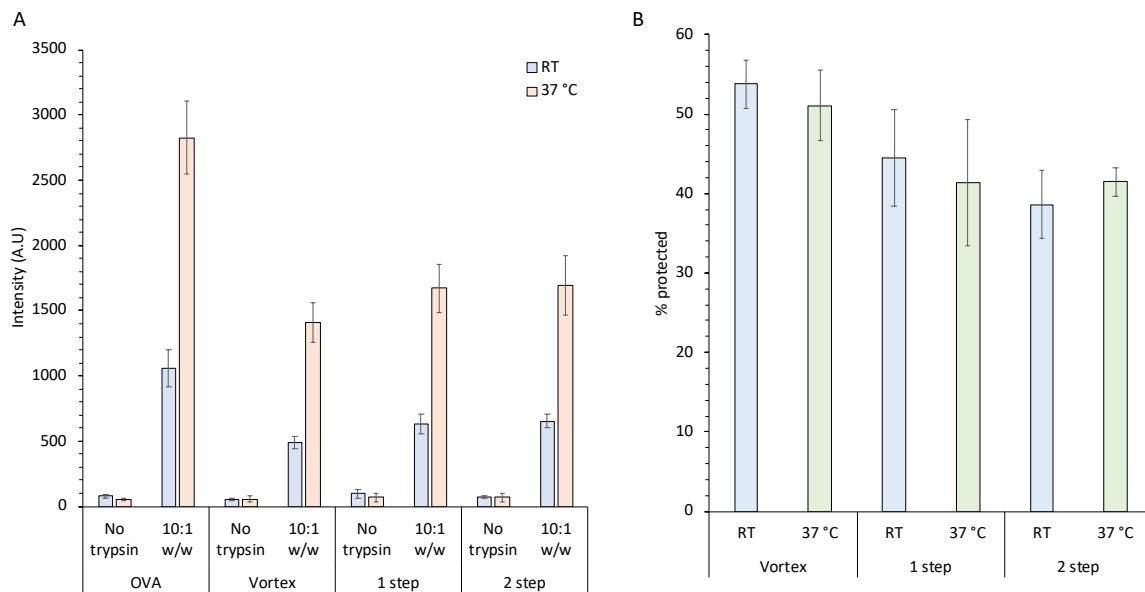
Figure 5.15 *Reduction of fluorescent intensity and reduced protein digestion using cationic liposomes. Liposomes and DQ-OVA adsorption (60:1 L:P) were manufactured using either the vortex, 1-step or 2-step methods using an initial lipid concentration of 24 mg/mL suspended in EtOH and final DQ-OVA concentration of 30 μg/mL. Formulations were then exposed to trypsin at a 10:1 v/v ratio and left for 4 h at either RT or 37 °C. Fluorescent intensities were then measured using an ex/em of 505/535 nm (figure 5.14A) allowing the %protection to be calculated from the emission intensity after each formulation is excited with the respective %protection (figue 5.14B) quantified following the equation outlined in (2.2). Results represent mean ± SD from 3 independent batches.*

When protection% capacity for each manufacturing method is compared, all formulations protected the protein even when bound on the outside. This work highlighted that the cationic liposomes could bind and protect protein even if surface adsorbed due to electrostatics. The researchers Korch and Birkman, using the liposomal formulation phosphatidylcholine:dicetyl phosphate:cholesterol (68:18:9 molar ratio), examined the impact of proteolytic digestion on entrapped and adsorbed protein [293]. Their results indicated that while entrapped protein had a higher degree of protection, surface adsorbed protein reduced digestion by approximately 40%, which the researchers attributed to possible refractory changes in the protein structure when adsorbed to the liposomes or as a result of the protein partially integrating within the bilayers [293]. Previous studies investigated the complex issue regarding protein adsorption to nanoparticles [237], and results showed that conformational changes in the protein structure occur, causing proteins to unfold upon mixing with nanoparticulate systems [294]. It has also been shown that bovine serum albumin (BSA) loses its secondary structure when adsorbed to vesicles with increasing size [295]. The

conformational change in the protein structure causes rearrangement on the liposome surface, leading to observed changes in the biophysical interactions [296, 297] and as such could alter enzymatic binding domains [298], leading to the differences observed in figure 5.15B where the larger 10:1 L:P offer the highest protection.

5.3.9 SDS-PAGE examination of liposome protein protection

Sodium dodecyl sulfate-polyacrylamide gel electrophoresis (SDS-PAGE) was also used to study protein protection offered by the cationic liposomal adjuvants. Enzyme concentrations were examined to determine if the 10:1 w/w trypsin:liposome ratio would fully digest selected protein concentrations and be suitable for the SDS-PAGE analysis. Using the same L:P ratio of 60:1 (final protein concentration of 40 µg/mL) used for section 5.7, various trypsin:liposome ratios were trialled to identify at what point complete protein digestion is achieved and if the result is comparable to the trypsin digestion ratio determined in figure 5.12.

From lane 2 in figure 5.16A, the OVA band without the addition of trypsin is at 43 kDa, with lanes 3 – 8 showing OVA exposed to increasing concentrations of trypsin. Lane 6 uses the same 10:1 w/w trypsin:protein ratio previously used. However, a faint band still appears at approximately 43 kDa from the SDS-PAGE gel. At lanes 7 and 8, which are 20:1 and 40:1 w/w trypsin:protein respectively, the OVA band at 43 kDa disappears with increasing intensities of the trypsin bands appearing at 25 and 18.4 kDa as the concentration of the enzyme increases. From this result in figure 5.16A, a 20:1 w/w trypsin:protein ratio (4 h at RT) was used for electrophoresis studies to ensure the complete digestion of the protein.

Using the 20:1 w/w trypsin:protein being a sufficient ratio for protein breakdown, a fluorescent quantitative protein protection assay (figure 5.16B) was run alongside the SDS-PAGE gel (figure 5.16C) using the same formulations manufactured using the 1-step microfluidic method at different L:P ratios. From the intensity values obtained in figure 5.16B, a concentration-dependent effect on the fluorescent intensity with higher protein concentrations eliciting greater intensities was observed. When %protection for each of the L:P ratios is calculated, the 10:1 L:P permitted protein protection of 40 ± 5%, which was significantly different ($p < 0.05$) from the 30:1 and 60:1 L:P (30 ± 2% and 30 ± 3% respectively).

While the fluorescent quantitative assay suggests that liposomes afforded protein protection, despite these values being less than those in figure 5.15B using a 10:1 w/w digestion mixture, the results in figure 5.16C contradict the findings. Negative and positive controls were set up in lanes 2 and 3 using 0.24 mg/mL of free protein, the final protein concentration at a 10:1 L:P following 1-step manufacturing (lane 2). This is mixed with 20:1 w/w trypsin:protein in lane 3 for the positive control, eliciting the expected results. Following the formulation of liposomes at a 10:1 L:P ratio without trypsin, the clear and intense band appears at 43 kDa in lane 4. However, upon the addition of trypsin, the protein is completely digested in lane 5. A similar effect is observed with the 30:1 L:P in lanes 6 and 7 and the 60:1 L:P in lanes 8 and 9.

Lane 1 = Protein ladder
Lane 2 = 40 ug/mL OVA
Lane 3 = 1:1 w/w
Lane 4 = 3:1 w/w
Lane 5 = 5:1 w/w
Lane 6 = 10:1 w/w
Lane 7 = 20:1 w/w
Lane 8 = 40:1 w/w

Lane 1 = Ladder
Lane 2 = 0.24 mg/mL OVA (-T)
Lane 3 = 0.24 mg/mL OVA (+T)
Lane 4 = 10:1 L:P (-T)
Lane 5 = 10:1 L:P (+T)
Lane 6 = 30:1 L:P (-T)
Lane 7 = 30:1 L:P (+T)
Lane 8 = 60:1 L:P (-T)
Lane 9 = 60:1 L:P (+T)
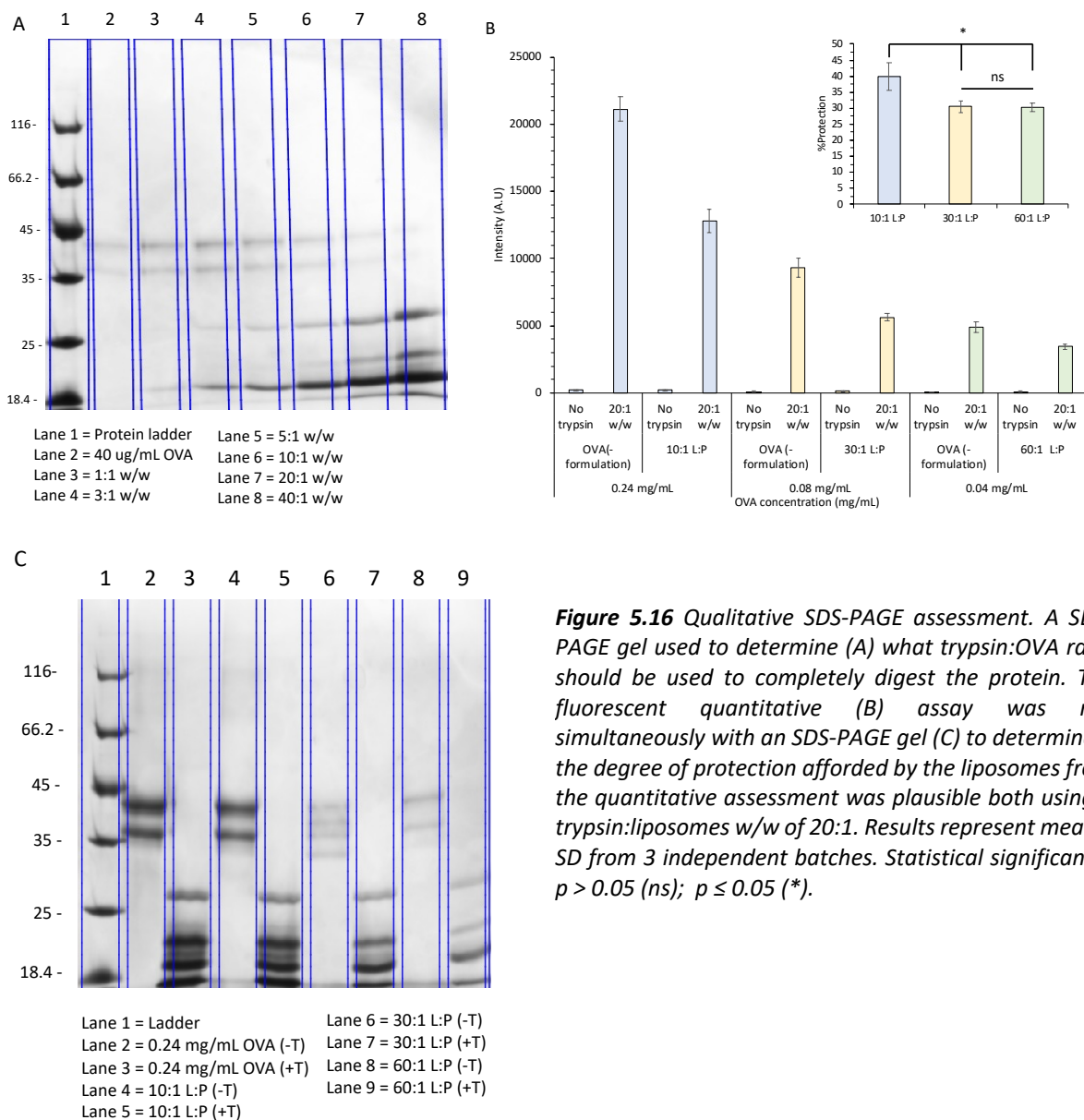
Figure 5.16 Qualitative SDS-PAGE assessment. A SDS-PAGE gel used to determine (A) what trypsin:OVA ratio should be used to completely digest the protein. The fluorescent quantitative (B) assay was ran simultaneously with an SDS-PAGE gel (C) to determine if the degree of protection afforded by the liposomes from the quantitative assessment was plausible both using a trypsin:liposomes w/w of 20:1. Results represent mean ± SD from 3 independent batches. Statistical significance: $p > 0.05$ (ns); $p \leq 0.05$ (*).

As the 1-step method was used exclusively in figure 5.16, the 2-step was also trailed and compared in figure 5.17 to check for differences resulting from changing the manufacturing method. Using a 10:1 L:P ratio in figure 5.17A, no significant difference in the fluorescent intensity or the %protection was measured (40 ± 5% and 38 ± 3% for the 1 and 2-step, respectively). The exact formulations, but using DQ-OVA, were run alongside the SDS-PAGE gel (figure 5.17B) to compare the two analytical methods. Again, this produced comparable results to that in figure 5.16C; mixing the formulation with trypsin led to complete digestion of the adsorbed protein both for the 1-step (lane 5) and 2-step (lane 7). An SDS-PAGE gel was also used to test the protein protection offered by liposomes prepared by the 1-step, 2-step, and vortex methods (60:1 L:P ratio). In figure 5.17C, a faint band at 43 kDa in lanes 2, 4, 6, and 8 (sample without trypsin for the 1-step, 2-step, and vortex method, respectively). This protein band disappears upon the samples being incubated with trypsin, showing the protein is digested by mixing with trypsin. This protein band disappears further, indicating complete digestion below detectable limits. In figure 5.17C, Lane 10 contains free trypsin without protein at an 800 μg/mL concentration to match the enzyme concentration used to digest 40 μg/mL of protein used in figure 5.16 and shows the same banding patterns observed in all the lanes, which include trypsin.
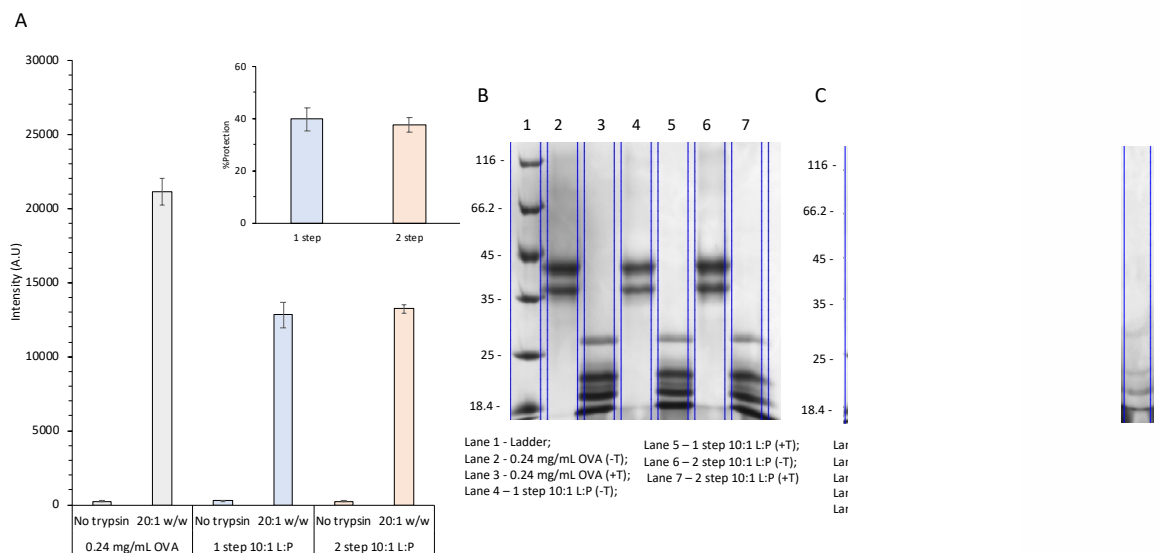
Figure 5.17 *1 vs 2-step manufacturing with protein protection assessed by quantitative and qualitative analysis. Liposomes were manufactured using an initial lipid concentration of 24 mg/mL at a 10:1 L:P ratio using the 1 or 2-step methods. Fluorescent quantitative assessment (A) was conducted simultaneously as an SDS-PAGE gel (B). A 60:1 L:P was additionally measured by SDS-PAGE using the 1 and 2-step production methods (C). A digestive mixture of 20:1 trypsin:liposomes (w/w) was used for the experiment. Results represent mean ± SD from 3 independent batches.*

These results highlight differences between SDS page protein detection and the fluorescent method developed. While comparable banding patterns were observed by Tanaka et al., who also mixed trypsin with OVA, it does not explain the differences between the developed quantitative method and SDS-PAGE results [299]. A possible explanation for the differences could be that DQ-OVA is composed of natural ovalbumin protein labelled with the fluorochrome BODIPY leading to self-quenching [300]. Upon digestion of DQ-OVA, the protease enzyme begins to digest the DQ-OVA leading to BODIFY fragments which reduces the self-quenching and generates fluorescent fragments [301]. Therefore, cleavage of peptide bonds within the carboxyl group of lysine or arginine [302] may result in fragments that would otherwise not be detected using the SDS-PAGE.

5.3.10 In vivo biodistribution of liposomal carriers and their associated protein subunits

Throughout this chapter, the cationic formulation DSPC:Chol:DDA formulated using different manufacturing platforms to control liposome complexing with the protein antigen effectively has been investigated. Studies from the past decade have highlighted the use of cationic liposomes for the effective delivery of sub-unit antigens through the formation of a depot at the injection site and the induction of different immune pathways to improve antigen delivery [95, 303, 304]. Various publications have highlighted multiple mechanisms by which cationic delivery systems deliver antigens and improve immune responses. For example, early work by Cox and Coulter postulated that through using cationic systems, antigens could be effectively delivered to antigen-presenting cells allowing for activation of the innate immune response. This was also supported by other researchers who highlighted the importance of delivering antigens to dendritic cells to invoke an immune response [305, 306]. However, other publications have also supported the observation that cationic formulations containing DDA can effectively be retained at the injection site through electrostatic interactions with negatively charged serum proteins leading to elevated Th1 responses [307]. Researchers have also shown that using DDA within formulations promotes the formation of a depot at the site of injection (SOI) [226, 308, 309]. Therefore, to investigate this further, the IVIS Spectrum *in vivo* imaging system was used to simultaneous tracking of both the liposomes and adsorbed

antigen over specific timepoints and gain an understanding if the formulations remain at the SOI as well as other organs and investigate whether liposome:protein ratios and different manufacturing methods affect the biodistribution.

5.3.10.1 Introduction of a lipophilic fluorescent tag has minimal impact on physical vesicle characteristics

Prior to beginning *in vivo* biodistribution studies, the formulation DSPC:Chol:DDA was made in EtOH, which was successfully formulated with comparable physical characteristics to that of MeOH as shown in figure 5.4 using the lead L:P of 60:1. To confirm the solvent has no impact on the 10:1 L:P or 30:1 L:P before working with animal models. As the basis of the L:P ratio was selected from the results in figure 5.2, formulations prepared by the 1 and 2-step method were compared against these results, which were produced using MeOH to determine any variations in the size and PDI (figure 5.18A) and zeta potential (figure 5.18B), which could have notable consequences in terms of the biodistribution. Liposomes formulated in EtOH and the 10:1 L:P and 30:1 L:P were significantly greater in size than those formulated in MeOH, with the 60:1 L:P corroborating the results obtained in figure 5.4. Using a 10:1 L:P, the liposomal-protein formulations prepared using EtOH by the 1 or 2-step methods were 1197 ± 64 nm and 1249 ± 24 nm in size, significantly ($p<0.05$) larger than the 10:1 L:P formulations prepared using MeOH (< 300 nm with a reduced PDI). A similar trend was observed using the 30:1 L:P with particles sizes of 396 ± 25 nm and 289 ± 15 nm for the 1 or 2-step formulations in EtOH, respectively (figure 5.18). Yet, there was no significant difference using the 60:1 L:P between MeOH and EtOH at either manufacturing method. Similarly, the biggest difference in the zeta potential was at the 10:1 L:P ratio. Using EtOH led to reduced zeta potentials from around 26 mV to 18 ± 2 mV for the 1-step, and for the 2-step, it was 17 ± 3 mV (figure 5.18). For the 30:1 L:P and 60:1 L:P, there was no significant difference in the zeta potentials compared to the formulations manufactured in MeOH (figure 5.18B).

Following these observations, EtOH was not used as a solvent for the *in vivo* investigations. Therefore, to match these as closely as possible, the following processes were implemented:

- 2-step method: a 1:1 FRR (15 mL/min TFR) with MeOH was used to manufacture the liposomes, followed by dialysis to remove residual solvent and then a 1:1 FRR adsorption step using the protein.

- 1-step method: a 9:1 FRR (15 mL/min TFR) with MeOH as the solvent. Dialysis was used to remove residual solvent.

Before examining the effect of L:P ratios and their impact on biodistribution, a stability study was conducted using the lipophilic dye $DiOC_{18}(7)$ (DiR) and fluorescent OVA conjugate, Alexa Fluor® 647 OVA (AF-647 OVA) to ensure sizes are maintained within the critical parameters identified for each L:P using the 1 and 2-step method. Double lipophilic dye and protein conjugate incorporation would allow simultaneous liposome and protein tracking upon *in vivo* injection. The stability study (formulations stored at 4 °C between measurements) would also allow for confirmation of the liposome:DiR ratio, which would be used (500:1 w/w [152]) and how this impacted the physical characteristics of formulations.
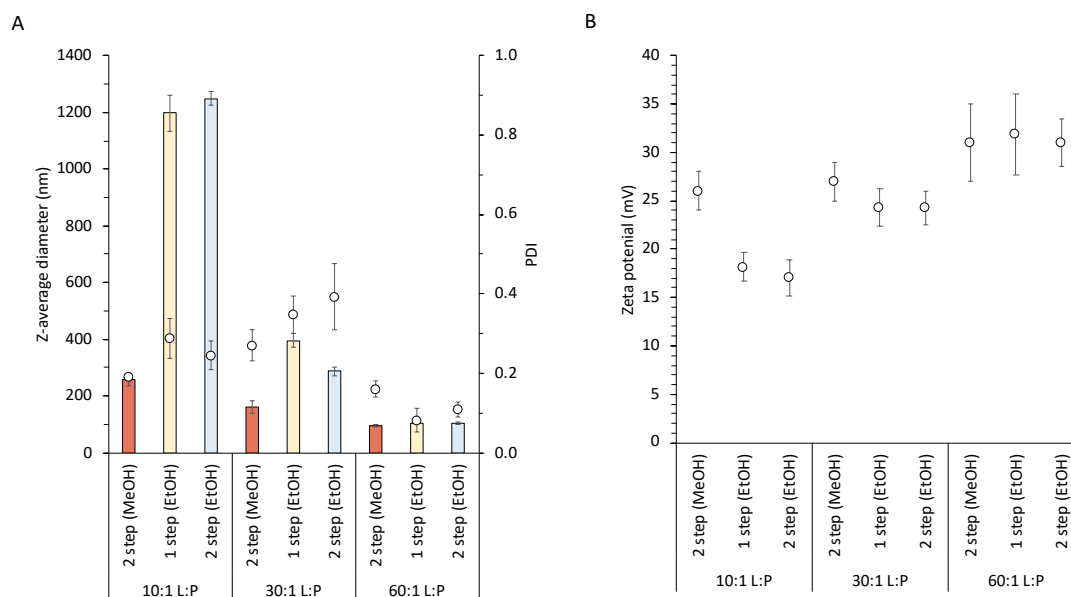
Figure 5.18 *Impact of solvent on different liposome:protein ratios. Liposomes were manufactured using an initial lipid concentration of 24 mg/mL in EtOH at 10:1 L:P; 30:1 L:P and 60:1 L:P using the 1 or 2-step methods and compared against a 2-step method using MeOH. Z-average and PDI measurements (A) of liposomes manufactured in EtOH were obtained along with zeta potentials (mV) and compared to formulations in MeOH. Results represent mean ± SD from 3 independent batches.*

Measuring the formulations over 14 days in figure 5.19 highlights that the most extensive variation in the physical characteristics of the liposomes occurs at a 10:1 L:P as shown in figure 5.19A and B. While the size at day 0 is for the liposomes manufactured with 2-step is comparable to the formulations without fluorescent dyes at approximately 260 nm, the formulation manufactured by 1-step using MeOH is larger at 410 nm; however, this plateaus at 500 nm after 5 days. In figure 5.19B, the PDI at day 0 for the florescent tagged formulations remained below 0.2 across the 14 days of the study. There was minimal impact on the liposome size upon inclusion of the dye in the 30:1 L:P (figure 5.19C) and 60:1 L:P (figure 5.19E) formulations which remained stable across the 14 days regardless of the manufacturing method. The PDI for the 30:1 L:P (figure 5.19D) and 60:1 L:P (figure 5.19F) indicated good uniformity across the 14 days.

One of the concerns for incorporating a lipophilic dye is the impact this can have on the immediate physical characterisation post liposome manufacturing and the effect this could cause on the stability due to the presence of the dye within the bilayer. In addition, DLS measurements were used to obtain particle size and uniformity. Light scattering used to define vesicle size and uniformity could be impacted by the adsorption and emission of DiR and AF647 dyes, which could interfere with the measurements [310]. At higher L:P ratios, there was minimal impact of the dyes. However, there were slight size variances between the unlabelled and labelled formulation in figure 5.19A using a 10:1 L:P. For all the L:P ratios examined in figure 5.19, the DiR concentration remained consistent using a 500:1 w/w lipid:DiR ratio, which is a lower concentration of DiR used with cationic liposomes DSPC:Chol:DDA 10:40:50 M ratio) [152]. The results suggest that due to the sizes and PDI at the 30:1 and 60:1 L:P aligning well with the unlabelled formulation, the DiR dye is not impacting on vesicle characterisation as the concentration is consistent for all investigated formulations and suggests that the dye is distributed uniformly throughout the bilayer which has been demonstrated using the lipophilic dye DiD within liposomes [311].
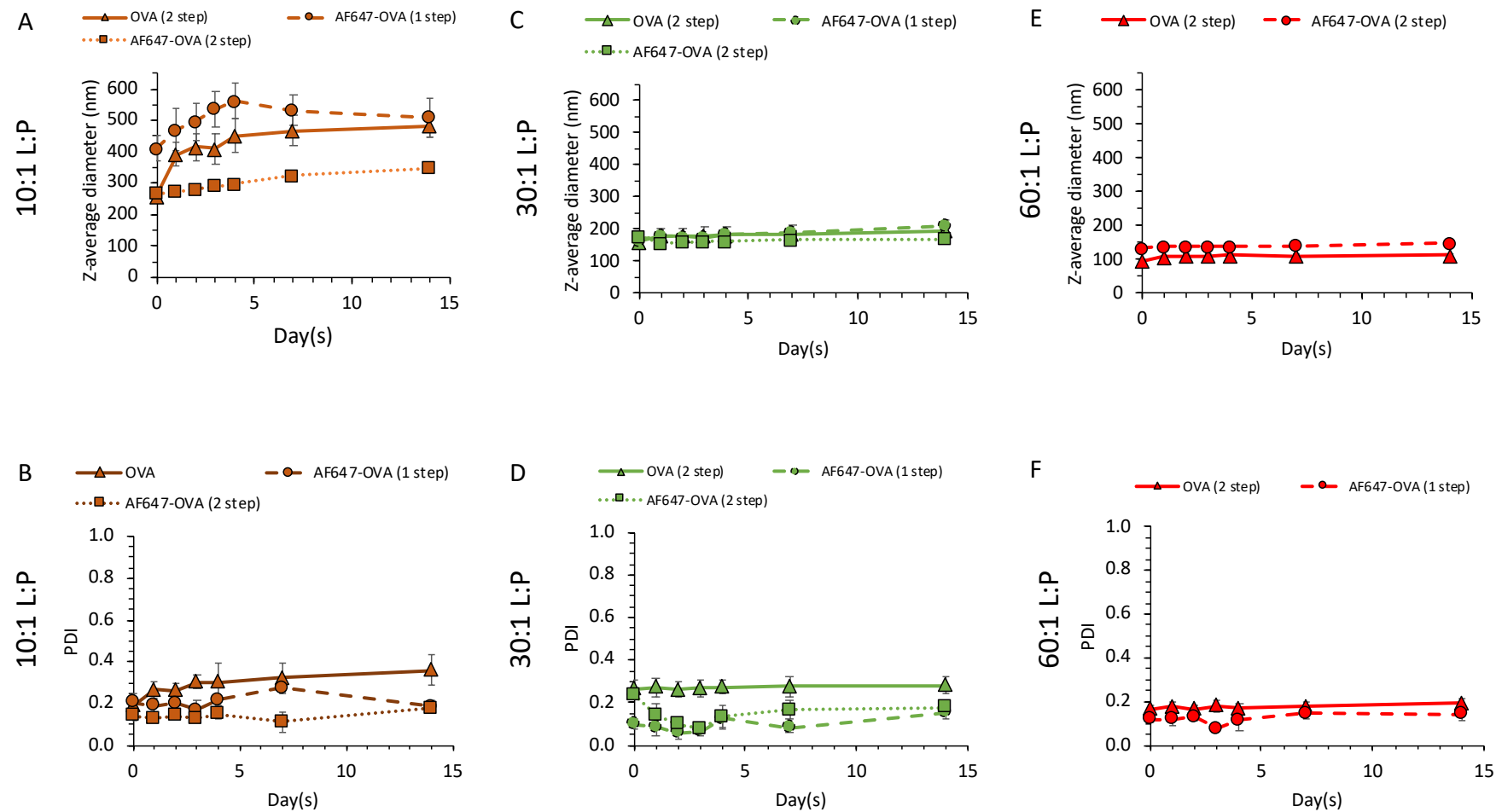
Figure 5.19 *Impact of fluorescent dyes on liposomal size and uniformity characteristics. Lipids were mixed with 500:1 w/w lipid:DiR in MeOH and mixed with AF647-OVA (45 kD) by either 1-step or 2-step mixing with size and PDI measurements recorded using the 10:1 L:P (A+B); 30:1 (C+D) and 60:1 (E+F) L:P over a period of 14 days. For the 2-step method an initial concentration of 4.8 mg/mL of lipids was used at a 1:1 FRR which was dialysed (14 kD membrane) immediately after production. A FRR of 1:1 was then used to adsorb protein at the respective L:P ratio. For 1-step a 9:1 FRR was used with an initial lipid concentration of 24 mg/mL and mixed with protein concentrations at the respective L:P ratios and dialysed (14 kD) immediately. Results represent mean ± SD from 3 independent batches.*

Most likely, the higher concentration of AF647-OVA within the 10:1 L:P caused changes in size and stability of the vesicles in figure 5.19A. As the size of the tagged protein is 45 kDa, which is not notably bigger than the untagged OVA (43 kDa), it is unlikely this would affect the vesicle size. Therefore, the size variances observed are more likely a result of dye adsorbing and emitting during size measuring. Despite the size differences observed in the 10:1 L:P, the size differences between the three L:P are not likely to cause variances in the biodistribution [71] as the biodistribution of these liposomes would be dictated by the cationic nature of the liposomes [115, 308].

5.3.10.2 Liposomes remain at the SOI and facilitate the controlled release of antigen

It has been shown that formulation pharmacokinetics can direct the immune response towards subunit antigens [21, 71]. Therefore, from these previous findings, conducting a biodistribution study using the 10:1, 30:1, and 60:1 L:P using either the 1 or 2-step manufacturing method would provide valuable results regarding the movement of liposomes and antigen upon intramuscular administration. Using the fluorescent OVA conjugate, Alexa Fluor® 647 OVA (AF-647 OVA), and the lipophilic dye $DiOC_{18}(7)$ (DiR) allows the study of both the movement of protein and liposomes respectively upon injection intramuscularly. Using free protein without a carrier, the results in figure 5.20A indicate the fast drainage of unbound protein after 24 h. By introducing a liposome carrier in all L:P tested, protein concentrations remained steady at the injection site for 9 days with no significant differences between the formulations. For the 10:1 L:P using the 1-step in figure 5.20B, after 9 days, the normalised flux was 74 ± 10 %, while for the 2-step in figure 5.20C, the normalised flux was 67 ± 12 %. Similar results ($p > 0.05$) were also obtained for the 30:1 L:P using the 1-step (figure 5.20D) and the 2-step (figure 5.20E) which were 64 ± 17 % and 82 ± 13 % and 60:1 by 1 and 2-step (figure 5.20F and G) with were measured to have a normalised flux of 82 ± 10% and 74 ± 11 % respectively.
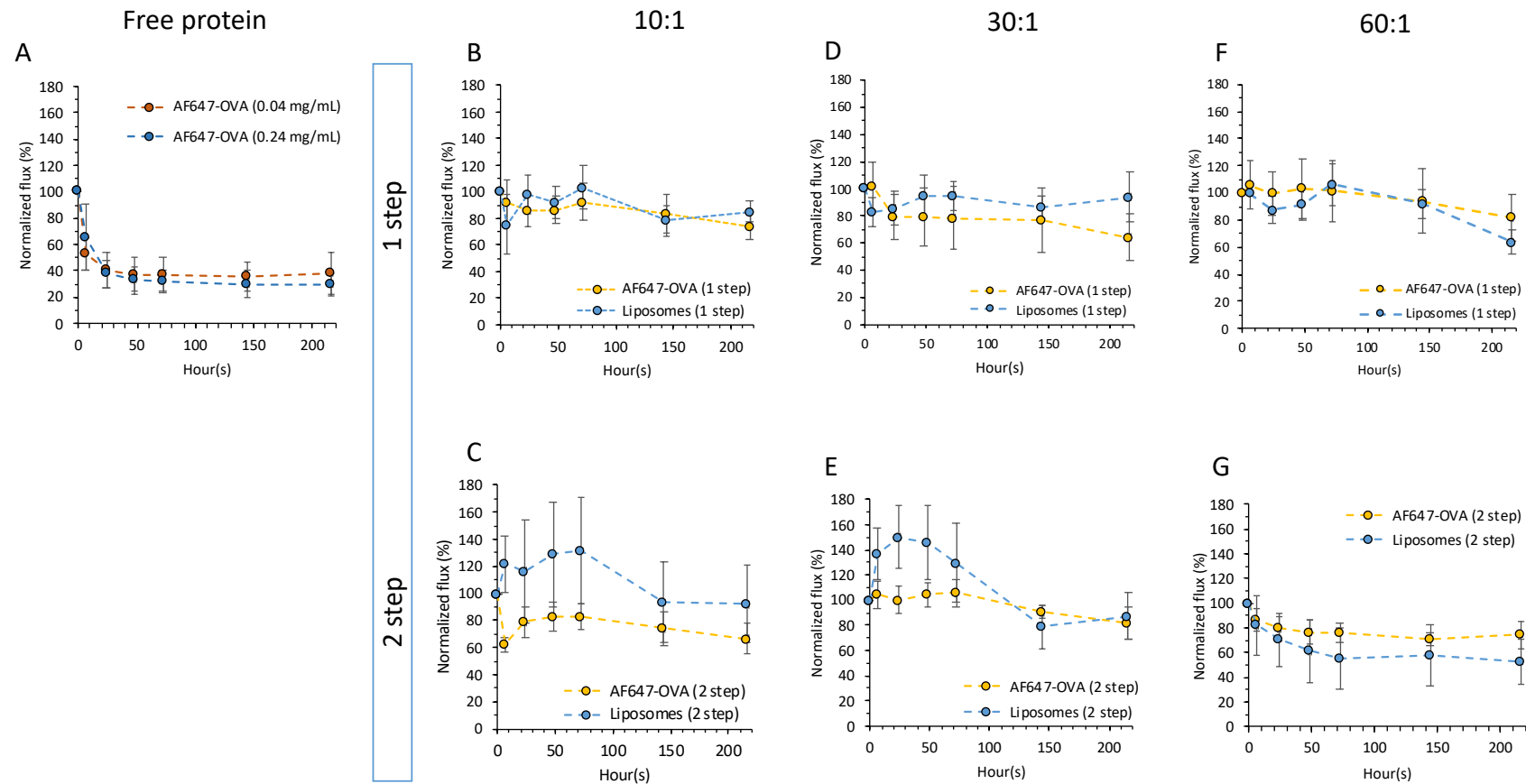
Figure 5.20 *In vivo biodistribution of liposomes and protein movement. Liposomes and protein were tracked upon 50 µL i.m administration of either 'free' AF647-OVA without a liposome carrier with two concentrations (A). Liposomes were manufactured by 1-step and 2-step at either 10:1 L:P (B + C); 30:1 L:P (D+E) or 60:1 L:P (F+G). For the 2-step method a initial concentration of 4.8 mg/mL of lipids was used at a 1:1 FRR which was dialysed (14 kD membrane) immediately after production. A FRR of 1:1 was then used to adsorb protein at the respective L:P ratio. For 1-step a 9:1 FRR was used with an initial lipid concentration of 24 mg/mL and mixed with protein concentrations at the respective L:P ratios and dialysed (14 kD) immediately. Results are represented as mean ± SD of 5 mice per experiment group.*

Interestingly, the results in figure 5.20 indicated that regardless of the L:P used, liposomes and their associated protein could be retained at the injection site. The results highlight that cationic liposomes interact with interstitial tissue at the injection site resulting in vesicle deposition [21, 312] and the sustained release of protein [313]. This effect could be overcome by incorporating PEG, which masks the surface charge and reduces electrostatic interactions between the formulation and interstitial tissue to increase blood circulation times if this was the desired pharmacokinetic profile [107. Figure 5.20 also demonstrate that swapping between the 1 and 2 step manufacturing methods allows for reproducible results for each of the respective L:P investigated and allow for similar biodistribution profiles to be achieved.

After the mice were terminated, organs that have a role in eliciting an adaptive immune response (inguinal/popliteal lymph nodes and spleen), in addition to those which facilitate pharmacokinetic metabolism and elimination (liver and kidneys), were removed to track the movement of the liposomes and antigen away from the SOI. Using the 10:1 L:P, figure 5.21A highlights the images and experimental layout to identify liposome accumulation by using an ex/em filter of 750/780 nm, which would not excite the AF647-OVA. The same organ layout was used for AF647-OVA analysis using an ex/em filter of 650/668 nm. Focussing on the AF647-OVA in figure 5.21B, the high total flux obtained from the liver is notable. However, this is autofluorescence from the high haemoglobin volume within the organ upon immediate imaging. Similar findings were observed in figure 5.21C and the other groups within the study. One of the critical organs of interest was the lymph nodes, specifically the draining inguinal and popliteal lymph due to their role within adaptive immunity. From figure 5.21B, there is a marginal elevation of the total flux present in the draining and non-draining inguinal and lymph nodes using the 2-step manufacturing method, which was also observed in figure 5.21C at the draining popliteal lymph nodes.
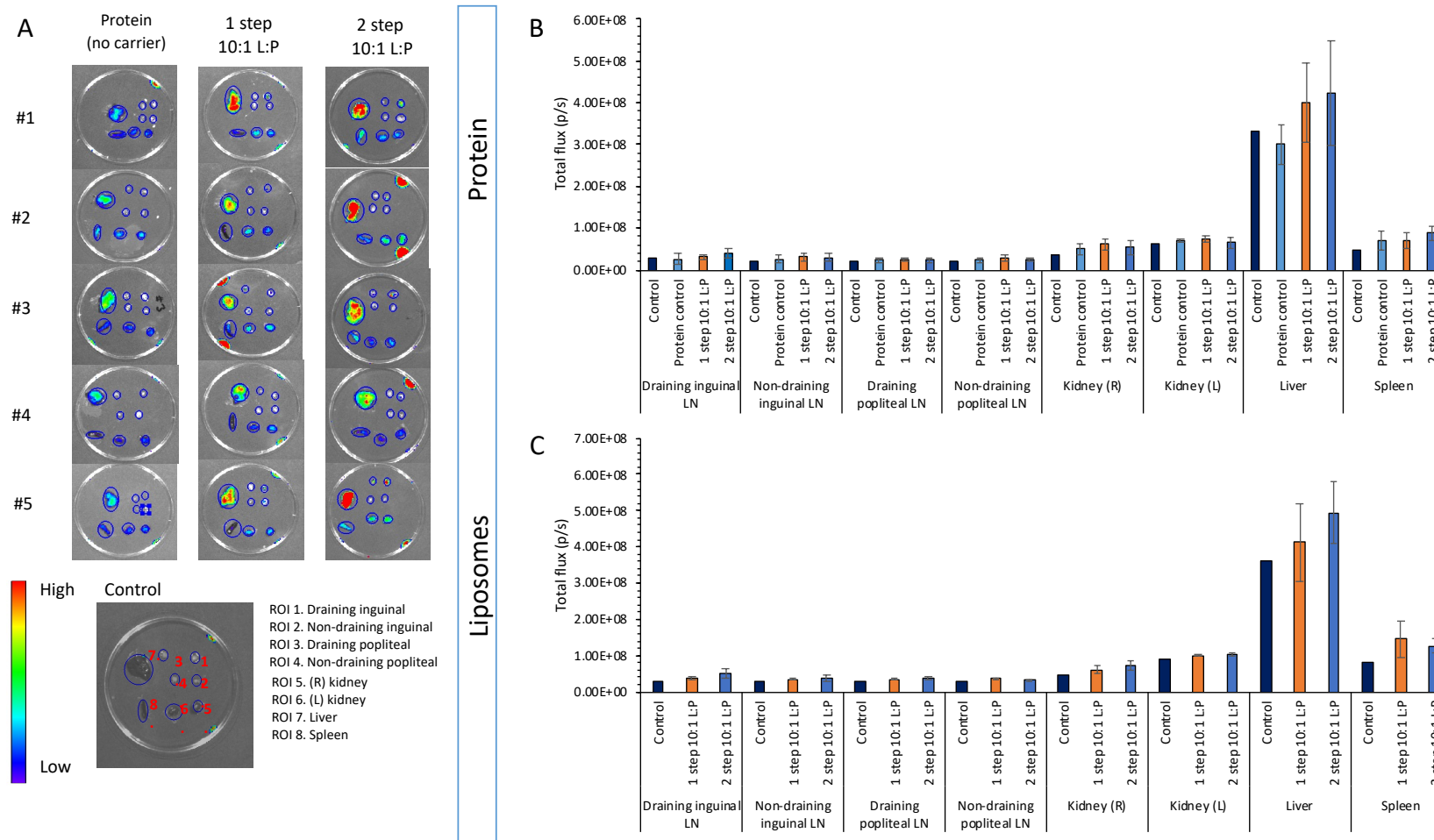
Figure 5.21 *Ex vivo analysis of key organs responsible for adaptive immune responses along with pharmacokinetic metabolism and elimination. Formulations manufactured by 1 and 2-step at a 10:1 L:P were imaged (A) to measure the total flux of AF647-OVA (B) and liposomes (C) by removing the inguinal and popliteal (both draining and non-draining) were dissected with kidneys (L+R); liver and spleen from mice in figure 5.18. AF647-OVA measurements were recorded using an ex/em of 650/680 nm while DiR labelled liposomes were measured using an ex/em of 710/780 nm.*

Using the IVIS for biodistribution analysis allows for the general tracking of particles, and using both AF-647 OVA and DiR permits the opportunity to follow the movement of protein and liposomes within one study. Evidence has shown that clearance of nanoparticles often occurs through their interaction with the mononuclear phagocytic system (MPS), where phagocytes uptake the nanoparticles [314-316] with clearance favouring stiffer NPs [317, 318]. To summarise, the results in figure 5.20 using both the 1 and 2-step manufacturing methods, using liposomes led to a strong interaction between the liposomes and injection site, allowing them to remain fixed at the SOI. However, while there were no statistical differences between the control values and formulations in figure 5.21B and C, there were increases in the total flux values at the lymph nodes and spleen compared to the control after 9 days. These results indicate that a shorter study could produce more statistically significant results and support the evidence that particles, when injected, can be trafficked away from the SOI to the draining lymph nodes by mononuclear phagocytes [319-321].

5.3.10.3 Rapid accumulation of antigen and liposomes at draining lymph nodes

Targeting secondary lymphatic tissue, such as the lymph nodes, is essential to elicit an adaptive immune response [322]. Encouragingly, increased total flux values after 9 days post-injection in figures 5.20 suggests that the formulations were drained away from the SOI. Therefore, to investigate this further, a short *in vivo* study was conducted to track drainage times away from the SOI using the 10:1 L:P manufactured by 1 and 2-step and identify the possible accumulation of liposomes and antigen within secondary lymphatic organs.

Delivery of AF647-OVA without the liposome carrier resulted in a high total flux at 0 h, as indicated by figure 5.22A. Nonetheless, rapid drainage from the SOI was noted: after 6 h, a drop of > 50%, and after 48 h, this dropped to 10 ± 4 % of the normalised flux (figure 5.22B). As shown from figure 5.20C, though there was a large increase in the total flux values at 6 h in the draining popliteal and inguinal lymph node, this was quickly cleared after 6 h. Antigen delivery was sustained at the SOI using a liposomal formulation, as shown in figure 5.22A for the 1-step and 2-step manufacturing methods. After 48 h, the normalised flux was 58 ± 14 %

and 67 ± 18 % for the 1 and 2-step methods, respectively, as shown in figure 5.21B. In terms of accumulation at the lymph nodes for the 1-step (figure 5.22D) and 2-step (figure 5.22E), the 1-step initially had a greater total flux value at the draining popliteal LN at the 6 h time point. Though, this diminished to $2.1 \times 10^7 \pm 9 \times 10^6$ p/s. On the other hand, the 2-step maintained a level of approximately 4×10^7 p/s across the 48 h at the draining popliteal lymph node. There was a greater accumulation of AF647-OVA at the draining popliteal lymph node for both manufacturing methods than the draining inguinal lymph node.

As expected, when the liposomes were tracked across 48 h, they remained at the injection site regardless of the manufacturing method used, as shown in figure 5.23A and B. Without liposomes, incorporation of DiR (500:1 w/w) was not possible, so no fluorescence was shown when AF647-OVA was used in figure 5.23C. However, using both the 1 and 2-step methods, liposomes accumulated at both the draining inguinal and popliteal lymph nodes, which were detected after the first 6 h time point in figure 5.23D and E. For both methods, there was a greater total flux at the popliteal lymph node when compared to the draining inguinal with limited accumulation at either draining or non-draining lymph nodes.

The sustained normalised flux using liposomes in figure 5.23B was expected due to the suspected electrostatic interaction the cationic liposomes have with interstitial proteins (such as heparan sulfates), which can cause aggregation at the SOI [61] with reduced draining of the formulations across the rest of the body [323, 324]. This effect has also been linked to favour the presentation to immune cells, which could also improve the immune response [307, 325]. The results obtained in figures 5.22 and 5.23 confirm previous assumptions made in section 5.8.2 that by conducting a shorter *in vivo* study, the tracking of liposomes and antigen away from the SOI can be analysed in greater detail and show greater levels of accumulation. However, an observation applied for both liposomal formulations and protein formulations in figure 5.22 and 5.23 was the levels of both protein and liposomes at the draining popliteal lymph node. Comparable observations were found by Roces et al., upon intramuscular injection [61]. This is predominantly a physiological driven effect as the popliteal lymph node is first draining lymph node the formulation would encounter by injection into the quadricep. After this, it would then move towards the inguinal lymph nodes,
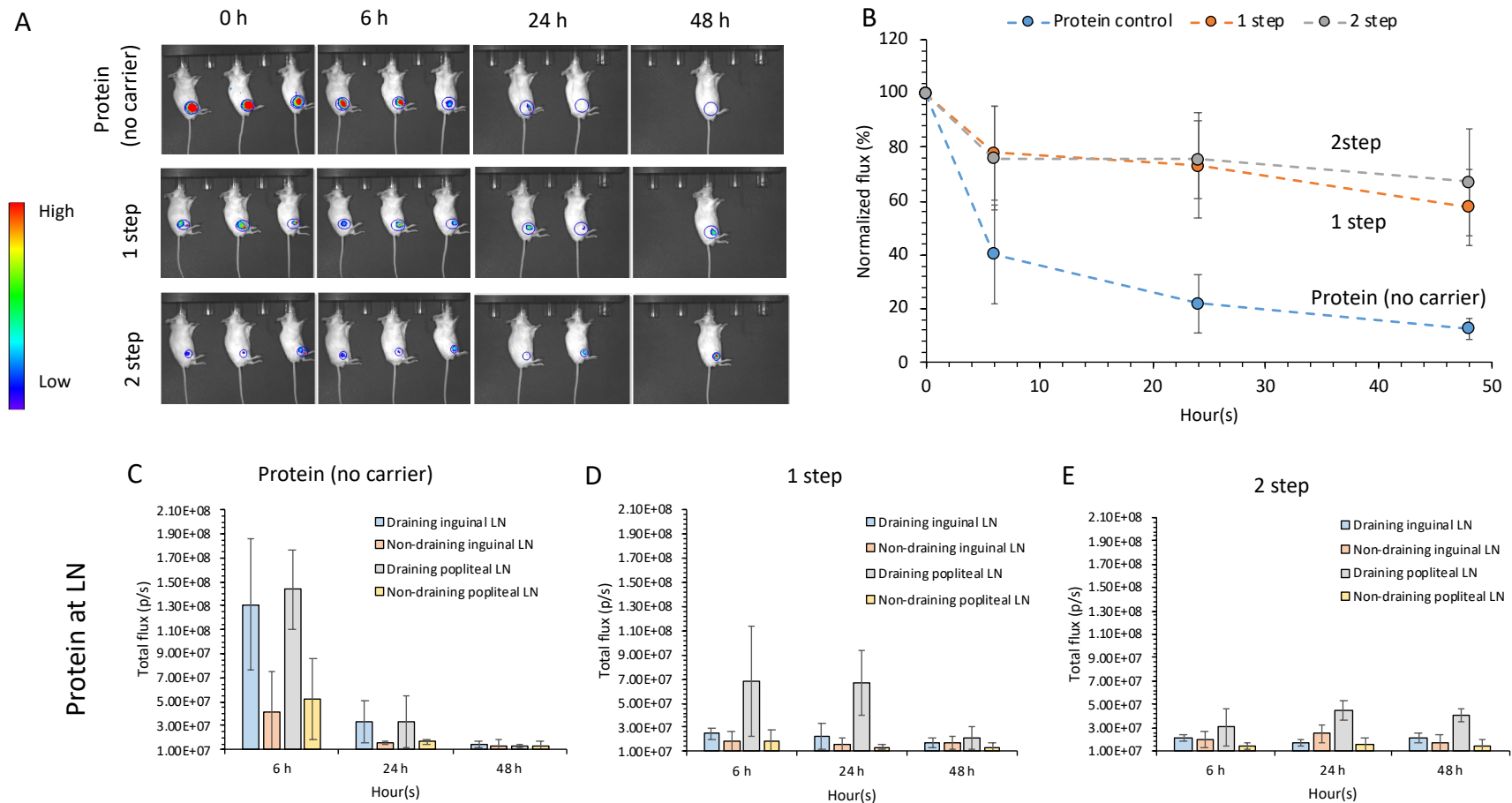
Figure 5.22 *Rapid draining of AF647-OVA away from SOI without a liposomal carrier. Mice were injected with 50 µL of a 10:1 L:P formulation manufactured by 1 or 2-step with fluorescent intensities for the protein measured at 0, 6, 24 and 48 h using an ex/em of 650/680 nm (A) allowing the normalised flux% to be extrapolated (B). The toal flux intensities from the fluorescent emission was measured for AF647-OVA (without a carrier) (C), 1 step (D) and 2 step (E) methods wre recorded at the inguinal and popliteal draining and non-draining lymph nodes. The draining and non-draining inguinal and popliteal lymph nodes were excised from mice to track and measure the accumulation of AF647-OVA over two days.*
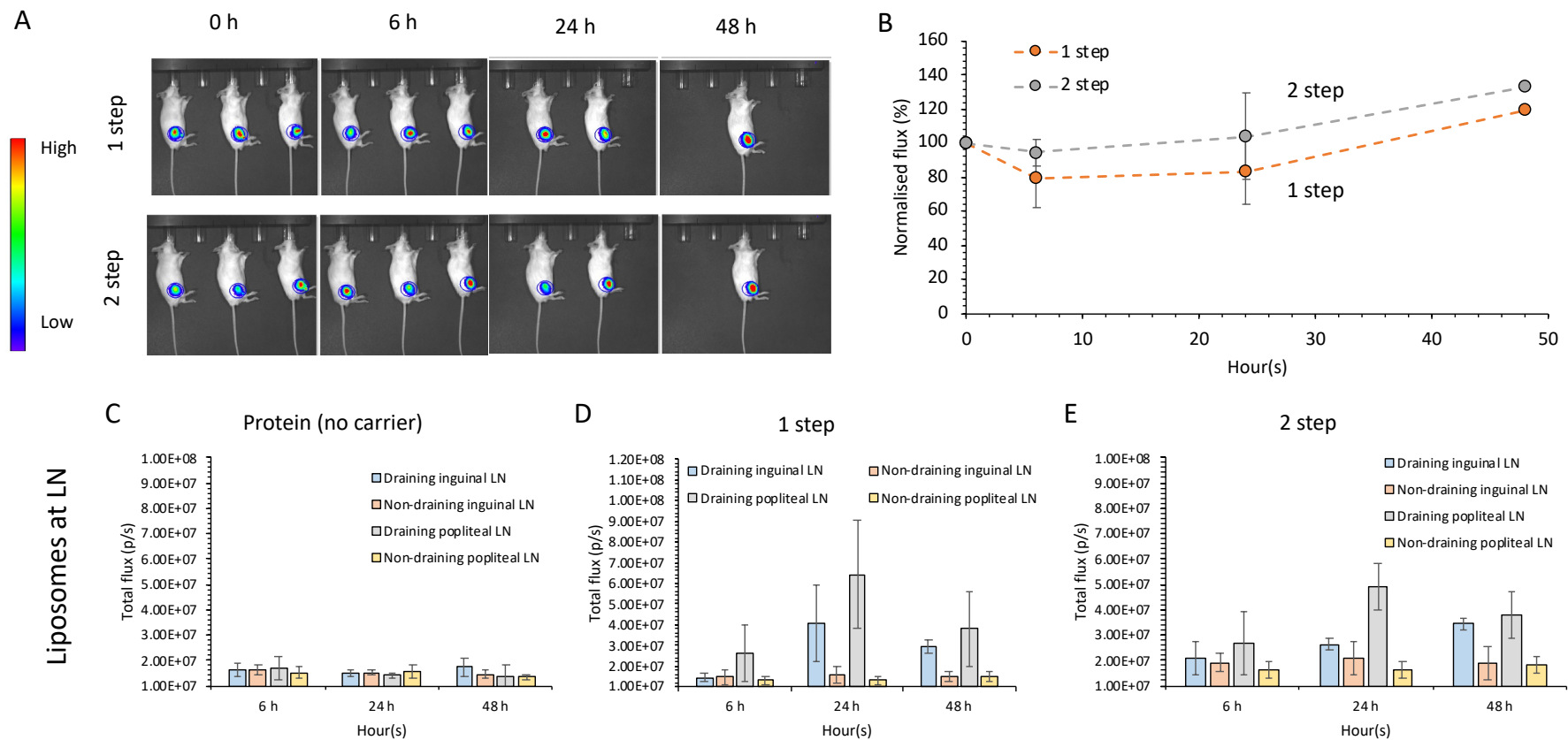
Figure 5.23 *Accumulation of liposomes at draining and non-draining inguinal and popliteal lymph nodes post injection. Mice were injected with 50 µL of a 10:1 L:P formulation manufactured by 1 or 2-step with fluorescent intensities for the liposomes measured at 0, 6, 24 and 48 h using an ex/em of 710/780 nm (A) allowing the normalised flux% to be extrapolated (B). The toal flux intensities from the fluorescent emission was measured for DiR labelled liposomes (without a carrier) (C), 1 step (D) and 2 step (E) methods wre recorded at the inguinal and popliteal draining and non-draining lymph nodes. The draining and non-draining inguinal and popliteal lymph nodes were excised from mice to track and measure the accumulation of AF647-OVA over two days.*

as shown in figure 5.23D and E, where elevated total flux values between 0 and 48 h were measured. The results gathered in section 5.8.3 have further indicated that manufacturing methods do not alter the formulations' kinetic profiles, despite the formulation's highly cationic nature and propensity for it to remain at the SOI. Based on the *in vivo* assessment of these liposomal formulations, the next step was to identify differences in immunological activity.

5.3.11 Liposome:protein ratio selection is a critical parameter to boost serum antibody responses

To assess the immunogenicity of the cationic formulation using different L:P ratio with the 1 and 2-step manufacturing methods, the protein subunit major out membrane protein (MOMP) was used as the vaccine antigen of *Chlamydia trachomatis (C.t).* MOMP has been used within preclinical studies [326-329] and recently the first clinical development of *C.t* vaccine using the cationic formulation DDA:TDB by Danish researchers at the Staten Serum Institut [10, 330] with improved immunogenicity profiles against the adjuvant aluminium hydroxide. Using the antigen would permit the evaluation for the controlled production of liposomal formulations and adsorption of the antigen with different L:P ratios, either 1 or 2-step microfluidic methods, to induce antigen-specific total IgG and subtypes in blood serum using a prime-boost vaccine regimen.

Before injection, as MOMP was replacing the model antigen OVA, characterisation of the 10:1, 30:1, and 60:1 L:P manufactured by 1 and 2-step was undertaken. At each L:P examined using the 1-step production method (figure 5.24A; B and C), the sizes obtained upon substitution with MOMP were comparable to those measured using OVA. Similarly, using the 2-step production method, the 30:1 and 60:1 L:P agreed with the formulations made with OVA. However, using the 10:1 L:P 1 step liposomal-MOMP formulation, the Z-average diameters of 717.1 ± 25.1 nm with a PDI > 0.5 was produced figure 5.24A). This was significantly (P<0.05) greater than the particle sizes obtained with the 1-step and with OVA or MOMP (figure 5.24A); thus, this formulation was dropped from the *in vivo* study. Measurements of the formulations were taken on days 0 and 21 before injection for each of

the L:P ratios examined (figure 5.24D – F) to ensure vesicles align with the Z-average diameter, PDI and zeta potential obtained in figure 5.24A - C before injection.

D

	1st Injection	2nd Injection
	10:1 L:P (1 step)	10:1 L:P (1 step)
Size (nm)	250 ± 6	256 ± 7
PDI	0.18 ± 0.03	0.19 ± 0.02
ZP (mV)	27 ± 2	31 ± 1

E

	1st Injection		2nd Injection	
	30:1 L:P (1 step)	30:1 L:P (2 step)	30:1 L:P (1 step)	30:1 L:P (2 step)
Size (nm)	124 ± 1	152 ± 7	119 ± 2	151 ± 3
PDI	0.18 ± 0.01	0.1 ± 0.01	0.21 ± 0.01	0.17 ± 0.03
ZP (mV)	35 ± 2	34 ± 2	35 ± 3	39 ± 3

F

	1st Injection		2nd Injection	
	60:1 L:P (1 step)	60:1 L:P (2 step)	60:1 L:P (1 step)	60:1 L:P (2 step)
Size (nm)	97 ± 5	109 ± 1	100 ± 5	103 ± 2
PDI	0.2 ± 0.01	0.09 ± 0.03	0.22 ± 0.02	0.15 ± 0.01
ZP (mV)	39 ± 2	40 ± 4	35 ± 2	39 ± 3

Figure 5.24 *Adsorption of MOMP onto liposomal surfaces and in vivo injection vesicle characteristics. Using 1 and 2-step manufacturing methods, MOMP was surface adsorbed at a L:P of 10:1 (A); 30:1 (B) and 60:1 (C). The formulations used for the immunogenicity study were produced on day 0 and day 21 with the size PDI and zeta potential measurements recoded for the 10:1 L:P (D), 30:1 L:P (E) and 60:1 L:P (F). All L:P examined for the immunogenicity study were produced by the 1 and 2 step methods, excluding the 10:1 L:P where the 1 step method was exclusively used. For the 2-step method a initial concentration of 4.8 mg/mL of lipids, suspended in MeOH, was used at a 1:1 FRR which was dialysed (14 kD membrane) immediately after production. A FRR of 1:1 was then used to adsorb protein at the respective L:P ratio. For 1-step a 9:1 FRR was used with an initial lipid concentration of 24 mg/mL in MeOH and was mixed with protein concentrations at the respective L:P ratios and dialysed (14 kD) immediately.*

Based on the results in figure 5.24, 5 formulations progressed to vaccine efficacy studies. Conducting an antibody immunogenicity study and examining total IgG, IgG1 and IgG2a highlighted trends between the different L:P ratios (10:1, 30:1 and 60:1) and manufacturing methods (1 step and 2 step) (Figure 5.25). A pattern was observed with the three antigen-specific IgG subtypes with the reciprocal endpoint titre growing in intensity as the adjuvant to protein ratio is increased from 21:1 to 126:1 moving from 10:1 up to 60:1 L:P (the DDA concentration remaining fixed at 5.05 mg/mL and the protein concentration decreasing from 240 µg/mL to 40 µg/mL from 10:1 to 60:1 L:P respectively). As the protein concentration decreases, there is also a reduction in vesicle size, which may also contribute. From 10:1 L:P with the 1-step strategy, the only significant differences (P<0.05) observed against the control was through induction of both MOMP specific IgG1 and IgG2a antibodies (figure 5.25B and C)

with no significant difference observed in total IgG subclass (figure 5.25A). The 10:1 L:P stimulated comparable reciprocal endpoint titre values for the IgG1 and IgG2a (figure 5.25E and F) subclasses to the 30:1 L:P after 48 days. Using the 60:1 L:P promoted the highest endpoint titre across the three antibodies investigated (figure 5.25G; H and I). The total IgG subclass provided the highest reciprocal endpoint (Figure 5.25G) with no significant difference between the IgG1 and IgG2a subclasses (figure 5.25H and I, respectively). When comparing the production methods, at both the 30:1 and 60:1, there was no significant difference in immune responses (Figure 5.25), highlighting the interchangeability in production strategies and its ability to induce comparable serum antibody responses.
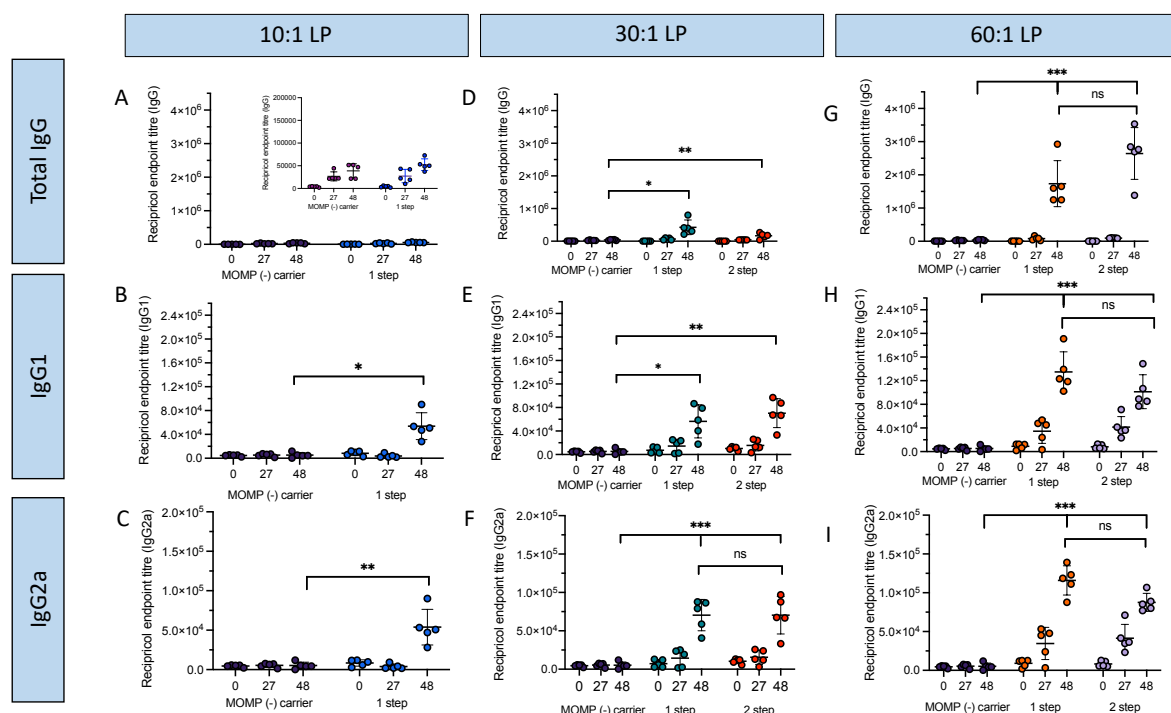
Figure 5.25 *Antibody immunogenicity study against MOMP using 1 and 2-step production strategies. Blood serum samples were taken from mice one day before injection along with days 27 and 48 with vaccine doses administered at 50 μL by I.M injection on day 0 and 28. Antibody specific ELISAs measured IgG; IgG1 and IgG2a for 10:1 L:P (A, B and C respectively); 30:1 L:P (D; E and F respectively) and 60:1 (G; H and I respectively). The lipid concentration for each L:P ratio was 2.4 mg/mL with a MOMP concentration of 240 μg/mL, 80 μg/mL and 40 μg/mL for the 10:1, 30:1 and 60:1 L:P respectively. The line represents the geometric mean for each group ± SD of 5 mice per experimental group.*

The results from the immunogenicity study were promising and highlighted two observations. The first is that regardless of IgG subtype, there was a trend where greater endpoint titres were observed a higher L:P ratios, and second that the effect of manufacture has no impact

on the endpoint titres. As the L:P ratio increases from 10:1 to 60:1 L:P, the ratio of adjuvant to protein is 6 times higher from 21:1 to 126:1 respectively, increasing the impact of the adjuvant at the injection site. The formulation DDA:TDB elicits robust antibody responses; yet, the researchers Hussain et al., demonstrated that altering the L:P by keeping the antigen concentration constant and reducing the DDA concentration through the incorporation of increasing concentrations of DSPC led to a reduction in IgG2b antibodies [325]. While the results in figure 5.25 use DSPC:Chol:DDA, the impact of increasing DDA concentrations on greater endpoint antibody titres agrees with the findings from Hussain et al., [325], underlining the impact DDA plays as an adjuvant. The incorporation of DDA within liposomes promotes the formation of a depot at the injection site [21, 225] (also shown in figure 5.20). The inclusion of DDA also enhances antigen uptake within dendritic cells, macrophages and B cells [238] and can traffic the antigen to the lymph node to T cells [309]. The DDA component is also of significant importance within the DDA:TDB formulation is crucial for Th1 and Th17 stimulation [331], which is discussed in greater detail within chapter 6. From figure 5.24, different liposome sizes were produced for each of the L:P ratios investigated with vesicles having a reduced size at an increased ratio of L:P, which could contribute to the different endpoint antibody titres observed. Again, using DDA:TDB liposomes, the impact of size was examined by producing MLV and SUV liposomes that were approximately 450 nm and 250 nm in size, respectively. In addition, 10 and 25% PEG was added to DDA:TDB to further reduce the size to approximately 145 nm and 120 nm, respectively [71]. These studies showed an increase in the early endpoint antibody titres, which was attributed to increased PEG concentrations, allowing for improved trafficking to draining lymph nodes. However, from day 24 onwards, there was no significant difference in the IgG titres obtained across the 4 sizes investigated [71]. Though, it was observed that the smaller vesicles containing PEG had reduced levels of cytokine production, particularly IFN-γ and IL-2, than their non-PEGylated counterparts and reduced splenocyte proliferation [71]. To summarise, within this study, using decreased concentrations of MOMP allowed for reduced vesicle sizes; however, vesicle size did not impact liposome immunogenicity. The increased adjuvant to protein ratio was crucial in inducing greater endpoint antibody titres.

5.4 Conclusion

This chapter outlines various manufacturing methods that allow for the refined production of cationic liposomes and controlled protein adsorption. Investigating and refining operational FRRs allowed formulations with reduced solvent content (< 10% v/v) and controlled protein adsorption. Building on these findings, different microfluidic protein subunit adsorption methods were investigated, all of which could function within a continuous platform. It was shown that using inline adsorption was not as effective as the 1 or 2-step methods, which permitted high loading efficiencies (> 65%), enhanced stability, and comparable vesicle morphologies. By conducting *in vivo* biodistribution investigations, it was shown that over 9 days, DSPC:Chol:DDA liposomes remained at the injection site and retained protein regardless of the L:P ratio used or manufacturing method. Further investigation also indicated drainage of protein and liposomes accumulated in secondary lymphatic organs. Following the immunogenicity study, the L:P ratio was crucial in promoting antigen-specific antibody titres. The 60:1 L:P formulation promoted high IgG and IgG subtype titres when compared against the 10:1 L:P, and 30:1 L:P formulations loaded the MOMP antigen. Despite the 60:1 L:P being the smallest vesicle with the lowest concentration of adsorbed antigen, the increased DDA:protein could have attributed to an improved adjuvant effect leading to stronger antibody titres obtained.

Chapter 6

Microfluidic preparation of adjuvanted SARS-CoV-2 spike protein: DDA:TDB vs DDA:PHAD®
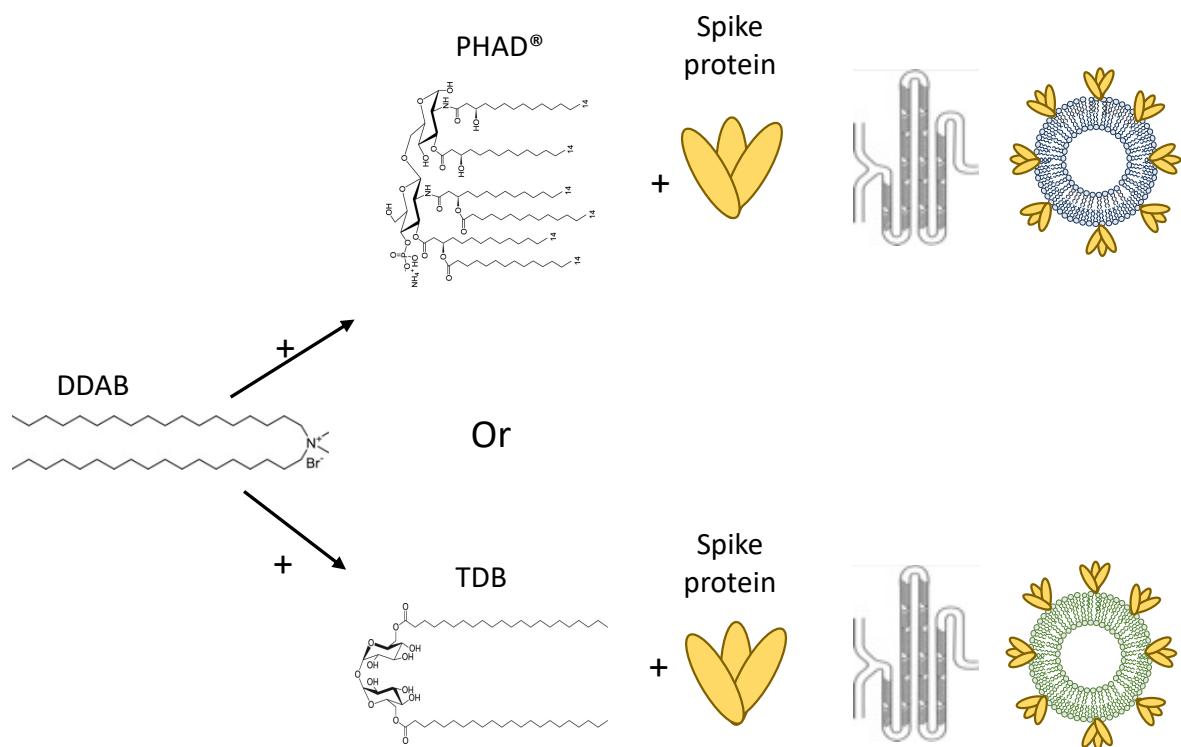
6.1 Introduction

At the time of planning chapter 6, the spike protein region was a key focus towards developing a COVID-19 vaccine, particularly the receptor-binding domain (RBD), which targets neutralisation of SARS-CoV-2 [332, 333]. The urgent requirement for a safe and effective vaccine has led to global collaborations allowing the use of RNA technology within two novels LNP formulations. Both Moderna [220] and Pfizer/BioNTech [221] utilised LNPs to deliver mRNA encoding for the spike protein region within 1 year. While the use of the spike protein region of SARS-CoV-2 has been targeted heavily for COVID-19 vaccines [334], the presentation of the protein varies substancially, leading to a broad range of vaccines to be developed (with 137 vaccines to progress into clinical development with 194 vaccines in pre-clinical development: access date 16th December 2021 [335]). Recent research has also indicated that using alternative COVID-19 vaccines for their "booster" dose in a 'mix and match' regimen (for example, using a Pfizer/BioNTech vaccine for the initial vaccination and the Moderna vaccine for the 2nd vaccination) allowed for more potent immune responses leading to higher spike-specific IgGs and neutralising antibodies compared to a homologous mRNA vaccine regimen [336-338]. The utilisation of a heterologous vaccine regimen approach not only broadens the COVID-19 vaccine portfolio allowing different vaccines to be used for various patient groups (i.e. elderly, immunocompromised, ethnic background) but also overcomes potential vaccine manufacturing issues and export delays to meet the 12 billion doses forecasted by the end of 2022 [339].

December 2021 and Feburary 2022 saw the European Medicines Agency (EMA) and MHRA respectively approve the first subunit vaccine against SARS-CoV-2 [340, 341], NovaVax, with further submissions to the FDA for emergency approval [342]. There are further phase I-II vaccine trials also reporting high titres of neutralising antibodies [343, 344] using protein subunits as possible future vaccine candidates against SARS-CoV-2. However, as the spike protein is not sufficiently immunogenic alone, an adjuvant is required to stimulate an innate immune response, such as Saponin within Matrix-MTM for the phase III subunit vaccine [343, 345]. Adjuvants function in various ways, such as forming a depot at the injection site, improving antigen uptake and presentation to APCs, allowing them to impact directly on the magnitude of Th1 and Th2 pathways [83, 346]. A potent liposomal adjuvant formulation,

known as CAF01, comprises of the dimethyldioctadecylammonium (DDA) and trehalose 6,6' – dibehenate (TDB) at the optimal w/w of 5:1 [267] used in phase I trials for adjuvating an Ag85B-ESAT-6 against tuberculosis [347] and has recently been used for adjuvating spike protein for SARS-CoV-2 following a single dose regimen [260]. DDA was used previously in chapter 5 and elicited antigen-specific antibodies, with additional research highlighting antibody and cell-mediated immunity [348]. DDA can self-assemble into closed bilayer vesicles; however, these are physically unstable [267], requiring additional lipids to stabilise the vesicle, such as DSPC or cholesterol, used in chapter 5. TDB was identified by the Staten Serum Institut, Denmark, to provide vesicle stabilisation and function as an immunostimulator promoting Th1 and Th17 responses by functioning as an agonist towards MINCLE receptors leading to activation of APCs [349-351]. Another vital adjuvant receptor arose from discovering pattern recognition receptors (PRRs) and their essential role in detecting pathogen-associated molecular patterns (PAMPs) from invading pathogens. Activation of PRRs leads to a cascade of pro-inflammatory responses and cytokines' triggering, leading to an adaptive immune response [352]. One of the best characterised PRRs is the toll-like receptor (TLR) [65] and are predominantly expressed on innate immune cells. For this particular reason, targeting TLRs has been an attractive target for adjuvants leading to the use of a TLR4 agonist, monophosphoryl lipid A (MPLA or MPL), within an HPV vaccine [353]. As MPLA was shown to be both a safe and immunogenic (predominantly Th1 biased), PHAD® was developed as a fully synthetic structural analogue which has already been demonstrated in human trials to boost antigen-specific T cells from formulation within an oil-in-water emulsion [354, 355].

The formulation of PHAD within a liposomal formulation presents a unique and novel opportunity to assess the applicability of the TLR4 adjuvant to deliver a spike trimer antigen by following the same formulation skeleton as CAF01 by simply swapping out TDB for PHAD and directly comparing the effectiveness of DDA:TDB and DDA:PHAD in a vaccine study.

6.2 Aim and objectives

The work within this chapter aimed to manufacture DDA:TDB and DDA:PHAD by microfluidics using the 2-step manufacturing method developed in chapter 5. The immunogenicity of the two vaccine adjuvants was then assessed following an *in vivo* vaccine study using the spike protein antigen using an intramuscular prime-boost regimen to identify the effectiveness of the two adjuvant systems at eliciting immunological responses for the protection against SARS-CoV-2. To achieve this, the following objectives were to:

1. Evaluate the size, PDI and zeta potential of DDA:TDB (5:1 w/w) and DDA:PHAD (5:1 w/w) with adsorbed OVA manufactured using the developed 2-step microfluidic manufacturing method to assess the physical differences between DDA:TDB and DDA:PHAD.

2. Conduct a formulation stability study of empty and OVA adsorbed formulations to evaluate the impact of antigen adsorption on DDA:TDB and DDA:PHAD has on vesicle stability.

3. Swap from the use of OVA to spike protein from SARS-CoV-2 as an active antigen to validate the vesicle size, PDI and zeta potential remains unchanged before conducting an *in vivo* vaccine iummunogenicty study and ensure that the desired formulation charactersitics are not altered as a result of swapping antigen.

4. Conduct antibody ELISAs on blood serum to analyse humoral responses from antigen-specific IgG subtypes and neutralising antibodies to investigate and compare adjuvant effectiveness between formulations containing TDB and PHAD.

5. Perform cytokine ELISAs to determine i) concentration of IL-1β from muscle serumand ii) IFN-γ concentrations from stimulated splenocytes for formulations containing TDB and PHAD and allow for the validation of a Th1 immune response in the formulations tested due to IL-1β being a precursor to IFN-γ.

6. Use a bead-based immunoassay to screen 12 cytokines, allowing insight into the activation of Th1, Th2 and Th17 and to compare and evaluate the degree of immune stimulation afforded by either TDB or PHAD.

6.3 Results and Discussion

6.3.1 Identification of suitable lipid concentrations for the production of DDA:TDB

Work outlined by Davidson et al. has shown that by using a DDA:TDB (CAF01) molar ratio of 8:1 (5:1 w/w) high immune responses could be achieved using a lipid film hydration method (LFH) [267]. CAF01 has been used extensively *in vivo* by i.m administration at a concentration of 250 µg/50 µg (DDA:TDB) in 50 µL [22, 260]. Roces et al. built on this work and proved that by using the solvent IPA it was possible to manufacture the formulation using microfluidics with operational parameters of 3:1 FRR and TFR of 10 mL/min [61]. To translate this work towards using EtOH, the same microfluidic operational parameters were used with a target of achieving a post microfluidic liposome concentration of 6 mg/mL to equate to the CAF01 concentrations previously investigated [22, 260].

The results in figure 6.1 outline these findings by varying the initial lipid concentrations from 12 to 24 mg/mL suspended in EtOH using a 3:1 FRR and 10 mL/min TFR. Vesicle physical characteristics were measured before and after solvent removal by dialysis (14 kDa dialysis membrane). The vesicles were shown to be cationic (figure 6.1A) across all the concentrations tested. Unsurprisingly, increasing DDA lipid concentrations allowed for vesicles of greater surface charges which increased from 25 ± 4 mV at an initial concentration of 12 mg/mL to 47 ± 6 mV at 24 mg/mL. There was no significant difference in the surface charge when measurements were recorded before or after dialysis for each concentration (figure 6.1A). When vesicles were measured pre-dialysis, there were no significant differences in the vesicle size with sizes around 1000 nm with high (>0.8) PDI (figure 6.1B). After solvent removal (figure 6.1C), the sizes across all initial concentrations reduced, and a lipid concentration effect was apparent. Using an initial concentration of 12 mg/mL, sizes of 118 ± 48 nm was achieved, which was significantly smaller than the vesicles formed at other concentrations (p ≤ 0.001). As the initial lipid concentration increased, vesicle size increased, and at the concentration of interest (24 mg/mL), vesicle sizes of 710 ± 100 nm with a high PDI (0.72 ± 0.04) were measured.
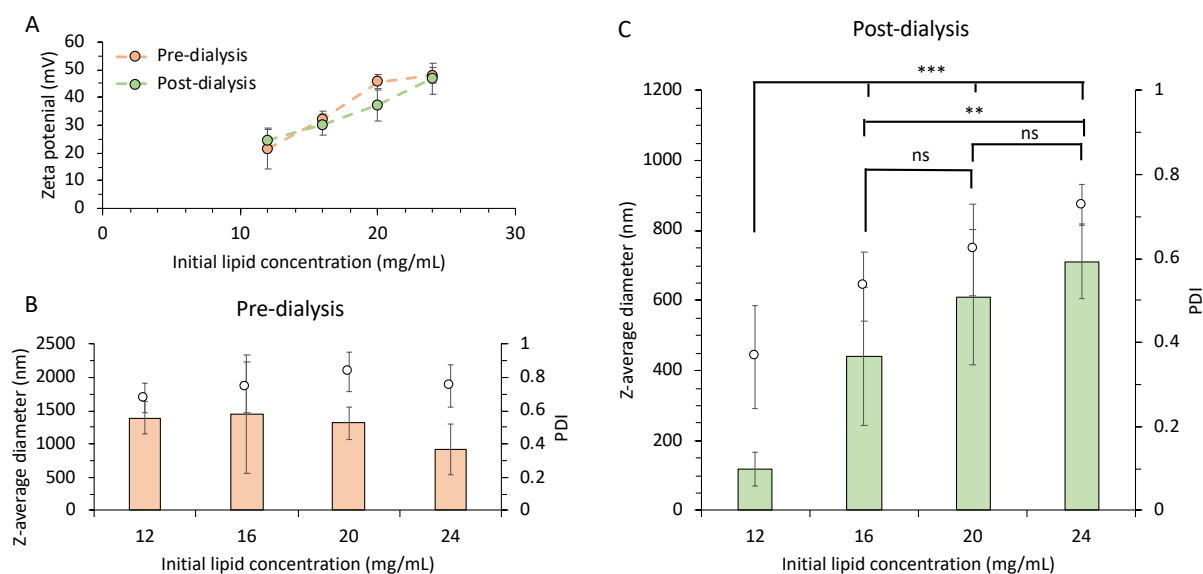
Figure 6.1 *Lipid concentration impacts DDA:TDB vesicle size. The initial lipid concentration was examined allow the zeta potential (A); Z-average diameter and (B) of vesicles produced by microfluidics at a 3:1 FRR and 10 mL/min TFR to be recorded before dialysis and the after dialysis (C). Lipids were dissolved in EtOH and initial concentrations between 12 – 24 mg/mL. Results represent mean ± SD of 3 independent batches: p > 0.05 (ns); p < 0.01 (**) and p < 0.001 (***).*

The study's objective was to investigate whether using the microfluidic parameters at 3:1 FRR and 10 mL/min would be suitable for producing liposomes when IPA was substituted for EtOH. A target vesicle size criteria were set between 200 – 500 nm [356] as this size can be achieved by sonication post-LFH in addition to vesicle sizes of approximately 250 nm achieved by microfluidics with IPA as shown by Roces et al., [61]. The results indicate an increase in size and PDI were observed due to increasing the initial lipid concentration. These results coincide with other publications and could be a result of the self-assembly mechanism previously described (chapters 3 and 4), whereby upon mixing of the solvent and aqueous phase, lipid discs begin to form, which are highly unstable, leading to the formation of vesicles to minimise the hydrophobicity at the lipid disc edge. However, if the change in polarity from the rapid mixing of the non-polar solvent with the polar aqueous phase is complete before the lipid particles have formed, then remaining lipids aggregate in an uncontrolled manner causing various sizes of liposomes. This results in increased polydispersity which can occur when the solvent to lipid ratio is not high enough, such as high initial lipid concentrations, as shown by increased vesicle sizes and coincides with previous publications [229, 357, 358]. While the

objective of the experiment was to identify a lead concentration to take forward for future studies, additional manufacturing optimisation work was shown to be required to achieve liposomes with reduced vesicle size and allow for comparable in vivo CAF01 lipid concentrations to be used.

6.3.1.1 Reduced antigen concentrations permit improved vesicle stability

The impact of the L:P ratio was examined as chapter 5 indicated L:P ratios to be a crucial attribute for vesicle stability [237]. From findings obtained in chapter 5, the 60:1 L:P was selected as the ratio to initially test as it was found to be an effective ratio promoting enhanced immunogencity and prolonged vesicle stability. A 150:1 L:P was also investigated as a high lipid to protein ratio would allow for reduced protein concentrations to be delivered and may improve vesicle stability as a result. Therefore, 150:1 L:P was compared against the 60:1 L:P and would allow 1 µg/50 µL (150:1 L:P) and 2.5 µg/50 µL (60:1 L:P) to be delivered intramuscularly in future *in vivo* studies.

A 24 mg/mL initial lipid stock in EtOH, heated to 60 °C, was used to produce the 60:1 L:P and 150 L:P. Using a 150:1 L:P, the Z-average diameter of the purified liposomes was 103 ± 24 nm with a PDI of 0.26 ± 0.03 (figure 6.2A), which were significantly different from the 60:1 L:P purified liposomes. A significant difference ($p \leq 0.001$) was observed when a greater protein concentration was used in the 60:1 L:P leading to a size of 167 ± 12 nm. Despite the increased size, the PDI (figure 6.2A) was not statistically different to the 150:1 L:P ($p > 0.05$) and was measured at 0.25 ± 0.05. Furthermore, despite a higher protein concentration being used, there was no effect at the 60:1 L:P on the zeta potential (41 ± 4 mV) for the purified liposomes and 37 ± 7 mV for the 60:1 L:P liposomes (figure 6.2B).
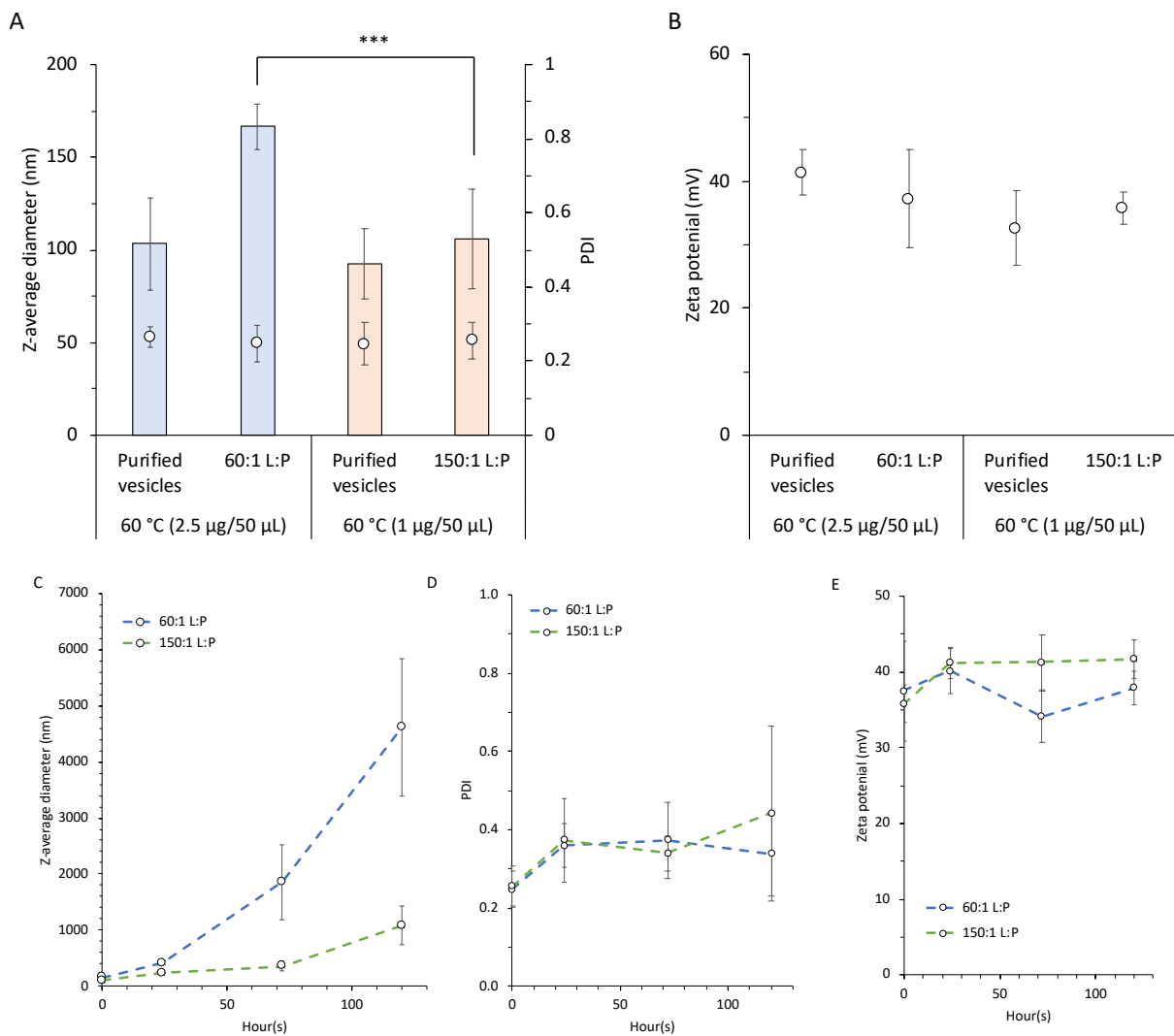
Figure 6.2 *Impact of increasing protein concentration on vesicle physical characteristics. The OVA concentration was increased from 1 µg/50 µL (150:1 L:P) to 2.5 µg/µL (60:1 L:P) to examine the influence on vesicle characteristics. The vesicle size and PDI (A) along with zeta potential (B) was measured before and after protein adsorption at the two L:P ratios. A stability study was conducted in figures C; D and E investigating Z-average diameter; PDI and zeta potential respectively and was terminated at 120 h as sizes exceeded 4000 nm with the 60:1 L:P formulation. An initial lipid concentration of 24 mg/mL and the same microfluidic operational parameters in table 6.1. Results represent mean ± SD of 3 independent batches: p < 0.001 (***).*

The stability study in figures 6.2C-D was stopped after 120 h following the results obtained in figure 6.2C where vesicle sizes exceed 4000 nm using a 60:1 L:P indicated a greater degree of vesicle instability than the 150:1 L:P liposomes. Given the increased sizes (figure 6.2C), higher PDI values (figure 6.2D) for the 60:1 L:P compared to those of the 150:1 L:P liposomes would

be expected. However, the PDI values for both L:P mirrored each other and were between 0.3 – 0.4 between 24 – 120 h. It was also observed in figure 6.4E, much like the findings in 6.3C, that the zeta potential cationic nature is preserved despite the increased aggregation allowing surface charges between 30 – 40 mV using the 150:1 L:P ratio. The results in figure 6.4 further verified the impact L:P has on the physical characteristics of vesicles, as discussed in chapter 5. Vesicular size increased because of increased protein concentrations to coat the liposomes (figure 6.2A) without impacting the surface charge. Additionally, the increased protein concentrations increased instability in the vesicles, as highlighted in figure 6.2C. After 24 h, the vesicles doubled in size comparable to the 150:1 L:P, though, after 74 h, the vesicles exceeded 1500 nm. Subsequently, due to the poor stability shown, the study was stopped after 4 days because the sizes exceeding 4000 nm indicated the L:P to be optimised should remain at 150:1 L:P.

The results in figure 6.2 indicate that while both formulations increase in size, the effect of vesicle aggregation is increased using higher protein concentrations as shown in the figure using the 60:1 L:P. Liposome suspensions with electrostatically adsorbed protein have been studied to understand colloidal behaviour by mixing a cationic formulation with α-lactalbumin or lysozyme, which is a negatively and positively charged proteins, respectively [359]. While a stability study was not conducted in the publication, aggregation was only observed between the cationic formulation and the α-lactalbumin, highlighting the impact of surface adsorbeded proteins have on colloidal behaviour. Protein concentrations were increased with aggregation observed between 0.02 to 18 protein:lipid (mol:mol) ratios. Interestingly, from cryo-TEM analysis, the increased protein concentrations significantly affected the morphology of the liposomes, highlighting bilayer restructuring. At a protein:lipid molar ratio of 0.003, the liposomes adopted a multivesicular morphology while at a higher protein:lipid molar ratio of 0.24 elongated lipid structures increased clustering. At this ratio, the bilayer thickness from an unloaded liposome had a bilayer thickness of 4-5 nm compared to 12 nm when loaded due to a more defined protein layer. The researchers Hamborg et al. theorised that greater adsorbeded protein concentrations increased rearrangement of the bilayer and than when reduced protein concentrations are adsorbeded which can thus impact vesicle stability [359].

6.3.2 Modification of the aqueous: Incorporating organic solvents to reduce vesicle sizes

To address the results in figure 6.2, an extensive study investigating microfluidic production methods was conducted using the 150:1 L:P as this was shown to be a more stable L:P ratio. Research by Schmidt et al., incorporated the water soluble solvent dimethyl sulfoxide (DMSO) within the buffer phase as this was shown to stabilise DDA:mycobacterial monomycolated glycerol (MMG) vesicles post-production [360]. Work conducted in chapter 5 highlighted that adjusting the L:P ratio for formulations can influence both the vesicle size and stability and indicated an L:P ratio of 150:1 permitted stable vesicles with sizes < 100 nm. Therefore, a decision was made to deliver 1 µg/50 µL in vivo as this was the same quantity of antigen delivered for the in vivo experiments in chapter 5. This initial 24 mg/mL concentration must be used, as described in table 6.1, following the 2 step manufacturing method to control antigen adsorption.

Table 6.1 Microfluidic operating parameters and concentrations of reagents for a 150:1 L:P formulation

Initial lipid concentration *(heated to at 60 °C)*	3:1 FRR & 10 mL/min at 60 °C	Post microfluidic concentration	1:1 FRR & 10 mL/min	Post microfluidic lipid and protein concentration	Lipid and protein in vivo dose (χ/50 µL)
24 mg/mL		6 mg/mL		3 mg/mL and 20 µg/mL	150 µg & 1 ug

The results of this modified production method are shown in Figure 6.2. Manufacturing the liposomes at 60 °C (figure 6.2A) still produced large vesicles (> 1500 nm) pre-dialysis with various size distributions (figure 6.2D). However, similar to the results in figure 6.1, the vesicle size was reduced after the solvent was removed (93 ± 18 nm; Figure 6.2A). Encouragingly, after protein adsorption using the 150:1 L:P ratio, there was no significant difference in the vesicle size with vesicles of 105 ± 28 nm and with little change in the PDI (0.24 ± 0.05 and 0.25 ± 0.05 for the purified liposomes and protein adsorbed liposomes respectively). Using the heating block resulted in no change in the zeta potential, which was maintained at 35 mV (figure 6.2C).

Upon introduction of 2.5% DMSO v/v within the Tris buffer along with the use of the heating block (60 °C), vesicles had sizes of 71 ± 12 nm (pre-dialysis; figure 6.2A) and PDI measurements of 0.41 ± 0.16 (figure 6.2B). However, the large standard deviation indicates that the formulation has not stabilised, as shown in figure 6.2E with two distinct vesicle populations. Post protein adsorption, the vesicle size was 95 ± 35 nm with a PDI of 0.34 ± 0.1, indicating the protein adsorption step helped stabilise the formulation with a comparable zeta potential of 34 ± 3 mV (figure 6.2C) to the formulation prepared without DMSO. EtOH was substituted for DMSO in the aqueous phase at the same 2.5 % v/v concentration to examine the effect of using the same lipid solvent. This led to larger unloaded vesicles (343 ± 169 nm; figure 6.2A), reducing the vesicle size and PDI after protein adsorption (98 ± 21 nm and 0.21 ± 0.03 respectively) with a zeta potential of 28 ± 5 mV.
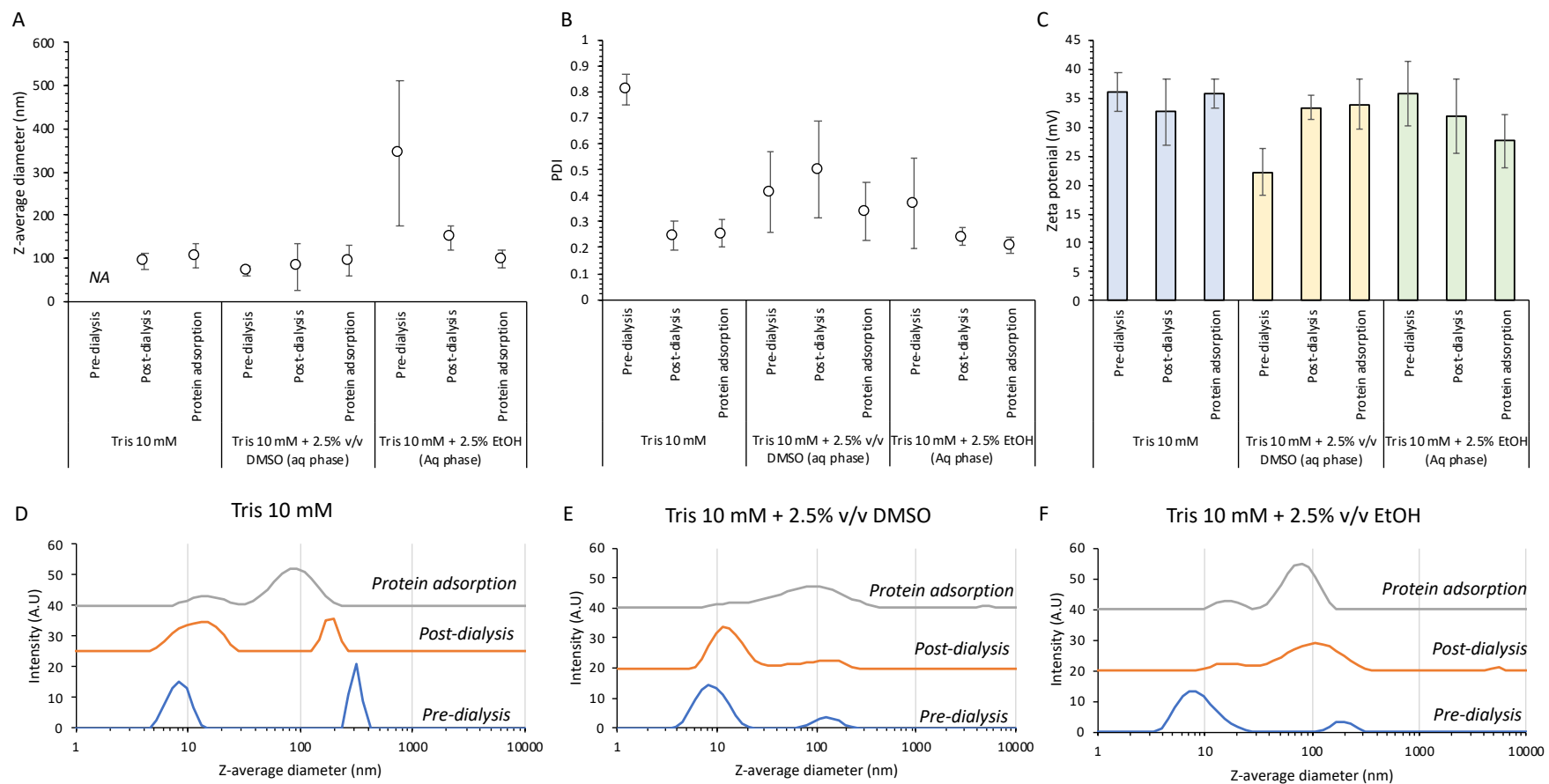
Figure 6.3 *Manufacturing optimisation to permit reduced vesicle sizes. Three manufacturing parameters were investigated to address vesicle size by either using a heating block to heat fluid streams to Tris 10 mM; incorporating 2.5% v/v DMSO or 2.5% v/v EtOH within the aqueous phase at a 150:1 L:P. The Z-average diameter (A); PDI (B) and zeta potential (C) was recorded for vesicles pre-dialysis; post-dialysis and protein adsorption. Intensity plots were generated for each step for empty vesicles using Tris 10 mM (D); 2.5% v/v DMSO (E) and 2.5% v/v EtOH (F) using an initial lipid concentration of 24 mg/mL and the same microfluidic operational parameters in table 6.1 using OVA as the antigen analogue. Results represent mean ± SD of 3 independent batches. In figure 6.2A NA was recorded pre-dialysis sizes using Tris 10 mM exclusively as sizes exceeded 1500*

To assess vesicle stability using the three different manufacturing methods, a two-week stability was conducted with produce liposomes physical characteristics monitored (figure 6.4). The results in figure 6.4A, D and G highlighted that after 24 h, using a 150:1 L:P ratio, the vesicles made using Tris + 60 °C, Tris + 2.5% DMSO or Tris + 2.5% EtOH produced vesicles which were shown to swell to approximately double their initial size for each of the conditions (shown in detail in table 6.2). A similar swelling effect was also demonstrated by measuring the empty vesicles, which doubled in vesicle size after 24 h (table 6.2). For both the empty and OVA loaded vesicles, the vesicle size continued to increase across the study duration resulting in sizes exceeding 4000 nm for all the formulations indicating high degrees of instability. The size also increased for the empty vesicles, and the difference was less extreme than the OVA loaded vesicles after 14 days. Using the 60 °C methods alone allowed for vesicles of 425 ± 105 nm while using the solvents led to larger vesicles which were 778 ± 93 nm and 754 ± 54 nm for using 2.5% DMSO and 2.5% EtOH, respectively.

By using the 60 °C methods, the PDI (figure 6.4B) increased from 0.24 ± 0.05 at 0 h to 0.47 ± 0.15 at 360 h, which had a marginally lower PDI than their empty vesicle counterparts also measured at 360 h, which were 0.52 ± 0.03. Using 2.5% DMSO figure 6.4E with empty vesicles, the vesicle PDI was between 0.5 – 0.6 across 0 h to 360 h. Whereas for loaded liposomes using 2.5% DMSO, the PDI when measured at 0 and 360 h was 0.34 ± 0.11 and 0.63 ± 0.27 respectively. Using 2.5% EtOH PDI increased throughout the study duration as shown in figure 6.4H for both the empty and loaded vesicles where after 360 days, they were recorded to be 0.79 ± 0.07 and 0.47 ± 0.09, respectively. The zeta potential for both the empty and loaded vesicles was shown to be stable using the three manufacturing methods and was between 30 to 40 mV across the 360 h study (figure 6.4C; F and I). By comparing the three production methods, each was able to produce vesicle sizes of approximately 100 nm post protein adsorption. However, there was no benefit in terms of vesicle stability by using either DMSO or EtOH at 2.5% within the aqueous inlet.

Modification of manufacturing parameters has allowed the production of purified and loaded liposomes to 100 nm (figure 6.3), which was impossible without manufacturing method refinement, as demonstrated in figure 6.1. Manufacturing at 60 °C ensures the lipids are
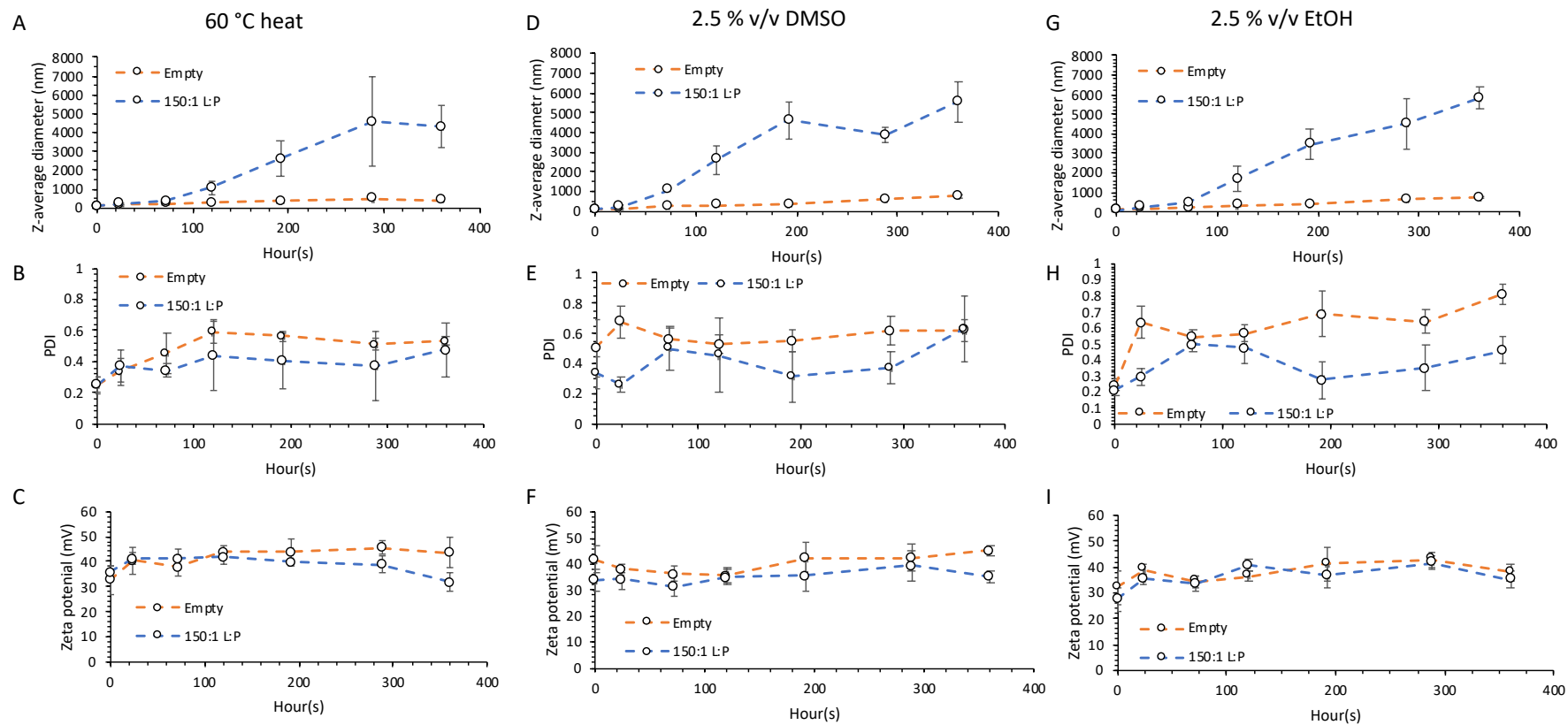
Figure 6.4 *Manufacturing methods and impact on empty and loaded vesicle stability. A stability study was conducted over 360 h with the Z-average diameter; PDI and zeta potential examined from manufacturing vesicles at 60 °C (A; B and C respectively); 2.5% v/v DMSO (D; E and F respectively) and 2.5% v/v EtOH (G; H and I respectively). An initial lipid concentration of 24 mg/mL and the same microfluidic operational parameters in table 6.1 using OVA as the antigen analogue. Samples were stored at 4 °C between measurements. Results represent mean ± SD of 3 independent batches.*

entirely dissolved and coincide with the use of the heating block from suspending DDA:TDB in IPA [61].

Table 6.2 *24 h vesicle stability measuring Z-average diameter and PDI at 0 and 24 h for (all produced at 60ºC) using a 150:1 L:P with three different aqueous phases*

Aqueous phase	Formulation	Z-average diameter (nm)		PDI	
		0 h	24 h	0 h	24 h
Tris Buffer	Empty	92 ± 18	181 ± 14	0.24 ± 0.05	0.33 ± 0.10
	150:1	105 ± 27	235 ± 10	0.26 ± 0.05	0.37 ± 0.10
Tris Buffer + 2.5% DMSO	Empty	80 ± 53	118 ± 23	0.50 ± 0.18	0.67 ± 0.10
	150:1	94 ± 35	226 ± 62	0.33 ± 0.10	0.25 ± 0.06
Tris Buffer + 2.5% EtOH	Empty	148 ± 29	187 ± 22	0.24 ± 0.03	0.62 ± 0.10
	150:1	98 ± 21	253 ± 8	0.21 ± 0.03	0.29 ± 0.05

In figure 6.3B, adding 2.5%, DMSO within the aqueous phase immediately reduced the vesicle size post microfluidic formation. This result builds on studies by Schmidt et al., where it was shown that the addition of 2.5% v/v DMSO within the buffer phase improved the stability of DDA based liposomes produced using microfluidics [360]. It has been shown that DMSO has a stabilising effect within lipid membranes due to DMSO forming hydrogen bonds with the polar surface of the membrane, which helps prevent orientational disorder of the lipid hydrocarbon chains [361]. Furthermore, using X-ray diffraction, the researchers Yu and Quinn [362] demonstrated that the thickness of a phosphatidylcholine (PC) bilayer could be decreased by using DMSO where it was found that DMSO inserts between the polar PC headgroups leading to bilayer conformation changes improving bilayer packing densities leading to a reduction in bilayer thickness. EtOH has also been shown to lead to bilayer modulation (as shown in section 3.3.5), whereby insertion of alcohols within the bilayer (hydroxyl group at the interfacial region and methyl groups towards the hydrophobic core) leads to size modulation. Raising the EtOH percentage during mixing by incorporating 2.5% v/v EtOH within the aqueous phase may act similarly.

A critical aspect of a liposomal adjuvant product is vesicle stability. While increasing operational temperatures to 60 °C in combination with incorporating water-soluble solvents

within the microfluidic buffer phase aided in the immediate reduction of Z-average diameters (figure 6.2), these vesicles increased in size on storage (Figure 6.4 and table 6.2). TDB has been demonstrated to stabilise the DDA bilayer, and bilayer formation is dependent on the presence of DDA [363], as demonstrated by Langmuir studies with sizes between 200 – 500 nm when prepared by LFH and not microfluidics. However, using microfluidics to form DDA:TDB liposomes, vesicles were below 200 – 500 nm but not stable (figure 6.3 and figure 6.4). The result suggests instability could arise from bilayer reconstruction leading to liposomal swelling. However, as these liposomes are highly cationic (figure 6.3) [226, 237, 364, 365], these vesicles should be stable according to DVLO theory [42-44] as the repulsive forces between cationic vesicles stability prevent aggregation. More likely, the instability occurs as a result of bilayer instability as it has been that DDA liposomes are highly unstable, which has led to the incorporation of additional lipids to reduce bilayer instability and improve bilayer packing densities, such as the incorporation of monophosphoryl lipid A (MPL) [364].

Further experiments conducted in external laboratories address DDA:TDB stability freeze-drying where it was found that incorporating 211 mM of trehalose preserves DDA:TDB without impacting in vivo efficacy. While the size increases are more evident in the loaded vesicles, potentially due to additional intermolecular forces between adsorbed proteins and vesicles [237], vesicle instability also occurs in the empty vesicles as shown in table 6.2. To address these stability issues, alterations in the formulation could be proposed by incorporating additional lipids to improve packing densities and bilayer stabilisation. An essential lipid that has already been discussed would be cholesterol. However, Kaur et al., observed that by incorporating cholesterol within DDA:TDB liposomal adjuvants bilayer elasticity was increased; yet, vital adjuvant properties including Th1 responses and cell uptake [226] were diminished as a result of cholesterol inclusion, meaning that other options need to be investigated to improve vesicle stability and maintain vaccine immunogenicity.

6.3.3 Reducing solvent polarity to enable microfluidic mixing of DDA:PHAD

Before modifying DDA:TDB further to allow for microfluidic mixing to proceed, the immune stimulator TDB was substituted for the TLR4 agonist PHAD to identify if vesicle instability also arose from microfluidic manufacturing. Following the same initial production parameters, a lipid stock of DDA:PHAD (5:1 w/w) was prepared in 100% EtOH at 60 °C before microfluidic mixing to solubilise the lipids.

The preparation of DDA:PHAD using 100% EtOH was not possible (figure 6.5A), most likely due to PHAD's chemical composition ($C_{96}H_{184}N_3O_{22}P$, figure 6.5B) and long non-polar alkyl chains. Therefore, using experience gained in chapter 3 and the role solvents can have on lipid suspensions, a mixture of EtOH and DMSO was initially tried at 80:20 v/v (both class 3 solvents). An 80:20 v/v mix was selected as it was hypothesised that the increased polarity using the formulation and solvent mixture would permit reduced liposome sizes, as shown in chapter 3. The introduction of this solvent mix in combination with heating to 60 °C enabled the complete dissolution of the solvent mixture (figure 6.5A), which allowed for liposome sizes of 41 ± 2 nm pre-purification and 42 ± 3 nm post-purification with PDIs of 0.3 (figure 6.5C) allowing for uniform distributions (figure 6.5D). Using an L:P of 150:1 to match the DDA:TDB vesicles led to a size increase of 52 ± 2 nm, with the PDI also maintained at 0.3 with a zeta potential ~30 mV.
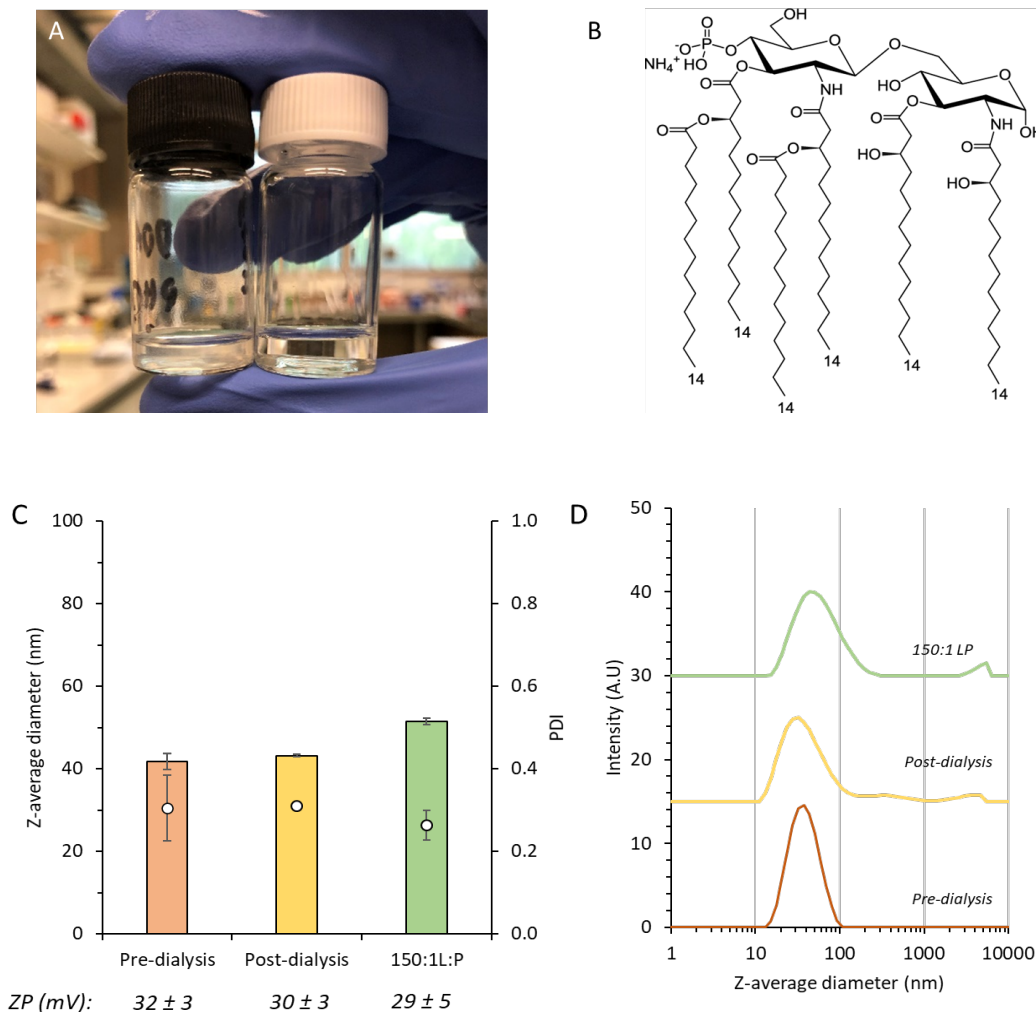
Figure 6.5 *Substitution of TDB for PHAD. Figure (A) depicts lipid solubility differences using 100% EtOH (left) and 80:20% v/v EtOH:DMSO (right) from the addition of PHAD (B; MW 1763.5 g/mol) where by lipid aggregation is observed from a cloudy solution falling out of suspension in 100% and a solubilised suspension using 80:20% v/v EtOH:DMSO. From using 80:20% EtOH:DMSO vesicle physical characteristics could be recorded (C) along with the generation of intensity plots (D). An initial lipid concentration of 24 mg/mL and the same microfluidic operational parameters in table 6.1. Results represent mean ± SD of 3 independent batches Results represent mean ± SD of 3 independent batches*

Interestingly when vesicle stability was investigated, when OVA was adsorbed, the rate of vesicle swelling decreased compared to empty liposomes over 360 h (figure 6.6A). Both the empty and loaded liposomes had near-identical sizes of 48 ± 6 nm and 52 ± 3 nm for the empty and loaded vesicles, respectively, in figure 6.6A. Both the empty and loaded vesicles followed a comparable rate of size increase from 0 to 192 h, after which the empty vesicles dramatically increased to 2812 ± 589 nm from 269 ± 72 nm, while at 192 h, the loaded vesicles

were measured to be 762 ± 20 nm. The empty vesicles increased to 4325 ± 879 nm after 360 h, while the loaded vesicles were smaller at 2002 ± 71 nm, which was an observation not seen using the DDA:TDB (figure 6.3). The PDI was shown to increase throughout the study for both empty and loaded vesicles with the empty vesicles at 0 h recording a PDI of 0.4 ± 0.1 and finishing at a PDI of 0.74 ± 0.17 at 360 h. The size differences at these two-time points were not significant (p > 0.05), with the loaded vesicles starting at a PDI of 0.32 ± 0.07 and finishing at 0.62 ± 0.05 at 360 h (figure 6.6B). Unlike the similar DDA:TDB formulation, there was no significant difference across the study duration using the empty and loaded vesicles when the zeta potential was measured with values between 30 – 40 mV being recorded (figure 6.6C).
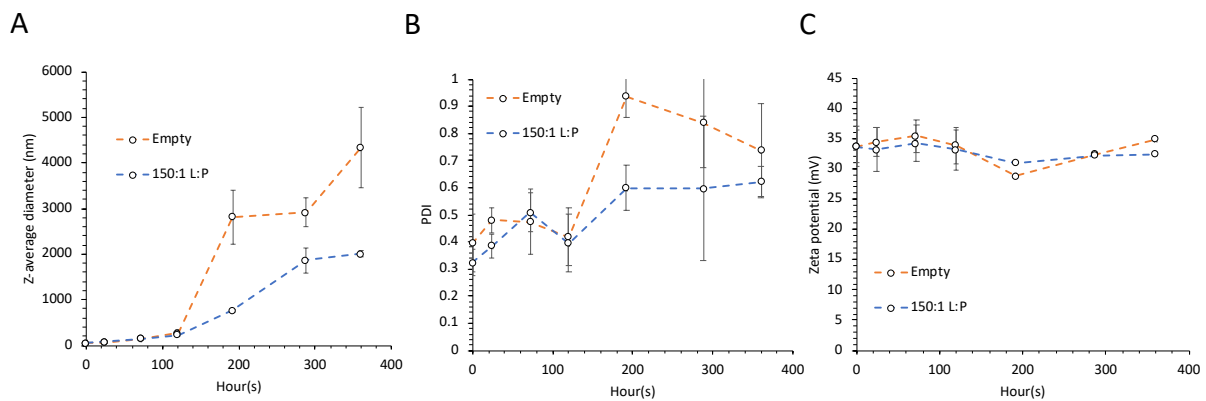
Figure 6.6 Assessment of DDA:PHAD stability. A stability study comparing empty and loaded vesicles with OVA was conducted with formulations stored at 4 °C between measurements. Z-average diameter (A); PDI (B) and zeta potential (C) was measured over a 360 h duration. An initial lipid concentration of 24 mg/mL and the same microfluidic operational parameters in table 6.1. Results represent mean ± SD of 3 independent batches.

Using DDA:PHAD, the results in figure 6.7A highlight good stability profiles across 48 h with sizes between 50 – 100 nm with PDIs maintained at 0.4 (figure 6.7B). The lack of aggregation led to stable particle concentrations over the 48 h between 2 – 6x10^{13} particles/mL (figure 6.7C). For the DDA:TDB, it has been shown that it is not possible to prepare vesicles of less than 100 nm, unlike the DDA:PHAD liposomes and that the 24 h stability has been poor with sizes doubling with 24 h (table 6.1). This is shown again in more detail in figure 6.7D, with sizes increasing from 108 ± 2 nm to 139 ± 1 nm within 10 h and further increased to 272 ± 2 nm after 48 h, which is significantly larger than the DDA:PHAD results. Interestingly, in figure 6.7E, despite the size increasing each hour, the PDI remained stable between 0.2 – 0.4, indicating that the vesicles are increasing in size at the same rate as each other. In figure 6.7F,

the concentration of particles at 0 h was 6×10^{13} particles/mL, which were maintained up until 10 h. However, this value begins to decrease from this point from 6×10^{13} particles/mL at 10 h to 2×10^{13} particles/mL after 48 h.
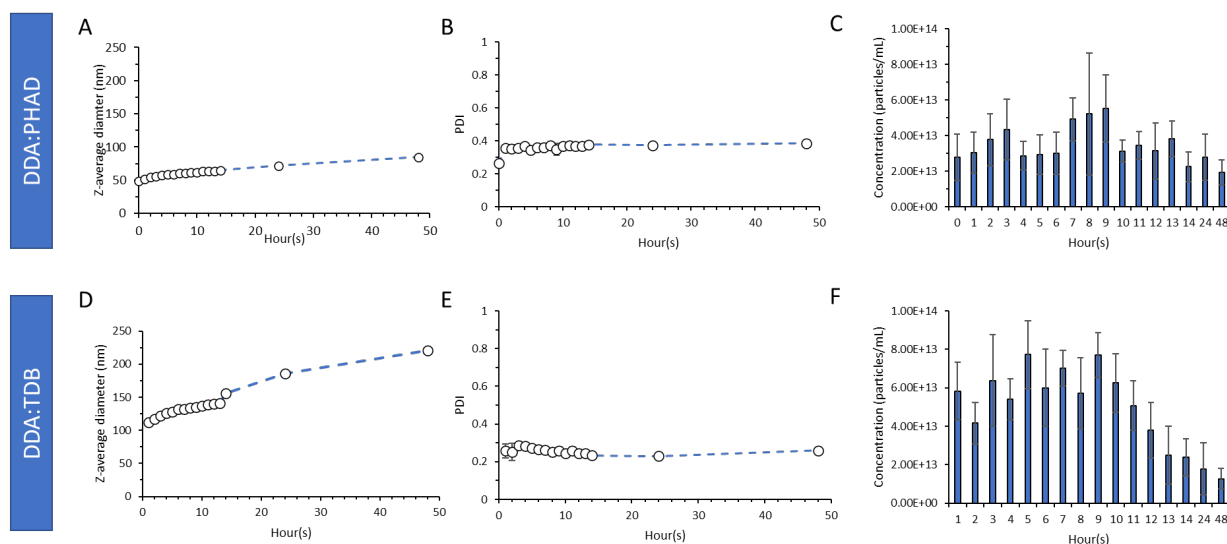
Figure 6.7 *48 h vesicle size and concentration analysis comparing DDA:TDB against DDA:PHAD. The vesicle size for DDA:PHAD (A) and DDA:TDB (D) was measured along with the PDI (B and E for DDA:PHAD and DDA:TDB respectively) as well as vesicle concentration (C and F for DDA:PHAD and DDA:TDB respectively). EtOH was used to suspended DDA:TDB lipids and EtOH:DMSO (80:20 v/v) was used to suspended DDA:PHAD lipids. An initial lipid concentration of 24 mg/mL and the same microfluidic operational parameters in table 6.1 was used for both formulations.*

Following the encouraging results in figure 6.6 using the solvent mixture of EtOH:DMSO (80:20 v/v) used for DDA:PHAD, the same mixture was used for DDA:TDB to identify if the reduced polarity would allow for more favourable sizes and stabilisation post-purification. The results in figure 6.8A indicate that post-manufacture, the liposomes were smaller than those achieved using 100 % EtOH (figure 6.2A), allowing for sizes of 474 ± 86 nm with a PDI of 0.49 ± 0.08. Post dialysis, the size was reduced but variable (290 ± 100 nm). The variability was reduced upon adsorption of OVA at 150:1 L:P, leading to sizes of 197 ± 50 nm (figure 6.8A). The PDI after protein adsorption was 0.31 ± 0.05, which was comparable to the PDI measurements using 100% EtOH. However, from the intensity plots in figure 6.8B, there were three vesicle populations, both post-purification and after protein adsorption, not seen in figure 6.2. There was no effect of using EtOH:DMSO on the zeta potential, which also allowed for vesicles with a surface charge between 30 – 40 mV (figure 6.8C).
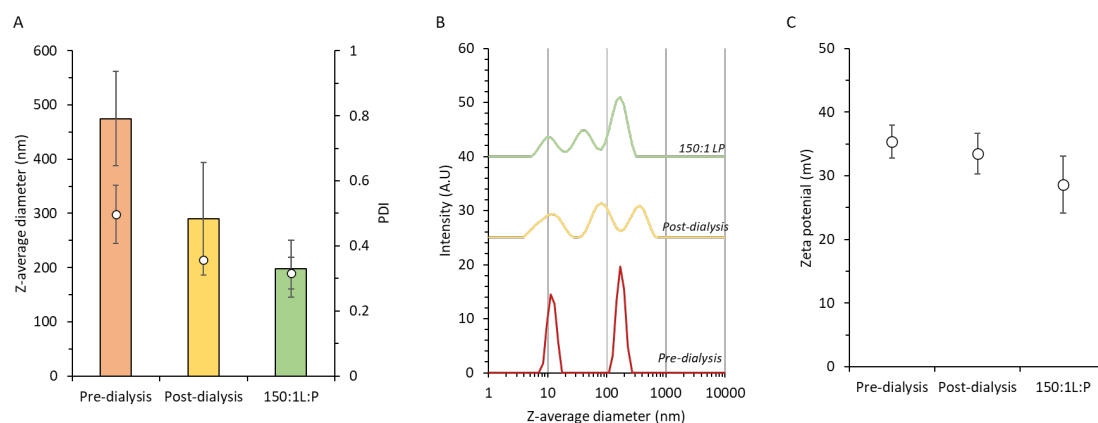
Figure 6.8 *Use of the 80:20 v/v EtOH:DMSO mix for formulating DDA:TDB. Using the solvent EtOH:DMSO solvent mixture for manufacturing DDA:PHAD, the same solvent mix was used for DDA:TDB to compare against vesicles manufactured using 100% EtOH. The vesicle size and PDI was measured (A) allowing for intensity plots (B). The zeta potential (C) was also measured across the manufacturing steps to identify any changes. An initial lipid concentration of 24 mg/mL and the same microfluidic operational parameters in table 6.1. Results represent mean ± SD of 3 independent batches.*

The results from section 6.3.3 have surmised the preparation of DDA:PHAD by microfluidics and the refinement processes involved in its production. The initial experiments conducted in figure 6.5 identified that it was not possible for DDA:PHAD to be dissolved in 100% EtOH (figure 6.5A) as this led to the lipids falling out of suspension. By reducing the polarity of the EtOH, more non-polar intermolecular bonds can occur between the long alkyl chains of the PHAD, improving miscibility allowing for uniform vesicles to form while maintaining vesicle sizes of < 100 nm (figure 6.5C and D). In addition, as short term vaccine stability has been a topic of concern using lipid-based vaccines against COVID-19 (current lipid-based COVID-19 vaccines must be used within 6 h post-suspension), a 48 h stability study was established to measure the rate of vesicle growth over 24 h. This was assessed by measuring vesicle size, PDI and particle concentration, allowing vesicle size ranges to be set, ensuring that the in vivo injections were maintained between set size parameters for each formulation.

However, much like DDA:TDB, long term vesicle instability (as shown in figure 6.6 for DDA:PHAD) remains problematic. Publications have already demonstrated that at a 5:1 w/w using DDA:TDB, DDA is the primary lipid involved in the formulation of liposomes [36], which could help explain the stability issues [366]. Using the bottom-up approach for manufacturing

SUVs with a high membrane curvature can increase bilayer pressures as described by Lichtenberg et al. [367] due to membrane curvature. The researchers Liu et al. highlighted in their study that lipid bilayers composed of one lipid have reduced fluidity and have a low resistance to bilayer pressures [366]. This was demonstrated by using various lipids and forming singular or binary component bilayers (1:1 w/w). The results highlight improved stability in the bilayers consisting of two components over the single component bilayers, which were demonstrated to be unstable using sum-frequency generation spectroscopy. Individual phospholipid geometry could also be a factor for instability of the membrane, as discussed by Cullis et al., [368]. Interestingly, as observed in figure 6.6, the adsorption of OVA reduced the vesicle growth rate when compared against the "empty" vesicles, which did not occur in DDA:TDB liposomes in figure 6.3. In DDA:PHAD liposomes, the presence of OVA on the surface of the liposome could seal 'pores' within the bilayer resulting from the lipid composition. Using ApoA1, Mittag et al. described similar findings and suggested that improved bilayer stability could arise from the protein inserting itself into the lipid and packing defects within the membrane [369].

Despite this, vesicle stability still represents a challenge, as highlighted by the more detailed size analysis measurements in figure 6.7, suggesting that formulation modification would be the next logical step to improve bilayer stability by increasing packing densities over more extended periods. Using a measuring technique developed by Malvern Panalytical, it was possible to measure absolute particle concentration distribution using multi-angle dynamic light scattering (MADLS®). As opposed to DLS measurements detected at one single angle, MADLS® uses several detection angles to obtain an improved resolution of the particle size distribution allowing data to be correlated from different vantage point leading to a greater resolution and extrapolation of the number of particles/mL to be calculated from weighted size distributions [370]. The results suggest in figure 6.7C that the particle concentration does not change using DDA:PHAD, which correlates well to the stable sizes (figure 6.6A) obtained across the 48 h duration. However, in figure 6.7F, the particle concentration begins to decrease from hour 11, which was the point when the vesicle sizes began to increase for DDA:TDB suggesting vesicle agglomeration. Following the results in figure 6.8, the solvent mixture of EtOH:DMSO was shown not to be beneficial, leading to larger vesicles post-purification compared to if 100% EtOH was used due to the reduced polarity leading to larger

lipid discs during microfluidic mixing. Reduced sizes were observed as protein was adsorbed due to higher osmotic pressures from the adsorbed protein, leading to reduced size [371, 372]. Therefore, from the results attained, a solvent mixture of EtOH:DSMO 80:20 v/v for DDA:PHAD liposomes and 100% EtOH for DDA:TDB was used when prepared liposomes by microfluidics.

6.3.4 Incorporation of helper lipids and polyethylene glycol to address stability during spike adsorption

The long-term stability of DDA:TDB and DDA:PHAD, when prepared by microfluidics at 150:1 L:P, was shown to be poor when the vesicle surface is coated with OVA. However, despite size increases occurring over the short term (< 6 h), the increased sizes shown in figure 6.7 were deemed acceptable given the stable PDIs. Current LNP COVID-19 vaccines were only approved for room temperature storage for 6 h after dilution. Therefore, before moving towards the in vivo studies to evaluate immunogenicity, the formulations were prepared in the same fashion using 150:1 L:P with the same 2-step manufacturing method but with the OVA substituted for the recombinant SARS-CoV-2 spike protein subunit (spike).

After purification (figure 6.9A) of the DDA:TDB, the size and PDI measurements were 89.6 ± 2.3 nm and 0.18 ± 0.02 respectively, with a zeta potential of 27 ± 3 mV, all of which aligns well with previous measurements. However, upon adsorption of the spike protein, the formulation rapidly aggregated, resulting in size measurements close to 4000 nm after immediate sizing post-production. Similar to DDA:TDB, using DDA:PHAD, the physical vesicle measurements aligned with previous results with sizes of 44 ± 1 nm and a PDI of 0.29 ± 0.02 (figure 6.9B) post-purification. It was hypothesised that following the results obtained using OVA (figure 6.5), it was expected that there would be not much variation in the vesicle size. However, following immediate measuring of the size, PDI and zeta potential, the vesicle size increased to 223 ± 2 nm with a PDI of 0.23 ± 0.02 and a decrease in the zeta potential from 25 ± 3 mV to 15 ± 1 mV. The vesicle stability was assessed after 1 h as this would be a realistic time duration between post-production and in vivo injection in our laboratory studies; nevertheless, this led to a significant jump in the vesicle size to 888 ± 19 mm.
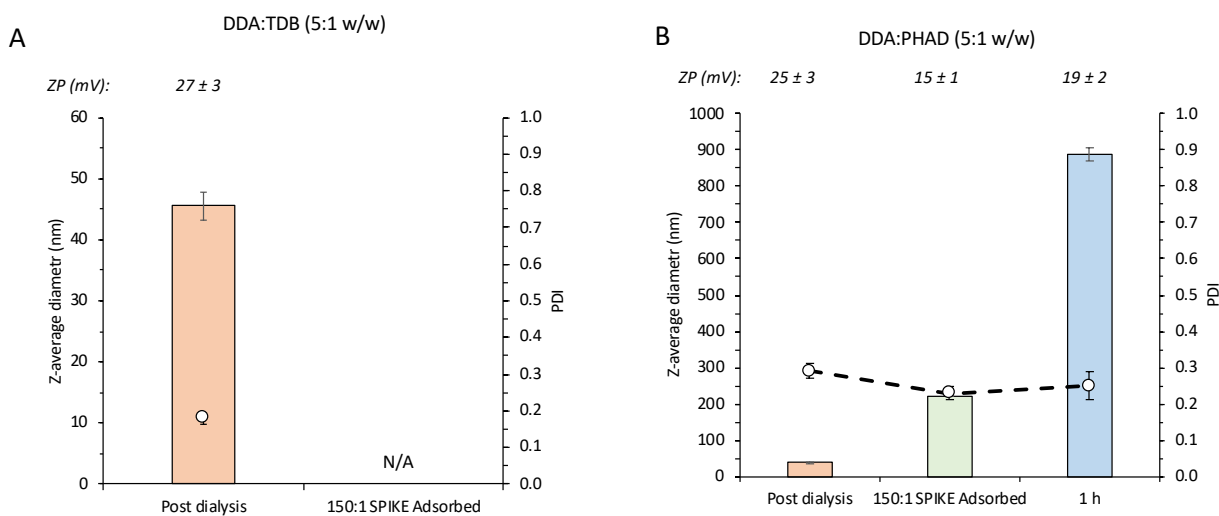
Figure 6.9 *Impact of spike adsorption on DDA:TDB and DDA:PHAD. The OVA antigen was substituted for spike trimer (134 kDa) to identify if vesicle characteristics were affected. Z-average diameter, PDI and zeta potential was measured for DDA:TDB (A) and DDA:PHAD (B) after dialysis, upon spike adsorption and 1 h after spike adsorption. An initial lipid concentration of 24 mg/mL and the same microfluidic operational parameters in table 6.1 with 100% EtOH used to solubilise the initial DDA:TDB lipid mixture and 80:20 v/v EtOH to solubilise the initial DDA:PHAD lipid mixture. Due to high costs and low quanity of spike protein available resulting from high global demand, the results represent mean ± SD of 1 batch.*

The results in figure 6.9 emphasise the impact increased protein molecular weights have on a formulation and the aggregation, which can occur from adsorbing larger compounds onto the surface. The molecular weight of OVA is 43 kDa, while for the spike protein, the molecular weight is 134 kDa which would explain the problems which have occurred in figure 6.9 as size increases and decreased stability was already observed using a smaller compound in previous figures. This could be resolved in future optimisation work by selecting a protein subunit with reduced molecular weight. For example, the S1 subunit of the spike protein has been identified as the subunit responsible for attachment of the protein to host receptors [373] and would reduce the molecular size to 75 kDa. An alternative thought is that if the spike protein is three times the molecular weight of OVA, then three times the quantity of lipid could be used to prevent instability. However, in this example, as a high initial lipid concentration is used (24 mg/mL), an initial lipid concentration of 72 mg/mL would be required, which would lead to solubility issues.

These results presented complications in developing the two formulations and progression towards in vivo studies and were detrimental to the microfluidic preparation of DDA:TDB and DDA:PHAD. The results in figure 6.9 only represent one replicate due to the high costs of the protein at the time of the data acquisition.

6.3.4.1 <u>Addition of a helper lipid to improve bilayer packing</u>

DSPC has been extensively used throughout chapters 3-5 and has been shown from the results to produce stable liposomes from its composition [374]. Therefore, to examine if DSPC can aid in stabilising DDA:TDB and DDA:PHAD bilayers, increasing concentrations of DSPC were used with the vesicle stability measured over 1 hour.

Initially looking at DDA:TDB based formulations, post purification, the vesicle sizes when 10% and 20% (w/w) DSPC were incorporated were 74 ± 11 nm and 91 ± 7 nm, respectively, with PDIs below 0.2 (figure 6.10). Increasing the DSPC content to 50% produced 50 ± 1 nm sized vesicles with a PDI of 0.67 ± 0.1 (figure 6.10A). After the protein adsorption step, the vesicle size and PDI increased. For example, using the 10% w/w DSPC, the vesicle size was 425 ± 2 nm with a PDI of 0.6 (figure 6.10A). This size increase was reduced by increasing DSPC content to 20% w/w, with sizes of 126 ± 2.6 nm and a PDI of 0.22 ± 0.01. For formulations containing 50% DSPC, sizes were similar to the 20% DSPC formulation (122 ± 1 nm); however, the PDI increased to 0.64 ± 0.03 (similar to the formulation without adsorbeded protein; figure 6.10A).

By incorporating DSPC (10, 20 or 50% w/w) into DDA:PHAD, there was no notable difference in size between the formulations nor change pre-and post-purification with sizes between 40 – 50 nm with PDIs between 0.3 – 0.4 (figure 6.10A), consistent with the results obtained in figure 6.5. For DDA:PHAD formulations containing 10% or 20% w/w DSPC, the with the addition of spike adsorption, the resulting particles were 126 ± 2 nm and 135 ± 6 nm (figure 6.10). This is in comparison to DDA:PHAD (no DSPC), where the liposomes increased in size to 223 ± 2 nm (figure 6.10A). For DDA:PHAD containing 50% DSPC, the size post-purification was 91 ± 30 nm, and after protein absorption increased to 133 ± 1 nm, and there was no

significant difference in PDI (figure 6.10A). When considering the zeta potential there was no significant difference between the formulations with or without DSPC at all concentrations tested with the formulations being cationic (25 – 30 mV; figure 6.10B).

As there was no benefit to increasing the DSPC content to 50% w/w, further studies focused on formulations containing 0, 10 or 20% DSPC and these formulations were left at 4 °C for 1 h to assess the stability (figures 6.10C and D). Without the inclusion of DSPC, the DDA:TDB measured 3874 ± 796 nm and, therefore, not measured after 1 h (figure 6.10C). In comparison, the DDA:PHAD increased to 888 ± 19 nm with a PDI of 0.25 after 1 h (from 223 ± 2 nm and 0.22 ± 0.015 at 0 h) (figure 6.10C and D). Formulations containing 10% DSPC increases in size and PDI occurred within 1 h (figure 6.10C). The greatest benefit was observed at 20% for DDA:TDB and DDA:PHAD. With DDA:TDB +20% DSPC, the vesicle size increased from 126 ± 3 nm to 172 ± 3 nm with the PDI maintained at 0.2, and for the DDA:PHAD, the size increased to 226 ± 8 nm from 135 ± 6 nm after 1 with a PDI of 0.45 ± 0.02 and 0.43 ± 0.02 (0 h and 1 h respectively; figure 6.10C and D).

DSPC was added to improve bilayer packing densities to address bilayer instability and reduce vesicle growth [86, 171, 174]. Therefore, the addition of neutral phospholipids with high Tm to supplement bilayer structural integrity could provide a possible solution by encouraging intermolecular attractions within the bilayer without affecting the cationic nature of the vesicles. As a result of the lipid shape and hydrophobicity to form aggregates, which depending on the lipid shape, will form micelles or bilayers [375, 376], PCs was shown to be an ideal contender for bilayer stabilisation, as highlighted by Cullis et al., who monitored non-bilayer phase behaviour in the presence of increasing PC concentrations [368]. The researchers observed that at 30% mol PC, the monolayer stabilised the bilayer, with additional research highlighting that smaller head groups and longer alkyl chains further promote bilayer formation [377]. The results highlighted that there was no additional benefit to increasing the concentration of DSPC to 50%, which also impacted the vesicle uniformity at these concentrations.
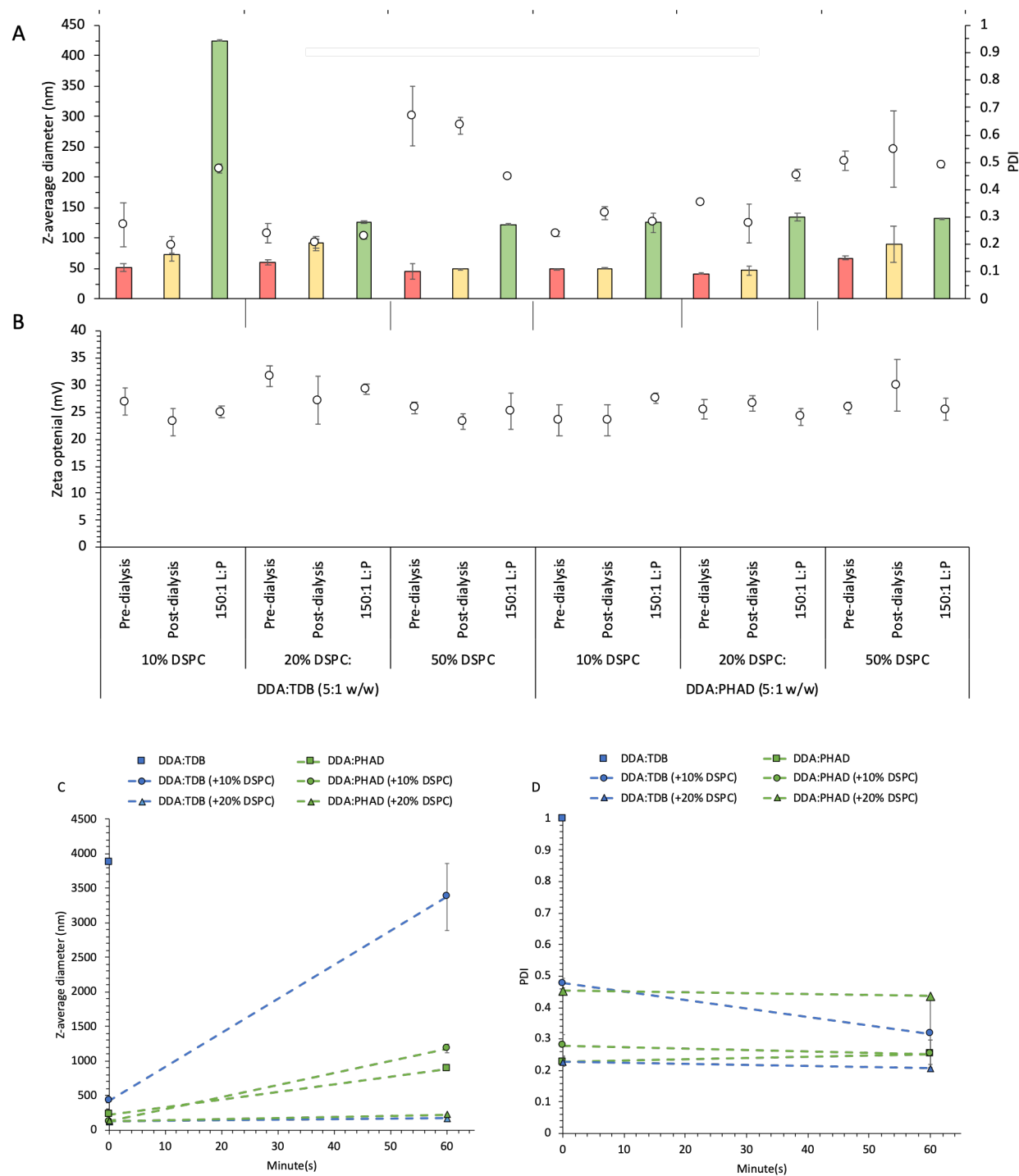
Figure 6.10 *Addition of helper lipid to improve vesicle stability post spike adsorption. To address vesicle stability disruptions caused by spike adsorption, 10% and 20% w/w DSPC was added to the lipid mixture of DDA:TDB and DDA:PHAD to measure the impact of Z-average diameter, PDI and zeta potential (A). A 1 h stability was also conducted for two formulations measuring Z-average diameter (C) and PDI (D) as this was the time frame set between protein adsorption and in vivo injection. An initial lipid concentration of 24 mg/mL and the same microfluidic operational parameters in table 6.1 with 100% EtOH used to solubilise the initial DDA:TDB lipid mixture and 80:20 v/v EtOH to solubilise the initial DDA:PHAD lipid mixture. Due to high costs and low quanity of spike protein available resulting from high global demand, the results represent mean ± SD of 1 batch.*

In similar studies, Nordly et al., added MPL, the non-synthetic form of PHAD, to DDA:TDB at two different concentrations (6 and 11 mol% or 5:1:1 and 5:1:2 w/w respectively) to study the physical-chemical characterisation when manufactured by lipid film hydration [364]. Similarly to the DSPC in figure 6.10, increasing concentrations of MPL (6 and 11 mol%) reduced the vesicle size from 544 ± 93 nm to 442 ± 76 nm with a PDI of approximately 0.3 at the two PDI concentrations. To confirm the changes in bilayer packing, a Langmuir-Blodgett study was conducted to test monolayer surface pressure. The addition of MPL further indicated that increased concentrations of MPL allowed increased surface pressures to be applied before monolayer collapse, indicating improved packing densities by preventing repulsion of positively charged DDA headgroups [364]. The publication also explored the differential gel-to-liquid phase transition temperature using differential calorimetry. It was found that the transition temperature of DDA:TDB (42.9 ± 0.1 °C) was reduced to 40.9 ± 0.3 °C when 6 mol% of MPL was incorporated with a thermogram profile similar to DDA:TDB suggesting that the MPL is uniformly distributed. However, when the 11 mol% of MPL was added, the main thermogram peak broadened with smaller peaks suggesting an uneven distribution of MPL within the bilayer. This observation could be used to describe the increased PDIs when 50% DSPC has been incorporated into the DDA:TDB and DDA:PHAD liposomes (figure 6.10A) where there could be an uneven distribution of DSPC within the bilayer at the higher concentrations. Using a comparable formulation to Nordly et al., the author's Tian et al. explored DDA:PHAD:TDB (250 µg:25 µg:50 µg/ 100 µL), an adjuvanted DNA vaccine against *Mycobacterium tuberculosis* [378]. The results highlighted the difficulties in stabilising DDA liposomes; however, incorporating PHAD and TDB ensured stability for up to 60 days for unloaded liposomes. While both studies [364, 378] proved that vesicle stability is maintained by adding MPL, these were in unloaded vesicles. In figure 6.10, TDB and PHAD were not tested as a combination, and the additional variable of protein adsorption could intensify liposome aggregation by intermolecular attracts between protein molecules, as previously discussed in chapters 5 and 6 [237].

6.3.4.2 Supplementation of DMG-PEG$_{2000}$ allows for sizes <100 nm

As discussed, the addition of 20% DSPC aids the short-term stability of the formulations, indicating that by improving the bilayer packaging, the formation of a stable bilayer helps

negate liposome growth. Furthermore, the incorporation of PEG has been discussed and is used in the liposomal formulation Caeylx [18], which hides surface charges improving circulation time. However, the inclusion of PEG can reduce immunogenicity in adjuvant liposomal formulations [379].

To investigate the impact of the addition of PEG, the percentage of DMG-PEG$_{2000}$ (DMG-PEG) was adjusted between 2 and 5% w/w within DDA:TDB:DSPC (20%) and DDA:PHAD:DSPC (20%) (this data was carried over from figure 6.10 to allow comparison). With DDA:TDB:DSPC (figure 6.11A) increasing the PEG% from 0 to 5% before protein adsorption had little impact on the vesicle size with vesicles remaining below 100 nm. However, by increasing the PEG% from 0 to 5% after protein adsorption allowed for reduced sizes to be obtained at higher PEG concentrations (at 0% the size was 130 nm while at 5% the size dropped to 80 nm). This trend was also observed in DDA:PHAD:DSPC (figure 6.11A) where similar sizes post dialysis were between 50 – 80 nm using a DMG-PEG concentration of between 0 – 5%. However, post protein adsorption the vesicle size dropped from 135 nm at 0% PEG to 98 nm and 78 nm at 2% and 5% DMG-PEG respectively. The PDI across 0 – 5% PEG post protein adsorption was approximetly 0.4.

When the zeta potential was measured for each of the formulations (figure 6.11B), at 0% PEG the surface charge was approximetly +30 mV for both DDA:TDB:DSPC and DDA:PHAD:DSPC. However, it was found that at increasing PEG% post-protein adsorption the zeta potential dropped +20 mV for DDA:TDB:DSPC and DDA:PHAD:DSPC at a 5% DMG-PEG.

From figure 6.11C when measuring the 12 h stability for 2 and 5% DMG-PEG formulations there was little change in the size at 0 h at 2 and 5% with both formulations remaing < 100 nm. The greatest benefit upon increasing the DMG-PEG percentage was the reduced size which the 5% afforded over the 2% after 12 h at 4 °C. After 12 h, the sizes measured were 400 ± 43 nm and 260 ± 4 nm for the 2% and 5% DMG-PEG respectively, with a greater PDI of 0.4 ± 0.12 observed at the 2% DMG-PEG concentration over the 5%, which was 0.28 ± 0.01. A similar pattern was also observed using the DDA:PHAD:DSPC with smaller vesicles obtained, adding increased concentrations of DMG-PEG. Working below 100 nm was permitted at 0 h with the two concentrations of DMG-PEG, with 2% DMG-PEG producing vesicle sizes of 98 ±

2 nm while with 5% DMG-PEG 78 ± 2 nm was obtained post spike absorption. Again, these also increased in size after 12 h to 367 ± 8 nm and 214 ± 4 nm for the 2% and 5% DMG-PEG, respectively figure 6.10A). Using the 5% DMG-PEG led to reduced PDIs of 0.41 ± 0.01 and 0.35 ± 0.05 at 0 h and 12 h when compared against the 2% DMG-PEG, which were 0.43 ± 0.07 and

A

B
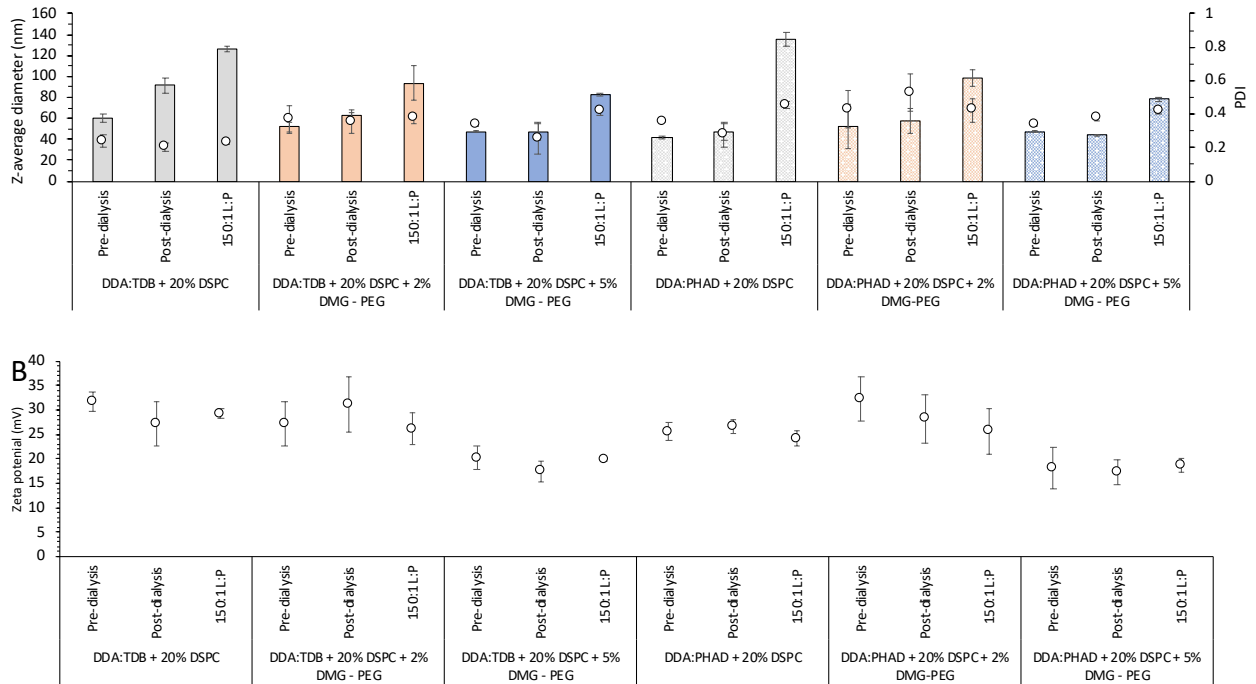
C

		0 h	12 h
DDA:TDB:DSPC:DMG-PEG(2%)	Z-average diameter (nm)	94	400
	PDI	0.37	0.39
DDA:TDB:DSPC:DMG-PEG(5%)	Z-average diameter (nm)	82	262
	PDI	0.41	0.29
DDA:PHAD:DSPC:DMG-PEG(2%)	Z-average diameter (nm)	98	367
	PDI	0.42	0.47
DDA:PHAD:DSPC:DMG-PEG(5%)	Z-average diameter (nm)	78	215
	PDI	0.41	0.35

Figure 6.11 Formulation modification to tackle vesicle instability. To further refine the formulation 0 – 5 % w/w of DMG-PEG$_{2000}$ was added to DDA:TBD:DSPC(20%) and DDA:PHAD:DSPC(20%) . Z-average and PDI (A) was measured at time of production and after the addition of spike protein to investigate vesicle stability. The zeta potential (B) was measured to track surface charge changes of increasing DMG-PEG concentrations. A 12 h stability study was conducted (C) to measure antigen loaded instability. An initial lipid concentration of 24 mg/mL and the same microfluidic operational parameters in table 6.1 with 100% EtOH used to solubilise the initial DDA:TDB lipid mixture and 80:20 v/v EtOH to solubilise the initial DDA:PHAD lipid mixture.

The incorporation of lipid-polymer was also investigated to bring the liposome sizes down to 100 nm, which were the sizes previously achieved using OVA without additional lipids to stabilise the formulation. PEG-lipids have been used in liposomal systems in clinical products. For example, DSPC-PEG was used in the chemotherapeutic drug Caelyx [380] and more appropriately in the Moderna RNA-LNP COVID-19 vaccine and Onpattro® (for siRNA delivery). A propriety PEG-lipid is also used within BioNTech/Pfizer's mRNA-LNP COVID-19 vaccine [381]. PEGylated liposomes have been described as sterically stabilised, which involved stabilisation of the membrane allowing retention of their API [382, 383]. In addition, researchers have also described an additional property that aids in the steric stabilisation of liposomes by PEGylation resulting from the attachment of PEG to a lipid [384]. As described by Tirosh et al., using large MW PEG (i.e. >2000 Da), which is covalently bound to a lipid headgroup, leads to steric exclusion of PEG from the liposome surface [16], promoting thermodynamic stabilisation of liposomes by dehydrating the lipid bilayer [385, 386], conversely PEG with an MW of < 750 Da leads to poor steric stabilisation as described by Needham and Kim [387].

The addition of PEG also improves colloidal stability through interlayer repulsions between liposomes and protein to protein interactions by overcoming attractive van der Waals forces [17, 387, 388] while maintaining liposome:protein interaction as demonstrated from early research by Needman et al. [388]. From the incorporation of 2% DMG-PEG and 5% DMG-PEG within DDA:TDB, sizes of less than 100 nm were achieved before protein adsorption, however, increased PEG concentrations allowed reduced sizes at 0 and 12 h to obtained post protein adsorption. There was a notable reduction in the zeta potential at higher PEG concentrations. It has been shown that as PEG mol% increases, the hydrophilic chains undergo conformational changes from a curled and ravelled "mushroom" confirmation occurs. In contrast, at >5% a "brush" conformation arises [389, 390] with the hydrophilic chains extending out from the surface. Therefore, as the PEG concentration increases the zeta potential is masked due to the increasing PEG concentration [71, 252]. A potentially negative characteristic of increasing PEG concentrations, particularly within vaccines, is that it has been shown that increased PEG concentrations can impact immunogenicity and reduce IgG2a antibody and IFN-γ levels [391].

6.3.5 In vivo immunogenicity study of immunostimulatory adjuvant formulations: TDB vs PHAD

Despite the size increases observed, sizes of 100 nm were achieved using microfluidics for both DDA:PHAD and DDA:TDB by incorporating DSPC (20% w/w) and DMG-PEG$_{2000}$ (2% w/w) post-manufacture (figure 6.11). As injections occur immediately following manufacture, the long-term stability (> 12 h) was not a barrier to progressing to in vivo efficacy testing. However, as previously discussed, PEGylated formulations alter desired immunogenicity [71]. Therefore, DDA:TDB and DDA:PHAD was also produced by LFH at a 150:1 L:P to compare the two immunostimulators. Therefore the study was designed to investigate:

1. To compare the immunogenic properties of cationic liposomes composed of DDA:TDB vs DDA:PHAD.

2. To test the impact DSPC and DMG-PEG (incorporated into the DDA:TDB and DDA:PHAD to support microfluidic manufacturing) on the immune responses elicited and compare them against formulations without DSPC and DMG-PEG.

As expected, the vesicles produced using the LFH were larger than those prepared by microfluidics owing to the top-down approach towards liposome production (figure 6.12). Post hydration, the vesicle size and PDI for DDA:TDB was 588 ± 77 nm and 0.1 ± 0.06, while for DDA:PHAD, the vesicle sizes was 516 ± 35 nm with a PDI of 0.1 ± 0.05 (figure 6.12A; p > 0.05). Upon absorption of spike protein, the size increased to 848 ± 19 nm and 836 ± 9 nm for DDA:TDB and DDA:PHAD respectively, with a PDI of 0.17 ± 0.07 and 0.2 ± 0.085 (figure 6.12A; p > 0.05).

Size measurements were taken 24 h later to observe the vesicles' long-term stability (figure 6.12A). Again size increases were observed for both formulations measured at 1057 ± 94 nm and 1293 ± 64 nm for DDA:TDB and DDA:PHAD, respectively. The PDI for DDA:TDB after 24 h was measured at 0.19 ± 0.07, which was comparable to the recording made at 0 h, the PDI for DDA:PHAD increased to 0.3 ± 0.02. The zeta potential before spike adsorption was 49 ± 5 mV for DDA:TDB and 42 ± 4 mV for DDA:PHAD (figure 6.12B). After adsorption of the spike protein was 37 ± 2 mV and 39 ± 3 mV at 0 h for DDA:TDB and DDA:PHAD, respectively, with no significant change after 24 h (figure 6.12B).
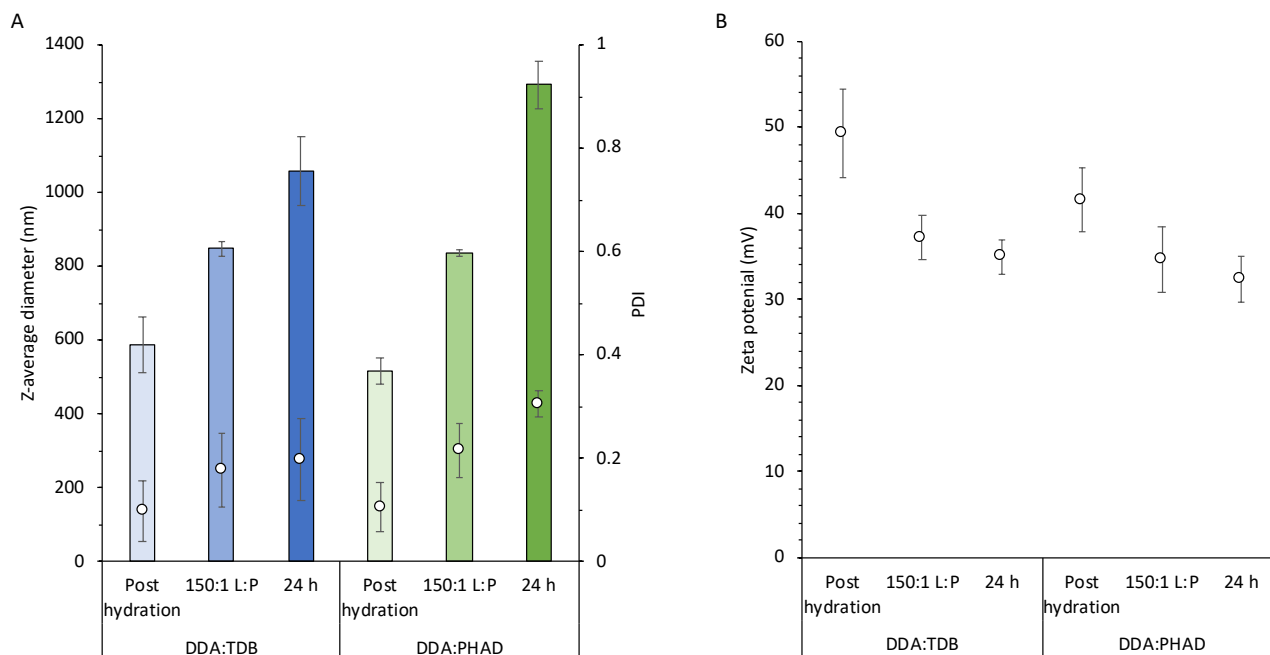
Figure 6.12 *Preparation of DDA:TDB and DDA:PHAD using lipid film hydration. DDA:TDB and DDA:PHAD were suspended in chloroform:MeOH 9:1 v/v with the organic solvent removed by rotary evaporation to form a thin lipid film. The film was hydrated and vortexed with Tris buffer, pH 7.4 10 mM at 40 ºC to a final total lipid concentration of 6 mg/mL. Subsequently, spike protein was gently mixed 1:1 v/v with the preformed vesicles leading to a final lipid concentration of 3 mg/mL and antigen concentration of 20 µg/mL (150:1 L:P). Liposome Z-average diameter and PDI (A) along with zeta potential (B) was measured immediately after lipid film hydration and the addition of spike protein. The same measurements were also repeated after 24 h from storage at 4 ºC.*

The sizes obtained from LFH in figure 6.12 are comparable and in line with those made by other researchers who have also produced DDA:TDB with adsorbed subunit protein [22]. Furthermore, the same stability profile was also observed by researchers from the Staten Serum Insitut, who also used a spike trimer with DDA:TDB prepared by LFH at an L:P of 60:1 [260].

The study plan is outlined in figure 6.13A, and each mouse would receive a final total spike concentration dose of 1 µg/50 µL and a total DDA:TDB/PHAD (5:1 w/w) concentration of 150 µg/50 µL. In addition to the DDA:TDB/PHAD formulations prepared by microfluidics or LFH, spike protein without a carrier was at the same final concentration matching the microfluidic and LFH formulations to act as a negative control (figure 6.13B), while AddaVax™ (squalene

oil in water emulsion) was used as a positive control (figure 6.13B) due to its known adjuvanted properties eliciting both Th1 and Th2 responses [392, 393] allowing it to be used as a formulation within Europe for influenza [394] and was mixed 1:1 v/v with spike protein to meet the same final concentrations as each of the examined.

The injection vesicle sizes and the PDI and zeta potential are listed in figure 6.13C on days 0 and 21. The results first highlight that on days 0 and 21, the physical characteristics of the vesicles are consistent on the prime and boost days and secondly that the vesicle size, PDI and zeta potenial match the values previously obtained in figure 6.11, and similarly the vesicle sizes for the LFH formulations meet the expected sizes obtained in figure 6.12.

Formulation	Day 0 (1st injection)			Day 21 (booster injection)		
	Z-average diameter (nm)	PDI	Zeta potential (mV)	Z-average diameter (nm)	PDI	Zeta potential (mV)
DDA:TDB:DSPC:DMG-PEG	85 ± 2	0.30 ± 0.01	30 ± 3	92 ± 1	0.23 ± 0.01	31 ± 2
DDA:PHAD:DSPC:DMG-PEG	90 ± 3	0.29 ± 0.01	30 ± 1	93 ± 3	0.18 ± 0.01	33 ± 2
DDA:TDB	852 ± 4	0.13 ± 0.01	39 ± 4	840 ± 4	0.24 ± 0.05	35 ± 3
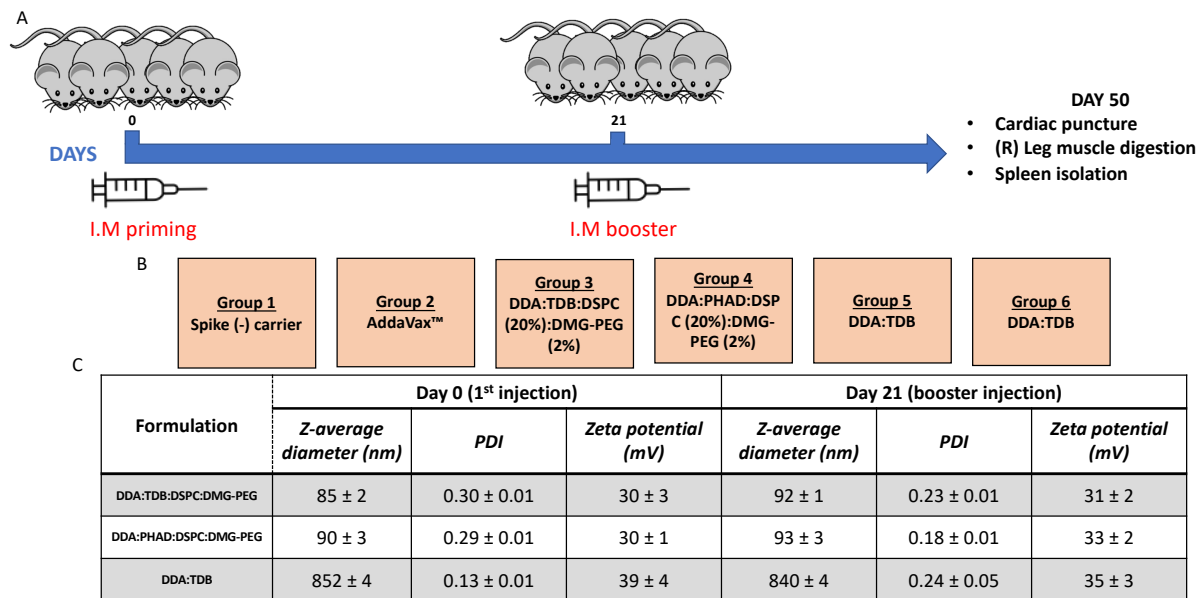
Figure 6.13 *Schematic of the vaccine immunogenicity investigation. The investigation would follow the timeline outlined in (A) using 5 mice per group. Six groups (B) were injected with either spike protein (without liposome carrier), AddaVax™, DDA:TDB:DSPC:DMG-PEG(2%), DDA:PHAD:DSPC:DMG-PEG(2%), DDA:TDB and DDA:PHAD on day 0 and 21 with termination on day 50. Liposomal formulations were prepared on the day of injection with the Z-average diameter, PDI and zeta potential (C) measured to ensure vesicle characteristics for each group were maintained across the investigation. Mice were injected by i.m with 50 μL containing 1 μg/50 μL of spike antigen within each of the 6 formulations examined.*

6.3.5.1 Activation of TLR4 pathways invokes robust IgG responses against adjuvanted spike

To assess the humoral response to the adjuvanted spike formulation, blood serum samples were collected on day 20 and day 50 with the results shown to induce IgG (total), IgG1 and IgG2a antibody isotypes (figure 6.14). From the results, a dose-response was observed following the booster injection across all antibody isotypes in the adjuvanted groups. For the

formulations composed of DDA:TDB/PHAD and incorporating DSPC and PEG, significant differences were shown with the immunostimulant PHAD producing higher reciprocal endpoint titre against IgG total (p ≤ 0.01) and IgG1 (p ≤ 0.001) with no significant differences arising with IgG2a (p > 0.05). The same trend was observed at day 50 in the specific antibody isotypes, with significant differences observed in IgG total (p ≤ 0.01) and IgG1 (p ≤ 0.001) with no difference in the reciprocal endpoint titres using IgG2a (p ≤ 0.001).

For formulations prepared by LFH, and composed of DDA:TDB or PHAD (without DSPC and PEG), again PHAD formulations produced significantly higher endpoint titres than TDB formulations in the antibody subtypes IgG total and IgG1 (p ≤ 0.001); however, for the IgG2a subtype, TDB promoted significantly (p ≤ 0.01) more robust responses (figure 6.14). Nevertheless, after the 2nd dose, the DDA:PHAD formulation elicited significantly (p ≤ 0.001) greater reciprocal endpoint titres in all three IgG types. Overall, from Figure 6.14 it can be seen that:

- A second dose enhanced antibody responses with all adjuvanted formulations.
- The inclusion of DSPC and PEG within the formulation reduced IgGT and IgG2a responses irrespective of the choice of immunostimulatory lipid (PHAD vs TDB).
- At day 50, DDA:PHAD (prepared by LFH) was shown to be the strongest adjuvant compared to the formulations (including the AddaVax positive control) in terms of IgG (total), IgG1 and IgG2a subtype responses.
- Overall, the liposomal PHAD formulations produce stronger responses than their TDB counterparts.
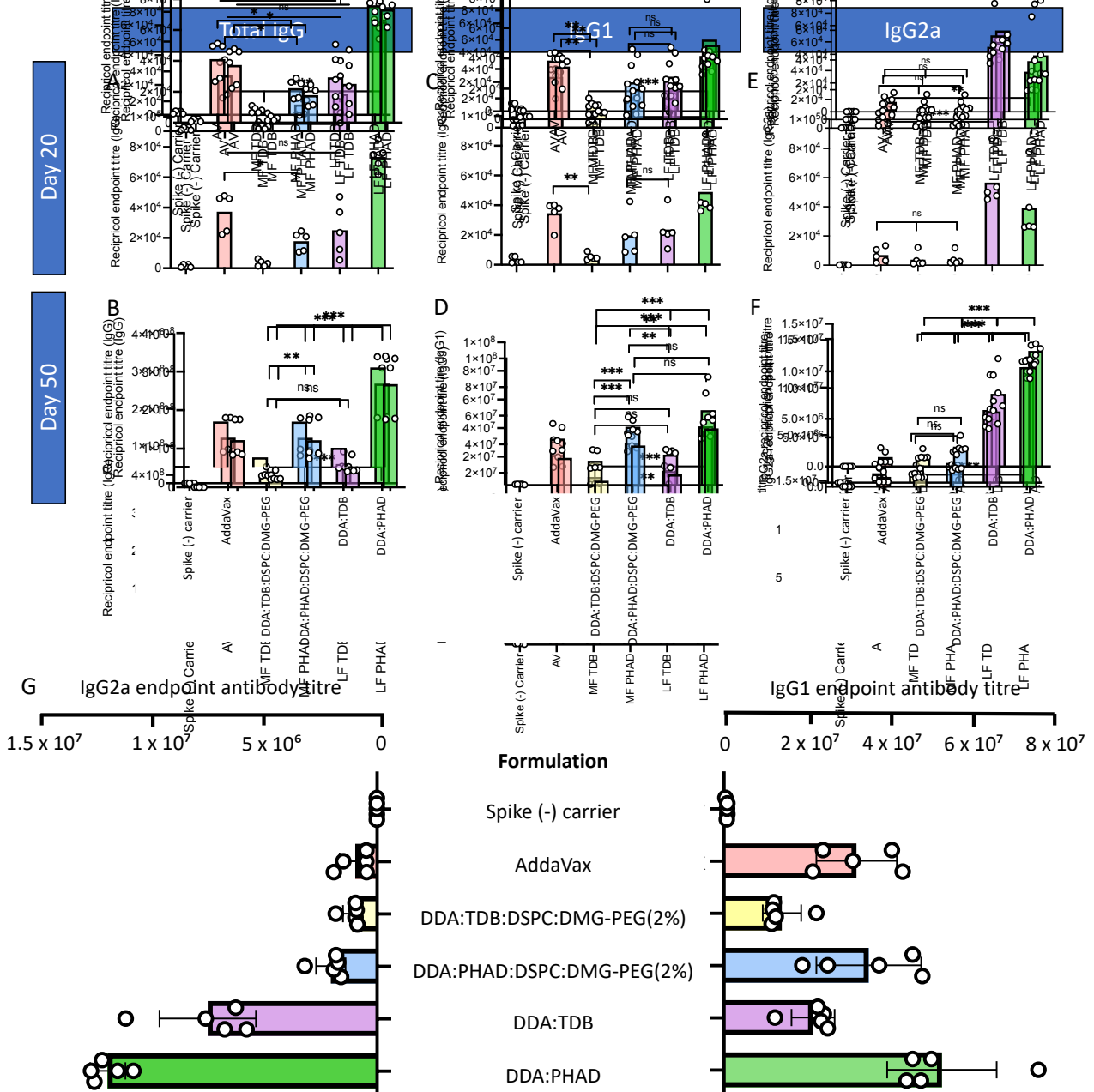
***Figure 6.14** Humoral immunogenicity assessment. Serum antibody titres were measured by ELISA from blood serum one day before the booster injection (day 20) and on the day of termination (day 50) with total IgG (A + B); IgG1 (C + D) and IgG2a (E + F) measured on the respective days. IgG2a and IgG1 endpoint antibody titres were also directly compared (G) on day 50 to assess the extent of antibody production from each of the groups. Both vertical and horizontal lines represent an average group value (n = 5): p > 0.05 (ns); p < 0.05 (*); p < 0.01 (**); p < 0.001 (***).*

In terms of mechanisms of action, TDB and PHAD activate different cellular pathways, which could result in the differences in humoral immunogenicity observed. TDB is a synthetic analogue of trehalose 6,6'-dumycolate (TDM) found in the mycobacterial membrane and is a known immunomodulator [395]. Yet, their branched mycolic acids are highly toxic and therefore not compatible with their role within a vaccine [396, 397], which led to the synthesis of TDB by replacing the branched mycolic acid groups [398]. TDB is a potent adjuvant that primarily induces Th1/Th17 immune responses by activating the MINCLE receptor activating Sky-Card9 pathways within antigen-presenting cells and has been described as the primary mechanism of action [399-401].

Much like TDB, PHAD is a proprietary lipid of Avanti, and a structural analogue of MPL used within human vaccines [402] and induces powerful Th1 immune responses [403, 404]. It has been shown that PHAD can invoke proinflammatory cytokines and CD4+ and CD8+ T cells through activation of toll-like receptor 4 (TLR4) [405]. Interestingly, a recent study highlighted the importance of TLR4 through the interaction of trimeric spike protein, leading to pro-inflammatory responses [406, 407]. Research has also highlighted the role of the TLR4 pathway; by investigating pro-inflammatory cytokine IL-1β levels in THP-1 cells infected with SARS-CoV-2, IL-1β production was shown to be inhibited by a TLR4-specific inhibitor "Resatorvid" leading to the researchers hypothesizing the importance of the TLR4 pathway for COVID-19 infections [408]. The results in Figure 6.14 support the evidence hypothesizing the importance of the TLR4 pathway.

When comparing formulations prepared with DSPC and PEG (using microfluidic manufacturing) and those without (prepared by LFH), there are two general differences: the lipid composition and the vesicle size (as shown in figure 6.13C). Vesicle trafficking from the injection site because of particle size has been investigated with results from Brewer et al, describing larger lipid vesicles that were > 500 nm had greater antigen trafficking than those vesicles which were < 150 nm [409]. Furthermore, in an earlier publication Brewer et al., also investigated lipid vesicle sizes to determine factors controlling the induction of Th1 and Th2 responses and highlighted immunogenic differences observed between antigen entrapped and antigens that are administered with a particulate. By formulating antigen within vesicles, researchers found that vesicles > 225 nm preferentially induce Th1 responses while vesicles

< 155 nm induced a Th2 response (shown by the increased production of IgG1 and the absence of IgG2a along with the upregulation of IL-5 within the lymph node) [410]. Indeed, a comparison can be made towards this study from the results in figure 6.14 as the formulations that were prepared by microfluidics were approximately 100 nm in size and elicited greater upregulation of IgG1 (Th2 response) than IgG2a (Th1 response) while the LFH vesicles produced greater IgG2a endpoint titres at day 50.

A more specific study using the formulation DDA:TDB investigated the pharmacokinetic and immunostimulatory responses (against the tuberculosis antigen Ag85B-ESAT-6) by varying the size of DDA:TDB liposomes [22]. The researchers observed that regardless of vesicle size, adjuvanted formulations could stimulate a Th1 response using DDA:TDB with no differences in IgG1 production across the sizes investigated. Again, in figure 6.14, using the DDA:TDB formulation, the study supports these findings, particularly for IgG1 and total IgG where no significant differences ($p > 0.05$) were observed in the reciprocal endpoint titres obtained with vesicles of 100 nm (microfluidic formulation) and 850 nm vesicles (LFH formulation) at day 50. However, this was not the case for IgG2a, with significant differences ($p < 0.001$) between the two formulations, both on days 21 and 50. Furthermore, this does not apply to formulations incorporating PHAD, which displayed greater total IgG endpoint titres on days 21 and 50 and greater IgG2a endpoint titres on days 21 and 50 suggesting other mechanisms at play.

An alternative hypothesis towards the humoral antibody responses from samples prepared by microfluidics and LFH could be because of the inclusion of DSPC and PEG to improve vesicle stability. In both DDA:TDB:DSPC:DMG-PEG and DDA:PHAD:DSPC:DMG-PEG, there was a significant drop in the endpoint titre measurements for IgG2a when compared against DDA:TDB and DDA:PHAD indicating that the Th1 pathway is not stimulated to the same extent as DDA:TDB and DDA:PHAD. This could be due to the incorporation of PEG, which can affect immune responses in DDA:TDB, specifically IgG2 production [71]. Despite PEGylated formulations promoting clearance away from the injection site and increased accumulation within draining lymph nodes [71], it was shown that the incorporation of PEG reduced IgG2 responses and maintained IgG1 antibodies when compared against non-PEGylated DDA:TDB. This supports the observations in figure 6.14 whereby on day 50, the IgG1 responses for both

DDA:TDB:DSPC:DMG-PEG and DDA:PHAD:DSPC:DMG-PEG were not significant to the respective counterparts when produced by LFH (p > 0.05). For IgG2a, the non-PEGylated formulations have endpoint titres significantly greater than their PEGylated counterparts.

It is unlikely the addition of DSPC made an impact on Th1 responses as it has been demonstrated in DDA:TDB formulations that by incrementally replacing the DDA component with DSPC reduced the Th1 mediated response [325]. In an additional study, Kastner et al., highlighted using the DDA:TDB formulation that addition of 25% DSPC had no significant impact on IgG concentrations, however, exceeding 25% led to significant reductions in cytokine production which did not occur at a DSPC concentration of 25% which produced comparable concentrations to DDA:TDB without DSPC [411]. As the concentration of DDA within the liposomal formulations used in figure 6.14 remained constant, it is unlikely to be the cause of the reduced IgG2a production in the formulations prepared by microfluidics. This coincides with additional publications highlighting DDA's role in eliciting Th1 mediated responses [307, 412, 413].

Overall, the results show PHAD is a stronger immunological adjuvant than TDB, and other factors can impact immune responses. To summarise, it has been hypothesised that a spike trimer acts via the TLR4 pathway, which could be used as a potential rationale for the increased immune activity observed using the TLR4 agonist PHAD [406-408]. In addition, physical vesicle characteristics could act as a Th1/Th2 immune pathway modifier where it has been demonstrated that smaller vesicles > 200 nm lead to increased IgG2 responses from the elevated production of IFN-γ [409, 410], which was observed in the figure 6.14 with elevated IgG2a responses in larger vesicles produced by LFH and IgG1 responses which are comparable to those of larger vesicles (p > 0.05). In addition, the effect of PEG could also impact the responses observed with the PEGylated formulations reducing IgG2a concentrations which have also been observed in separate findings [71].

The development of a balanced Th1/Th2 immune response is of particular importance for vaccine development and the avoidance of vaccine enhanced disease (VED), leading to the enhanced clinical symptoms of the disease after vaccination. In early research, vaccine-associated enhanced respiratory disease (VAERD) has been linked to a Th2-biased immune

response in children that were vaccinated using whole-inactivated virus vaccines against the respiratory syncytial virus (RSV) and measles virus [414, 415], which has also been implicated in animal experiments for the previous SARS-CoV outbreak [416, 417]. From the results, in figure 6.14G, there is a slight bias towards Th2 based immunity with DDA:TDB provides a more favourable Th1/Th2 profile, leading towards a more Th1-biased response, which is generally more considered to be favourable towards providing anti-viral immunity [418].

6.3.5.2 Upregulation of neutralising antibody production against SARS-CoV-2

Following the outbreak of SARS-CoV-2 a primary objective was to understand the mechanism by which the virus enters the cell. Following the first outbreak of SARS-CoV in 2002, it was found that the transmembrane protein spike facilitates viral entry into human cells [419, 420]. The spike protein contains two subunits, S1 and S2, with the receptor-binding domain (RBD) contained within the S1 subunit [421], which binds to the angiotensin-converting enzyme 2 on the surface of epithelial cells in the upper respiratory tract [419], leading the production of a subset of RBD spike antibodies which can block viral entry called neutralisation. It has been found that there is a strong relationship between those infected with COVID-19 and increased concentrations of neutralising antibodies [422] and a reliable correlate of protection [333, 423, 424]. In addition, blocking the RBD has been shown to offer protection in animal studies. Therefore, upregulation of neutralising antibodies from a vaccine presents an attractive component towards providing protection and the induction of T cells that have been shown to conduct different immune processes [260, 425]. However, the ideal immune profile for a vaccine is still for deliberation in terms of protection against COVID-19, with multiple strategies discussed [426]. The experiment conducted in figure 6.15 involved a competitive ELISA and measures neutralising antibodies present in mouse serum from blood taken on day 50 by preventing RBD binding to an ACE2 receptor. The presence of neutralising antibodies in the serum is detected by reducing optical density (OD), indicating the inhibition of spike (RBD) – ACE2 binding.

The results in figure 6.15 show that without an adjuvanted carrier, the spike protein provided < 20% inhibition whereas for the positive control, AddaVax, led to 63 ± 8 %. There was no statistical difference (p > 0.05) between the two microfluidic preparations and DDA:TDB

which elicited 33 ± 8%; 40 ± 5% and 38 ± 9% inhibition for DDA:TDB:DSPC:DMG-PEG; DDA:PHAD:DSPC:DMG-PEG and DDA:TDB respectively. The formulation DDA:PHAD led to 60 ± 11% inhibition which had a high degree of statistical significance compared to DDA:TDB:DSPC:DMG-PEG ($p < 0.001$) as well as DDA:PHAD:DSPC:DMG-PEG and DDA:TDB ($p < 0.01$). DDA:PHAD was not significantly different when compared against the positive control ($p > 0.05$).
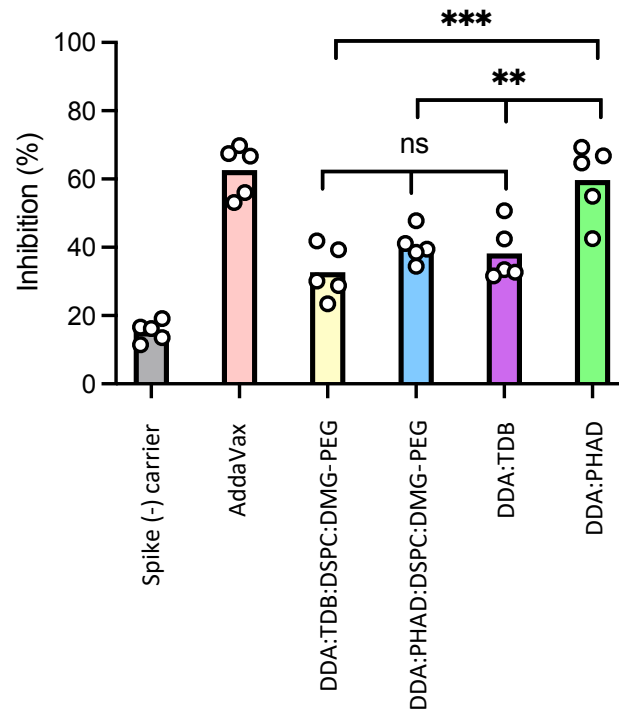
Figure 6.15 Adjuvanted formulations promote neutralising antibody production. Neutralising antibodies were detected in blood serum using an ELISA with SARS-CoV-2 spike (RBD) recombinant protein precoated on a 96 well plate with the presence of neutralising antibodies measured by a reduction in the OD. Vertical lines represent an average group value (n = 5): p > 0.05 (ns); p < 0.01 (**); p < 0.001 (***).

The findings in figure 6.15 further support the use of an adjuvanted formulation to deliver the spike subunit leading to significantly lower levels of inhibition (%) than the adjuvant formulations ($p < 0.001$). These results are supported by other studies [260] showing that 45 days after following a single injection, the squalene-based oil-in-water adjuvant (AddaVax) was not significantly different from the DDA:TDB group. However, it was observed that neutralising activity was detected after 7 days post-inoculation using the AddaVax group. As the results in figure 6.15 are from a prime-boost regimen, direct comparisons cannot be

made, particularly as the importance of the booster injection has shown to be vital at eliciting an immune response (figure 6.14).

6.3.5.3 Activation of caspase-I receptors to induce Th1 responses

The activity of IL-1β was monitored at the site of injection derived from the right thigh muscle. IL-1β is a highly potent pro-inflammatory cytokine [427] upregulated in response to an innate immune response. Activation of caspase-I by a group of receptors called 'NLRP1 inflammasomes' was identified by Martinon et al. [428] in 2002 and was found to induce inflammation in response to potentially infectious agents [429]. Activated caspase-I receptors then allow for the processing of IL-1β and IL-18, which induce IFN-γ cytokines [427, 430]. Examining IL-1β at the SOI would highlight caspase-I activation and induction of IFN-γ (Th1 response).

From the results in figure 6.16A, there was an increase in the concentration of IL-1β at the SOI in all the adjuvanted groups compared to the spike protein. Interestingly, despite DDA:PHAD proving to be the most potent IgG (figure 6.14) and neutralising antibody inducer (figure 6.15), the DDA:PHAD:DSPC:DMG-PEG formulation was shown to lead to significantly higher concentrations (p < 0.01) of IL-1β with the muscle at the SOI. Comparing DDA:PHAD:DSPC:DMG-PEG to DDA:TDB; DDA:PHAD and the antigen delivery by emulsion (AV), the differences were shown to be highly significant (p < 0.001) with significant differences also observed between DDA:TDB:DSPC:DMG-PEG and DDA:TDB (p < 0.01). In addition, the other formulation prepared by microfluidics, DDA:TDB:DSPC:DMG-PEG, was also shown to induce significantly greater concentrations of IL-1β when compared to its counterpart prepared by LFH (p < 0.01), however, there was no significant difference when the formulation was compared to DDA:PHAD (p > 0.05).

Focusing on formulations prepared by LFH, the familiar pattern of PHAD eliciting a more potent response was also shown, with concentrations of IL-1β being significantly greater than those incorporating TDB (p < 0.05). Interestingly, the IL-1β results align well with the patterns observed in the IFN-γ concentrations from stimulated splenocytes in figures 6.16B.

DDA:PHAD:DSPC:DMG-PEG, much like in figure 6.16A, was significantly greater than the other groups examined (figure 6.16B). It was highly significant when compared against AddaVax, DDA:TDB:DSPC:DMG-PEG and DDA:TDB (p < 0.001) and significant when compared to DDA:PHAD (p < 0.05). There was shown to be no significant differences in the IFN-γ concentration between the remaining adjuvanted formulations (p > 0.05).
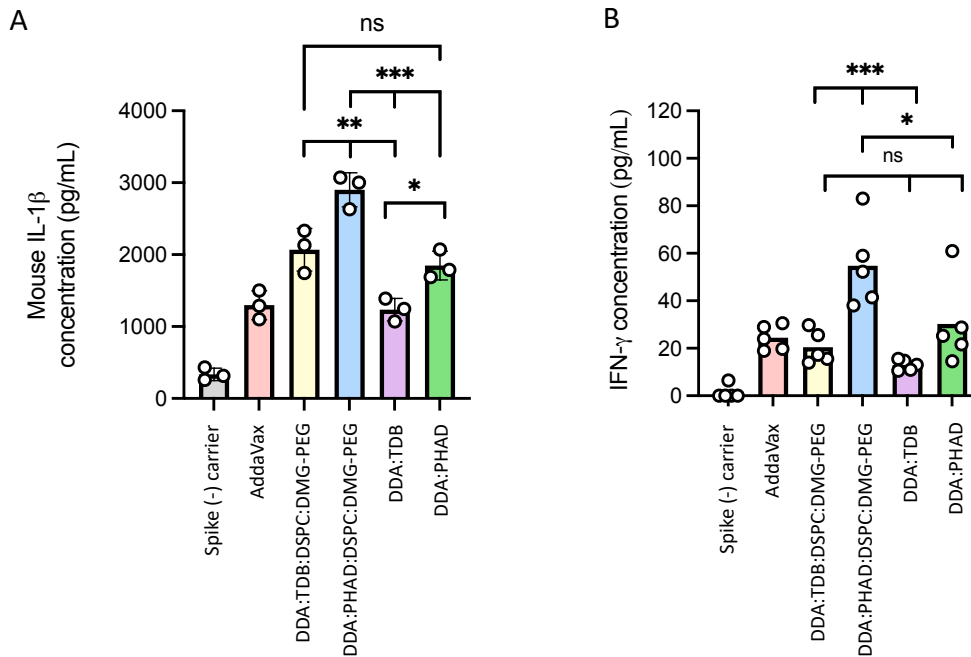
Figure 6.16 *Activation of caspase-I receptors at the site of injection and downstream-stimulation of IFN-γ. On the day of termination (day 50), the right hind leg of the mouse was removed with the muscle serum analysed for the pro-inflammatory cytokine IL-1β at the SOI (A). In addition, the spleen was removed with cells stimulated with 1 µg/mL of antigen (B) to allow quantification of IFN-γ for each of the respective groups. Vertical bars represent an average group value (n = 5): p > 0.05 (ns); p < 0.05 (*); p < 0.01 (**); p < 0.001 (***).*

The results obtained in figure 6.16 support the role of IL-1β within a Th1 response due to the increased concentrations of IFN-γ in groups with raised levels of IL-1β [427, 430, 431]. The presence of IL-1β at the SOI suggests the adjuvanted formulations can activate caspase-I receptors leading to the production of IL-1β and IL-18, which are strong inducers of IFN-γ.

6.3.5.4 Implementation of a bead-based immunoassay to screen cytokines and identify leading Th pathways

A screen of cytokines was investigated from restimulated splenocytes to gain a deeper insight into immune pathway activation. By screening a panel of cytokines allows for identifying Th1,

Th2, Th9, Th17, and Th22 induced immunity elicited by each formulation. The role of Th17 within vaccine-based immunity is becoming more documented and provided clear evidence that the Th1/Th2 pathways are not the immune responses generating host immunity [432-434]. In addition, upregulation of IL-17 could be an essential cytokine to target given that It has been shown to play a critical function within infections, particularly at the mucosa [435] and evidence of host Th17 cytokine immune responses caused by COVID-19 [436]. Various cytokines (figure 6.17A) from restimulated splenocytes were simultaneously quantified using a bead-based immunoassay and flow cytometry. The splenocytes were stimulated by either media (negative control; not shown), ConA (positive control; not shown), or spike antigen. Figure 6.17B indicated that various cytokines were activated by different degrees when plotted as a fold change against the spike protein group. The objective of this work was to identify the cytokine pathways that each formulation primarily acted on. Indeed it is clear there are complexities in terms of some cytokines playing a role in multiple T helper subtypes, ergo, to simplify this slightly, cytokines will be grouped as Th1, Th2, and Th17 subtypes for this thesis, given that it has been indicated that these Th subtypes have a critical role in acquired immunity and these subtypes primarily produce the cytokines IL-6, TNF-α and IFN-γ (in addition to IL-1 and IL-12 where were not investigated) which have been shown to be key cytokines stimulated in SARS-CoV-2 infection [437, 438].

A

T helper subtype	Associated cytokines examined
Th1	IL-2; IL-6; IL-10; IFN-γ; TNF-α
Th2	IL-4; IL-5; IL-6; IL-10; IL-13; IFN-γ
Th17	IL-6; IL-10; IL-17A; IL-17F; IL-22; IFN-γ; TNF-α

B
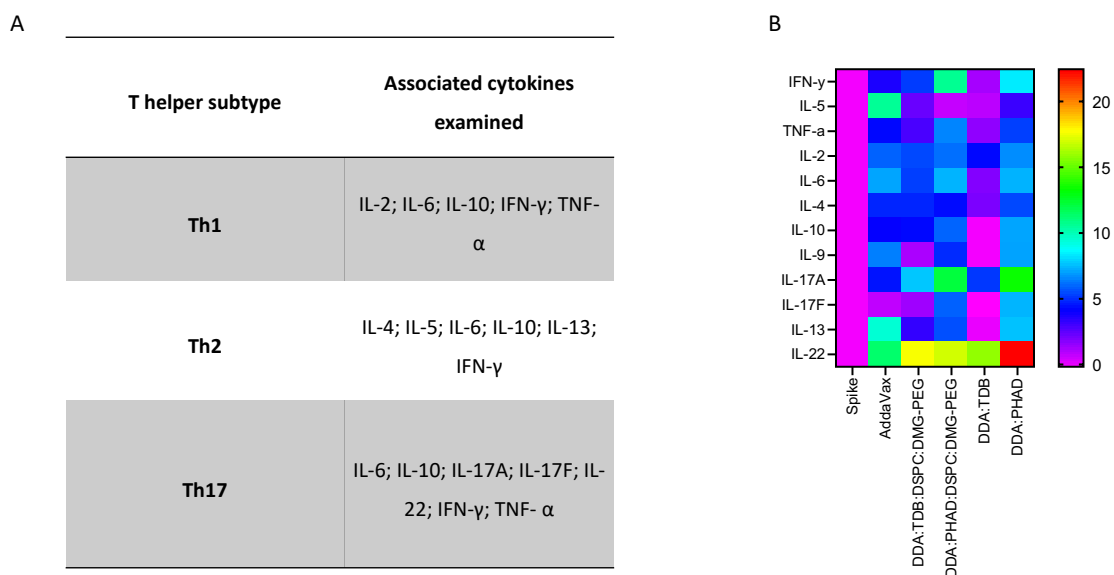
Figure 6.17 *Examination of Th1; Th2 and Th17 based cytokines through a bead-based immunoassay. A range of cytokines was examined using a bead-based immunoassay allowing for the identification of activated T helper*

subtypes with a focus on Th1; Th2 and Th17 (A). From the analysis, a heatmap was plotted (B) from the fold change against the spike protein group with results expressed as a log(2).

6.3.5.4.1 _Formulations containing PHAD allow more robust Th1 cytokine responses_

To examine the cytokines and their associated pathways, the Th1 subtype was examined by initially looking at IL-2 (figure 6.18A). Spike protein alone was shown not to invoke a sufficiently measurable result through stimulation either with the media or antigen. Despite the AddaVax group and DDA:PHAD:DSPC:DMG-PEG group eliciting a response greater than the negative control, this was shown not to be significant against the adjuvanted formulations ($p > 0.05$) with the only significant difference arising from the DDA:PHAD and DDA:TDB ($p < 0.01$).

Despite IL-6 (figure 6.18B) being a controversial cytokine due to its affinity within multiple Th1; Th2; Th17 and others, it was grouped within the Th1 subtype; however, it is generally referred to simply as a "proinflammatory cytokine". For this purpose, as it was found to provide a comparable T cell activation stimulation pattern when the antigen was used to IL-2, it was grouped within the Th1 subtype. With the AddaVax, DDA:PHAD:DSPC:DMG-PEG and DDA:PHAD groups producing concentrations greater than the negative control. However, there were no significant differences between the groups. As for the DDA:PHAD:DSPC:DMG-PEG group one mouse had a concentration of 4500 pg/mL, while in the DDA:PHAD group, one mouse measured 1 pg/mL, which made it hard to determine statistical significance between the groups.

Statistical differences were obtained from investigating IL-10 (figure 6.18C) with DDA:PHAD leading to significantly greater concentrations ($p < 0.001$) than AddaVax. Both the DDA:PHAD:DSPC:DMG-PEG and DDA:PHAD was shown to elicit greater IL-10 concentrations. However, within the DDA:PHAD group, two outliers produced IL-10 concentrations of 444 and 558 pg/mL. Interestingly, DDA:PHAD:DSPC:DMG-PEG was shown to elicit higher IFN-γ (figure 6.18D) concentrations which coincide with the results figure 6.16.
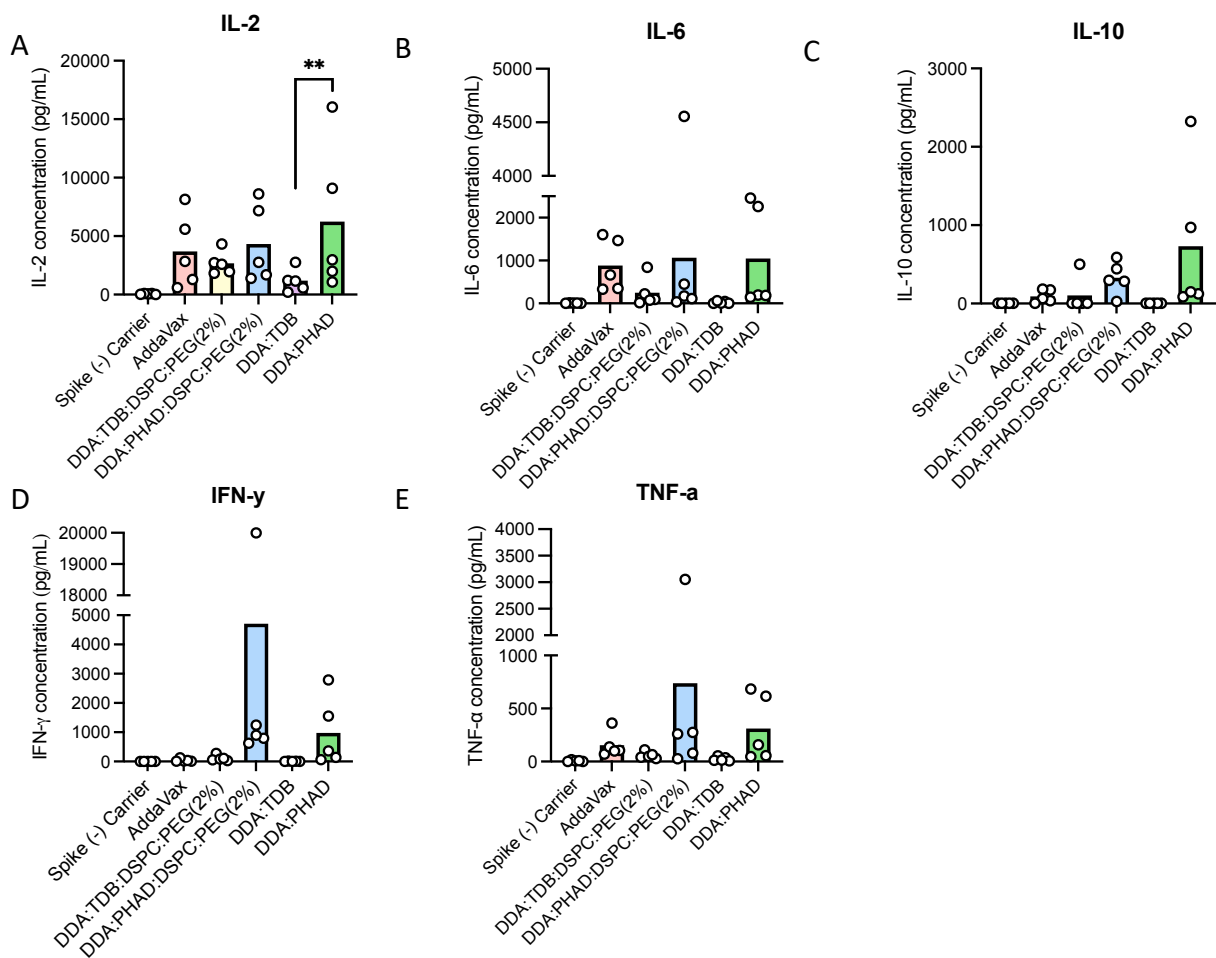
Figure 6.18 *PHAD based formulations promote Th1 cytokines. It is not unusual for one cytokine to have a role in other T helper subtypes, however, IL-2 (A); IL-6 (B); IL-10 (C); IFN-γ (D) and TNF-α (E) have been grouped with the Th1 subtype within this figure. T cell responses were measured by stimulating splenocytes with 1 μg/mL of spike protein 29 days after the booster injection. Vertical bars represent an average group value (n = 5): $p > 0.05$ (ns); $p < 0.01$ (**).*

The investigation of Th1 cytokines after immunisation of adjuvanted formulations with spike protein showed an increased response to formulations that incorporated PHAD instead of TDB. It has been shown that DDA:TDB stimulates robust Th1 responses towards TB antigens (such as Ag85B-ESAT6 or H56) from IL-2 and IFN-γ levels [224]. However, this was not shown in figure 6.17, with little to no response observed using TDB formulations. However, differences in the study methods could explain why the Th1 cytokine results DDA:TDB were not comparable to the study, such as the use of C57BL/6 mice, which strongly promote IFN-γ production compared to other mouse strains, and as such stimulate Th1 pathways to a greater extent than BALB/c mice.

In addition, within this study, spleens were harvested 4 weeks after the 2nd booster injection compared to 4 days after the administration of the 3rd booster injection within the referenced study [224]. Within the context of COVID-19, IL-2 has been proportionally linked to the severity of the disease [439]. IL-2 also plays a key role in the production of T cells and functioning as a mediator between the T-cell receptor and antigen [440]. The results suggest that at the restimulation antigen concentration tested, those formulations incorporating PHAD and the use of AddaVax lead to improved spike presentation and T cells priming.

IL-6 was the next cytokine to be examined and is a cytokine that is readily detected during a humoral response as it has a functional role for B cell differentiation and T cell differentiation towards Th1, Th2 and Th17 subtypes [441] in addition to the inflammatory response [442, 443]. As reviewed Jones [441], the definition of IL-6 is highly complex due to the numerous interplays has with other cytokines, such as upregulating of IL-2 within the lymph nodes, promoting a Th1 response [444, 445], and induction of Th2 responses through the promotion of IL-4 [446] in addition to the findings highlighting the involvement it has with the differentiation of naïve T cells to Th17 subtypes [447]. Using the same restimulation concentration of spike as IL-2, an absence in the response of TDB formulations when compared against PHAD was shown. However, one mouse in the DDA:PHAD group was an outlier and skewed the results. Significant differences were observed when IL-10 was investigated and saw a reduction in the concentrations elicited by AddaVax for IL-10 ($p < 0.01$). Again, IL-10 is a complex cytokine and plays a role in Th1, Th2 and Th17 [448, 449], making it hard to differentiate the affected pathway. However, the results obtained in figure 6.18 suggests that the Th2 pathway is most likely not affected due to increased Th2 specific cytokines. There were increased concentrations of IL-10 using the two microfluidic samples; however, these were shown not to be significant ($p > 0.05$). Interestingly, studies have demonstrated IL-10 production to be enhanced by including DSPC with DDA:TDB [325] which was observed by an approximately 2-fold increase in IL-10 concentration produced by DDA:TDB:DSPC:DMG-PEG compared against DDA:TDB (figure 6.17). Low concentrations of IL-10 for DDA:TDB and AddaVax were also detected in an additional study delivery spike protein Both IFN-γ and TNF-α are important Th1 cytokines for activating antigen-presenting cells and upregulation of phagocytic activity. It has also been shown that monophosphoryl lipid A

(MPLA), from which PHAD is based, strongly enhances IFN- γ secretion through its interaction with TLRs on the APC surface membrane [450] and as such led to the incorporation of MPLA within a vaccine against human papillomavirus (HPV) called Ceravix [271, 353]. In addition, TLR4 agonists have also been described to upregulate NF-κB transcriptase leading to the upregulation of TNF- α and IL-6 [40], as shown in figure 6.17. By activation of these cytokines, the adaptive immune system is enhanced, leading to and stimulating the maturation of APCs as described by Pasare et al., [451]. Indeed, the literature regarding the IFN-γ and TNF-α expression from TLR4 agonists supports figure 6.17, showing that formulations incorporating PHAD permitted strong responses. In contrast, the literature strongly supports DDA:TDB producing a high concentration of IFN-γ and TNF-α against Ag85B-ESAT-6 [21, 22, 347]. This was not shown in the results obtained with formulations containing the TLR4 agonist producing a more robust result.

6.3.5.4.2 *Comparable Th2 cytokine stimulation from TDB and PHAD*

Specific Th2 cytokines were also investigated as part of the cytokine panel investigated. The first was IL-5 (figure 6.19A), a pro-inflammatory cytokine associated with pro-inflammatory responses such as allergies and respiratory conditions such as asthma [452]. Following re-stimulation with the antigen, there was little to no response in T-cell activity across all the liposomal formulations. In contrast, for the AddaVax formulation, there was high activity eliciting results that were at least 1000-fold higher than the examined liposomal formulations. In addition, a comparable cytokine that is also expressed highly in pro-inflammatory conditions is IL-13 [453, 454]. Again, the AddaVax group was shown to produce high levels of IL-13 (figure 6.19B) when compared against the liposomal formulations and was highly significant when compared to DDA:TDB:DSPC:DMG-PEG and DDA:TDB ($p < 0.001$) as well as significantly greater than DDA:PHAD:DSPC:DMG-PEG. From re-stimulating the DDA:PHAD group with antigen led to a marginal increase in the concentration and thus was shown to be not statistically significant when compared against the AddaVax group ($p > 0.05$). The last Th2 specific cytokine investigated was IL-4 (figure 6.19C), which elicited low cytokine concentrations across all the adjuvant formulations investigated. In addition to IL-13, IL-4 is an archetypal Th2 response cytokine [455] leading to the suppression of crucial Th1 cytokines, such as IFN-γ, if concentrations of IL-4 are high. Both the AddaVax group and DDA:TDB:DSPC:DMG-PEG and DDA:PHAD:DSPC:DMG-PEG led to IL-4 concentrations between

50 -100 pg/mL with lower concentrations of IL-4 observed in the LF-TDB group with recordings of < 20 pg/mL when stimulated with the antigen. As for the DDA:PHAD group, higher concentrations were observed, with two outliers producing 206 and 210 pg/mL concentrations. However, despite these higher values, the other three mice had concentrations between 20 – 30 pg/mL and were shown not to be statistically greater than the other adjuvanted formulations examined (p > 0.05).
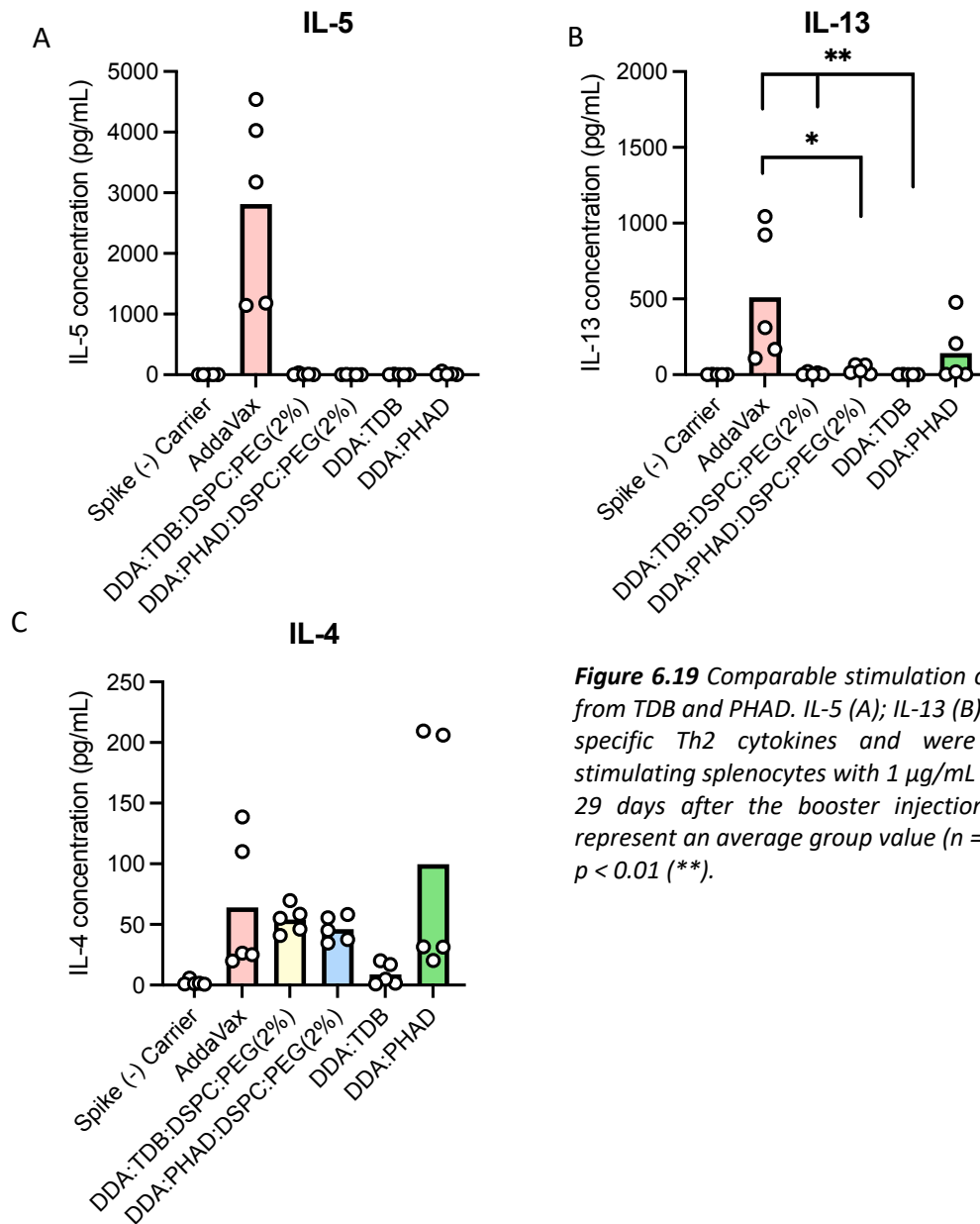
Figure 6.19 *Comparable stimulation of Th2 cytokines from TDB and PHAD. IL-5 (A); IL-13 (B) and IL-4 (C) are specific Th2 cytokines and were measured by stimulating splenocytes with 1 µg/mL of SPIKE protein 29 days after the booster injection. Vertical bars represent an average group value (n = 5): p < 0.05 (*); p < 0.01 (**).*

The reduced Th2 cytokine concentrations in figure 6.18 support the high Th1 cytokine concentrations observed in figure 6.17 due to the antagonistic relationship Th1 and Th2 have between each other as high Th2 cytokine concentrations result in low Th1 cytokine concentrations and vice versa [456, 457]. As viral infections predominantly stimulate a Th2 response, while larger organisms such as parasites elicit a greater Th2 response [454], reduced Th2 cytokines would be beneficial to prevent the suppression of Th1 cytokines. Furthermore, the Th1 response from DDA: TDB is often characterised by low IL-4 concentrations described by Christensen et al. when delivering the tuberculous antigen AG58B-ESAT-6 with near matching IL-4 concentrations obtained in figure 6.18 (approximately 20 pg/mL) for DDA: TDB prepared by lipid film hydration for their study investigating the impact of disaccharides on the preservation of protein biostructures and liposomes [365].

Both MPL and PHAD have been shown to elicit strong Th1 mediated immunity coupled with reduced Th2 specific cytokines such as IL-5 and IL-4 [355, 458]. The results in figure 6.18 further support these findings as both large reductions in the two cytokine concentrations were observed when compared against the cytokine concentrations produced with Th1 mediated cytokines. Despite the mechanism of action for AddaVax not being completely established, it has been shown that AddaVax encourages an influx of APCs to the injection site [320, 392], leading to the internalisation of the antigen and trafficking to the lymph nodes, which have been established as a strategic targeting site for vaccine adjuvants [459, 460]. AddaVax, in addition to a Th1 response, has been shown to stimulate Th2 immune responses [392-394]. This is confirmed by the results in figure 6.18, where AddaVax was shown to stimulate IL5, IL-13 and IL-4.

6.3.5.4.3 *TLR4 activation by PHAD promotes Th17 pathway activation*

Interestingly, the results obtained from the cytokine panel investigated the efficient stimulation of Th17 mediated T cells from formulations containing DDA:PHAD adsorbing spike protein (figure 6.20). Since 2005 after the discovery of the 3rd T cell subset, known as Th17, the role the cytokine plays within immunity has led to the evolution of the field as it was long thought Th1 cells lead to cell-mediated immunity from intracellular pathogens while Th2 cells invoke humoral immunity from parasites [432, 434]. However, it was found that auto-

inflammatory diseases acted independently from Th1 and Th2 pathways, which prompted a Th17 T cell population [461]. Th17 is characterised by its stimulation of IL-17 and plays a vital role within immunity as it permits downstream upregulation of pro-inflammatory cytokines and recruitment of APCs [462]. Within the context of COVID-19, IL-6 has presented as a key cytokine involved in mediating an inflammatory response in patients infected with SARS-CoV-2 with a with positive relationship between IL-6 and disease severity [463]. While the desired immune pathway activation for a COVID-19 vaccine is not currently known, it has been shown that immune enhancement is linked towards IL-6 and IL-8 production, both of which are prominent cytokines towards Th17 differentiation, highlighting advantageous benefits towards Th17 activation [436, 464, 465].

From initially looking at IL-17A in figure 6.20A, both the DDA:PHAD:DSPC:DMG-PEG and DDA:PHAD led to elevated levels of IL-17A production, with significantly increased levels (p < 0.05) observed when compared against all formulations excluding DDA:PHAD:DSPC:DMG-PEG were there was shown to be no significant difference (p > 0.05). Remarkably there was little T cell stimulation in both the AddaVax group in addition to the formulations containing TBD with concentration levels less than 180 pg/mL excluding one outlier mouse from the DDA:TDB:DSPC:DMG-PEG group, which produced an IL-17A concentration of 1590 pg/mL. The other IL-17 subtype, IL-17F (figure 6.20B), was also shown to be stimulated by the two formulations containing PHAD. However, DDA:PHAD was shown to be a more potent adjuvant than DDA:PHAD:DSPC:DMG-PEG and stimulated IL-17F to a greater extent than DDA:PHAD:DSPC:DMG-PEG (500 pg/mL and 150 pg/mL respectively). IL-22 (figure 6.20C) was only found to be stimulated by DDA:PHAD out of all the groups tested and was shown to be statistically different when compared against the other groups (p < 0.05). Overall, the results in figure 6.20 highlight that PHAD, similar to the robust activation of Th1 cytokines in figure 6.18, activates Th17 pathways to a greater extent than TDB.

A IL-17A

B IL-17F

C IL-22
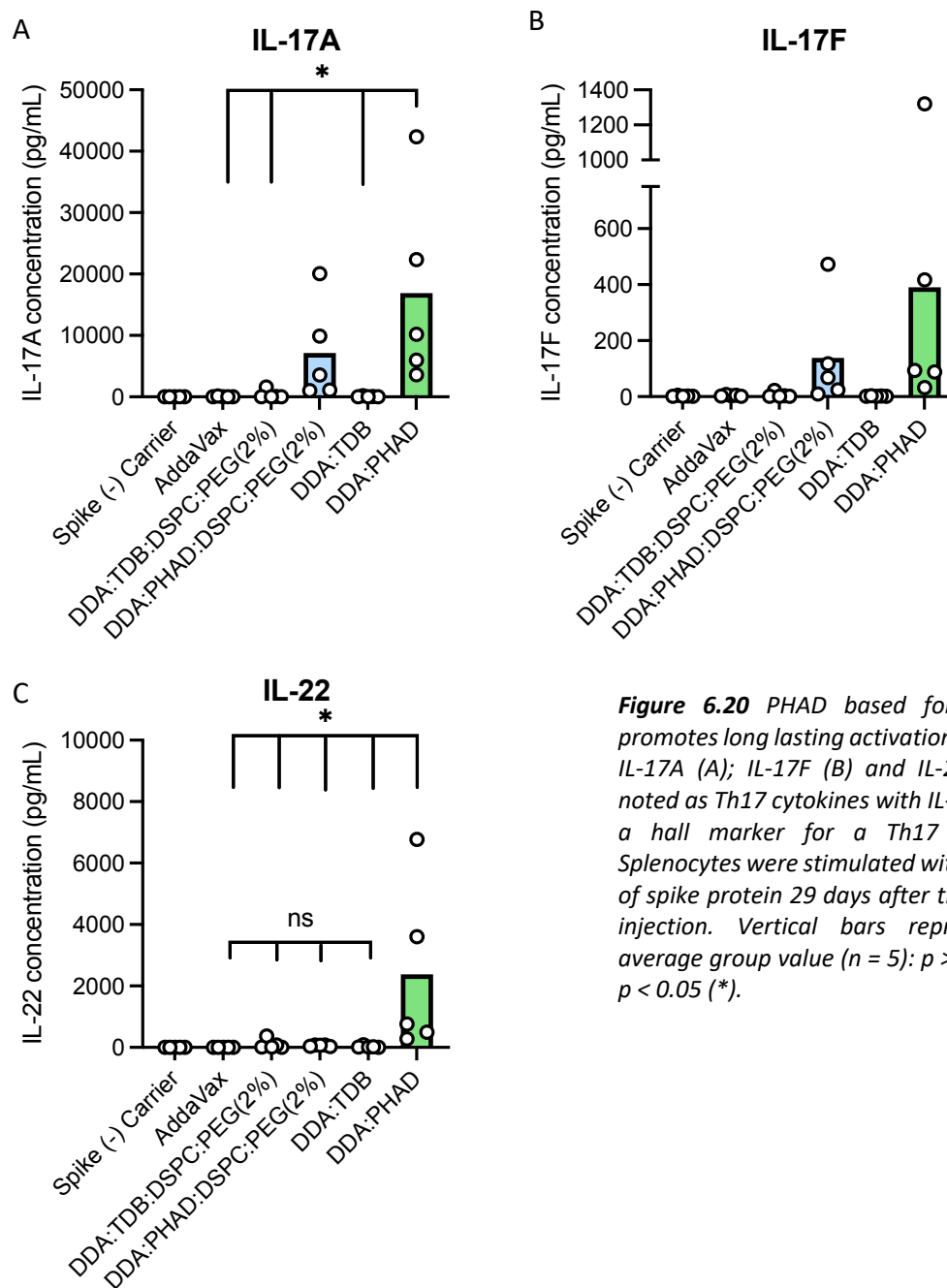
Figure 6.20 *PHAD based formulations promotes long lasting activation of IL-17A. IL-17A (A); IL-17F (B) and IL-22 (C) are noted as Th17 cytokines with IL-17A being a hall marker for a Th17 response. Splenocytes were stimulated with 1 μg/mL of spike protein 29 days after the booster injection. Vertical bars represent an average group value (n = 5): p > 0.05 (ns); p < 0.05 (*).*

IL-17A is a hallmark for Th17 pathway activation and functions as a pro-inflammatory cytokine typically associated with chronic inflammatory diseases such as rheumatoid arthritis [156, 157] and its mechanistic actions implicated within cell differentiation and proliferation [466]. Interestingly, IL-17A has also been suggested to amplify inflammatory immune responses by stimulating the production of IL-1; IL-6 and TNF-α cytokines [467], leading to the development of targeted IL-17 therapeutic blocking [468]. Within this context, formulations incorporating PHAD in figure 6.20A lead to a robust IL-17A cytokine response of which formulations

prepared by lipid film hydration were significantly different from formulations containing TDB and the AddaVax group suggesting, along with supporting literature, that using a TLR agonist leads to Th17 upregulation [469, 470]. The activation of FcR has characterised formulations containing TDB and upregulation of Th17 pathways upregulate innate immune responses and can direct Th17 immune responses by selectively activating the FcRγ-Syk-Card9 pathway in APCs [349] and delivering the TB antigen Ag85B-ESAT-6 [224]; however, this was not demonstrated in figure 6.20. Th17 cells have also been identified as crucial T cells involved in the host defence against fungi and bacteria. While this has no direct correlation towards intracellular pathogens, it is evident that PHAD functions as an active adjuvant within this cellular pathway.

6.3.5.4.4 *Liposomal formulation allow for a Th1-biased cytokine response*

The evaluation of the Th1/Th2 balanced response can be further extrapolated from stimulated splenocytes using key cytokines that are produced from specific Th1 and Th2 subtypes. Using IFN-γ as a key marker for Th1 pathway stimulation and IL-4, IL-5 and IL-13 as classical Th2 cytokines [220], a ratio between the two can be calculated to determine skewed Th responses.

Broadly, from the liposomal formulations, there was a Th1 bias with increased production of IFN-γ, while for the o/w emulsion, there was greater stimulation of IL-5 and IL-13, leading to a more pronounced Th2 response. As shown in figure 6.18D, DDA:PHAD:DSPC:DMG-PEG had significantly greater production of IFN-γ, which has caused the Th1 bias observed within this group in figure 6.21. DDA:TDB:DPSC:DMG-PEG was also shown to be Th1 biased in IFN-γ:IL-5 and IFN-γ:IL-13 with balanced production of IFN-γ and IL-4. A similar IFN-γ:IL4 profile was also observed in DDA:TDB. There was significant IL-5 production in the DDA:TDB from when splenocytes were stimulated, leading to minimal Th1 skewing. The ratio of Th1/Th2 remained consistent for DDA:PHAD with comparable ratios observed for IFN-γ:IL-4, IFN-γ:IL-5 and IFN-γ:IL-13.
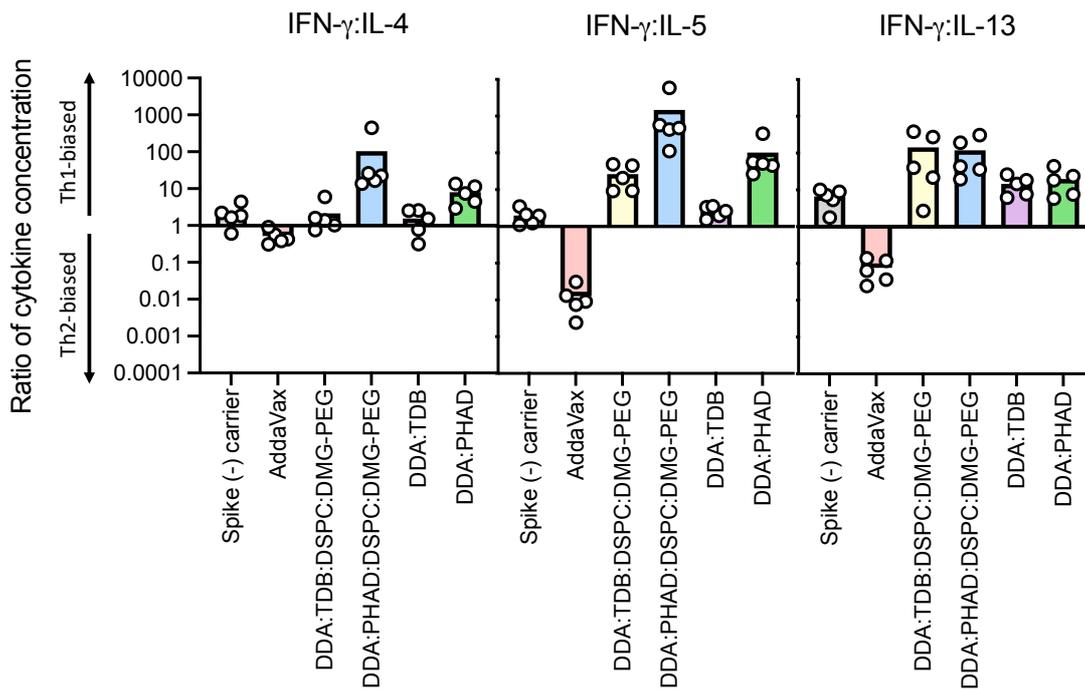
Figure 6.21 *Th1-skewed liposome cytokine responses. The ratio of IFN-γ to either IL-4, IL-5 or IL-13 cytokine concentrations were calculated to determine the Th1 or Th2 biased response from the cytokine invoked from stimulated splenocytes with 1 μg/mL of spike protein 29 days after the booster injection. Vertical bars represent an average group value (n = 5).*

Recent literature has indicated the importance of a Th1-biased skew in the immune response to provide protection and subsequent re-infection of SARS-CoV-2 [426, 471, 472] with avoidance of VAERD. The results in figure 6.21 are encouraging as it suggests that the Th2 immune is avoided from cytokines investigated in all liposomal formulations when splenocytes are stimulated with 1 μg/mL of spike antigen. Together with the IgG subclasses (figure 6.14) obtained from blood serum, presenting a slight Th2 bias, and cytokine results (figure 6.21) from stimulated splenocytes indicates that a balanced Th1 and Th2 response can be obtained in all liposomal formulations examined.

6.4 Conclusion

The use of subunit vaccines for COVID-19 could provide an alternative vaccine type to the novel vaccine technologies which are currently used. Microfluidic technology also lends itself as a powerful manufacturing method for scalable translation of formulations made at the lab bench to GMP volumes with improved potential for implementation within a continuous production setting. Manufacturing DDA:TDB and DDA:PHAD was successfully achieved using the smaller OVA proteins, but stability issues arose from using the larger spike protein. From modification of the formulation, it was possible to produce and control liposome physical characteristics to sizes less than 100 nm for both DDA:TDB and DDA:PHAD from the addition of DSPC and DMG-PEG$_{2000}$ though both formulations require further optimisation to address vesicle stability. In terms of antibody analysis, all adjuvanted formulations provided a robust response with the DDA:PHAD produced by lipid film provided significantly higher antibody responses. Investigating neutralising antibody production, the results highlighted that DDA:PHAD prepared by lipid film hydration was significantly greater than the other liposome formulations investigated with comparable results obtained to a positive control (o/w emulsion). By exploring IL-1β at the SOI, caspase-I receptors were activated, largely by DDA:PHAD prepared by microfluidics indicating the adjuvants' role at stimulating a Th1 response, supported this by elevated concentrations of IFN-γ when examined by ELISA and bead-array for this group. Formulations incorporating PHAD allowed for increased Th1 and Th17 cytokines with IFN-γ, IL-2, IL-10, IL17A and IL-22, which were the critical cytokines elicited from the immunostimulator. From this work, both DDA:TDB and DDA:PHAD can be manufactured by both lipid film hydration and microfluidics with physical characteristics controlled by the addition of PEG, allowing for the enhanced neutralising antibody production using DDA:PHAD, furthermore, the use of PHAD is a potent adjuvant and strongly influenced Th1 and Th17 pathways four weeks after the booster injection. The results obtained demonstrate that a spike subunit protein can be effectively adjuvanted, eliciting neutralising antibodies and T cell responses using both DDA:TDB and a novel DDA:PHAD formulation supporting the use of subunit vaccines against SARS-CoV-2.

Chapter 7

Overall Conclusion

7.1 Introduction

The main aim of this thesis was to investigate and develop scalable manufacturing methods to produce adjuvanted protein subunit liposomal vaccines. Liposomes are a highly flexible and adaptable drug delivery system that has been extensively studied for the delivery of both small molecules and biologics, along with the first FDA approved use of siRNA for rare disease treatment of hereditary transthyretin amyloidosis (Patisiran). While recent global events during the acquisition of data and writing of this thesis have significantly advanced both the vaccine and genetic nanomedicine fields, the use of protein subunits within vaccines remains a highly attractive and heavily researched field. Indeed they may offer a safer alternative to live attenuated vaccines, which have been shown to be among the most effective methods for preventing the spread of disease [473]. However, the delivery of protein subunits is poorly immunogenic due to the poor stimulation of APCs (mainly dendritic cells) [474], leading to the inclusion of adjuvants to mount an immune response.

Adjuvants allow the stimulation of the APCs and can be divided into immunostimulants and delivery systems. The use of TDB within DDA:TDB (CAF01) is a particularly effective compound for both mounting and modulating immune responses for the delivery of protein subunits leading it to be a heavily investigated formulation. Recent progress has drawn significant attention to pattern recognition receptors, particularly the use of TLRs agonists, which have been classed as a newer generation of vaccines and have shown to control the generation of humoral and cell-mediated immune responses [474, 475]. Liposomes are unique delivery systems and present themselves to provide significant potential as an adjuvant by allowing critical formulation attributes such as particle size, charge, location of antigen (entrapped or adsorbed), choice of lipid and SOI, which have been shown to elicit specific immune response and biodistribution impacting on the efficacy of the vaccine [70, 224, 266, 325, 476]

To support the translation of liposomal adjuvants to the market, efficacious liposomal formulation attributes identified in pre-clinical candidates must be maintained during progression from the lab bench to GMP to maintain vaccine efficacy. As the physicochemical

attributes of a potential liposome candidate are a result of the manufacturing method adopted, scale-up complications can arise if critical manufacturing conditions are not identified. Therefore, it is crucial that manufacturing methods can be easily scaled and controlled without changing critical operational parameters during scale-up. The use of a bottom-up strategy during the primary research stages allows for precise process control of each manufacturing operation parameter and circumvents scale-up complexities that can impact market authorisation for potential new liposomal adjuvants.

7.2 Identification of a novel microfluidic critical process parameter

The initial portion of this thesis investigated a potential new critical microfluidic attribute that can be used to control physical characteristics. This would provide a valuable tool for formulation scientists to meet possible formulation regulatory criteria and vesicle sizes that are particularly important for biodistribution, allowing for enhanced efficacy and reduced off-target toxicity. While an extensive range of attributes has already been researched and published, such as FRR, TFR, lipid concentration and buffer media, the use of solvent and their effects on liposomal formulations have not been investigated extensively. The choice of solvent is also crucially important in regards to residual solvent within the formulation, and there is a heavy emphasis on the selection of class 3 solvents as these have been indicated to be least toxic and, in turn, protects patients from potential adverse events as outlined in the ICH guidelines [154]. Therefore, understanding solvent polarity and the impact on the formulation characteristics could allow the selection of less harmful solvents during manufacturing and achieve the desired formulation properties.

Using a low-volume high throughput production, it was possible to gain insight into the impact of solvent polarity on vesicle size using MeOH, EtOH, and isopropyl. While the size changes between MeOH and EtOH were low, using IPA, which is less polar, led to increased sizes and that using lipids with longer alkyl chain lengths permitted smaller vesicles that align with previous findings [117] regardless of solvent choice. It was also shown that increasing cholesterol concentrations led to reduced vesicle sizes which was attributed to cholesterol improving bilayer packing densities, allowing increased bilayer elasticity and rapid closure of

lipid discs and that at higher cholesterol levels. The effect of solvent polarity on the vesicle is diminished, suggesting that ordered packing of the lipid bilayer supersedes solvent selection. It was also found that by using solvent mixtures, liposome sizes can be precisely controlled using microfluidics, with larger liposomes achieved using lower polarity mixtures. Using DSPC:Chol, solvent selection did not affect formulation stability across 7 days. Each formulation produced by the solvents investigated provided comparable release profiles of encapsulated protein (f_2> 50) with 80% of protein released after 72 h, which RP-HPLC successfully assessed. Upon investigation of solvent morphology, it was identified that MeOH and EtOH allowed the production of SUV, which was previously observed in independent findings [153], but that IPA led to the formation of vesicles with multiple bilayers. By applying a hypothesised mechanism for liposome formulation during microfluidics by Zook and Vreeland [91], a possible explanation for this effect could be that due to larger lipid discs forming as a result of a more non-polar solvent from increased lipid solubility and prolonged duration to hydrate the solvent leading to larger lipid discs engulfing smaller discs with multiple bilayers.

This work identified solvent selection as a crucial microfluidic parameter for controlling vesicle size and highlighted the advantageous use of EtOH as a choice of solvent for large-scale manufacturing. In addition to other known critical microfluidic attributes for controlling liposome physical properties, solvent selection should be considered during the design and development of microfluidic manufacturing processes.

7.3 Systematic mapping analysis of microfluidic geometries

Microfluidics is a novel manufacturing technology to produce liposomes but has recently gained significant attention for its use in the development of the Moderna COVID-19 vaccine [220, 477] and the first siRNA therapy patisiran (Onpattro®; Alnylam) [478, 479]. COVID-19 has highlighted the necessity for scalable manufacturing, providing a direct path from research conducted at the lab bench to GMP. The SHM architecture is well-established and cited over 100 times [209]. However, the complexity of the design presents practical limitations in terms of consistent fabrication of herringbone structures at the micro-scale. This

leads to complicated and costly production costs, and due to the multidimensional dependencies and size of the herringbone structures, throughput speeds are reduced, hindering final product volumes expected from a GMP facility without parallelisation. To address this, a novel microfluidic architecture was investigated with a simplified design, and centrifugal mixing would permit greater throughput speeds to be achieved. Therefore, the aim was to systematically map the two cartridges using critical microfluidic parameters and manufacture the formulation DSPC:Chol with an entrapped subunit on the lab bench scale and completely scale-up to GMP without any changes to critical manufacturing process parameters.

From work conducted in chapter 4, to assess formulation reproducibility from the cartridge formulation, critical liposomal quality criteria were set before beginning experimentation of a Z-average diameter of between 50 – 70 nm, a PDI of < 0.2, zeta potential of – 5 to – 10 mV and protein encapsulation of between 26 – 36 %. These criteria were also carried across for formulations manufactured by both pre-clinical and GMP production scales. Using the critical quality requirements from lab bench-scale testing, both the SHM and TrM cartridges were effectively mapped, producing liposomes within the specification set with protein encapsulation assessed by micro-BCA and RP-HPLC. It was also identified that the two cartridges could produce liposomes with entrapped proteins using different formulations that were not statistically different in terms of size, PDI, ZP or EE%. In addition, other critical microfluidic operational parameters were tested, such as the FRR, TFR and solvent choice and liposomes compared from the two cartridges, which again found no statistical differences in the liposomes produced when critical operational parameters were altered.

Furthermore, before progressing to GMP testing, liposome morphology and protein release kinetics were assessed from the liposomes made by the two microfluidic architectures. The results indicated that the SUV morphology, which is achieved using the SHM cartridge using DSPC:Chol was maintained when using the TrM cartridge and that protein release kinetics was highly comparable. Using the TrM architecture, the TFR was increased to 60 mL/min for pre-clinical manufacturing and 200 mL/min for clinical manufacturing using the same FRR of 3:1 and lipid/protein concentrations used at the lab bench when producing the formulation at 12 mL/min. At the increased speeds of 60 mL/min and 200 mL/min, the liposomes' Z-

average was successfully maintained between $60 - 70$ nm with PDIs < 0.2 and EE% of $25 - 35$ %.

The microfluidic mapping study was crucial to maintain liposomal attributes using a different microfluidic architecture, particularly when switching from a chaotic advection mixing method to centrifugal mixing. The work within the chapter successfully mapped the two cartridges. Additionally, it demonstrated the premise that a scale-independent production method allows complete progression from the lab bench to GMP without changing additional operational parameters or affecting physical-chemical liposome characteristics. Furthermore, implementing a TrM architecture negates the requirement for parallelisation when moving to GMP, which would be needed with the SHM design and multiple individual pumps and pressure monitoring to achieve the same production volumes. Overall this work highlights that a microfluidic manufacturing process can permit the rapid translation and production pathway of primary research and development to GMP production of nanomedicines.

7.4 Development of a continuous microfluidic manufacturing process for liposomal subunit vaccines

Building on chapter 4, the next step in chapter 5 was to develop a microfluidic method allowing the controlled adsorption of protein subunits using the cationic lipid DDA. For the surface adsorption of protein onto cationic liposomes, manually pipetting and mixing is a common technique; however, It is clear that automating processes is a driving force within the pharmaceutical industry [230, 272, 480, 481]. Utilising microfluidics allows precise manufacturing criteria, such as mixing speeds and ratios, to finely control physical liposomal attributes that have been shown to impact immune responses [22, 67, 69, 224]. The main objective of chapter 5 was to identify a lead microfluidic manufacturing method that would allow the potential of liposomes production and protein adsorption within one operation. The formulation was to be assessed by physical characterisation, protection of antigen and conduction of an *in vivo* biodistribution and immunogenicity study to assess if an immune response eliciting antigen trafficking and stimulation of antigen-specific antibodies can be successfully invoked.

The results highlighted that L:P ratios were critical criteria to consider in terms of vesicle stability leading to the selection of 10:1, 30:1, and 60:1 L:P to be further developed as this allowed for the assessment of different vesicle sizes, which were also stable over 14 days. By optimising FRR selection, reduced solvent content of < 10% could be used for the controlled adsorption of proteins. From this, three different continuous microfluidic protein adsorption methods were investigated. The results indicated that using an inline adsorption method where the protein was added directly after the microfluidic mixer was not as effective as the 1 or 2 step mixing methods, which incorporated protein mixing within the micromixer. By mixing the protein and liposomes within the micromixer, greater protein adsorption efficiencies, improved stability and uniform morphology were achieved. Investigating in vivo biodistribution highlighted that using DSPC:Chol:DDA (10:5:4 w/w) using the 1 and 2 step manufacturing methods, liposomes could remain at the SOI and retain protein which was detectable after 216 h. Upon ex vivo analysis, liposomes were detected at the lymph nodes highlighting potential trafficking of the formulation away from the SOI. Given the importance the lymphatics play within an immune response [61, 482, 483], a short lymphatic biodistribution was conducted, highlighting an increased accumulation of protein and liposomes within secondary lymphatic organs. The study was finalised by conducting an immunogenicity study investigating using the 1 step and 2 step at L:P ratios of 10:1, 30:1 and 60:1 using the antigen MOMP.

Interestingly, using the MOMP antigen, it was impossible to fabricate a stable vesicle at a 10:1 L:P using the 2 step manufacturing method, highlighting that different microfluidic mixing methods can significantly impact vesical characteristics. The L:P was identified as a crucial attribute for invoking a humoral response where it was shown that a 60:1 L:P led to the greatest antigen-specific IgG titres from the L:P ratios investigated. While size has been shown to impact immune response, the result observed was most likely due to the increased DDA:protein ratio leading to a more powerful adjuvant effect leading to greater stimulation of IgGs.

The results within chapter 5 demonstrate the successful use of microfluidics to refine operational parameters to tightly control protein adsorption, which allows the production of

preformed liposomes and adsorption of protein within the one operation that removes manual operator input and allows implementation within a continuous production setting. Such a process allows the movement away from batch processing and precisely control each aspect of nanomedicine production.

7.5 Microfluidic preparation of adjuvanted SARS-CoV-2 spike protein

Given the development of a microfluidic production platform enabling antigen-controlled coating onto cationic liposomes, the next step was to include an immunostimulator to promote humoral and cytokine responses. CAF01 is a potent adjuvant comprising of DDA, which was used in chapter 5 in addition to TDB at a 5:1 w/w ratio. CAF01 has been shown to promote Th1-biased immune responses in studies including tuberculosis and chlamydia, leading to high IgG antibody production and elevated IFN-γ [10, 22, 60]. While the effects of CAF01 are well described, substituting TBD for the TLR4 agonist PHAD (DDA:PHAD 5:1 w/w), an MPLA synthetic derivative, presented a novel opportunity to evaluate in vivo performance by adjuvating the SARS-CoV-2 SPIKE protein.

Building on previous research following the successful microfluidic preparation of DDA:TDB using IPA, the same operational parameters were used to formulate DDA:TDB using EtOH, given that the EtOH has been used extensively throughout this thesis. While both DDA:TDB and DDA:PHAD presented unexpected challenges following the use of EtOH within a microfluidic setup with the initial lipid concentrations selected, the introduction of heating blocks and solvent mixtures to ensure lipids were suspended allowed the production of uniform vesicles that were < 100 nm when OVA was adsorbed. However, switching the antigen OVA for SPIKE led to additional complexities in formulation stability leading to the refinement of the formulation by incorporation of DSPC (20% w/w) and DMG-PEG$_{2000}$ (2%), which was required to control the vesicle size and promote stability. A consequence of the addition of DSPC and DMG-PEG$_{2000}$ is the effect this can have on immune profiles [21, 71, 379]. Therefore, DDA:TDB and DDA:PHAD were produced using lipid film hydration to allow a more robust comparison between the two adjuvants without the possible interference of DSPC and DMG-PEG$_{2000}$ impacting immune profiles. Overall, from the immunological analysis

conducted, formulations containing PHAD was shown to be more potent than formulations containing TDB. By assessing neutralising antibodies, DDA:PHAD elicited high antibody titres that were significantly different from the other liposomal adjuvants examined with a comparable antibody titre to AddaVax. The results also demonstrate that all adjuvanted formulations examined are potent antigen-specific antibody stimulators, particularly IgG1, with high antibody titres obtained after 4 weeks from blood serum following the booster injection. By collecting muscle serum at the SOI, IL-1β was shown to be upregulated from the formulation DDA:PHAD:DSPC:DMG-PEG. This formulation also led to increased IFN-γ concentrations when splenocytes were stimulated with the antigen and assessed by ELISA and a bead-based immunoassay indicating the adjuvants role in invoking a Th1 response. Formulations containing PHAD consistently allowed for increased Th1 and Th17 cytokines.

From this work, it has been demonstrated that both DDA:TDB and DDA:PHAD can be effectively manufactured using lipid film hydration and microfluidics by incorporating additional lipids to control and stabilise vesicle sizes though further work could be conducted to extend the stability profile. It was also indicated that PHAD functions as a potent adjuvant and strongly stimulates Th1 and Th17 immune pathways along with neutralising antibody production following booster injection. This work provides the foundations for using a novel liposomal formulation, promoting future studies for adjuvating other antigens or refining DDA:PHAD and allowing the preparation of stable vesicles produced by microfluidics.

7.6 Concluding remarks and future work

In recent times, scalable manufacturing has become increasingly more attractive for the preparation of lipid nanomedicines enabling the rapid translation of formulations produced on the lab bench to large scale batches with tightly controlled vesicle attributes. Microfluidics enables a complete path for lipid nanomedicine production, allowing small volumes to be used for primary research through to industrial volumes without the requirement to adjust operational parameters, which can affect vesicle characteristics such as particle size, polydispersity and zeta potential, which are crucially essential for adjuvant performance. While large, centralised manufacturing is the status quo for therapeutic development,

microfluidics also opens the exciting future for decentralised manufacturing permitting lipid nanomedicines to be manufactured and administered at specific localised sites eliminating storage and supply chain challenges, providing significant regulatory changes.

Within this thesis, both neutral and cationic liposomes have been effectively produced allowing for either entrapment or surface adsorbed protein antigens. Using a model formulation comprised of DSPC:Chol with the entrapped model antigen ovalbumin, microfluidics has been shown to produce liposomes of < 1 mL all the way through to GMP production 200 mL/min without alteration to formulation characteristics or entrapped capabilities. Furthermore, the use of tangential flow filtration as scalable of purification technology was also shown to be an effective technique for removing residual solvents and impurities within the formulation. Using DSPC:Chol also demonstrated that solvent polarity to be an additional microfluidic operational parameter that can be effectively used to refine further and fine-tune vesicle attributes. The delivery of protein subunits continues to be an attractive form of vaccination and to streamline and automate the manufacturing process, and various mixing methods were developed and assessed in vivo to investigate efficacy. It was highlighted that the 1 and 2 step production techniques could be effectively used, allowing expected biodistribution kinetics for cationic liposomes to be maintained and induce enhanced IgG antibody titres using the MOMP antigen using the 60:1 L:P. Vaccination against COVID-19 is still ongoing, with a protein subunit vaccine now in phase III trials allowing an increased range of vaccine types to be used. Using DDA:TDB and DDA:PHAD manufactured by both lipid film hydration and microfluidics allowed the delivery of adjuvanted SPIKE protein and effectively promoted antigen-specific IgG responses. The use of PHAD allowed for an enhanced cytokine response highlighting that Th1 and Th17 pathways with stimulating the cytokines IFN-γ, IL-2, IL-10, IL17A and IL-22 are shown to be critical cytokines elicited by DDA:PHAD.

Future studies should focus on supporting the scalable production of liposomal productions and, particularly, the microfluidic preparation of DDA:PHAD given the in vivo results indicating PHAD to be a potent adjuvant. Using the S1 SPIKE protein subunit instead of the SPIKE trimer could help address the stability issues upon adsorption onto preformed liposomes. Furthermore, additional lipids could be screened, such as cholesterol, to improve bilayer

packaging; however, the use of additional lipids should be avoided until necessary, given the impact this can have on immune responses. Unfortunately, such screening studies were not possible within this thesis, given the cost of PHAD and SPIKE protein. Once a stable formulation can be produced by microfluidics, future in vivo additional immunological assessments for adjuvating SARS-CoV-2 SPIKE protein could be considered. These could include IL-6 within the muscle serum at the SOI given its role to induce IFN-γ would be a pivotal result to support a Th1-biased immune response.

Given that COVID-19 infection is a respiratory syndrome, it could also be interesting to excise lung tissue following a vaccine study along with the spleen and compare both antibody and cytokine analysis given that published vaccines have shown to be efficacious in the lungs of vaccinated animals [220, 484]. The overall success of the adjuvant could be further assessed by challenging the mice to a COVID-19 strain to assess the potential success of the developed adjuvanted vaccine. Ultimately, microfluidics is a well-placed platform within both lab-scale research and large scale GMP manufacturing that has proven to be an effective tool to develop a range of liposomal formulations to effectively deliver protein subunits and activate crucial adaptive immune responses which are required for an efficacious vaccine adjuvant system.

References

[1] D. Papahadjopoulos, S. Nir, S. Ohki, Permeability properties of phospholipid membranes: Effect of cholesterol and temperature, Biochimica et Biophysica Acta: Biomembranes, 266 (1972) 561-583.

[2] G. Gregoriadis, B.E. Ryman, Liposomes as carriers of enzymes or drugs: a new approach to the treatment of storage diseases, Biochemical Journal, 124 (1971) 58.

[3] G. Gregoriadis, B.E. Ryman, Lysosomal localization of -fructofuranosidase-containing liposomes injected into rats, Biochem J, 129 (1972) 123-133.

[4] M.C. Smith, R.M. Crist, J.D. Clogston, S.E. McNeil, Zeta potential: a case study of cationic, anionic, and neutral liposomes, Anal Bioanal Chem, 409 (2017) 5779-5787.

[5] A.R. Mohammed, N. Weston, A.G. Coombes, M. Fitzgerald, Y. Perrie, Liposome formulation of poorly water soluble drugs: optimisation of drug loading and ESEM analysis of stability, Int J Pharm, 285 (2004) 23-34.

[6] A. Laouini, C. Jaafar-Maalej, I. Limayem-Blouza, S. Sfar, C. Charcosset, H. Fessi, Preparation, Characterization and Applications of Liposomes: State of the Art, Journal of Colloid Science and Biotechnology, 1 (2012) 147-168.

[7] C. Zylberberg, S. Matosevic, Pharmaceutical liposomal drug delivery: a review of new delivery systems and a look at the regulatory landscape, Drug Deliv, 23 (2016) 3319-3329.

[8] G. Vitiello, A. Falanga, A.A. Petruk, A. Merlino, G. Fragneto, L. Paduano, S. Galdiero, G. D'Errico, Fusion of raft-like lipid bilayers operated by a membranotropic domain of the HSV-type I glycoprotein gH occurs through a cholesterol-dependent mechanism, Soft Matter, 11 (2015) 3003-3016.

[9] S. Joshi, M.T. Hussain, C.B. Roces, G. Anderluzzi, E. Kastner, S. Salmaso, D.J. Kirby, Y. Perrie, Microfluidics based manufacture of liposomes simultaneously entrapping hydrophilic and lipophilic drugs, International Journal of Pharmaceutics, 514 (2016) 160-168.

[10] S. Abraham, H.B. Juel, P. Bang, H.M. Cheeseman, R.B. Dohn, T. Cole, M.P. Kristiansen, K.S. Korsholm, D. Lewis, A.W. Olsen, L.R. McFarlane, S. Day, S. Knudsen, K. Moen, M. Ruhwald, I. Kromann, P. Andersen, R.J. Shattock, F. Follmann, Safety and immunogenicity of the chlamydia vaccine candidate CTH522 adjuvanted with CAF01 liposomes or aluminium hydroxide: a first-in-human, randomised, double-blind, placebo-controlled, phase 1 trial, Lancet Infect Dis, 19 (2019) 1091-1100.

[11] G. Poste, D. Papahadjopoulos, Lipid vesicles as carriers for introducing materials into cultured cells: influence of vesicle lipid composition on mechanism(s) of vesicle incorporation into cells, Proc Natl Acad Sci U S A, 73 (1976) 1603-1607.

[12] F. Szoka, Jr., D. Papahadjopoulos, Procedure for preparation of liposomes with large internal aqueous space and high capture by reverse-phase evaporation, Proc Natl Acad Sci U S A, 75 (1978) 4194-4198.

[13] S. Shah, V. Dhawan, R. Holm, M.S. Nagarsenker, Y. Perrie, Liposomes: Advancements and innovation in the manufacturing process, Adv Drug Deliv Rev, (2020).

[14] A.E. Green, P.G. Rose, Pegylated liposomal doxorubicin in ovarian cancer, International journal of nanomedicine, 1 (2006) 229-239.

[15] Y. Barenholz, Doxil(R)--the first FDA-approved nano-drug: lessons learned, Journal of controlled release : official journal of the Controlled Release Society, 160 (2012) 117-134.

[16] O. Tirosh, Y. Barenholz, J. Katzhendler, A. Priev, Hydration of Polyethylene Glycol-Grafted Liposomes, Biophysical Journal, 74 (1998) 1371-1379.

[17] M.L. Immordino, F. Dosio, L. Cattel, Stealth liposomes: review of the basic science, rationale, and clinical applications, existing and potential, Int J Nanomedicine, 1 (2006) 297-315.

[18] A. Gabizon, R. Catane, B. Uziely, B. Kaufman, T. Safra, R. Cohen, F. Martin, A. Huang, Y. Barenholz, Prolonged Circulation Time and Enhanced Accumulation in Malignant Exudates of Doxorubicin Encapsulated in Polyethylene-glycol Coated Liposomes, Cancer Research, 54 (1994) 987.

[19] Z. Symon, A. Peyser, D. Tzemach, O. Lyass, E. Sucher, E. Shezen, A. Gabizon, Selective delivery of doxorubicin to patients with breast carcinoma metastases by stealth liposomes, Cancer, 86 (1999) 72-78.

[20] U. Bulbake, S. Doppalapudi, N. Kommineni, W. Khan, Liposomal Formulations in Clinical Use: An Updated Review, Pharmaceutics, 9 (2017).

[21] M. Henriksen-Lacey, V.W. Bramwell, D. Christensen, E.M. Agger, P. Andersen, Y. Perrie, Liposomes based on dimethyldioctadecylammonium promote a depot effect and enhance immunogenicity of soluble antigen, Journal of controlled release : official journal of the Controlled Release Society, 142 (2010) 180-186.

[22] M. Henriksen-Lacey, A. Devitt, Y. Perrie, The vesicle size of DDA:TDB liposomal adjuvants plays a role in the cell-mediated immune response but has no significant effect on antibody production, Journal of controlled release : official journal of the Controlled Release Society, 154 (2011) 131-137.

[23] M. Alam, C.T. Hartrick, Extended-release epidural morphine (DepoDur): an old drug with a new profile, Pain Pract, 5 (2005) 349-353.

[24] C.T. Hartrick, G. Martin, G. Kantor, J. Koncelik, G. Manvelian, Evaluation of a single-dose, extended-release epidural morphine formulation for pain after knee arthroplasty, J Bone Joint Surg Am, 88 (2006) 273-281.

[25] A. Castiglioni, A History of Medicine, Taylor & Francis, 2019.

[26] S. Plotkin, History of vaccination, Proc Natl Acad Sci U S A, 111 (2014) 12283-12287.

[27] B. Greenwood, The contribution of vaccination to global health: past, present and future, Philosophical Transactions of the Royal Society B: Biological Sciences, 369 (2014) 20130433.

[28] D. Gouglas, T. Thanh Le, K. Henderson, A. Kaloudis, T. Danielsen, N.C. Hammersland, J.M. Robinson, P.M. Heaton, J.-A. Røttingen, Estimating the cost of vaccine development against epidemic infectious diseases: a cost minimisation study, The Lancet Global Health, 6 (2018) e1386-e1396.

[29] J.-A. Røttingen, D. Gouglas, M. Feinberg, S. Plotkin, K.V. Raghavan, A. Witty, R. Draghia-Akli, P. Stoffels, P. Piot, New vaccines against epidemic infectious diseases, New England journal of medicine, 376 (2017) 610-613.

[30] Z. Andreadakis, A. Kumar, R.G. Román, S. Tollefsen, M. Saville, S. Mayhew, The COVID-19 vaccine development landscape, Nature reviews. Drug discovery, 19 (2020) 305-306.

[31] J.P. Cramer, Principles of Immunization, in: Travel Medicine, 2019, pp. 65-73.

[32] S. Gordon, Pattern recognition receptors: doubling up for the innate immune response, Cell, 111 (2002) 927-930.

[33] E.P. Widmaier, H. Raff, K.T. Strang, A.J. Vander, Vander's human physiology : the mechanisms of body function, 2016.

[34] T. Lawrence, The nuclear factor NF-kappaB pathway in inflammation, Cold Spring Harb Perspect Biol, 1 (2009) a001651-a001651.

[35] R. Medzhitov, Toll-like receptors and innate immunity, Nature Reviews Immunology, 1 (2001) 135-145.

[36] C. Murdoch, A. Finn, Chemokine receptors and their role in inflammation and infectious diseases, Blood, 95 (2000) 3032-3043.

[37] I.A. Khalil, K. Kogure, H. Akita, H. Harashima, Uptake pathways and subsequent intracellular trafficking in nonviral gene delivery, Pharmacol Rev, 58 (2006) 32-45.

[38] P. Guermonprez, J. Valladeau, L. Zitvogel, C. Théry, S. Amigorena, Antigen presentation and T cell stimulation by dendritic cells, Annu Rev Immunol, 20 (2002) 621-667.

[39] N.L. La Gruta, S. Gras, S.R. Daley, P.G. Thomas, J. Rossjohn, Understanding the drivers of MHC restriction of T cell receptors, Nature Reviews Immunology, 18 (2018) 467-478.

[40] A. Iwasaki, R. Medzhitov, Toll-like receptor control of the adaptive immune responses, Nat Immunol, 5 (2004) 987-995.

[41] D.R. Forsdyke, Lymphocyte repertoire selection and intracellular self/non-self-discrimination: historical overview, Immunol Cell Biol, 93 (2015) 297-304.

[42] X. Michelet, S. Garg, B.J. Wolf, A. Tuli, P. Ricciardi-Castagnoli, M.B. Brenner, MHC Class II Presentation Is Controlled by the Lysosomal Small GTPase, Arl8b, The Journal of Immunology, 194 (2015) 2079.

[43] J.S. Blum, P.A. Wearsch, P. Cresswell, Pathways of antigen processing, Annu Rev Immunol, 31 (2013) 443-473.

[44] E. Ghanem, S. Fritzsche, M. Al-Balushi, J. Hashem, L. Ghuneim, L. Thomer, H. Kalbacher, P. van Endert, E. Wiertz, R. Tampé, S. Springer, The transporter associated with antigen processing (TAP) is active in a post-ER compartment, Journal of Cell Science, 123 (2010) 4271.

[45] J.M.S. Pearce, Louis Pasteur and rabies: a brief note, J Neurol Neurosurg Psychiatry, 73 (2002) 82-82.

[46] I. Hajj Hussein, N. Chams, S. Chams, S. El Sayegh, R. Badran, M. Raad, A. Gerges-Geagea, A. Leone, A. Jurjus, Vaccines Through Centuries: Major Cornerstones of Global Health, Frontiers in Public Health, 3 (2015).

[47] T. Cernuschi, S. Malvolti, E. Nickels, M. Friede, Bacillus Calmette-Guérin (BCG) vaccine: A global assessment of demand and supply balance, Vaccine, 36 (2018) 498-506.

[48] Y. Perrie, R. Kaur, M. Henriksen-Lacey, Vaccines, in: I.F. Uchegbu, A.G. Schätzlein, W.P. Cheng, A. Lalatsa (Eds.) Fundamentals of Pharmaceutical Nanoscience, Springer New York, New York, NY, 2013, pp. 465-491.

[49] L. Roberts, Polio outbreaks in the DRC threaten eradication effort, in, American Association for the Advancement of Science, 2018.

[50] K.M. Thompson, D.A. Kalkowska, Logistical challenges and assumptions for modeling the failure of global cessation of oral poliovirus vaccine (OPV), Expert review of vaccines, 18 (2019) 725-736.

[51] G. Leroux-Roels, Unmet needs in modern vaccinology: adjuvants to improve the immune response, Vaccine, 28 Suppl 3 (2010) C25-36.

[52] X. Zhang, V. Goel, H. Attarwala, M.T. Sweetser, V.A. Clausen, G.J. Robbie, Patisiran Pharmacokinetics, Pharmacodynamics, and Exposure-Response Analyses in the Phase 3 APOLLO Trial in Patients With Hereditary Transthyretin-Mediated (hATTR) Amyloidosis, J Clin Pharmacol, 60 (2020) 37-49.

[53] P.F. McKay, K. Hu, A.K. Blakney, K. Samnuan, J.C. Brown, R. Penn, J. Zhou, C.R. Bouton, P. Rogers, K. Polra, P.J.C. Lin, C. Barbosa, Y.K. Tam, W.S. Barclay, R.J. Shattock, Self-amplifying RNA SARS-CoV-2 lipid nanoparticle vaccine candidate induces high neutralizing antibody titers in mice, Nature Communications, 11 (2020) 3523.

[54] A.B. Vogel, L. Lambert, E. Kinnear, D. Busse, S. Erbar, K.C. Reuter, L. Wicke, M. Perkovic, T. Beissert, H. Haas, S.T. Reece, U. Sahin, J.S. Tregoning, Self-Amplifying RNA Vaccines Give

Equivalent Protection against Influenza to mRNA Vaccines but at Much Lower Doses, Mol Ther, 26 (2018) 446-455.

[55] L.A. Brito, M. Chan, C.A. Shaw, A. Hekele, T. Carsillo, M. Schaefer, J. Archer, A. Seubert, G.R. Otten, C.W. Beard, A.K. Dey, A. Lilja, N.M. Valiante, P.W. Mason, C.W. Mandl, S.W. Barnett, P.R. Dormitzer, J.B. Ulmer, M. Singh, D.T. O'Hagan, A.J. Geall, A cationic nanoemulsion for the delivery of next-generation RNA vaccines, Mol Ther, 22 (2014) 2118-2129.

[56] A.T. Glenny, C.G. Pope, H. Waddington, U. Wallace, Immunological notes. XVII–XXIV, The Journal of Pathology and Bacteriology, 29 (1926) 31-40.

[57] G. Gregoriadis, I. Gursel, M. Gursel, B. McCormack, Liposomes as immunological adjuvants and vaccine carriers, Journal of Controlled Release, 41 (1996) 49-56.

[58] M. Kool, K. Fierens, B.N. Lambrecht, Alum adjuvant: some of the tricks of the oldest adjuvant, J Med Microbiol, 61 (2012) 927-934.

[59] A.C. Allison, G. Gregoriadis, Liposomes as immunological adjuvants, Nature, 252 (1974) 252-252.

[60] D. Christensen, L. Bollehuus Hansen, R. Leboux, W. Jiskoot, J.P. Christensen, P. Andersen, J. Dietrich, A Liposome-Based Adjuvant Containing Two Delivery Systems with the Ability to Induce Mucosal Immunoglobulin A Following a Parenteral Immunization, ACS Nano, 13 (2019) 1116-1126.

[61] C.B. Roces, S. Khadke, D. Christensen, Y. Perrie, Scale-Independent Microfluidic Production of Cationic Liposomal Adjuvants and Development of Enhanced Lymphatic Targeting Strategies, Mol Pharm, 16 (2019) 4372-4386.

[62] A. Di Pasquale, S. Preiss, F. Tavares Da Silva, N. Garcon, Vaccine Adjuvants: from 1920 to 2015 and Beyond, Vaccines (Basel), 3 (2015) 320-343.

[63] S. Tandrup Schmidt, C. Foged, K.S. Korsholm, T. Rades, D. Christensen, Liposome-Based Adjuvants for Subunit Vaccines: Formulation Strategies for Subunit Antigens and Immunostimulators, Pharmaceutics, 8 (2016).

[64] A.K. Dey, I.K. Srivastava, Novel adjuvants and delivery systems for enhancing immune responses induced by immunogens, Expert review of vaccines, 10 (2011) 227-251.

[65] M.S. Duthie, H.P. Windish, C.B. Fox, S.G. Reed, Use of defined TLR ligands as adjuvants within human vaccines, Immunol Rev, 239 (2011) 178-196.

[66] T. Mazumdar, K. Anam, N. Ali, Influence of phospholipid composition on the adjuvanticity and protective efficacy of liposome-encapsulated Leishmania donovani antigens, J Parasitol, 91 (2005) 269-274.

[67] A. Badiee, A. Khamesipour, A. Samiei, D. Soroush, V.H. Shargh, M.T. Kheiri, F. Barkhordari, W. Robert Mc Master, F. Mahboudi, M.R. Jaafari, The role of liposome size on the type of immune response induced in BALB/c mice against leishmaniasis: rgp63 as a model antigen, Exp Parasitol, 132 (2012) 403-409.

[68] J.M. Brewer, L. Tetley, J. Richmond, F.Y. Liew, J. Alexander, Lipid vesicle size determines the Th1 or Th2 response to entrapped antigen, J Immunol, 161 (1998) 4000-4007.

[69] T. Nakanishi, J. Kunisawa, A. Hayashi, Y. Tsutsumi, K. Kubo, S. Nakagawa, H. Fujiwara, T. Hamaoka, T. Mayumi, Positively charged liposome functions as an efficient immunoadjuvant in inducing immune responses to soluble proteins, Biochem Biophys Res Commun, 240 (1997) 793-797.

[70] C. Foged, C. Arigita, A. Sundblad, W. Jiskoot, G. Storm, S. Frokjaer, Interaction of dendritic cells with antigen-containing liposomes: effect of bilayer composition, Vaccine, 22 (2004) 1903-1913.

[71] R. Kaur, V.W. Bramwell, D.J. Kirby, Y. Perrie, Manipulation of the surface pegylation in combination with reduced vesicle size of cationic liposomal adjuvants modifies their clearance kinetics from the injection site, and the rate and type of T cell response, Journal of controlled release : official journal of the Controlled Release Society, 164 (2012) 331-337.

[72] Y. Perrie, E. Kastner, R. Kaur, A. Wilkinson, A.J. Ingham, A case-study investigating the physicochemical characteristics that dictate the function of a liposomal adjuvant, Hum Vaccin Immunother, 9 (2013) 1374-1381.

[73] Y. Zhou, J. Kopeček, Biological rationale for the design of polymeric anti-cancer nanomedicines, J Drug Target, 21 (2013) 1-26.

[74] X.-R. Qi, Zhao, Zhuang, Comparative study of the in vitro and in vivo characteristics of cationic and neutral liposomes, International Journal of Nanomedicine, (2011).

[75] J.H. Senior, K.R. Trimble, R. Maskiewicz, Interaction of positively-charged liposomes with blood: implications for their application in vivo, Biochim Biophys Acta, 1070 (1991) 173-179.

[76] C.R. Miller, B. Bondurant, S.D. McLean, K.A. McGovern, D.F. O'Brien, Liposome−Cell Interactions in Vitro: Effect of Liposome Surface Charge on the Binding and Endocytosis of Conventional and Sterically Stabilized Liposomes, Biochemistry, 37 (1998) 12875-12883.

[77] J.P. Behr, B. Demeneix, J.P. Loeffler, J. Perez-Mutul, Efficient gene transfer into mammalian primary endocrine cells with lipopolyamine-coated DNA, Proc Natl Acad Sci U S A, 86 (1989) 6982-6986.

[78] X. Gao, L. Huang, A novel cationic liposome reagent for efficient transfection of mammalian cells, Biochem Biophys Res Commun, 179 (1991) 280-285.

[79] D.P. Vangasseri, Z. Cui, W. Chen, D.A. Hokey, L.D. Falo, Jr., L. Huang, Immunostimulation of dendritic cells by cationic liposomes, Mol Membr Biol, 23 (2006) 385-395.

[80] K. Lappalainen, I. Jääskeläinen, K. Syrjänen, A. Urtti, S. Syrjänen, Comparison of cell proliferation and toxicity assays using two cationic liposomes, Pharm Res, 11 (1994) 1127-1131.

[81] H. Lv, S. Zhang, B. Wang, S. Cui, J. Yan, Toxicity of cationic lipids and cationic polymers in gene delivery, Journal of controlled release : official journal of the Controlled Release Society, 114 (2006) 100-109.

[82] Y. Tanaka, M. Taneichi, M. Kasai, T. Kakiuchi, T. Uchida, Liposome-coupled antigens are internalized by antigen-presenting cells via pinocytosis and cross-presented to CD8 T cells, PloS one, 5 (2010) e15225-e15225.

[83] Y. Perrie, F. Crofts, A. Devitt, H.R. Griffiths, E. Kastner, V. Nadella, Designing liposomal adjuvants for the next generation of vaccines, Advanced Drug Delivery Reviews, 99 (2016) 85-96.

[84] G. Gregoriadis, C. Davis, Stability of liposomes invivo and invitro is promoted by their cholesterol content and the presence of blood cells, Biochemical and Biophysical Research Communications, 89 (1979) 1287-1293.

[85] B. Moghaddam, M.H. Ali, J. Wilkhu, D.J. Kirby, A.R. Mohammed, Q. Zheng, Y. Perrie, The application of monolayer studies in the understanding of liposomal formulations, Int J Pharm, 417 (2011) 235-244.

[86] T.A. Daly, M. Wang, S.L. Regen, The Origin of Cholesterol's Condensing Effect, Langmuir, 27 (2011) 2159-2161.

[87] L. Redondo-Morata, M.I. Giannotti, F. Sanz, Influence of Cholesterol on the Phase Transition of Lipid Bilayers: A Temperature-Controlled Force Spectroscopy Study, Langmuir, 28 (2012) 12851-12860.

[88] P. Andersen, Effective vaccination of mice against Mycobacterium tuberculosis infection with a soluble mixture of secreted mycobacterial proteins, Infect Immun, 62 (1994) 2536-2544.

[89] D.J. Kirby, R. Kaur, E.M. Agger, P. Andersen, V.W. Bramwell, Y. Perrie, Developing solid particulate vaccine adjuvants: surface bound antigen favours a humoural response, whereas entrapped antigen shows a tendency for cell mediated immunity, Curr Drug Deliv, 10 (2013) 268-278.

[90] S.E. McNeil, I. Rosenkrands, E.M. Agger, P. Andersen, Y. Perrie, Subunit vaccines: distearoylphosphatidylcholine-based liposomes entrapping antigen offer a neutral alternative to dimethyldioctadecylammonium-based cationic liposomes as an adjuvant delivery system, J Pharm Sci, 100 (2011) 1856-1865.

[91] J.M. Zook, W.N. Vreeland, Effects of temperature, acyl chain length, and flow-rate ratio on liposome formation and size in a microfluidic hydrodynamic focusing device, Soft Matter, 6 (2010) 1352.

[92] A. Jahn, S.M. Stavis, J.S. Hong, W.N. Vreeland, D.L. DeVoe, M. Gaitan, Microfluidic Mixing and the Formation of Nanoscale Lipid Vesicles, ACS Nano, 4 (2010) 2077-2087.

[93] A. Jahn, W.N. Vreeland, D.L. DeVoe, L.E. Locascio, M. Gaitan, Microfluidic Directed Formation of Liposomes of Controlled Size, American Chemical Society 23 (2007) 6289-6293.

[94] O.K. Nag, V. Awasthi, Surface engineering of liposomes for stealth behavior, Pharmaceutics, 5 (2013) 542-569.

[95] P.-J. Cardona, A. Milicic, R. Kaur, A. Reyes-Sandoval, C.-K. Tang, J. Honeycutt, Y. Perrie, A.V.S. Hill, Small Cationic DDA:TDB Liposomes as Protein Vaccine Adjuvants Obviate the Need for TLR Agonists in Inducing Cellular and Humoral Responses, PLoS ONE, 7 (2012).

[96] K. Karlsen, K.S. Korsholm, R. Mortensen, S.M. Ghiasi, P. Andersen, C. Foged, D. Christensen, A stable nanoparticulate DDA/MMG formulation acts synergistically with CpG ODN 1826 to enhance the CD4$^+$ T-cell response, Nanomedicine (Lond), 9 (2014) 2625-2638.

[97] M.G. Carstens, M.G. Camps, M. Henriksen-Lacey, K. Franken, T.H. Ottenhoff, Y. Perrie, J.A. Bouwstra, F. Ossendorp, W. Jiskoot, Effect of vesicle size on tissue localization and immunogenicity of liposomal DNA vaccines, Vaccine, 29 (2011) 4761-4770.

[98] A.D. Bangham, A Correlation between Surface Charge and Coagulant Action of Phospholipids, Nature, 192 (1961) 1197-1198.

[99] A.D. Bangham, M.M. Standish, J.C. Watkins, Diffusion of univalent ions across the lamellae of swollen phospholipids, Journal of molecular biology, 13 (1965) 238-252.

[100] R.D. Worsham, V. Thomas, S.S. Faird, Potential of Continous Manufacturing for Liposomal Drug Products, Biotechnology Journal, 14 (2019).

[101] I.V. Zhigaltsev, N. Belliveau, I. Hafez, A.K. Leung, J. Huft, C. Hansen, P.R. Cullis, Bottom-up design and synthesis of limit size lipid nanoparticle systems with aqueous and triglyceride cores using millisecond microfluidic mixing, Langmuir, 28 (2012) 3633-3640.

[102] L.A. Meure, N.R. Foster, F. Dehghani, Conventional and dense gas techniques for the production of liposomes: a review, AAPS PharmSciTech, 9 (2008) 798-809.

[103] S. Batzri, E.D. Korn, Single bilayer liposomes prepared without sonication, Biochimica et Biophysica Acta (BBA) - Biomembranes, 298 (1973) 1015-1019.

[104] C. Jaafar-Maalej, R. Diab, V. Andrieu, A. Elaissari, H. Fessi, Ethanol injection method for hydrophilic and lipophilic drug-loaded liposome preparation, Journal of Liposome Research, 20 (2010) 228-243.

[105] S. Hauschild, U. Lipprandt, A. Rumplecker, U. Borchert, A. Rank, R. Schubert, S. Forster, Direct preparation and loading of lipid and polymer vesicles using inkjets, Small, 1 (2005) 1177-1180.

[106] C. Li, Y. Deng, A novel method for the preparation of liposomes: Freeze drying of monophase solutions, Journal of Pharmaceutical Sciences, 93 (2004) 1403-1414.

[107] A. Wagner, K. Vorauer-Uhl, G. Kreismayr, H. Katinger, The crossflow injection technique: An improvment of the ethanol injection method, Journal of Liposome Research, 12 (2002) 259-270.

[108] P. Shrimal, G. Jadeja, S. Patel, A review on novel methodologies for drug nanoparticle preparation: Microfluidic approach, Chemical Engineering Research and Design, 153 (2020) 728-756.

[109] R. Barnadas-Rodríguez, M. Sabés, Factors involved in the production of liposomes with a high-pressure homogenizer, International journal of pharmaceutics, 213 (2001) 175-186.

[110] M. Riaz, Liposomes preparation methods, Pak J Pharm Sci, 9 (1996) 65-77.

[111] A. Wagner, K. Vorauer-Uhl, Liposome technology for industrial purposes, J Drug Deliv, 2011 (2011) 591325.

[112] A. Akbarzadeh, R. Rezaei-Sadabady, S. Davaran, S.W. Joo, N. Zarghami, Y. Hanifehpour, M. Samiei, M. Kouhi, K. Nejati-Koshki, Liposome: classification, preparation, and applications, Nanoscale Res Lett, 8 (2013) 102-102.

[113] F. Bally, D.K. Garg, C.A. Serra, Y. Hoarau, N. Anton, C. Brochon, D. Parida, T. Vandamme, G. Hadziioannou, Improved size-tunable preparation of polymeric nanoparticles by microfluidic nanoprecipitation, Polymer, 53 (2012) 5045-5051.

[114] B.H. Weigl, R.L. Bardell, C.R. Cabrera, Lab-on-a-chip for drug development, Advanced Drug Delivery Reviews, 55 (2003) 349-377.

[115] G. Lou, G. Anderluzzi, S. Woods, C.W. Roberts, Y. Perrie, A novel microfluidic-based approach to formulate size-tuneable large unilamellar cationic liposomes: Formulation, cellular uptake and biodistribution investigations, Eur J Pharm Biopharm, 143 (2019) 51-60.

[116] C. Webb, S. Khadke, S.T. Schmidt, C.B. Roces, N. Forbes, G. Berrie, Y. Perrie, The Impact of Solvent Selection: Strategies to Guide the Manufacturing of Liposomes Using Microfluidics, Pharmaceutics, 11 (2019).

[117] N. Forbes, M.T. Hussain, M.L. Briuglia, D.P. Edwards, J.H.T. Horst, N. Szita, Y. Perrie, Rapid and scale-independent microfluidic manufacture of liposomes entrapping protein incorporating in-line purification and at-line size monitoring, Int J Pharm, 556 (2019) 68-81.

[118] D. van Swaay, A. deMello, Microfluidic methods for forming liposomes, Lab Chip, 13 (2013) 752-767.

[119] C. van Ballegooie, A. Man, I. Andreu, B.D. Gates, D. Yapp, Using a Microfluidics System to Reproducibly Synthesize Protein Nanoparticles: Factors Contributing to Size, Homogeneity, and Stability, Processes, 7 (2019).

[120] N. Dimov, E. Kastner, M. Hussain, Y. Perrie, N. Szita, Formation and purification of tailored liposomes for drug delivery using a module-based micro continuous-flow system, Scientific Reports, 7 (2017).

[121] M. Guimaraes Sa Correia, M.L. Briuglia, F. Niosi, D.A. Lamprou, Microfluidic manufacturing of phospholipid nanoparticles: Stability, encapsulation efficacy, and drug release, Int J Pharm, 516 (2017) 91-99.

[122] W.S. Lin, N. Malmstadt, Liposome production and concurrent loading of drug simulants by microfluidic hydrodynamic focusing, Eur Biophys J, 48 (2019) 549-558.

[123] T.M. Squires, S.R. Quake, Microfluidics: Fluid physics at the nanoliter scale, Reviews of Modern Physics, 77 (2005) 977-1026.

[124] A.J. DeMello, Control and detection of chemical reactions in microfluidic systems, Nature, 442 (2006) 394-402.

[125] D.A. Beard, Taylor dispersion of a solute in a microfluidic channel, Journal of Applied Physics, 89 (2001) 4667-4669.

[126] N.-T. Nguyen, Z. Wu, Micromixers—a review, Journal of Micromechanics and Microengineering, 15 (2005) R1-R16.

[127] H.A. Stone, A.D. Stroock, A. Ajdari, Engineering Flows in Small Devices, Annual Review of Fluid Mechanics, 36 (2004) 381-411.

[128] L. Capretto, W. Cheng, M. Hill, X. Zhang, Micromixing Within Microfluidic Devices, in: B. Lin (Ed.) Microfluidics: Technologies and Applications, Springer Berlin Heidelberg, Berlin, Heidelberg, 2011, pp. 27-68.

[129] A.D. Stroock, S.K. Dertinger, A. Ajdari, I. Mezić, H.A. Stone, G.M. Whitesides, Chaotic Mixer for Microchannels, American Association for the Advancement of Science, 295 (2002) 647-651.

[130] M. Bayareh, M.N. Ashani, A. Usefian, Active and passive micromixers: A comprehensive review, Chemical Engineering and Processing - Process Intensification, 147 (2020) 107771.

[131] T.M. Floyd-Smith, J.P. Golden, P.B. Howell, F.S. Ligler, Characterization of passive microfluidic mixers fabricated using soft lithography, Microfluidics and Nanofluidics, 2 (2006) 180-183.

[132] K. Ward, Z.H. Fan, Mixing in microfluidic devices and enhancement methods, J Micromech Microeng, 25 (2015).

[133] M.A. Obeid, I. Khadra, A. Albaloushi, M. Mullin, H. Alyamani, V.A. Ferro, Microfluidic manufacturing of different niosomes nanoparticles for curcumin encapsulation: Physical characteristics, encapsulation efficacy, and drug release, Beilstein J Nanotechnol, 10 (2019) 1826-1832.

[134] T. Yanagi, K. Tachikawa, R. Wilkie-Grantham, A. Hishiki, K. Nagai, E. Toyonaga, P. Chivukula, S. Matsuzawa, Lipid Nanoparticle-mediated siRNA Transfer Against PCTAIRE1/PCTK1/Cdk16 Inhibits In Vivo Cancer Growth, Mol Ther Nucleic Acids, 5 (2016) e327.

[135] P.B. Howell, Jr., D.R. Mott, J.P. Golden, F.S. Ligler, Design and evaluation of a Dean vortex-based micromixer, Lab Chip, 4 (2004) 663-669.

[136] Y. Wang, Q. Dong, P. Wang, Numerical Investigation on Fluid Flow in a 90-Degree Curved Pipe with Large Curvature Ratio, Mathematical Problems in Engineering, 2015 (2015) 548262.

[137] N.M. Belliveau, J. Huft, P.J. Lin, S. Chen, A.K. Leung, T.J. Leaver, A.W. Wild, J.B. Lee, R.J. Taylor, Y.K. Tam, C.L. Hansen, P.R. Cullis, Microfluidic Synthesis of Highly Potent Limit-size Lipid Nanoparticles for In Vivo Delivery of siRNA, Mol Ther Nucleic Acids, 1 (2012) e37.

[138] L.K. Yeo, T.O.B. Olusanya, C.S. Chaw, A.A. Elkordy, Brief Effect of a Small Hydrophobic Drug (Cinnarizine) on the Physicochemical Characterisation of Niosomes Produced by Thin-Film Hydration and Microfluidic Methods, Pharmaceutics, 10 (2018).

[139] Y. Morikawa, T. Tagami, A. Hoshikawa, T. Ozeki, The Use of an Efficient Microfluidic Mixing System for Generating Stabilized Polymeric Nanoparticles for Controlled Drug Release, Biological and Pharmaceutical Bulletin, 41 (2018) 899-907.

[140] J.A. Kulkarni, Y.Y.C. Tam, S. Chen, J. Zaifman, P.R. Cullis, S. Biswas, Rapid synthesis of lipid nanoparticles containing hydrophobic inorganic nanoparticles, Nanoscale, 9 (2017).

[141] S. Ding, C.A. Serra, N. Anton, W. Yu, T.F. Vandamme, Production of dry-state ketoprofen-encapsulated PMMA NPs by coupling micromixer-assisted nanoprecipitation and spray drying, Int J Pharm, 558 (2019) 1-8.

[142] A. Dobhal, A. Kulkarni, P. Dandekar, R. Jain, A microreactor-based continuous process for controlled synthesis of poly-methyl-methacrylate-methacrylic acid (PMMA) nanoparticles, Journal of Materials Chemistry B, 5 (2017) 3404-3417.

[143] S. de Paiva Lacerda, F. Espitalier, V. Hoffart, M.I. Ré, Liquid anti-solvent recrystallization to enhance dissolution of CRS 74, a new antiretroviral drug, Drug Development and Industrial Pharmacy, 41 (2015) 1910-1920.

[144] X. Zhang, H. Chen, F. Qian, Y. Cheng, Preparation of itraconazole nanoparticles by anti-solvent precipitation method using a cascaded microfluidic device and an ultrasonic spray drier, Chemical Engineering Journal, 334 (2018) 2264-2272.

[145] P. Patil, G. Khairnar, J. Naik, Preparation and statistical optimization of Losartan Potassium loaded nanoparticles using Box Behnken factorial design: Microreactor precipitation, Chemical Engineering Research and Design, 104 (2015) 98-109.

[146] M. Bramosanti, L. Chronopoulou, F. Grillo, A. Valletta, C. Palocci, Microfluidic-assisted nanoprecipitation of antiviral-loaded polymeric nanoparticles, Colloids and Surfaces A: Physicochemical and Engineering Aspects, 532 (2017) 369-376.

[147] L. Chronopoulou, C. Sparago, C. Palocci, A modular microfluidic platform for the synthesis of biopolymeric nanoparticles entrapping organic actives, Journal of Nanoparticle Research, 16 (2014).

[148] R.R. Hood, W.N. Vreeland, D.L. DeVoe, Microfluidic remote loading for rapid single-step liposomal drug preparation, Lab Chip, 14 (2014) 3359-3367.

[149] S.D. Schaber, D.I. Gerogiorgis, R. Ramachandran, J.M.B. Evans, P.I. Barton, B.L. Trout, Economic Analysis of Integrated Continuous and Batch Pharmaceutical Manufacturing: A Case Study, Industrial & Engineering Chemistry Research, 50 (2011) 10083-10092.

[150] FDA, Drug shortages: Root causes and potential solutions, in: D.S.T. Force (Ed.), 2019, pp. 1 - 124.

[151] D.G. Fatouros, S.G. Antimisiaris, Effect of amphiphilic drugs on the stability and zeta-potential of their liposome formulations: a study with prednisolone, diazepam, and griseofulvin, J Colloid Interface Sci, 251 (2002) 271-277.

[152] D. Chatzikleanthous, S.T. Schmidt, G. Buffi, I. Paciello, R. Cunliffe, F. Carboni, M.R. Romano, D.T. O'Hagan, U. D'Oro, S. Woods, C.W. Roberts, Y. Perrie, R. Adamo, Design of a novel vaccine nanotechnology-based delivery system comprising CpGODN-protein conjugate anchored to liposomes, Journal of Controlled Release, 323 (2020) 125-137.

[153] D. Carugo, E. Bottaro, J. Owen, E. Stride, C. Nastruzzi, Liposome production by microfluidics: potential and limiting factors, Sci Rep, 6 (2016) 25876.

[154] ICH, Harmonised Tripartite Guideline, Impurities: Guideline for residual solvents Q3C (R5), Current Step, 4 (2016) 1-25.

[155] J.S. Hong, S.M. Stavis, S.H. DePaoli Lacerda, L.E. Locascio, S.R. Raghavan, M. Gaitan, Microfluidic directed self-assembly of liposome-hydrogel hybrid nanoparticles, Langmuir, 26 (2010) 11581-11588.

[156] Malvern, Dynamic Light Scattering : An Introduction in 30 Minutes, in, 2014.

[157] E. Kastner, Y. Perrie, Particle Size Analysis of Micro and Nanoparticles, in: A. Müllertz, Y. Perrie, T. Rades (Eds.) Analytical Techniques in the Pharmaceutical Sciences, Springer New York, New York, NY, 2016, pp. 677-699.

[158] ISO, ISO 22412:2017 Particle size analysis — Dynamic light scattering (DLS), in, International Organization for Standardization, Geneva, Switzerland, 2017.

[159] K. Hac-Wydro, P. Wydro, A. Jagoda, J. Kapusta, The study on the interaction between phytosterols and phospholipids in model membranes, Chem Phys Lipids, 150 (2007) 22-34.

[160] M.L. Briuglia, C. Rotella, A. McFarlane, D.A. Lamprou, Influence of cholesterol on liposome stability and on in vitro drug release, Drug Deliv Transl Res, 5 (2015) 231-242.

[161] A. Reis, C.M. Spickett, Chemistry of phospholipid oxidation, Biochim Biophys Acta, 1818 (2012) 2374-2387.

[162] R. Michel, T. Plostica, L. Abezgauz, D. Danino, M. Gradzielski, Control of the stability and structure of liposomes by means of nanoparticles, Soft Matter, 9 (2013).

[163] J.W. Virden, J.C. Berg, Sodium chloride-induced aggregation of dipalmitoylphoshpatidylglycerol small unilamellar vesicles with varying amounts of incorporated cholesterol, Langmuir, 8 (1992) 1532-1537.

[164] S.C. Semple, A. Chonn, P.R. Cullis, Influence of cholesterol on the association of plasma proteins with liposomes, Biochemistry, 35 (1996) 2521-2525.

[165] R.M. Epand, R.F. Epand, S. Maekawa, The arrangement of cholesterol in membranes and binding of NAP-22, Chem Phys Lipids, 122 (2003) 33-39.

[166] G. Gregoriadis, Drug entrapment in liposomes, FEBS Lett, 36 (1973) 292-296.

[167] L. Krupp, A.V. Chobanian, P.I. Brecher, The in vivo transformation of phospholipid vesicles to a particle resembling HDL in the rat, Biochemical and Biophysical Research Communications, 72 (1976) 1251-1258.

[168] G. Scherphof, F. Roerdink, M. Waite, J. Parks, Disintegration of phosphatidylcholine liposomes in plasma as a result of interaction with high-density lipoproteins, Biochim Biophys Acta, 542 (1978) 296-307.

[169] C. Kirby, J. Clarke, G. Gregoriadis, Effect of the Cholesterol Content of Small Unilamellar Liposomes on their Stability in vivo and in vitro, Journal of Biochemistry, 186 (1979) 591-598.

[170] B.D. Ladbrooke, R.M. Williams, D. Chapman, Studies on lecithin-cholesterol-water interactions by differential scanning calorimetry and X-ray diffraction, Biochim Biophys Acta, 150 (1968) 333-340.

[171] R.A. Demel, B. De Kruyff, The function of sterols in membranes, Biochim Biophys Acta, 457 (1976) 109-132.

[172] S. Imaizumi, I. Hatta, Binary Mixtures of Phospholipids and Cholesterol Studied by Dynamic Heat Capacity Measurements, Journal of the Physical Society of Japan, 53 (1984) 4476-4487.

[173] I. Hatta, Temperature scanning X-ray diffraction at phase transitions of biologically related lipid assemblies: Special attention to cholestrol-rich state, Journal of Thermal Analysis and Calorimetry, 82 (2005) 189-192.

[174] J. Genova, I. Bivas, R. Marinov, Cholesterol influence on the bending elasticity of lipid membranes, Colloids and Surfaces A: Physicochemical and Engineering Aspects, 460 (2014) 79-82.

[175] G.N. Devaraj, S.R. Parakh, R. Devraj, S.S. Apte, B.R. Rao, D. Rambhau, Release studies on niosomes containing fatty alcohols as bilayer stabilizers instead of cholesterol, J Colloid Interface Sci, 251 (2002) 360-365.

[176] M. Maeki, Y. Fujishima, Y. Sato, T. Yasui, N. Kaji, A. Ishida, H. Tani, Y. Baba, H. Harashima, M. Tokeshi, Understanding the formation mechanism of lipid nanoparticles in microfluidic devices with chaotic micromixers, PLoS One, 12 (2017) e0187962.

[177] A. Jahn, W.N. Vreeland, D.L. DeVoe, L.E. Locascio, M. Gaitan, Microfluidic Directed Formation of Liposomes of Controlled Size, American Chemical Society, 23 (2007) 6289-6293.

[178] M. Wehbe, A. Malhotra, M. Anantha, J. Roosendaal, A.W.Y. Leung, D. Plackett, K. Edwards, R. Gilabert-Oriol, M.B. Bally, A simple passive equilibration method for loading carboplatin into pre-formed liposomes incubated with ethanol as a temperature dependent permeability enhancer, Journal of controlled release : official journal of the Controlled Release Society, 252 (2017) 50-61.

[179] R. Tran, S. Ho, P. Dea, Effects of ethanol on lipid bilayers with and without cholesterol: the distearoylphosphatidylcholine system, Biophys Chem, 110 (2004) 39-47.

[180] Helgi I. Ingólfsson, Olaf S. Andersen, Alcohol's Effects on Lipid Bilayer Properties, Biophysical Journal, 101 (2011) 847-855.

[181] J.W. Zeng, P.L. Chong, Interactions between pressure and ethanol on the formation of interdigitated DPPC liposomes: a study with Prodan fluorescence, Biochemistry, 30 (1991) 9485-9491.

[182] J.A. Barry, K. Gawrisch, Direct NMR evidence for ethanol binding to the lipid-water interface of phospholipid bilayers, Biochemistry, 33 (1994) 8082-8088.

[183] A. Belay, E. Libnedengel, H.K. Kim, Y.H. Hwang, Effects of solvent polarity on the absorption and fluorescence spectra of chlorogenic acid and caffeic acid compounds: determination of the dipole moments, Luminescence, 31 (2016) 118-126.

[184] A. Zizzari, M. Bianco, L. Carbone, E. Perrone, F. Amato, G. Maruccio, F. Rendina, V. Arima, Continuous-Flow Production of Injectable Liposomes via a Microfluidic Approach, Materials (Basel), 10 (2017).

[185] Merck, A Hands-On Guide to Ultrafiltration/ Diafiltra®tion Optimization using Pellicon Cassettes, in, 2013, pp. 1-12
.

[186] G.H. Bio-Science, Cross Flow Filtration Method Handbook, in, 2014, pp. 1-82.

[187] M.T. Hussain, N. Forbes, Y. Perrie, Comparative Analysis of Protein Quantification Methods for the Rapid Determination of Protein Loading in Liposomal Formulations, Pharmaceutics, 11 (2019).

[188] L. Sercombe, T. Veerati, F. Moheimani, S.Y. Wu, A.K. Sood, S. Hua, Advances and Challenges of Liposome Assisted Drug Delivery, Front Pharmacol, 6 (2015) 286.

[189] A.S. Fauci, H.C. Lane, R.R. Redfield, Covid-19 — Navigating the Uncharted, New England Journal of Medicine, 382 (2020) 1268-1269.

[190] Y. Dong, T. Dai, Y. Wei, L. Zhang, M. Zheng, F. Zhou, A systematic review of SARS-CoV-2 vaccine candidates, Signal Transduction and Targeted Therapy, 5 (2020) 237.

[191] E.J. Anderson, N.G. Rouphael, A.T. Widge, L.A. Jackson, P.C. Roberts, M. Makhene, J.D. Chappell, M.R. Denison, L.J. Stevens, A.J. Pruijssers, A.B. McDermott, B. Flach, B.C. Lin, N.A. Doria-Rose, S. O'Dell, S.D. Schmidt, K.S. Corbett, P.A. Swanson, 2nd, M. Padilla, K.M. Neuzil, H. Bennett, B. Leav, M. Makowski, J. Albert, K. Cross, V.V. Edara, K. Floyd, M.S. Suthar, D.R. Martinez, R. Baric, W. Buchanan, C.J. Luke, V.K. Phadke, C.A. Rostad, J.E. Ledgerwood, B.S. Graham, J.H. Beigel, Safety and Immunogenicity of SARS-CoV-2 mRNA-1273 Vaccine in Older Adults, N Engl J Med, 383 (2020) 2427-2438.

[192] N. Pardi, M.J. Hogan, F.W. Porter, D. Weissman, mRNA vaccines - a new era in vaccinology, Nat Rev Drug Discov, 17 (2018) 261-279.

[193] Y. Zhang, G. Zeng, H. Pan, C. Li, Y. Hu, K. Chu, W. Han, Z. Chen, R. Tang, W. Yin, X. Chen, Y. Hu, X. Liu, C. Jiang, J. Li, M. Yang, Y. Song, X. Wang, Q. Gao, F. Zhu, Safety, tolerability, and immunogenicity of an inactivated SARS-CoV-2 vaccine in healthy adults aged 18–59 years: a

randomised, double-blind, placebo-controlled, phase 1/2 clinical trial, The Lancet Infectious Diseases, 21 (2021) 181-192.

[194] ISRCTN17072692, Clinical trial to assess the safety of a coronavirus vaccine in healthy men and women, in, 2020.

[195] NCT04480957, Ascending Dose Study of Investigational SARS-CoV-2 Vaccine ARCT-021 in Healthy Adult Subjects, in, 2020.

[196] A.K. Blakney, P. Deletic, P.F. McKay, C.R. Bouton, M. Ashford, R.J. Shattock, A. Sabirsh, Effect of complexing lipids on cellular uptake and expression of messenger RNA in human skin explants, Journal of Controlled Release, 330 (2021) 1250-1261.

[197] A. Jahn, W.N. Vreeland, M. Gaitan, L.E. Locascio, Controlled Vesicle Self-Assembly in Microfluidic Channels with

Hydrodynamic Focusing, Journal of the American Chemical Society, 126 (2004) 2672-2675.

[198] S. Khadke, C.B. Roces, A. Cameron, A. Devitt, Y. Perrie, Formulation and manufacturing of lymphatic targeting liposomes using microfluidics, Journal of controlled release : official journal of the Controlled Release Society, (2019).

[199] M.A. Ansari, K.-Y. Kim, K. Anwar, S.M. Kim, A novel passive micromixer based on unbalanced splits and collisions of fluid streams, Journal of Micromechanics and Microengineering, 20 (2010).

[200] C.K. Chung, T.R. Shih, B.H. Wu, C.K. Chang, Design and mixing efficiency of rhombic micromixer with flat angles, Microsystem Technologies, 16 (2010) 1595-1600.

[201] M. Juraeva, D.J. Kang, Mixing Performance of a Cross-Channel Split-and-Recombine Micro-Mixer Combined with Mixing Cell, Micromachines (Basel), 11 (2020).

[202] A.U. Andar, R.R. Hood, W.N. Vreeland, D.L. Devoe, P.W. Swaan, Microfluidic preparation of liposomes to determine particle size influence on cellular uptake mechanisms, Pharm Res, 31 (2014) 401-413.

[203] R.R. Shah, D.T. O'Hagan, M.M. Amiji, L.A. Brito, The impact of size on particulate vaccine adjuvants, Nanomedicine, 9 (2014) 2671-2681.

[204] P.C. Soema, G.J. Willems, W. Jiskoot, J.P. Amorij, G.F. Kersten, Predicting the influence of liposomal lipid composition on liposome size, zeta potential and liposome-induced dendritic cell maturation using a design of experiments approach, Eur J Pharm Biopharm, 94 (2015) 427-435.

[205] R.J. Kessler, D.D. Fanestil, Interference by lipids in the determination of protein using bicinchoninic acid, Anal Biochem, 159 (1986) 138-142.

[206] J. Colletier, Chaize, B,, Winterhlater, M., Fournuer D., Protein encapsulation in liposomes: efficiency depends on interactions between protein and phospholipid bilayer, BMC Biotechnology, 2 (2002) 1-8.

[207] R. Molinaro, M. Evangelopoulos, J.R. Hoffman, C. Corbo, F. Taraballi, J.O. Martinez, K.A. Hartman, D. Cosco, G. Costa, I. Romeo, M. Sherman, D. Paolino, S. Alcaro, E. Tasciotti, Design and Development of Biomimetic Nanovesicles Using a Microfluidic Approach, Adv Mater, 30 (2018) e1702749.

[208] S.W.Z. Lim, Y.S. Wong, B. Czarny, S. Venkatraman, Microfluidic-directed self-assembly of liposomes: Role of interdigitation, Journal of Colloid and Interface Science, 578 (2020) 47-57.

[209] C. Webb, N. Forbes, C.B. Roces, G. Anderluzzi, G. Lou, S. Abraham, L. Ingalls, K. Marshall, T.J. Leaver, J.A. Watts, J.W. Aylott, Y. Perrie, Using microfluidics for scalable manufacturing of nanomedicines from bench to GMP: A case study using protein-loaded liposomes, International Journal of Pharmaceutics, 582 (2020).

[210] M. Mijajlovic, D. Wright, V. Zivkovic, J.X. Bi, M.J. Biggs, Microfluidic hydrodynamic focusing based synthesis of POPC liposomes for model biological systems, Colloids Surf B Biointerfaces, 104 (2013) 276-281.

[211] E. Kastner, R. Kaur, D. Lowry, B. Moghaddam, A. Wilkinson, Y. Perrie, High-throughput manufacturing of size-tuned liposomes by a new microfluidics method using enhanced statistical tools for characterization, International Journal of Pharmaceutics, 477 (2014) 361-368.

[212] S.M. Phapal, P. Sunthar, Influence of micro-mixing on the size of liposomes self-assembled from miscible liquid phases, Chem Phys Lipids, 172-173 (2013) 20-30.

[213] D. Talley, B. Cutak, E. Rathbone, T. Al -Kolla, D. Allison, J. Blasberg, K. Kao, M. Caple, Synthechol™ Ynthetic Cholesterol for Cholesterol Dependent Cell Culture — Development of Non-Animal Derived Chemically Defined NS0 Medium, in: F. Gòdia, M. Fussenegger (Eds.) Animal Cell Technology Meets Genomics, Springer Netherlands, Dordrecht, 2005, pp. 577-580.

[214] M. Sedighi, S. Sieber, F. Rahimi, M.-A. Shahbazi, A.H. Rezayan, J. Huwyler, D. Witzigmann, Rapid optimization of liposome characteristics using a combined microfluidics and design-of-experiment approach, Drug Delivery and Translational Research, 9 (2019) 404-413.

[215] P. Pradhan, J. Guan, D. Lu, P.G. Wang, L.J. Lee, R.J. Lee, A facile microfluidic method for production of liposomes, Anticancer Res, 28 (2008) 943-947.

[216] J.M.H. Kremer, M.W. Van der Esker, C. Pathmamanoharan, P.H. Wiersema, Vesicles of variable diameter prepared by a modified injection method, Biochemistry, 16 (1977) 3932-3935.

[217] E.V. Orlova, M.B. Sherman, W. Chiu, H. Mowri, L.C. Smith, A.M. Gotto, Three-dimensional structure of low density lipoproteins by electron cryomicroscopy, Proceedings of the National Academy of Sciences, 96 (1999) 8420-8425.

[218] D. Kirschneck, G. Tekautz, Integration of a Microreactor in an Existing Production Plant, Chemical Engineering & Technology, 30 (2007) 305-308.

[219] M.J. Huter, J. Strube, Model-Based Design and Process Optimization of Continuous Single Pass Tangential Flow Filtration Focusing on Continuous Bioprocessing, Processes, 7 (2019).

[220] K.S. Corbett, D.K. Edwards, S.R. Leist, O.M. Abiona, S. Boyoglu-Barnum, R.A. Gillespie, S. Himansu, A. Schafer, C.T. Ziwawo, A.T. DiPiazza, K.H. Dinnon, S.M. Elbashir, C.A. Shaw, A. Woods, E.J. Fritch, D.R. Martinez, K.W. Bock, M. Minai, B.M. Nagata, G.B. Hutchinson, K. Wu, C. Henry, K. Bahl, D. Garcia-Dominguez, L. Ma, I. Renzi, W.P. Kong, S.D. Schmidt, L. Wang, Y. Zhang, E. Phung, L.A. Chang, R.J. Loomis, N.E. Altaras, E. Narayanan, M. Metkar, V. Presnyak, C. Liu, M.K. Louder, W. Shi, K. Leung, E.S. Yang, A. West, K.L. Gully, L.J. Stevens, N. Wang, D. Wrapp, N.A. Doria-Rose, G. Stewart-Jones, H. Bennett, G.S. Alvarado, M.C. Nason, T.J. Ruckwardt, J.S. McLellan, M.R. Denison, J.D. Chappell, I.N. Moore, K.M. Morabito, J.R. Mascola, R.S. Baric, A. Carfi, B.S. Graham, SARS-CoV-2 mRNA vaccine design enabled by prototype pathogen preparedness, Nature, 586 (2020) 567-571.

[221] A.B. Vogel, I. Kanevsky, Y. Che, K.A. Swanson, A. Muik, M. Vormehr, L.M. Kranz, K.C. Walzer, S. Hein, A. Güler, J. Loschko, M.S. Maddur, A. Ota-Setlik, K. Tompkins, J. Cole, B.G. Lui, T. Ziegenhals, A. Plaschke, D. Eisel, S.C. Dany, S. Fesser, S. Erbar, F. Bates, D. Schneider, B. Jesionek, B. Sänger, A.-K. Wallisch, Y. Feuchter, H. Junginger, S.A. Krumm, A.P. Heinen, P. Adams-Quack, J. Schlereth, S. Schille, C. Kröner, R. de la Caridad Güimil Garcia, T. Hiller, L. Fischer, R.S. Sellers, S. Choudhary, O. Gonzalez, F. Vascotto, M.R. Gutman, J.A. Fontenot, S.

Hall-Ursone, K. Brasky, M.C. Griffor, S. Han, A.A.H. Su, J.A. Lees, N.L. Nedoma, E.H. Mashalidis, P.V. Sahasrabudhe, C.Y. Tan, D. Pavliakova, G. Singh, C. Fontes-Garfias, M. Pride, I.L. Scully, T. Ciolino, J. Obregon, M. Gazi, R. Carrion, K.J. Alfson, W.V. Kalina, D. Kaushal, P.-Y. Shi, T. Klamp, C. Rosenbaum, A.N. Kuhn, Ö. Türeci, P.R. Dormitzer, K.U. Jansen, U. Sahin, BNT162b vaccines protect rhesus macaques from SARS-CoV-2, Nature, 592 (2021) 283-289.

[222] P.A. Bovier, Epaxal: a virosomal vaccine to prevent hepatitis A infection, Expert review of vaccines, 7 (2008) 1141-1150.

[223] R. Mischler, I.C. Metcalfe, Inflexal V a trivalent virosome subunit influenza vaccine: production, Vaccine, 20 Suppl 5 (2002) B17-23.

[224] M. Henriksen-Lacey, D. Christensen, V.W. Bramwell, T. Lindenstrom, E.M. Agger, P. Andersen, Y. Perrie, Liposomal cationic charge and antigen adsorption are important properties for the efficient deposition of antigen at the injection site and ability of the vaccine to induce a CMI response, Journal of controlled release : official journal of the Controlled Release Society, 145 (2010) 102-108.

[225] D. Christensen, M. Henriksen-Lacey, A.T. Kamath, T. Lindenstrøm, K.S. Korsholm, J.P. Christensen, A.-F. Rochat, P.-H. Lambert, P. Andersen, C.-A. Siegrist, Y. Perrie, E.M. Agger, A cationic vaccine adjuvant based on a saturated quaternary ammonium lipid have different in vivo distribution kinetics and display a distinct CD4 T cell-inducing capacity compared to its unsaturated analog, Journal of controlled release : official journal of the Controlled Release Society, 160 (2012) 468-476.

[226] R. Kaur, M. Henriksen-Lacey, J. Wilkhu, A. Devitt, D. Christensen, Y. Perrie, Effect of incorporating cholesterol into DDA:TDB liposomal adjuvants on bilayer properties, biodistribution, and immune responses, Mol Pharm, 11 (2014) 197-207.

[227] M.L. De Temmerman, J. Rejman, J. Demeester, D.J. Irvine, B. Gander, S.C. De Smedt, Particulate vaccines: on the quest for optimal delivery and immune response, Drug Discov Today, 16 (2011) 569-582.

[228] C.B. Roces, E. Kastner, P. Stone, D. Lowry, Y. Perrie, Rapid Quantification and Validation of Lipid Concentrations within Liposomes, Pharmaceutics, 8 (2016).

[229] C.B. Roces, G. Lou, N. Jain, S. Abraham, A. Thomas, G.W. Halbert, Y. Perrie, Manufacturing Considerations for the Development of Lipid Nanoparticles Using Microfluidics, Pharmaceutics, 12 (2020).

[230] N.S. Arden, A.C. Fisher, K. Tyner, L.X. Yu, S.L. Lee, M. Kopcha, Industry 4.0 for pharmaceutical manufacturing: Preparing for the smart factories of the future, Int J Pharm, 602 (2021) 120554.

[231] M. Sarkis, A. Bernardi, N. Shah, M.M. Papathanasiou, Emerging Challenges and Opportunities in Pharmaceutical Manufacturing and Distribution, Processes, 9 (2021).

[232] C. Su, Y. Xia, J. Sun, N. Wang, L. Zhu, T. Chen, Y. Huang, D. Liang, Liposomes Physically Coated with Peptides: Preparation and Characterization, Langmuir, 30 (2014) 6219-6227.

[233] P. Skupin-Mrugalska, T. Zalewski, P.A. Elvang, G. Nowaczyk, M. Czajkowski, H. Piotrowska-Kempisty, Insight into theranostic nanovesicles prepared by thin lipid hydration and microfluidic method, Colloids and Surfaces B: Biointerfaces, 205 (2021) 111871.

[234] D. Pozzi, C. Marchini, F. Cardarelli, A. Rossetta, V. Colapicchioni, A. Amici, M. Montani, S. Motta, P. Brocca, L. Cantù, G. Caracciolo, Mechanistic Understanding of Gene Delivery Mediated by Highly Efficient Multicomponent Envelope-Type Nanoparticle Systems, Molecular Pharmaceutics, 10 (2013) 4654-4665.

[235] F. Giulimondi, L. Digiacomo, D. Pozzi, S. Palchetti, E. Vulpis, A.L. Capriotti, R.Z. Chiozzi, A. Laganà, H. Amenitsch, L. Masuelli, G. Peruzzi, M. Mahmoudi, I. Screpanti, A. Zingoni, G.

Caracciolo, Interplay of protein corona and immune cells controls blood residency of liposomes, Nature Communications, 10 (2019) 3686.

[236] D. Pozzi, C. Marianecci, M. Carafa, C. Marchini, M. Montani, A. Amici, G. Caracciolo, Programmed packaging of multicomponent envelope-type nanoparticle system for gene delivery, Applied Physics Letters, 96 (2010) 183702.

[237] M. Hamborg, L. Jorgensen, A.R. Bojsen, D. Christensen, C. Foged, Protein antigen adsorption to the DDA/TDB liposomal adjuvant: effect on protein structure, stability, and liposome physicochemical characteristics, Pharm Res, 30 (2013) 140-155.

[238] K.S. Korsholm, E.M. Agger, C. Foged, D. Christensen, J. Dietrich, C.S. Andersen, C. Geisler, P. Andersen, The adjuvant mechanism of cationic dimethyldioctadecylammonium liposomes, Immunology, 121 (2007) 216-226.

[239] V.P. Zhdanov, B. Kasemo, Adsorption of proteins on a lipid bilayer, European Biophysics Journal, 39 (2010) 1477-1482.

[240] C.D. Walkey, W.C. Chan, Understanding and controlling the interaction of nanomaterials with proteins in a physiological environment, Chemical Society Reviews, 41 (2012) 2780-2799.

[241] S. Tenzer, D. Docter, J. Kuharev, A. Musyanovych, V. Fetz, R. Hecht, F. Schlenk, D. Fischer, K. Kiouptsi, C. Reinhardt, Rapid formation of plasma protein corona critically affects nanoparticle pathophysiology, Nature nanotechnology, 8 (2013) 772-781.

[242] T. Cedervall, I. Lynch, S. Lindman, T. Berggård, E. Thulin, H. Nilsson, K.A. Dawson, S. Linse, Understanding the nanoparticle–protein corona using methods to quantify exchange rates and affinities of proteins for nanoparticles, Proceedings of the National Academy of Sciences, 104 (2007) 2050-2055.

[243] I. Lynch, K.A. Dawson, Protein-nanoparticle interactions, Nano today, 3 (2008) 40-47.

[244] S.R. Saptarshi, A. Duschl, A.L. Lopata, Interaction of nanoparticles with proteins: relation to bio-reactivity of the nanoparticle, Journal of Nanobiotechnology, 11 (2013) 26.

[245] S. May, D. Harries, A. Ben-Shaul, Lipid demixing and protein-protein interactions in the adsorption of charged proteins on mixed membranes, Biophysical journal, 79 (2000) 1747-1760.

[246] H. Moustaoui, J. Saber, I. Djeddi, Q. Liu, D. Movia, A. Prina-Mello, J. Spadavecchia, M. Lamy de la Chapelle, N. Djaker, A protein corona study by scattering correlation spectroscopy: a comparative study between spherical and urchin-shaped gold nanoparticles, Nanoscale, 11 (2019) 3665-3673.

[247] W. Shang, J.H. Nuffer, J.S. Dordick, R.W. Siegel, Unfolding of ribonuclease A on silica nanoparticle surfaces, Nano Lett, 7 (2007) 1991-1995.

[248] S.H. Lacerda, J.J. Park, C. Meuse, D. Pristinski, M.L. Becker, A. Karim, J.F. Douglas, Interaction of gold nanoparticles with common human blood proteins, ACS Nano, 4 (2010) 365-379.

[249] H.C. Loughrey, K.F. Wong, L.S. Choi, P.R. Cullis, M.B. Bally, Protein-liposome conjugates with defined size distributions, Biochim Biophys Acta, 1028 (1990) 73-81.

[250] R. Bredehorst, F.S. Ligler, A.W. Kusterbeck, E.L. Chang, B.P. Gaber, C.W. Vogel, Effect of covalent attachment of immunoglobulin fragments on liposomal integrity, Biochemistry, 25 (1986) 5693-5698.

[251] T.D. Heath, R.T. Fraley, D. Papahdjopoulos, Antibody targeting of liposomes: cell specificity obtained by conjugation of F(ab')2 to vesicle surface, Science, 210 (1980) 539-541.

[252] C.B. Roces, E.C. Port, N.N. Daskalakis, J.A. Watts, J.W. Aylott, G.W. Halbert, Y. Perrie, Rapid scale-up and production of active-loaded PEGylated liposomes, International Journal of Pharmaceutics, 586 (2020) 119566.

[253] M.H. Ali, B. Moghaddam, D.J. Kirby, A.R. Mohammed, Y. Perrie, The role of lipid geometry in designing liposomes for the solubilisation of poorly water soluble drugs, Int J Pharm, 453 (2013) 225-232.

[254] M. Hamborg, L. Jorgensen, A.R. Bojsen, D. Christensen, C. Foged, Protein Antigen Adsorption to the DDA/TDB Liposomal Adjuvant: Effect on Protein Structure, Stability, and Liposome Physicochemical Characteristics, Pharmaceutical Research, 30 (2013) 140-155.

[255] A. Badamchi-Zadeh, P.F. McKay, B.T. Korber, G. Barinaga, A.A. Walters, A. Nunes, J.P. Gomes, F. Follmann, J.S. Tregoning, R.J. Shattock, A Multi-Component Prime-Boost Vaccination Regimen with a Consensus MOMP Antigen Enhances Chlamydia trachomatis Clearance, Frontiers in Immunology, 7 (2016).

[256] D. Gall, The adjuvant activity of aliphatic nitrogenous bases, Immunology, 11 (1966) 369-386.

[257] L.A. Hilgers, H. Snippe, DDA as an immunological adjuvant, Res Immunol, 143 (1992) 494-503; discussion 574-496.

[258] C. Klinguer, A. Beck, P. De-Lys, M.C. Bussat, A. Blaecke, F. Derouet, J.Y. Bonnefoy, T.N. Nguyen, N. Corvaïa, D. Velin, Lipophilic quaternary ammonium salt acts as a mucosal adjuvant when co-administered by the nasal route with vaccine antigens, Vaccine, 19 (2001) 4236-4244.

[259] C. Klinguer-Hamour, C. Libon, H. Plotnicky-Gilquin, M.-C. Bussat, L. Revy, T. Nguyen, J.-Y. Bonnefoy, N. Corvaïa, A. Beck, DDA adjuvant induces a mixed Th1/Th2 immune response when associated with BBG2Na, a respiratory syncytial virus potential vaccine, Vaccine, 20 (2002) 2743-2751.

[260] K. Worzner, D.J. Sheward, S.T. Schmidt, L. Hanke, J. Zimmermann, G. McInerney, G.B. Karlsson Hedestam, B. Murrell, D. Christensen, G.K. Pedersen, Adjuvanted SARS-CoV-2 spike protein elicits neutralizing antibodies and CD4 T cell responses after a single immunization in mice, EBioMedicine, 63 (2021) 103197.

[261] I. Rosenkrands, E.M. Agger, A.W. Olsen, K.S. Korsholm, C.S. Andersen, K.T. Jensen, P. Andersen, Cationic liposomes containing mycobacterial lipids: a new powerful Th1 adjuvant system, Infect Immun, 73 (2005) 5817-5826.

[262] L. Holten-Andersen, T.M. Doherty, K.S. Korsholm, P. Andersen, Combination of the cationic surfactant dimethyl dioctadecyl ammonium bromide and synthetic mycobacterial cord factor as an efficient adjuvant for tuberculosis subunit vaccines, Infect Immun, 72 (2004) 1608-1617.

[263] Y. Li, X.-L. Cui, Q.-S. Chen, J. Yu, H. Zhang, J. Gao, D.-X. Sun, G.-Q. Zhang, Cationic liposomes induce cytotoxicity in HepG2 via regulation of lipid metabolism based on whole-transcriptome sequencing analysis, BMC Pharmacology and Toxicology, 19 (2018) 43.

[264] S. Cui, Y. Wang, Y. Gong, X. Lin, Y. Zhao, D. Zhi, Q. Zhou, S. Zhang, Correlation of the cytotoxic effects of cationic lipids with their headgroups, Toxicology Research, 7 (2018) 473-479.

[265] M.J. Bennett, A.M. Aberle, R.P. Balasubramaniam, J.G. Malone, R.W. Malone, M.H. Nantz, Cationic Lipid-Mediated Gene Delivery to Murine Lung: Correlation of Lipid Hydration with in Vivo Transfection Activity, Journal of Medicinal Chemistry, 40 (1997) 4069-4078.

[266] C. Lonez, M. Vandenbranden, J.M. Ruysschaert, Cationic lipids activate intracellular signaling pathways, Adv Drug Deliv Rev, 64 (2012) 1749-1758.

[267] J. Davidsen, I. Rosenkrands, D. Christensen, A. Vangala, D. Kirby, Y. Perrie, E.M. Agger, P. Andersen, Characterization of cationic liposomes based on dimethyldioctadecylammonium

and synthetic cord factor from M. tuberculosis (trehalose 6,6'-dibehenate)-a novel adjuvant inducing both strong CMI and antibody responses, Biochim Biophys Acta, 1718 (2005) 22-31.

[268] R.B. Campbell, S.V. Balasubramanian, R.M. Straubinger, Phospholipid-cationic lipid interactions: influences on membrane and vesicle properties, Biochimica et Biophysica Acta (BBA) - Biomembranes, 1512 (2001) 27-39.

[269] R.J. Bose, Y. Arai, J.C. Ahn, H. Park, S.H. Lee, Influence of cationic lipid concentration on properties of lipid-polymer hybrid nanospheres for gene delivery, Int J Nanomedicine, 10 (2015) 5367-5382.

[270] A. Milicic, R. Kaur, A. Reyes-Sandoval, C.-K. Tang, J. Honeycutt, Y. Perrie, A.V.S. Hill, Small Cationic DDA:TDB Liposomes as Protein Vaccine Adjuvants Obviate the Need for TLR Agonists in Inducing Cellular and Humoral Responses, PLOS ONE, 7 (2012) e34255.

[271] A.M. Didierlaurent, S. Morel, L. Lockman, S.L. Giannini, M. Bisteau, H. Carlsen, A. Kielland, O. Vosters, N. Vanderheyde, F. Schiavetti, D. Larocque, M. Van Mechelen, N. Garçon, AS04, an aluminum salt- and TLR4 agonist-based adjuvant system, induces a transient localized innate immune response leading to enhanced adaptive immunity, J Immunol, 183 (2009) 6186-6197.

[272] B. Ding, Pharma Industry 4.0: Literature review and research opportunities in sustainable pharmaceutical supply chains, Process Safety and Environmental Protection, (2018).

[273] P. Taboada, S. Barbosa, E. Castro, M. Gutiérrez-Pichel, V. Mosquera, Effect of solvation on the structure conformation of human serum albumin in aqueous–alcohol mixed solvents, Chemical Physics, 340 (2007) 59-68.

[274] H.Y. Hu, H.N. Du, Alpha-to-beta structural transformation of ovalbumin: heat and pH effects, J Protein Chem, 19 (2000) 177-183.

[275] J. Jaspe, S.J. Hagen, Do Protein Molecules Unfold in a Simple Shear Flow?, Biophysical Journal, 91 (2006) 3415-3424.

[276] M.-R. Toh, G.N. Chiu, Liposomes as sterile preparations and limitations of sterilisation techniques in liposomal manufacturing, Asian Journal of Pharmaceutical Sciences, 8 (2013) 88-95.

[277] D.L. Carlson, K.D. Than, A.L. Roberts, Acid-and base-catalyzed hydrolysis of chloroacetamide herbicides, Journal of agricultural and food chemistry, 54 (2006) 4740-4750.

[278] G. Shim, M.-G. Kim, J.Y. Park, Y.-K. Oh, Application of cationic liposomes for delivery of nucleic acids, Asian journal of pharmaceutical sciences, 8 (2013) 72-80.

[279] P. Nakhaei, R. Margiana, D.O. Bokov, W.K. Abdelbasset, M.A. Jadidi Kouhbanani, R.S. Varma, F. Marofi, M. Jarahian, N. Beheshtkhoo, Liposomes: Structure, Biomedical Applications, and Stability Parameters With Emphasis on Cholesterol, Frontiers in bioengineering and biotechnology, 9 (2021) 705886-705886.

[280] A.R. Mohammed, V.W. Bramwell, A.G. Coombes, Y. Perrie, Lyophilisation and sterilisation of liposomal vaccines to produce stable and sterile products, Methods, 40 (2006) 30-38.

[281] J.H. Crowe, L.M. Crowe, Factors affecting the stability of dry liposomes, Biochimica et Biophysica Acta (BBA) - Biomembranes, 939 (1988) 327-334.

[282] K.L. Koster, M.S. Webb, G. Bryant, D.V. Lynch, Interactions between soluble sugars and POPC (1-palmitoyl-2-oleoylphosphatidylcholine) during dehydration: vitrification of sugars alters the phase behavior of the phospholipid, Biochimica et Biophysica Acta (BBA) - Biomembranes, 1193 (1994) 143-150.

[283] W. Abdelwahed, G. Degobert, S. Stainmesse, H. Fessi, Freeze-drying of nanoparticles: formulation, process and storage considerations, Adv Drug Deliv Rev, 58 (2006) 1688-1713.

[284] J.H. Crowe, F.A. Hoekstra, L.M. Crowe, Anhydrobiosis, Annual Review of Physiology, 54 (1992) 579-599.

[285] L.M. Crowe, D.S. Reid, J.H. Crowe, Is trehalose special for preserving dry biomaterials?, Biophys J, 71 (1996) 2087-2093.

[286] G. Gregoriadis, D. Davis, A. Davies, Liposomes as immunological adjuvants: antigen incorporation studies, Vaccine, 5 (1987) 145-151.

[287] N.A. Latif, B.K. Bachhawat, The effect of surface-coupled antigen of liposomes in immunopotentiation, Immunol Lett, 15 (1987) 45-51.

[288] G.R. Matyas, N.M. Wassef, M. Rao, C.R. Alving, Induction and detection of antibodies to squalene, J Immunol Methods, 245 (2000) 1-14.

[289] H. Snippe, J.E. van Dam, A.J. van Houte, J.M. Willers, J.P. Kamerling, J.F. Vliegenthart, Preparation of a semisynthetic vaccine to Streptococcus pneumoniae type 3, Infect Immun, 42 (1983) 842-844.

[290] M.R. Villegas, A. Baeza, M. Vallet-Regí, Nanotechnological Strategies for Protein Delivery, Molecules, 23 (2018).

[291] Y.S. Chen, Y.C. Hung, W.H. Lin, G.S. Huang, Assessment of gold nanoparticles as a size-dependent vaccine carrier for enhancing the antibody response against synthetic foot-and-mouth disease virus peptide, Nanotechnology, 21 (2010) 195101.

[292] A. Quarta, M. Rodio, M. Cassani, G. Gigli, T. Pellegrino, L.L. Del Mercato, Multilayered Magnetic Nanobeads for the Delivery of Peptides Molecules Triggered by Intracellular Proteases, ACS Appl Mater Interfaces, 9 (2017) 35095-35104.

[293] B. Niels Henrik, L.K. David, Protection of protein from bacterial degradation by submicron particles, Aquatic Microbial Ecology, 16 (1999) 265-272.

[294] M.P. Vincent, S. Bobbala, N.B. Karabin, M. Frey, Y. Liu, J.O. Navidzadeh, T. Stack, E.A. Scott, Surface chemistry-mediated modulation of adsorbed albumin folding state specifies nanocarrier clearance by distinct macrophage subsets, Nature Communications, 12 (2021) 648.

[295] P. Roach, D. Farrar, C.C. Perry, Surface Tailoring for Controlled Protein Adsorption: Effect of Topography at the Nanometer Scale and Chemistry, Journal of the American Chemical Society, 128 (2006) 3939-3945.

[296] A.E. Nel, L. Mädler, D. Velegol, T. Xia, E.M.V. Hoek, P. Somasundaran, F. Klaessig, V. Castranova, M. Thompson, Understanding biophysicochemical interactions at the nano–bio interface, Nature Materials, 8 (2009) 543-557.

[297] M.S. Ehrenberg, A.E. Friedman, J.N. Finkelstein, G. Oberdörster, J.L. McGrath, The influence of protein adsorption on nanoparticle association with cultured endothelial cells, Biomaterials, 30 (2009) 603-610.

[298] O.A. Turapov, G.V. Mukamolova, A.R. Bottrill, M.K. Pangburn, Digestion of native proteins for proteomics using a thermocycler, Anal Chem, 80 (2008) 6093-6099.

[299] N. Tanaka, Y. Morimoto, Y. Noguchi, T. Tada, T. Waku, S. Kunugi, T. Morii, Y.-F. Lee, T. Konno, N. Takahashi, The mechanism of fibril formation of a non-inhibitory serpin ovalbumin revealed by the identification of amyloidogenic core regions, The Journal of biological chemistry, 286 (2011) 5884-5894.

[300] M.K. Mansour, E. Latz, S.M. Levitz, Cryptococcus neoformans Glycoantigens Are Captured by Multiple Lectin Receptors and Presented by Dendritic Cells, The Journal of Immunology, 176 (2006) 3053.

[301] P. Rivera-Gil, S. De Koker, B.G. De Geest, W.J. Parak, Intracellular Processing of Proteins Mediated by Biodegradable Polyelectrolyte Capsules, Nano Letters, 9 (2009) 4398-4402.

[302] R.J. Simpson, Fragmentation of protein using trypsin, CSH Protoc, 2006 (2006).

[303] M. Henriksen-Lacey, V. Bramwell, Y. Perrie, Radiolabelling of Antigen and Liposomes for Vaccine Biodistribution Studies, Pharmaceutics, 2 (2010) 91-104.

[304] B.D. Freimark, H.P. Blezinger, V.J. Florack, J.L. Nordstrom, S.D. Long, D.S. Deshpande, S. Nochumson, K.L. Petrak, Cationic lipids enhance cytokine and cell influx levels in the lung following administration of plasmid: cationic lipid complexes, J Immunol, 160 (1998) 4580-4586.

[305] J. Banchereau, R.M. Steinman, Dendritic cells and the control of immunity, Nature, 392 (1998) 245-252.

[306] J.C. Cox, A.R. Coulter, Adjuvants--a classification and review of their modes of action, Vaccine, 15 (1997) 248-256.

[307] M. Henriksen-Lacey, D. Christensen, V.W. Bramwell, T. Lindenstrøm, E.M. Agger, P. Andersen, Y. Perrie, Comparison of the depot effect and immunogenicity of liposomes based on dimethyldioctadecylammonium (DDA), 3β-[N-(N',N'-Dimethylaminoethane)carbomyl] cholesterol (DC-Chol), and 1,2-Dioleoyl-3-trimethylammonium propane (DOTAP): prolonged liposome retention mediates stronger Th1 responses, Mol Pharm, 8 (2011) 153-161.

[308] G. Lou, G. Anderluzzi, S. Tandrup Schmidt, S. Woods, S. Gallorini, M. Brazzoli, F. Giusti, I. Ferlenghi, R. Johnson, C.W. Roberts, D.T. O'Hagan, B.C. Baudner, Y. Perrie, Delivery of self-amplifying mRNA vaccines by cationic lipid nanoparticles: The impact of cationic lipid selection, Journal of Controlled Release, (2020).

[309] D. Christensen, M. Henriksen-Lacey, A. Kamath, T. Lindenstrøm, K. Korsholm, J. Christensen, A.-F. Rochat, P.-H. Lambert, P. Andersen, C.-A. Siegrist, Y. Perrie, E. Agger, A cationic vaccine adjuvant based on a saturated quaternary ammonium lipid have different in vivo distribution kinetics and display a distinct CD4 T cell-inducing capacity compared to its unsaturated analog, Journal of controlled release : official journal of the Controlled Release Society, 160 (2012) 468-476.

[310] D. Geißler, C. Gollwitzer, A. Sikora, C. Minelli, M. Krumrey, U. Resch-Genger, Effect of fluorescent staining on size measurements of polymeric nanoparticles using DLS and SAXS, Analytical Methods, 7 (2015) 9785-9790.

[311] S.J. Tan, K. Nakahara, K. Sou, S. Takeoka, An Assay to Evaluate the Function of Liposomal Platelet Substitutes Delivered to Platelet Aggregates, Frontiers in Bioengineering and Biotechnology, 7 (2019).

[312] Y. Zhuang, Y. Ma, C. Wang, L. Hai, C. Yan, Y. Zhang, F. Liu, L. Cai, PEGylated cationic liposomes robustly augment vaccine-induced immune responses: Role of lymphatic trafficking and biodistribution, Journal of controlled release : official journal of the Controlled Release Society, 159 (2012) 135-142.

[313] S.T. Schmidt, C.L. Olsen, H. Franzyk, K. Wørzner, K.S. Korsholm, T. Rades, P. Andersen, C. Foged, D. Christensen, Comparison of two different PEGylation strategies for the liposomal adjuvant CAF09: Towards induction of CTL responses upon subcutaneous vaccine administration, European journal of pharmaceutics and biopharmaceutics : official journal of Arbeitsgemeinschaft fur Pharmazeutische Verfahrenstechnik e.V, 140 (2019) 29-39.

[314] E. Blanco, H. Shen, M. Ferrari, Principles of nanoparticle design for overcoming biological barriers to drug delivery, Nat Biotechnol, 33 (2015) 941-951.

[315] S. Schwartz, Jr., Unmet needs in developing nanoparticles for precision medicine, Nanomedicine (Lond), 12 (2017) 271-274.

[316] C. von Roemeling, W. Jiang, C.K. Chan, I.L. Weissman, B.Y.S. Kim, Breaking Down the Barriers to Precision Cancer Nanomedicine, Trends in Biotechnology, 35 (2017) 159-171.

[317] J. Key, A.L. Palange, F. Gentile, S. Aryal, C. Stigliano, D. Di Mascolo, E. De Rosa, M. Cho, Y. Lee, J. Singh, P. Decuzzi, Soft Discoidal Polymeric Nanoconstructs Resist Macrophage Uptake and Enhance Vascular Targeting in Tumors, ACS Nano, 9 (2015) 11628-11641.

[318] Y. Hui, X. Yi, F. Hou, D. Wibowo, F. Zhang, D. Zhao, H. Gao, C.X. Zhao, Role of Nanoparticle Mechanical Properties in Cancer Drug Delivery, ACS Nano, 13 (2019) 7410-7424.

[319] G.J. Randolph, K. Inaba, D.F. Robbiani, R.M. Steinman, W.A. Muller, Differentiation of phagocytic monocytes into lymph node dendritic cells in vivo, Immunity, 11 (1999) 753-761.

[320] M. Dupuis, K. Denis-Mize, A. LaBarbara, W. Peters, I.F. Charo, D.M. McDonald, G. Ott, Immunization with the adjuvant MF59 induces macrophage trafficking and apoptosis, Eur J Immunol, 31 (2001) 2910-2918.

[321] A.G. Harmsen, B.A. Muggenburg, M.B. Snipes, D.E. Bice, The role of macrophages in particle translocation from lungs to lymph nodes, Science, 230 (1985) 1277.

[322] D.T. O'Hagan, M. Singh, Microparticles as vaccine adjuvants and delivery systems, Expert review of vaccines, 2 (2003) 269-283.

[323] L.O. De Serrano, D.J. Burkhart, Liposomal vaccine formulations as prophylactic agents: design considerations for modern vaccines, J Nanobiotechnology, 15 (2017) 83.

[324] R. Nisini, N. Poerio, S. Mariotti, F. De Santis, M. Fraziano, The Multirole of Liposomes in Therapy and Prevention of Infectious Diseases, Front Immunol, 9 (2018) 155.

[325] M.J. Hussain, A. Wilkinson, V.W. Bramwell, D. Christensen, Y. Perrie, Th1 immune responses can be modulated by varying dimethyldioctadecylammonium and distearoyl-sn-glycero-3-phosphocholine content in liposomal adjuvants, Journal of Pharmacy and Pharmacology, 66 (2014) 358-366.

[326] S. Pal, I. Theodor, E.M. Peterson, L.M. de la Maza, Immunization with the Chlamydia trachomatis mouse pneumonitis major outer membrane protein can elicit a protective immune response against a genital challenge, Infect Immun, 69 (2001) 6240-6247.

[327] G. Sun, S. Pal, J. Weiland, E.M. Peterson, L.M. de la Maza, Protection against an intranasal challenge by vaccines formulated with native and recombinant preparations of the Chlamydia trachomatis major outer membrane protein, Vaccine, 27 (2009) 5020-5025.

[328] C.M. Farris, S.G. Morrison, R.P. Morrison, CD4+ T cells and antibody are required for optimal major outer membrane protein vaccine-induced immunity to Chlamydia muridarum genital infection, Infect Immun, 78 (2010) 4374-4383.

[329] Y. Yuan, Y.X. Zhang, N.G. Watkins, H.D. Caldwell, Nucleotide and deduced amino acid sequences for the four variable domains of the major outer membrane proteins of the 15 Chlamydia trachomatis serovars, Infect Immun, 57 (1989) 1040-1049.

[330] C. Thoma, First chlamydia vaccine trial in humans, Nature Reviews Urology, 16 (2019) 566-566.

[331] K. Wørzner, J. Hvannastein, S.T. Schmidt, C. Foged, I. Rosenkrands, G.K. Pedersen, D. Christensen, Adsorption of protein antigen to the cationic liposome adjuvant CAF®01 is required for induction of Th1 and Th17 responses but not for antibody induction, Eur J Pharm Biopharm, 165 (2021) 293-305.

[332] L. Du, G. Zhao, Z. Kou, C. Ma, S. Sun, V.K. Poon, L. Lu, L. Wang, A.K. Debnath, B.J. Zheng, Y. Zhou, S. Jiang, Identification of a receptor-binding domain in the S protein of the novel human coronavirus Middle East respiratory syndrome coronavirus as an essential target for vaccine development, J Virol, 87 (2013) 9939-9942.

[333] T.F. Rogers, F. Zhao, D. Huang, N. Beutler, A. Burns, W.T. He, O. Limbo, C. Smith, G. Song, J. Woehl, L. Yang, R.K. Abbott, S. Callaghan, E. Garcia, J. Hurtado, M. Parren, L. Peng, S. Ramirez, J. Ricketts, M.J. Ricciardi, S.A. Rawlings, N.C. Wu, M. Yuan, D.M. Smith, D. Nemazee, J.R. Teijaro, J.E. Voss, I.A. Wilson, R. Andrabi, B. Briney, E. Landais, D. Sok, J.G. Jardine, D.R. Burton, Isolation of potent SARS-CoV-2 neutralizing antibodies and protection from disease in a small animal model, Science, 369 (2020) 956-963.

[334] L. Dai, G.F. Gao, Viral targets for vaccines against COVID-19, Nat Rev Immunol, 21 (2021) 73-82.

[335] WHO, COVID-19 vaccine tracker and landscape, in, World Health Organization, https://www.who.int/publications/m/item/draft-landscape-of-covid-19-candidate-vaccines, 2021.

[336] T. Schmidt, V. Klemis, D. Schub, J. Mihm, F. Hielscher, S. Marx, A. Abu-Omar, L. Ziegler, C. Guckelmus, R. Urschel, S. Schneitler, S.L. Becker, B.C. Gärtner, U. Sester, M. Sester, Immunogenicity and reactogenicity of heterologous ChAdOx1 nCoV-19/mRNA vaccination, Nat Med, 27 (2021) 1530-1535.

[337] A.M. Borobia, A.J. Carcas, M. Pérez-Olmeda, L. Castaño, M.J. Bertran, J. García-Pérez, M. Campins, A. Portolés, M. González-Pérez, M.T.G. Morales, Immunogenicity and reactogenicity of BNT162b2 booster in ChAdOx1-S-primed participants (CombiVacS): a multicentre, open-label, randomised, controlled, phase 2 trial, The Lancet, 398 (2021) 121-130.

[338] R.H. Shaw, A. Stuart, M. Greenland, X. Liu, J.S.N. Van-Tam, M.D. Snape, Heterologous prime-boost COVID-19 vaccination: initial reactogenicity data, The Lancet, 397 (2021) 2043-2046.

[339] A. Irwin, What it will take to vaccinate the world against COVID-19, Nature, 592 (2021) 176-178.

[340] EMA, EMA recommends Nuvaxovid for authorisation in the EU, in, European Medicines Agency https://www.ema.europa.eu/en/news/ema-recommends-nuvaxovid-authorisation-eu, 2021.

[341] MHRA, Novavax COVID-19 vaccine Nuvaxovid approved by MHRA, in, Medicines and Healthcare products Regulatory Agency https://www.gov.uk/government/news/novavax-covid-19-vaccine-nuvaxovid-approved-by-mhra, 2022.

[342] Novavax, Novavax Submits Request to the U.S. FDA for Emergency Use Authorization of COVID-19 Vaccine, in, https://ir.novavax.com/2022-01-31-Novavax-Submits-Request-to-the-U-S-FDA-for-Emergency-Use-Authorization-of-COVID-19-Vaccine, 2022.

[343] C. Keech, G. Albert, I. Cho, A. Robertson, P. Reed, S. Neal, J.S. Plested, M. Zhu, S. Cloney-Clark, H. Zhou, G. Smith, N. Patel, M.B. Frieman, R.E. Haupt, J. Logue, M. McGrath, S. Weston, P.A. Piedra, C. Desai, K. Callahan, M. Lewis, P. Price-Abbott, N. Formica, V. Shinde, L. Fries, J.D. Lickliter, P. Griffin, B. Wilkinson, G.M. Glenn, Phase 1-2 Trial of a SARS-CoV-2 Recombinant Spike Protein Nanoparticle Vaccine, N Engl J Med, 383 (2020) 2320-2332.

[344] M. Mandolesi, D.J. Sheward, L. Hanke, J. Ma, P. Pushparaj, L. Perez Vidakovics, C. Kim, M. Àdori, K. Lenart, K. Loré, X. Castro Dopico, J.M. Coquet, G.M. McInerney, G.B. Karlsson Hedestam, B. Murrell, SARS-CoV-2 protein subunit vaccination of mice and rhesus macaques elicits potent and durable neutralizing antibody responses, Cell Reports Medicine, 2 (2021).

[345] P.T. Heath, E.P. Galiza, D.N. Baxter, M. Boffito, D. Browne, F. Burns, D.R. Chadwick, R. Clark, C. Cosgrove, J. Galloway, A.L. Goodman, A. Heer, A. Higham, S. Iyengar, A. Jamal, C. Jeanes, P.A. Kalra, C. Kyriakidou, D.F. McAuley, A. Meyrick, A.M. Minassian, J. Minton, P. Moore, I. Munsoor, H. Nicholls, O. Osanlou, J. Packham, C.H. Pretswell, A. San Francisco

Ramos, D. Saralaya, R.P. Sheridan, R. Smith, R.L. Soiza, P.A. Swift, E.C. Thomson, J. Turner, M.E. Viljoen, G. Albert, I. Cho, F. Dubovsky, G. Glenn, J. Rivers, A. Robertson, K. Smith, S. Toback, Safety and Efficacy of NVX-CoV2373 Covid-19 Vaccine, New England Journal of Medicine, 385 (2021) 1172-1183.

[346] G. Del Giudice, R. Rappuoli, A.M. Didierlaurent, Correlates of adjuvanticity: A review on adjuvants in licensed vaccines, Semin Immunol, 39 (2018) 14-21.

[347] J.T. van Dissel, S.A. Joosten, S.T. Hoff, D. Soonawala, C. Prins, D.A. Hokey, D.M. O'Dee, A. Graves, B. Thierry-Carstensen, L.V. Andreasen, M. Ruhwald, A.W. de Visser, E.M. Agger, T.H.M. Ottenhoff, I. Kromann, P. Andersen, A novel liposomal adjuvant system, CAF01, promotes long-lived Mycobacterium tuberculosis-specific T-cell responses in human, Vaccine, 32 (2014) 7098-7107.

[348] L. Hilgers, H. Snippe, DDA as an immunological adjuvant, Research in immunology, 143 (1992) 494-503; discussion 574.

[349] K. Werninghaus, A. Babiak, O. Groß, C. Hölscher, H. Dietrich, E.M. Agger, J. Mages, A. Mocsai, H. Schoenen, K. Finger, Adjuvanticity of a synthetic cord factor analogue for subunit Mycobacterium tuberculosis vaccination requires FcRγ–Syk–Card9–dependent innate immune activation, Journal of Experimental Medicine, 206 (2009) 89-97.

[350] E. Ishikawa, T. Ishikawa, Y.S. Morita, K. Toyonaga, H. Yamada, O. Takeuchi, T. Kinoshita, S. Akira, Y. Yoshikai, S. Yamasaki, Direct recognition of the mycobacterial glycolipid, trehalose dimycolate, by C-type lectin Mincle, Journal of experimental medicine, 206 (2009) 2879-2888.

[351] H. Schoenen, B. Bodendorfer, K. Hitchens, S. Manzanero, K. Werninghaus, F. Nimmerjahn, E.M. Agger, S. Stenger, P. Andersen, J. Ruland, Cutting edge: Mincle is essential for recognition and adjuvanticity of the mycobacterial cord factor and its synthetic analog trehalose-dibehenate, The Journal of Immunology, 184 (2010) 2756-2760.

[352] D.T. O'Hagan, R.N. Lodaya, G. Lofano, The continued advance of vaccine adjuvants – 'we can work it out', Seminars in Immunology, 50 (2020) 101426.

[353] A. Monie, C.-F. Hung, R. Roden, T.C. Wu, Cervarix: a vaccine for the prevention of HPV 16, 18-associated cervical cancer, Biologics, 2 (2008) 97-105.

[354] H. Behzad, A.L.W. Huckriede, L. Haynes, B. Gentleman, K. Coyle, J.C. Wilschut, T.R. Kollmann, S.G. Reed, J.E. McElhaney, GLA-SE, a synthetic toll-like receptor 4 agonist, enhances T-cell responses to influenza vaccine in older adults, J Infect Dis, 205 (2012) 466-473.

[355] R.N. Coler, S.L. Baldwin, N. Shaverdian, S. Bertholet, S.J. Reed, V.S. Raman, X. Lu, J. DeVos, K. Hancock, J.M. Katz, T.S. Vedvick, M.S. Duthie, C.H. Clegg, N. Van Hoeven, S.G. Reed, A Synthetic Adjuvant to Enhance and Expand Immune Responses to Influenza Vaccines, PLOS ONE, 5 (2010) e13677.

[356] A.K. Blakney, P.F. McKay, D. Christensen, B.I. Yus, Y. Aldon, F. Follmann, R.J. Shattock, Effects of cationic adjuvant formulation particle type, fluidity and immunomodulators on delivery and immunogenicity of saRNA, Journal of controlled release : official journal of the Controlled Release Society, 304 (2019) 65-74.

[357] T.A. Balbino, N.T. Aoki, A.A.M. Gasperini, C.L.P. Oliveira, A.R. Azzoni, L.P. Cavalcanti, L.G. de la Torre, Continuous flow production of cationic liposomes at high lipid concentration in microfluidic devices for gene delivery applications, Chemical Engineering Journal, 226 (2013) 423-433.

[358] J. Trevisan, L. Cavalcanti, C. Oliveira, L. Torre, M.H. Santana, Technological Aspects of Scalable Processes for the Production of Functional Liposomes for Gene Therapy, in, 2011.

[359] M. Hamborg, F. Rose, L. Jorgensen, K. Bjorklund, H.B. Pedersen, D. Christensen, C. Foged, Elucidating the mechanisms of protein antigen adsorption to the CAF/NAF liposomal

vaccine adjuvant systems: Effect of charge, fluidity and antigen-to-lipid ratio, Biochimica et Biophysica Acta (BBA) - Biomembranes, 1838 (2014) 2001-2010.

[360] S.T. Schmidt, D. Christensen, Y. Perrie, Applying Microfluidics for the Production of the Cationic Liposome-Based Vaccine Adjuvant CAF09b, Pharmaceutics, 12 (2020).

[361] V.I. Gordeliy, M.A. Kiselev, P. Lesieur, A.V. Pole, J. Teixeira, Lipid Membrane Structure and Interactions in Dimethyl Sulfoxide/Water Mixtures, Biophysical Journal, 75 (1998) 2343-2351.

[362] Z.W. Yu, P.J. Quinn, Solvation effects of dimethyl sulphoxide on the structure of phospholipid bilayers, Biophys Chem, 70 (1998) 35-39.

[363] D. Christensen, D. Kirby, C. Foged, E.M. Agger, P. Andersen, Y. Perrie, H.M. Nielsen, α,α'-trehalose 6,6'-dibehenate in non-phospholipid-based liposomes enables direct interaction with trehalose, offering stability during freeze-drying, Biochimica et Biophysica Acta (BBA) - Biomembranes, 1778 (2008) 1365-1373.

[364] P. Nordly, E. Agger, P. Andersen, H. Nielsen, C. Foged, Incorporation of the TLR4 Agonist Monophosphoryl Lipid A Into the Bilayer of DDA/TDB Liposomes: Physico-Chemical Characterization and Induction of CD8+ T-Cell Responses In Vivo, Pharmaceutical research, 28 (2010) 553-562.

[365] D. Christensen, C. Foged, I. Rosenkrands, H.M. Nielsen, P. Andersen, E.M. Agger, Trehalose preserves DDA/TDB liposomes and their adjuvant effect during freeze-drying, Biochimica et Biophysica Acta (BBA) - Biomembranes, 1768 (2007) 2120-2129.

[366] W. Liu, Z. Wang, L. Fu, R.M. Leblanc, E.C.Y. Yan, Lipid Compositions Modulate Fluidity and Stability of Bilayers: Characterization by Surface Pressure and Sum Frequency Generation Spectroscopy, Langmuir, 29 (2013) 15022-15031.

[367] D. Lichtenberg, E. Freire, C.F. Schmidt, Y. Barenholz, P.L. Felgner, T.E. Thompson, Effect of surface curvature on stability, thermodynamic behavior, and osmotic activity of dipalmitoylphosphatidylcholine single lamellar vesicles, Biochemistry, 20 (1981) 3462-3467.

[368] P.R. Cullis, M.J. Hope, C.P.S. Tilcock, Lipid polymorphism and the roles of lipids in membranes, Chem Phys Lipids, 40 (1986) 127-144.

[369] J.J. Mittag, B. Kneidl, T. Preiβ, M. Hossann, G. Winter, S. Wuttke, H. Engelke, J.O. Rädler, Impact of plasma protein binding on cargo release by thermosensitive liposomes probed by fluorescence correlation spectroscopy, European Journal of Pharmaceutics and Biopharmaceutics, 119 (2017) 215-223.

[370] J. Austin, C. Minelli, D. Hamilton, M. Wywijas, H.J. Jones, Nanoparticle number concentration measurements by multi-angle dynamic light scattering, Journal of Nanoparticle Research, 22 (2020) 108.

[371] J. Wolfram, K. Suri, Y. Yang, J. Shen, C. Celia, M. Fresta, Y. Zhao, H. Shen, M. Ferrari, Shrinkage of pegylated and non-pegylated liposomes in serum, Colloids and Surfaces B: Biointerfaces, 114 (2014) 294-300.

[372] J. Pencer, G.F. White, F.R. Hallett, Osmotically Induced Shape Changes of Large Unilamellar Vesicles Measured by Dynamic Light Scattering, Biophysical Journal, 81 (2001) 2716-2728.

[373] A.M. de Haan Cornelis, E. te Lintelo, Z. Li, M. Raaben, T. Wurdinger, J. Bosch Berend, J.M. Rottier Peter, Cooperative Involvement of the S1 and S2 Subunits of the Murine Coronavirus Spike Protein in Receptor Binding and Extended Host Range, Journal of Virology, 80 (2006) 10909-10918.

[374] J.L. Thewalt, M. Bloom, Phosphatidylcholine: cholesterol phase diagrams, Biophysical Journal, 63 (1992) 1176-1181.

[375] V.A. Frolov, A.V. Shnyrova, J. Zimmerberg, Lipid polymorphisms and membrane shape, Cold Spring Harb Perspect Biol, 3 (2011) a004747-a004747.

[376] I.M. Hafez, P.R. Cullis, Roles of lipid polymorphism in intracellular delivery, Adv Drug Deliv Rev, 47 (2001) 139-148.

[377] C.P.S. Tilcock, Lipid polymorphism, Chem Phys Lipids, 40 (1986) 109-125.

[378] M. Tian, Z. Zhou, S. Tan, X. Fan, L. Li, N. Ullah, Formulation in DDA-MPLA-TDB Liposome Enhances the Immunogenicity and Protective Efficacy of a DNA Vaccine against Mycobacterium tuberculosis Infection, Frontiers in immunology, 9 (2018) 310-310.

[379] R. Kaur, V.W. Bramwell, D.J. Kirby, Y. Perrie, Pegylation of DDA:TDB liposomal adjuvants reduces the vaccine depot effect and alters the Th1/Th2 immune responses, Journal of controlled release : official journal of the Controlled Release Society, 158 (2012) 72-77.

[380] T.M. Allen, P.R. Cullis, Liposomal drug delivery systems: From concept to clinical applications, Advanced Drug Delivery Reviews, 65 (2013) 36-48.

[381] L. Schoenmaker, D. Witzigmann, J.A. Kulkarni, R. Verbeke, G. Kersten, W. Jiskoot, D.J.A. Crommelin, mRNA-lipid nanoparticle COVID-19 vaccines: Structure and stability, International Journal of Pharmaceutics, 601 (2021) 120586.

[382] Y. Barenholz, Liposome application: problems and prospects, Current Opinion in Colloid & Interface Science, 6 (2001) 66-77.

[383] D.D. Lasic, F.J. Martin, Stealth liposomes, CRC press, 1995.

[384] J.M. Harris, S. Zalipsky, A.C.S. Staff, Poly (ethylene glycol), American Chemical Society Washington, DC, 1997.

[385] R. Nisini, N. Poerio, S. Mariotti, F. De Santis, M. Fraziano, The Multirole of Liposomes in Therapy and Prevention of Infectious Diseases, Frontiers in Immunology, 9 (2018).

[386] A. Priev, A.M. Samuni, O. Tirosh, Y. Barenholz, The role of hydration in stabilization of liposomes: resistance to oxidative damage of PEG-grafted liposomes, in: Targeting of Drugs 6, Springer, 1998, pp. 147-167.

[387] D. Needham, D.H. Kim, PEG-covered lipid surfaces: bilayers and monolayers, Colloids and Surfaces B: Biointerfaces, 18 (2000) 183-195.

[388] D. Needham, T.J. McIntosh, D.D. Lasic, Repulsive interactions and mechanical stability of polymer-grafted lipid membranes, Biochimica et Biophysica Acta (BBA) - Biomembranes, 1108 (1992) 40-48.

[389] C. Allen, N. Santos, R. Gallagher, G. Chiu, Y. Shu, W. Li, S. Johnstone, A. Janoff, L. Mayer, M. Webb, M. Bally, Controlling the Physical Behavior and Biological Performance of Liposome Formulations Through Use of Surface Grafted Poly(ethylene Glycol), Bioscience reports, 22 (2002) 225-250.

[390] H.I. Labouta, M.J. Gomez-Garcia, C.D. Sarsons, T. Nguyen, J. Kennard, W. Ngo, K. Terefe, N. Iragorri, P. Lai, K.D. Rinker, D.T. Cramb, Surface-grafted polyethylene glycol conformation impacts the transport of PEG-functionalized liposomes through a tumour extracellular matrix model, RSC Advances, 8 (2018) 7697-7708.

[391] S. Bibi, R. Kaur, M. Henriksen-Lacey, S.E. McNeil, J. Wilkhu, E. Lattmann, D. Christensen, A.R. Mohammed, Y. Perrie, Microscopy imaging of liposomes: from coverslips to environmental SEM, Int J Pharm, 417 (2011) 138-150.

[392] S. Calabro, E. Tritto, A. Pezzotti, M. Taccone, A. Muzzi, S. Bertholet, E. De Gregorio, D.T. O'Hagan, B. Baudner, A. Seubert, The adjuvant effect of MF59 is due to the oil-in-water emulsion formulation, none of the individual components induce a comparable adjuvant effect, Vaccine, 31 (2013) 3363-3369.

[393] G. Ott, G.L. Barchfeld, D. Chernoff, R. Radhakrishnan, P. van Hoogevest, G. Van Nest, MF59. Design and evaluation of a safe and potent adjuvant for human vaccines, Pharm Biotechnol, 6 (1995) 277-296.

[394] J.-H. Fang, M. Hora, The Adjuvant MF59: A 10-Year Perspective Gary Ott, Ramachandran Radhakrishnan, in: D.T. O'Hagan (Ed.) Vaccine Adjuvants: Preparation Methods and Research Protocols, Springer New York, Totowa, NJ, 2000, pp. 211-228.

[395] A. Bekierkunst, I.S. Levij, E. Yarkoni, E. Vilkas, E. Lederer, Suppression of Urethan-Induced Lung Adenomas in Mice Treated with Trehalose-6,6-Dimycolate (Cord Factor) and Living Bacillus Calmette Guérin, Science, 174 (1971) 1240-1242.

[396] R.L. Hunter, M. Olsen, C. Jagannath, J.K. Actor, Trehalose 6,6'-Dimycolate and Lipid in the Pathogenesis of Caseating Granulomas of Tuberculosis in Mice, The American Journal of Pathology, 168 (2006) 1249-1261.

[397] R.L. Hunter, N. Venkataprasad, M.R. Olsen, The role of trehalose dimycolate (cord factor) on morphology of virulent M. tuberculosis in vitro, Tuberculosis, 86 (2006) 349-356.

[398] D. Christensen, Chapter 17 - Development and Evaluation of CAF01, in: V.E.J.C. Schijns, D.T. O'Hagan (Eds.) Immunopotentiators in Modern Vaccines (Second Edition), Academic Press, 2017, pp. 333-345.

[399] C. Desel, K. Werninghaus, M. Ritter, K. Jozefowski, J. Wenzel, N. Russkamp, U. Schleicher, D. Christensen, S. Wirtz, C. Kirschning, E.M. Agger, C.P. da Costa, R. Lang, The Mincle-Activating Adjuvant TDB Induces MyD88-Dependent Th1 and Th17 Responses through IL-1R Signaling, PLOS ONE, 8 (2013) e53531.

[400] H. Schoenen, B. Bodendorfer, K. Hitchens, S. Manzanero, K. Werninghaus, F. Nimmerjahn, E.M. Agger, S. Stenger, P. Andersen, J. Ruland, G.D. Brown, C. Wells, R. Lang, Cutting Edge: Mincle Is Essential for Recognition and Adjuvanticity of the Mycobacterial Cord Factor and its Synthetic Analog Trehalose-Dibehenate, The Journal of Immunology, 184 (2010) 2756.

[401] K. Werninghaus, A. Babiak, O. Groß, C. Hölscher, H. Dietrich, E.M. Agger, J. Mages, A. Mocsai, H. Schoenen, K. Finger, F. Nimmerjahn, G.D. Brown, C. Kirschning, A. Heit, P. Andersen, H. Wagner, J. Ruland, R. Lang, Adjuvanticity of a synthetic cord factor analogue for subunit Mycobacterium tuberculosis vaccination requires FcRγ–Syk–Card9–dependent innate immune activation, Journal of Experimental Medicine, 206 (2009) 89-97.

[402] T. Bharucha, D. Ming, J. Breuer, A critical appraisal of 'Shingrix', a novel herpes zoster subunit vaccine (HZ/Su or GSK1437173A) for varicella zoster virus, Human vaccines & immunotherapeutics, 13 (2017) 1789-1797.

[403] N.F. Eng, N. Bhardwaj, R. Mulligan, F. Diaz-Mitoma, The potential of 1018 ISS adjuvant in hepatitis B vaccines: HEPLISAV™ review, Hum Vaccin Immunother, 9 (2013) 1661-1672.

[404] S.G. Reed, M. Tomai, M.J. Gale, Jr., New horizons in adjuvants for vaccine development, Curr Opin Immunol, 65 (2020) 97-101.

[405] D. Carter, N. van Hoeven, S. Baldwin, Y. Levin, E. Kochba, A. Magill, N. Charland, N. Landry, K. Nu, A. Frevol, J. Ashman, Z.K. Sagawa, A.M. Beckmann, S.G. Reed, The adjuvant GLA-AF enhances human intradermal vaccine responses, Sci Adv, 4 (2018) eaas9930-eaas9930.

[406] M. Bhattacharya, A.R. Sharma, B. Mallick, G. Sharma, S.-S. Lee, C. Chakraborty, Immunoinformatics approach to understand molecular interaction between multi-epitopic regions of SARS-CoV-2 spike-protein with TLR4/MD-2 complex, Infect Genet Evol, 85 (2020) 104587-104587.

[407] A. Choudhury, S. Mukherjee, In silico studies on the comparative characterization of the interactions of SARS-CoV-2 spike glycoprotein with ACE-2 receptor homologs and human TLRs, J Med Virol, 92 (2020) 2105-2113.

[408] Y. Zhao, M. Kuang, J. Li, L. Zhu, Z. Jia, X. Guo, Y. Hu, J. Kong, H. Yin, X. Wang, F. You, SARS-CoV-2 spike protein interacts with and activates TLR41, Cell Research, 31 (2021) 818-820.

[409] J.M. Brewer, K.G. Pollock, L. Tetley, D.G. Russell, Vesicle size influences the trafficking, processing, and presentation of antigens in lipid vesicles, J Immunol, 173 (2004) 6143-6150.

[410] J.M. Brewer, L. Tetley, J. Richmond, F.Y. Liew, J. Alexander, Lipid Vesicle Size Determines the Th1 or Th2 Response to Entrapped Antigen, The Journal of Immunology, 161 (1998) 4000.

[411] E. Kastner, M.J. Hussain, V.W. Bramwell, D. Christensen, Y. Perrie, Correlating liposomal adjuvant characteristics to in-vivo cell-mediated immunity using a novel Mycobacterium tuberculosis fusion protein: a multivariate analysis study, J Pharm Pharmacol, 67 (2015) 450-463.

[412] K.S. Korsholm, R.V. Petersen, E.M. Agger, P. Andersen, T-helper 1 and T-helper 2 adjuvants induce distinct differences in the magnitude, quality and kinetics of the early inflammatory response at the site of injection, Immunology, 129 (2010) 75-86.

[413] L. Holten-Andersen, T. Doherty, K. Korsholm, P. Andersen, Combination of the cationic surfactant dimethyl dioctadecyl ammonium bromide and synthetic mycobacterial cord factor as an efficient adjuvant for tuberculosis subunit vaccines, Infection and immunity, 72 (2004) 1608-1617.

[414] H.W. Kim, J.G. Canchola, C.D. Brandt, G. Pyles, R.M. Chanock, K. Jensen, R.H. Parrott, Respiratory syncytial virus disease in infants despite prior administration of antigenic inactivated vaccine, American journal of epidemiology, 89 (1969) 422-434.

[415] V.A. Fulginiti, J.J. Eller, A.W. Downie, C.H. Kempe, Altered reactivity to measles virus: atypical measles in children previously immunized with inactivated measles virus vaccines, Jama, 202 (1967) 1075-1080.

[416] M. Bolles, D. Deming, K. Long, S. Agnihothram, A. Whitmore, M. Ferris, W. Funkhouser, L. Gralinski, A. Totura, M. Heise, A double-inactivated severe acute respiratory syndrome coronavirus vaccine provides incomplete protection in mice and induces increased eosinophilic proinflammatory pulmonary response upon challenge, Journal of virology, 85 (2011) 12201-12215.

[417] D. Deming, T. Sheahan, M. Heise, B. Yount, N. Davis, A. Sims, M. Suthar, J. Harkema, A. Whitmore, R. Pickles, Vaccine efficacy in senescent mice challenged with recombinant SARS-CoV bearing epidemic and zoonotic spike variants, PLoS medicine, 3 (2006) e525.

[418] L.M. Snell, I. Osokine, D.H. Yamada, J.R. De la Fuente, H.J. Elsaesser, D.G. Brooks, Overcoming CD4 Th1 Cell Fate Restrictions to Sustain Antiviral CD8 T Cells and Control Persistent Virus Infection, Cell reports, 16 (2016) 3286-3296.

[419] M. Hoffmann, H. Kleine-Weber, S. Schroeder, N. Krüger, T. Herrler, S. Erichsen, T.S. Schiergens, G. Herrler, N.-H. Wu, A. Nitsche, M.A. Müller, C. Drosten, S. Pöhlmann, SARS-CoV-2 Cell Entry Depends on ACE2 and TMPRSS2 and Is Blocked by a Clinically Proven Protease Inhibitor, Cell, 181 (2020) 271-280.e278.

[420] T. Kuiken, R.A.M. Fouchier, M. Schutten, G.F. Rimmelzwaan, G. van Amerongen, D. van Riel, J.D. Laman, T. de Jong, G. van Doornum, W. Lim, A.E. Ling, P.K.S. Chan, J.S. Tam, M.C. Zambon, R. Gopal, C. Drosten, S. van der Werf, N. Escriou, J.-C. Manuguerra, K. Stöhr, J.S.M. Peiris, A.D.M.E. Osterhaus, Newly discovered coronavirus as the primary cause of severe acute respiratory syndrome, The Lancet, 362 (2003) 263-270.

[421] L. Du, Y. He, Y. Zhou, S. Liu, B.-J. Zheng, S. Jiang, The spike protein of SARS-CoV — a target for vaccine and therapeutic development, Nature Reviews Microbiology, 7 (2009) 226-236.

[422] L. Premkumar, B. Segovia-Chumbez, R. Jadi, D.R. Martinez, R. Raut, A. Markmann, C. Cornaby, L. Bartelt, S. Weiss, Y. Park, C.E. Edwards, E. Weimer, E.M. Scherer, N. Rouphael, S. Edupuganti, D. Weiskopf, L.V. Tse, Y.J. Hou, D. Margolis, A. Sette, M.H. Collins, J. Schmitz, R.S. Baric, A.M. de Silva, The receptor binding domain of the viral spike protein is an immunodominant and highly specific target of antibodies in SARS-CoV-2 patients, Sci Immunol, 5 (2020).

[423] D.S. Khoury, D. Cromer, A. Reynaldi, T.E. Schlub, A.K. Wheatley, J.A. Juno, K. Subbarao, S.J. Kent, J.A. Triccas, M.P. Davenport, Neutralizing antibody levels are highly predictive of immune protection from symptomatic SARS-CoV-2 infection, Nat Med, 27 (2021) 1205-1211.

[424] K. McMahan, J. Yu, N.B. Mercado, C. Loos, L.H. Tostanoski, A. Chandrashekar, J. Liu, L. Peter, C. Atyeo, A. Zhu, Correlates of protection against SARS-CoV-2 in rhesus macaques, Nature, 590 (2021) 630-634.

[425] S.L. Swain, K.K. McKinstry, T.M. Strutt, Expanding roles for CD4+ T cells in immunity to viruses, Nature Reviews Immunology, 12 (2012) 136-148.

[426] M. Jeyanathan, S. Afkhami, F. Smaill, M.S. Miller, B.D. Lichty, Z. Xing, Immunological considerations for COVID-19 vaccine strategies, Nature Reviews Immunology, 20 (2020) 615-632.

[427] C.A. Dinarello, Proinflammatory cytokines, Chest, 118 (2000) 503-508.

[428] F. Martinon, K. Burns, J. Tschopp, The inflammasome: a molecular platform triggering activation of inflammatory caspases and processing of proIL-beta, Mol Cell, 10 (2002) 417-426.

[429] H. Guo, J.B. Callaway, J.P.Y. Ting, Inflammasomes: mechanism of action, role in disease, and therapeutics, Nature Medicine, 21 (2015) 677-687.

[430] G. Fenini, E. Contassot, L.E. French, Potential of IL-1, IL-18 and Inflammasome Inhibition for the Treatment of Inflammatory Skin Diseases, Frontiers in Pharmacology, 8 (2017).

[431] C.A. Dinarello, D. Novick, A.J. Puren, G. Fantuzzi, L. Shapiro, H. Mühl, D.Y. Yoon, L.L. Reznikov, S.H. Kim, M. Rubinstein, Overview of interleukin-18: more than an interferon-gamma inducing factor, J Leukoc Biol, 63 (1998) 658-664.

[432] L.E. Harrington, R.D. Hatton, P.R. Mangan, H. Turner, T.L. Murphy, K.M. Murphy, C.T. Weaver, Interleukin 17–producing CD4+ effector T cells develop via a lineage distinct from the T helper type 1 and 2 lineages, Nature immunology, 6 (2005) 1123-1132.

[433] C.L. Langrish, Y. Chen, W.M. Blumenschein, J. Mattson, B. Basham, J.D. Sedgwick, T. McClanahan, R.A. Kastelein, D.J. Cua, IL-23 drives a pathogenic T cell population that induces autoimmune inflammation, Journal of Experimental Medicine, 201 (2005) 233-240.

[434] H. Park, Z. Li, X.O. Yang, S.H. Chang, R. Nurieva, Y.-H. Wang, Y. Wang, L. Hood, Z. Zhu, Q. Tian, A distinct lineage of CD4 T cells regulates tissue inflammation by producing interleukin 17, Nature immunology, 6 (2005) 1133-1141.

[435] S.A. Khader, S.L. Gaffen, J.K. Kolls, Th17 cells at the crossroads of innate and adaptive immunity against infectious diseases at the mucosa, Mucosal Immunol, 2 (2009) 403-411.

[436] P.J. Hotez, M.E. Bottazzi, D.B. Corry, The potential role of Th17 immune responses in coronavirus immunopathology and vaccine-induced immune enhancement, Microbes Infect, 22 (2020) 165-167.

[437] E. Aleebrahim-Dehkordi, B. Molavi, M. Mokhtari, N. Deravi, M. Fathi, T. Fazel, M. Mohebalizadeh, P. Koochaki, P. Shobeiri, A. Hasanpour-Dehkordi, T helper type (Th1/Th2)

responses to SARS-CoV-2 and influenza A (H1N1) virus: From cytokines produced to immune responses, Transplant Immunology, 70 (2022) 101495.

[438] V.J. Costela-Ruiz, R. Illescas-Montes, J.M. Puerta-Puerta, C. Ruiz, L. Melguizo-Rodríguez, SARS-CoV-2 infection: The role of cytokines in COVID-19 disease, Cytokine Growth Factor Rev, 54 (2020) 62-75.

[439] C. Huang, Y. Wang, X. Li, L. Ren, J. Zhao, Y. Hu, L. Zhang, G. Fan, J. Xu, X. Gu, Clinical features of patients infected with 2019 novel coronavirus in Wuhan, China, The lancet, 395 (2020) 497-506.

[440] R.Y. Lan, C. Selmi, M.E. Gershwin, The regulatory, inflammatory, and T cell programming roles of interleukin-2 (IL-2), J Autoimmun, 31 (2008) 7-12.

[441] S.A. Jones, Directing Transition from Innate to Acquired Immunity: Defining a Role for IL-6, The Journal of Immunology, 175 (2005) 3463.

[442] R.M. McLoughlin, J. Witowski, R.L. Robson, T.S. Wilkinson, S.M. Hurst, A.S. Williams, J.D. Williams, S. Rose-John, S.A. Jones, N. Topley, Interplay between IFN-γ and IL-6 signaling governs neutrophil trafficking and apoptosis during acute inflammation, The Journal of Clinical Investigation, 112 (2003) 598-607.

[443] H. Yasukawa, M. Ohishi, H. Mori, M. Murakami, T. Chinen, D. Aki, T. Hanada, K. Takeda, S. Akira, M. Hoshijima, T. Hirano, K.R. Chien, A. Yoshimura, IL-6 induces an anti-inflammatory response in the absence of SOCS3 in macrophages, Nature Immunology, 4 (2003) 551-556.

[444] S. Ohshima, Y. Saeki, T. Mima, M. Sasai, K. Nishioka, S. Nomura, M. Kopf, Y. Katada, T. Tanaka, M. Suemura, Interleukin 6 plays a key role in the development of antigen-induced arthritis, Proceedings of the National Academy of Sciences, 95 (1998) 8222-8226.

[445] M. Yamamoto, K. Yoshizaki, T. Kishimoto, H. Ito, IL-6 is required for the development of Th1 cell-mediated murine colitis, The Journal of Immunology, 164 (2000) 4878-4882.

[446] S. Diehl, M. Rincón, The two faces of IL-6 on Th1/Th2 differentiation, Mol Immunol, 39 (2002) 531-536.

[447] A. Kimura, T. Kishimoto, IL-6: regulator of Treg/Th17 balance, Eur J Immunol, 40 (2010) 1830-1835.

[448] Y.J. Heo, Y.B. Joo, H.J. Oh, M.K. Park, Y.M. Heo, M.L. Cho, S.K. Kwok, J.H. Ju, K.S. Park, S.G. Cho, S.H. Park, H.Y. Kim, J.K. Min, IL-10 suppresses Th17 cells and promotes regulatory T cells in the CD4+ T cell population of rheumatoid arthritis patients, Immunol Lett, 127 (2010) 150-156.

[449] M.J. McGeachy, D.J. Cua, Th17 cell differentiation: the long and winding road, Immunity, 28 (2008) 445-453.

[450] N. Surendran, A. Simmons, M.E. Pichichero, TLR agonist combinations that stimulate Th type I polarizing responses from human neonates, Innate Immun, 24 (2018) 240-251.

[451] C. Pasare, R. Medzhitov, Toll pathway-dependent blockade of CD4+ CD25+ T cell-mediated suppression by dendritic cells, Science, 299 (2003) 1033-1036.

[452] C. Pelaia, G. Paoletti, F. Puggioni, F. Racca, G. Pelaia, G.W. Canonica, E. Heffler, Interleukin-5 in the Pathophysiology of Severe Asthma, Frontiers in Physiology, 10 (2019).

[453] L. Li, Y. Xia, A. Nguyen, Y.H. Lai, L. Feng, T.R. Mosmann, D. Lo, Effects of Th2 cytokines on chemokine expression in the lung: IL-13 potently induces eotaxin expression by airway epithelial cells, J Immunol, 162 (1999) 2477-2487.

[454] B. Spellberg, J.E. Edwards, Jr., Type 1/Type 2 Immunity in Infectious Diseases, Clinical Infectious Diseases, 32 (2001) 76-102.

[455] H.-J. Kim, H. Cantor, CD4 T-cell subsets and tumor immunity: the helpful and the not-so-helpful, Cancer immunology research, 2 (2014) 91-98.

[456] K.S. Rosenthal, D.H. Zimmerman, Vaccines: all things considered, Clin Vaccine Immunol, 13 (2006) 821-829.

[457] T.R. Mosmann, S. Sad, The expanding universe of T-cell subsets: Th1, Th2 and more, Immunol Today, 17 (1996) 138-146.

[458] S. Lousada-Dietrich, P.S. Jogdand, S. Jepsen, V.V. Pinto, S.B. Ditlev, M. Christiansen, S.O. Larsen, C.B. Fox, V.S. Raman, R.F. Howard, T.S. Vedvick, G. Ireton, D. Carter, S.G. Reed, M. Theisen, A synthetic TLR4 agonist formulated in an emulsion enhances humoral and Type 1 cellular immune responses against GMZ2 – A GLURP–MSP3 fusion protein malaria vaccine candidate, Vaccine, 29 (2011) 3284-3292.

[459] F.D. Batista, N.E. Harwood, The who, how and where of antigen presentation to B cells, Nature Reviews Immunology, 9 (2009) 15-27.

[460] S.F. Gonzalez, S.E. Degn, L.A. Pitcher, M. Woodruff, B.A. Heesters, M.C. Carroll, Trafficking of B cell antigen in lymph nodes, Annual review of immunology, 29 (2011) 215-233.

[461] P. Miossec, J.K. Kolls, Targeting IL-17 and TH 17 cells in chronic inflammation, Nature reviews Drug discovery, 11 (2012) 763-776.

[462] L.A. Tesmer, S.K. Lundy, S. Sarkar, D.A. Fox, Th17 cells in human disease, Immunol Rev, 223 (2008) 87-113.

[463] E.J. Rubin, D.L. Longo, L.R. Baden, Interleukin-6 Receptor Inhibition in Covid-19 — Cooling the Inflammatory Soup, New England Journal of Medicine, 384 (2021) 1564-1565.

[464] L. Liu, Q. Wei, Q. Lin, J. Fang, H. Wang, H. Kwok, H. Tang, K. Nishiura, J. Peng, Z. Tan, Anti–spike IgG causes severe acute lung injury by skewing macrophage responses during acute SARS-CoV infection, JCI insight, 4 (2019).

[465] F. Yasui, C. Kai, M. Kitabatake, S. Inoue, M. Yoneda, S. Yokochi, R. Kase, S. Sekiguchi, K. Morita, T. Hishima, Prior immunization with severe acute respiratory syndrome (SARS)-associated coronavirus (SARS-CoV) nucleocapsid protein causes severe pneumonia in mice infected with SARS-CoV, The Journal of Immunology, 181 (2008) 6337-6348.

[466] F. Maione, G.M. Casillo, F. Raucci, C. Salvatore, G. Ambrosini, L. Costa, R. Scarpa, F. Caso, M. Bucci, Interleukin-17A (IL-17A): A silent amplifier of COVID-19, Biomedicine & Pharmacotherapy, 142 (2021) 111980.

[467] Z. Xu, L. Shi, Y. Wang, J. Zhang, L. Huang, C. Zhang, S. Liu, P. Zhao, H. Liu, L. Zhu, Pathological findings of COVID-19 associated with acute respiratory distress syndrome, The Lancet respiratory medicine, 8 (2020) 420-422.

[468] O. Pacha, M.A. Sallman, S.E. Evans, COVID-19: a case for inhibiting IL-17?, Nature Reviews Immunology, 20 (2020) 345-346.

[469] M.G. Kattah, M.T. Wong, M.D. Yocum, P.J. Utz, Cytokines secreted in response to Toll-like receptor ligand stimulation modulate differentiation of human Th17 cells, Arthritis Rheum, 58 (2008) 1619-1629.

[470] E. Davila, J. Kolls, A "Toll" for Th17 cell expansion, Journal of leukocyte biology, 88 (2010) 5-7.

[471] N. Le Bert, A.T. Tan, K. Kunasegaran, C.Y. Tham, M. Hafezi, A. Chia, M.H.Y. Chng, M. Lin, N. Tan, M. Linster, SARS-CoV-2-specific T cell immunity in cases of COVID-19 and SARS, and uninfected controls, Nature, 584 (2020) 457-462.

[472] T. Sekine, A. Perez-Potti, O. Rivera-Ballesteros, K. Strålin, J.-B. Gorin, A. Olsson, S. Llewellyn-Lacey, H. Kamal, G. Bogdanovic, S. Muschiol, Robust T cell immunity in convalescent individuals with asymptomatic or mild COVID-19, Cell, 183 (2020) 158-168. e114.

[473] P.M. Moyle, Biotechnology approaches to produce potent, self-adjuvanting antigen-adjuvant fusion protein subunit vaccines, Biotechnol Adv, 35 (2017) 375-389.

[474] S.G. Reed, M.T. Orr, C.B. Fox, Key roles of adjuvants in modern vaccines, Nature Medicine, 19 (2013) 1597-1608.

[475] C. Maisonneuve, S. Bertholet, D.J. Philpott, E. De Gregorio, Unleashing the potential of NOD- and Toll-like agonists as vaccine adjuvants, Proceedings of the National Academy of Sciences, 111 (2014) 12294-12299.

[476] D. Mohanan, B. Slütter, M. Henriksen-Lacey, W. Jiskoot, J.A. Bouwstra, Y. Perrie, T.M. Kündig, B. Gander, P. Johansen, Administration routes affect the quality of immune responses: A cross-sectional evaluation of particulate antigen-delivery systems, Journal of Controlled Release, 147 (2010) 342-349.

[477] K.J. Hassett, K.E. Benenato, E. Jacquinet, A. Lee, A. Woods, O. Yuzhakov, S. Himansu, J. Deterling, B.M. Geilich, T. Ketova, C. Mihai, A. Lynn, I. McFadyen, M.J. Moore, J.J. Senn, M.G. Stanton, Ö. Almarsson, G. Ciaramella, L.A. Brito, Optimization of Lipid Nanoparticles for Intramuscular Administration of mRNA Vaccines, Molecular Therapy - Nucleic Acids, 15 (2019) 1-11.

[478] A. Akinc, M.A. Maier, M. Manoharan, K. Fitzgerald, M. Jayaraman, S. Barros, S. Ansell, X. Du, M.J. Hope, T.D. Madden, B.L. Mui, S.C. Semple, Y.K. Tam, M. Ciufolini, D. Witzigmann, J.A. Kulkarni, R. van der Meel, P.R. Cullis, The Onpattro story and the clinical translation of nanomedicines containing nucleic acid-based drugs, Nature Nanotechnology, 14 (2019) 1084-1087.

[479] EMA, Onpattro Assessment Report, in, European Medicines Agency, 2018.

[480] S.M. Paul, D.S. Mytelka, C.T. Dunwiddie, C.C. Persinger, B.H. Munos, S.R. Lindborg, A.L. Schacht, How to improve R&D productivity: the pharmaceutical industry's grand challenge, Nat Rev Drug Discov, 9 (2010) 203-214.

[481] V. Sainz, J. Conniot, A.I. Matos, C. Peres, E. Zupancic, L. Moura, L.C. Silva, H.F. Florindo, R.S. Gaspar, Regulatory aspects on nanomedicines, Biochem Biophys Res Commun, 468 (2015) 504-510.

[482] N. Benne, J. van Duijn, J. Kuiper, W. Jiskoot, B. Slutter, Orchestrating immune responses: How size, shape and rigidity affect the immunogenicity of particulate vaccines, Journal of controlled release : official journal of the Controlled Release Society, 234 (2016) 124-134.

[483] G.K. Pedersen, K. Worzner, P. Andersen, D. Christensen, Vaccine Adjuvants Differentially Affect Kinetics of Antibody and Germinal Center Responses, Front Immunol, 11 (2020) 579761.

[484] R. Zhou, P. Wang, Y.-C. Wong, H. Xu, S.-Y. Lau, L. Liu, B.W.-Y. Mok, Q. Peng, N. Liu, K.-F. Woo, S. Deng, R.C.-Y. Tam, H. Huang, A.J. Zhang, D. Zhou, B. Zhou, C.-Y. Chan, Z. Du, D. Yang, K.-K. Au, K.-Y. Yuen, H. Chen, Z. Chen, Nasal prevention of SARS-CoV-2 infection by intranasal influenza-based boost vaccination in mouse models, EBioMedicine, 75 (2022).